Technical Report CHL-97-7
April 1997

US Army Corps of Engineers
Waterways Experiment Station

Physical Model Studies for Riprap Design of Tow-Induced Forces

by Sandra K. Martin

Prepared for Headquarters, U.S. Army Corps of Engineers

Technical Report CHL-97-7
April 1997

Physical Model Studies for Riprap Design of Tow-Induced Forces

by Sandra K. Martin

U.S. Army Corps of Engineers
Waterways Experiment Station
3909 Halls Ferry Road
Vicksburg, MS 39180-6199

Final report

Approved for public release; distribution is unlimited

Prepared for U.S. Army Corps of Engineers
Washington, DC 20314-1000

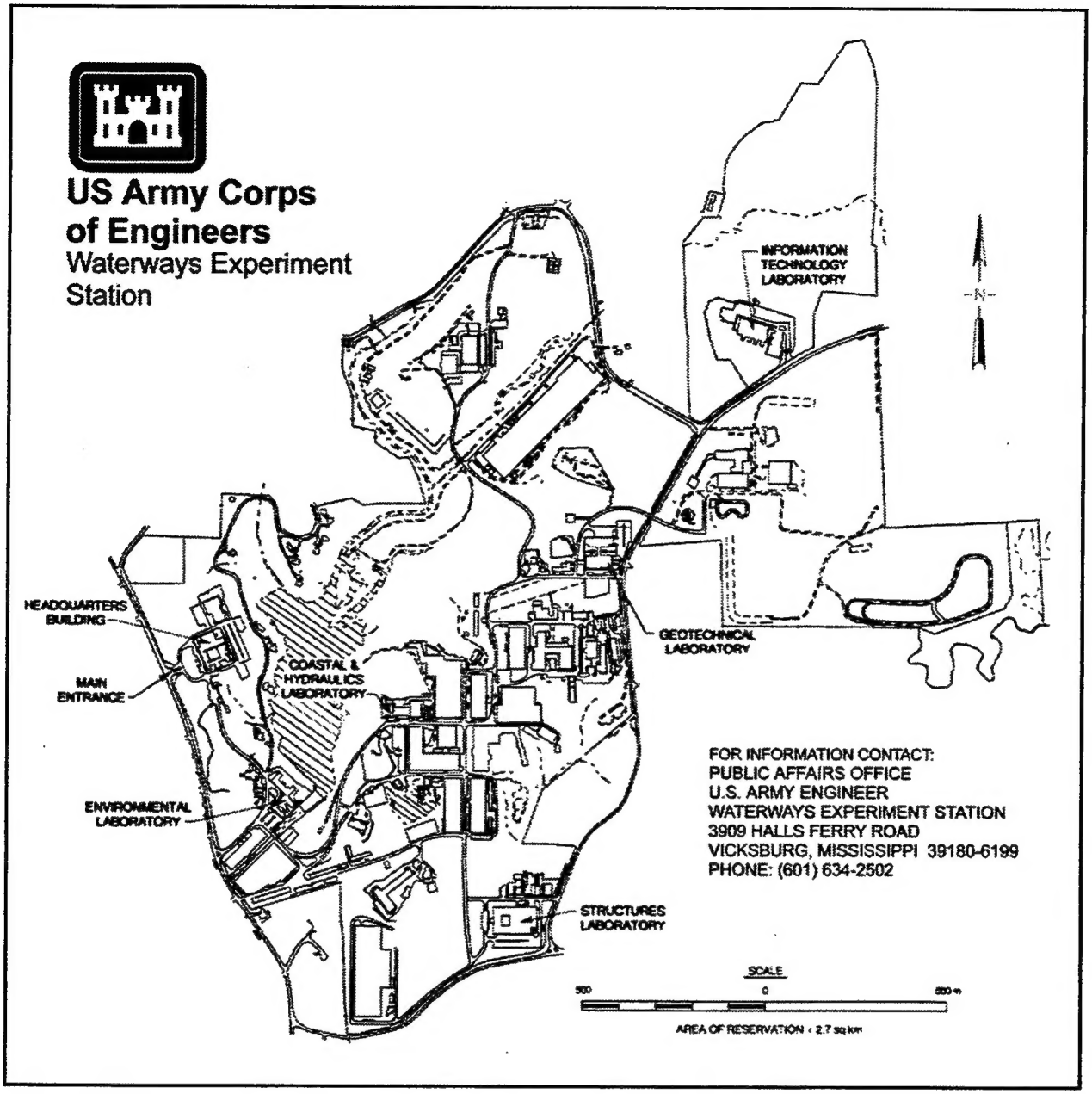

Waterways Experiment Station Cataloging-in-Publication Data

Martin, Sandra K.

Physical model studies for riprap design of tow-induced forces / by Sandra K. Martin ; prepared for U.S. Army Corps of Engineers.

260 p. : ill. ; 28 cm. — (Technical report ; CHL-97-7)

Includes bibliographic references.

1. Inland navigation. 2. Riprap. 3. Towboats. I. United States. Army. Corps of Engineers. II. U.S. Army Engineer Waterways Experiment Station. III. Coastal and Hydraulics Laboratory (U.S. Army Engineer Waterways Experiment Station) IV. Title. V. Series: Technical report (U.S. Army Engineer Waterways Experiment Station) ; CHL-97-7.

TA7 W34 no.CHL-97-7

Table of Contents

List of Tables

List of Figures

Preface

This study was funded by Headquarters, U.S. Army Corps of Engineers, and conducted from Fiscal Year 1990 to 1993 by Dr. Sandra K. Martin, Navigation Effects Group, Navigation Division, Hydraulics Laboratory (HL), U.S. Army Engineer Waterways Experiment Station (WES). The research was conducted under the general supervision of Mr. R. A. Sager, Acting Director, HL; Mr. R. F. Athow, Acting Assistant Director, HL; and Dr. Larry L. Daggett, Chief, Navigation Division; and under the direct supervision of Dr. Stephen T. Maynord, Navigation Effects Group Leader, who provided technical guidance throughout the study.

This report is a dissertation in partial fulfillment of the requirements for the degree of Doctor of Philosophy from the University of Memphis, Memphis, TN.

The author would like to thank the many people who helped with this effort. Ms. Sheila Knight, Navigation Effects Group, performed the data collection for the entire study. Others who assisted with the project were Messrs. Douglas M. White, Spillways and Channels Branch, Hydraulic Structures Division, HL; Bobby Bottin, Contractor; Van E. Stewart, Calvin Buie, and James Cessna, all of the Locks, Reservoirs, and Fisheries Hydrodynamics Branch, Hydraulic Structures Division; and Ms. Olie Blansett, Contractor. The author would also like to thank the Dissertation Committee members of the University of Memphis, especially Dr. Jerry Anderson, Chairman, for their input.

At the time of publication of this report, Director of WES was Dr. Robert W. Whalin. Commander was COL Bruce K. Howard, EN.

Notation

a, a_1	Coefficients
A	Representative wave amplitude or the runup, ft (m)
A	Area eroded, ft^2 (m^2)
A_b	Cross-sectional area of the submerged barges at mid-ship, ft^2 (m^2)
A_c	Channel cross-sectional area before drawdown, ft^2 (m^2)
A_w	Wetted cross-sectional area of channel at mid-ship of the barges, ft^2 (m^2)
b_t	Top width of channel at waterline, ft (m)
b_w	Bottom width of channel, ft (m)
B_s	Vessel beam width, ft (m)
c, c_1	Coefficients
C_D	Drag coefficient
C_I	Inertia coefficient
C_L	Lift coefficient
C_q	Total force coefficient
C	Constant
C_{fr}	Coefficient of drag
d	Draft of barges, ft (m)

d_b Depth of breaking waves, ft (m)

D Diameter of stone, ft (m)

D_{act} Actual stone diameter used in each model test, ft (m)

D_{eq} Equivalent stone diameter, ft (m)

D_{50} Diameter of stone protection for which 50% is lighter by weight, ft (m)

F_d Draft Froude number

F_h Vessel Froude number

F_q Total force

F_p Forces parallel to the bank

F_{Y*} Vessel Froude number defined by Bhowmik

F_D Drag force

F_I Inertia force

F_L Lift force

F_N Forces normal to the bank

F_P Forces parallel to the bank

F_T Resultant hydrodynamic force acting on slope

g Gravitational constant, 32.2 ft/s^2 (9.81 m/s^2)

h Depth of undisturbed water level, ft (m)

h_f Front wave, ft (m)

H Height of attacking wave, ft (m)

H_i Maximum secondary wave height, ft (m)

H_{max} Maximum wave height, ft (m)

H_{mo} Energy-based, zero-moment wave height, ft (m)

H_s Significant wave height and stone diameter, ft (m)

H_T Total head, ft (m)

i_f Gradient of the front wave

i_{max} Gradient of transversal stern wave

k_1 , k_d , K_ϕ , K_{down} , K_{up} , K , K_1 , K_2, K_3 Coefficients used in stability factors

k_1 Volume shape factor, $\pi/6$ for spheres

k_2 Area shape factor, $\pi/4$ for spheres

k_s Bottom roughness, ft (m)

K_{act} Actual K_3 value corresponding to model

K_{max} Maximum K_3 value for normalizing diameters

L Length of slope, ft

L_p Airy wave length, ft (m)

L_s Length of ship at waterline, ft (m)

L_{wi} Wave length, ft (m)

n Blockage ratio

N Normal force resisting motion

N Number of waves

N_s Dimensionless stability number

N_{sz} Stability number at zero damage

P_1 Normal force lifting stone

R	Parallel force resisting motion
R_D	Particle Reynolds number
R_e	Wave Reynolds number
R_E	Wave Reynolds number
R_{max}	Maximum wave runup, ft (m)
R_N	Reynolds number
R_u	Wave runup, ft (m)
R_z	Wave runup associated with zero-damage wave height, ft (m)
s	Distance between ship's side and water's edge, ft (m)
S	Distance from wave gage to sailing line, ft (m)
S	Damage level
S_f	Safety factor
T	Wave period, sec
T_i	Average wave period, sec
T_p	Period of peak wave energy density, sec
T_z	Wave period at zero damage, sec
u	Directional velocity, fps (mps)
u_c	Return current near bank, fps (mps)
u_{max}	Maximum current in stern wave, fps (mps)
u_r	Return current, fps (mps)
u_{rm}	Maximum return current, fps (mps)
u_{yb}	Lateral current away from bow, fps (mps)

u_{ys} Lateral current toward stern, fps (mps)

V Jet efflux velocity, fps (mps)

V_L Limiting speed of vessel, fps (mps)

V_R Water particle velocity parallel to breakwater side slope, fps (mps)

V_s Speed of tow relative to earth, fps (mps)

W_B Buoyant weight of stone, lb (kg)

W_r Unit weight of stone, lb (kg)

W_{50} Unit weight of stone which is 50 percent lighter by weight, lb (kg)

x Distance a water particle moves due to u_r, ft (m)

y Eccentricity or distance from centerline channel to centerline tow, ft (m)

Y^* Water depth minus draft, ft (m)

y_t Distance from centerline of vessel to midway up slope, ft (m)

z Drawdown, ft (m)

z_{ave} Average drawdown, ft (m)

z_{max} Transversal stern wave, ft (m)

z_{zero} Channel factor

α Angle slope makes with horizontal

α_1, α_2 Coefficient to determine seconday waves

β Angle wave makes to bank

γ_r Specific weight of stone, lb/ft^3 (kg/m^3)

γ_w Specific weight of water, lb/ft^3 (kg/m^3)

Δ $\frac{\gamma_r}{\gamma_w} - 1$

ξ Surf similarity parameter

ξ_L Surf similarity parameter using local wave length

ξ_z Surf similarity parameter at zero damage

θ Angle between wave propagation and sailing line

λ Wave length, ft (m)

ν Kinematic viscosity of water, ft^2/s (m^2/s)

ρ Density of water, $slug/ft^3$ (kg/m^3)

τ_c Critical shear stress, lb/ft^2 (kg/m^2)

τ_m Maximum shear stress, lb/ft^2 (kg/m^2)

ϕ Natural angle of repose

ψ Flow parameter

ω Radian frequency

$\forall$ Displacement volume of ship, ft^3 (m^3)

1 Introduction

Background

As commercial towboats navigate inland waterways, physical forces in the form of waves and currents are generated. In confined or restricted waterways, these vessel-induced forces can have a significant effect on the surrounding environment. Evaluating the impacts of navigation-induced forces on the riverine environment has become a topic of serious discussion and intense debate in recent years.

Technical studies related to navigation effects investigate the characteristics of the physical forces produced by moving vessels and determine the effects of these forces from both an engineering and a biological perspective. Bank stability, bed stability, sediment transport, maneuverability of the vessel through the waterway, sill heights at locks, and collisions with structures are a few of the reasons evaluation of forces is important from an engineering design perspective. Environmental concerns range from propeller jet turbulence impacts on fish larvae, wave energy on aquatic vegetation, to sediment resuspension and transport in critical shoreline habitat areas and adjacent backwaters.

Minimizing shoreline erosion can be critical for the protection of valuable resources whether they are man-made or natural. Shoreline erosion, among other things, can lead

to loss of habitat, can expose important archaeological sites, and can threaten the structural integrity of flood control and navigation projects. This research focuses on the protection of banks from forces produced by commercial vessels underway on inland navigable waterways using stone slope protection.

Riprap is a classical solution to bank stability problems whether related to wave-induced forces or flow-induced velocities. Minimization of rock size can result in substantial savings in a bank protection project. Design guidance related to riprap design for waves was originally developed for protection of coastal shorelines. Beginning with a formulation developed by Iribarren (1948), Hudson (1957) reformulated an equation, still widely accepted and used, that relates stone weight to wave height. Criteria for riprap design in open channel flows has been studied and developed by many, including Maynord (1988).

The Delft Hydraulics Laboratory, the Netherlands, has conducted research and produced design methodologies for riprap design in constricted waterways due to vessel-generated forces. Site-specific studies have been conducted at the U.S. Army Engineer Waterways Experiment Station (WES), Vicksburg, MS, for the Tennessee-Tombigbee Waterway (Maynord and Oswalt 1986) and for locks and dams on the Ohio River. The Ohio River studies for the U.S. Army Corps of Engineers, Huntington District (Martin 1989), suggested that rather small stone sizes exhibit stability under reasonable vessel operating conditions. Verification of this premise could result in considerable savings to inland navigation projects by reducing the size, and consequently, blanket thickness, of stone protection in heavily navigated reaches of commercial waterways. Savings have

already been realized on the Point Marion Lock approach on the Monongahela River based on site-specific studies recommending a reduction in the riprap size over the proposed stone (Maynord 1989).

The U.S. Army Corps of Engineers have recently been, and are currently, authorized to construct major rehabilitation projects on several inland locks and dams with studies underway on many more. In the approach channels to these locks, where the major potential causal mechanism for bank erosion can be attributed to commercial tow traffic, a generalized approach is needed to minimize the need for site-specific studies and to insure safe and economical stone slope protection. Sorensen (1986), in his investigations of existing criteria for the design of bank protection from vessel-generated waves, concludes, "significant improvements can be made in the quality of this design information so less conservative and more economical designs can be made with more confidence."

Objective

The main objective of this research was to develop a riprap sizing procedure for protecting bank slopes from tow-induced forces generated by commercial traffic on United States navigable waterways. A commercial tow consists of multiple barge units pushed by a towboat. The riprap design applications were in essentially slack water canals or natural channels with small ratios of wetted channel cross-sectional areas to

submerged vessel cross-sectional areas. A secondary emphasis was placed on presentation of existing methods for quantifying tow-induced forces.

Although not recognized as an objective prior to this study, considerable knowledge was obtained regarding scale effects in physical model studies. Low Reynolds values during testing and the test materials' natural angle of repose were found to contribute to stone instability.

Approach

This research scrutinized existing methods for sizing riprap by (a) the review of literature, (b) analyzing physical model data from previous site-specific studies, and (c) supplemental data through additional physical model testing. Applicability of existing techniques and guidance were compared to results obtained through the model tests. Recommendations for riprap sizing were made to satisfy research objectives.

The existing and supplemental riprap stability tests were conducted at two model scales by exposing different gradations of model stone on two bank slopes with repetitive passes of a model tow (towboat and variable barge configurations). The tow's draft, speed, and sailing line were varied. Several water depths were used during testing. All tests were conducted in generally confined channels with no ambient currents.

2 Literature Review

Existing Methods for Predicting Physical Forces

Definitions

Vessel-induced water motion or navigation effects can be classified in three general categories according to the mechanisms that caused the effects (a) the displacement motion of the vessel in the channel or the primary wave system, (b) waves produced by dynamic ship theory or secondary waves, and (c) propeller jets. Methods coupling all the dynamics of vessel motion that quantify the three-dimensional (3-D) forces produced do not exist. Therefore, the three basic areas of vessel-induced water motion are studied in pieces based on conservation of energy or momentum, slender body theory, and empirical approaches (Blaauw et al. 1984).

The vessel's displacement motion produces long period changes in water-surface elevations and some rather characteristic current patterns around and beneath the vessel. This phenomena can be explained in much the same manner as a piston moving through a cylinder. As the vessel moves faster through the channel the fluid must change directions and water levels to satisfy the principles of energy and continuity. Figure 1 shows the

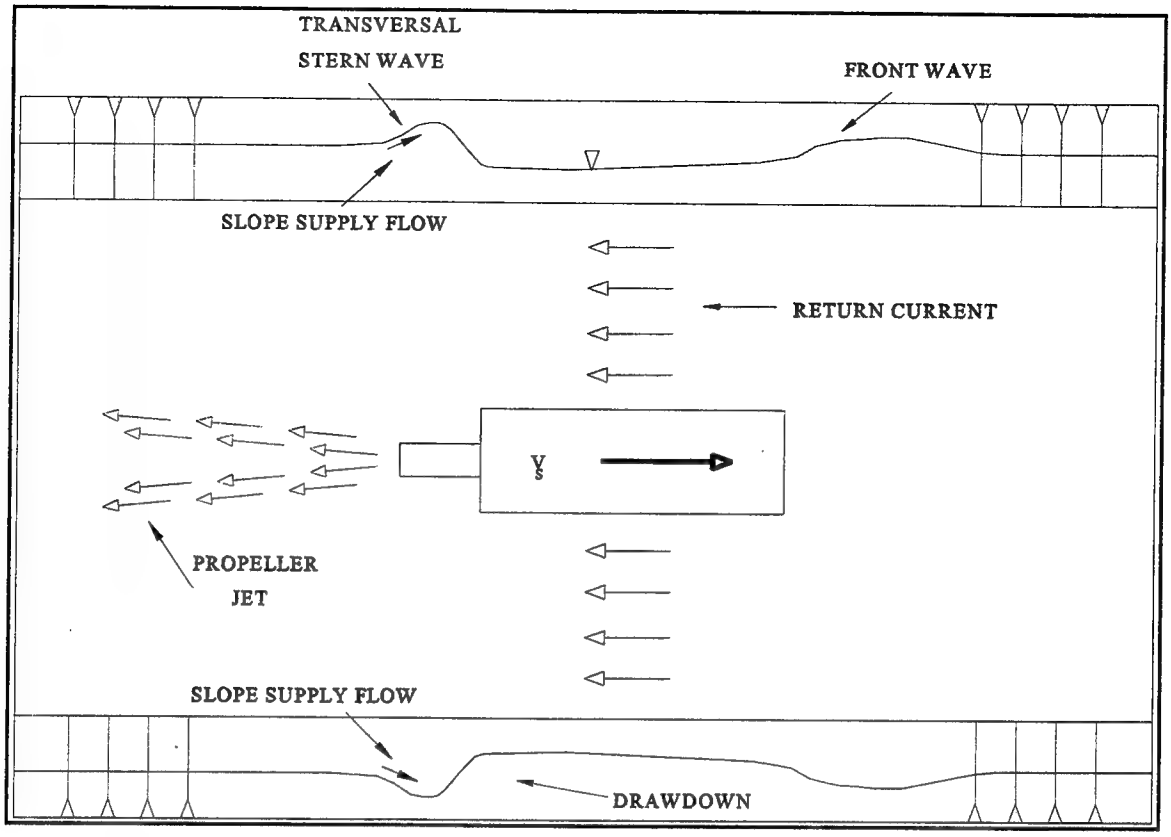

Figure 1. Schematic of primary navigation effects

primary components of this motion in plan view. Major water level changes are attributed to the front or bow wave, drawdown, and transversal stern wave. Major velocity components are the return current and slope supply flow. The strength of these forces is primarily a function of the vessel speed and its size relative to the channel. The current beneath the vessel is a force not shown. The shear forces and velocities generated in this region can be critical to the channel bed, but do not influence the stability of the channel banks.

Secondary waves include the entire wave spectrum formed by the pressure disturbance on the hull of the moving vessel. The vessel creates transverse and diverging waves intersecting at peaks which form a distinct pattern in deep water (Verhey and Bogaerts 1989). The shape of the vessel hull and the speed of the vessel dictate the magnitude of these waves. Figure 2 is a diagram showing this wave pattern in plan view.

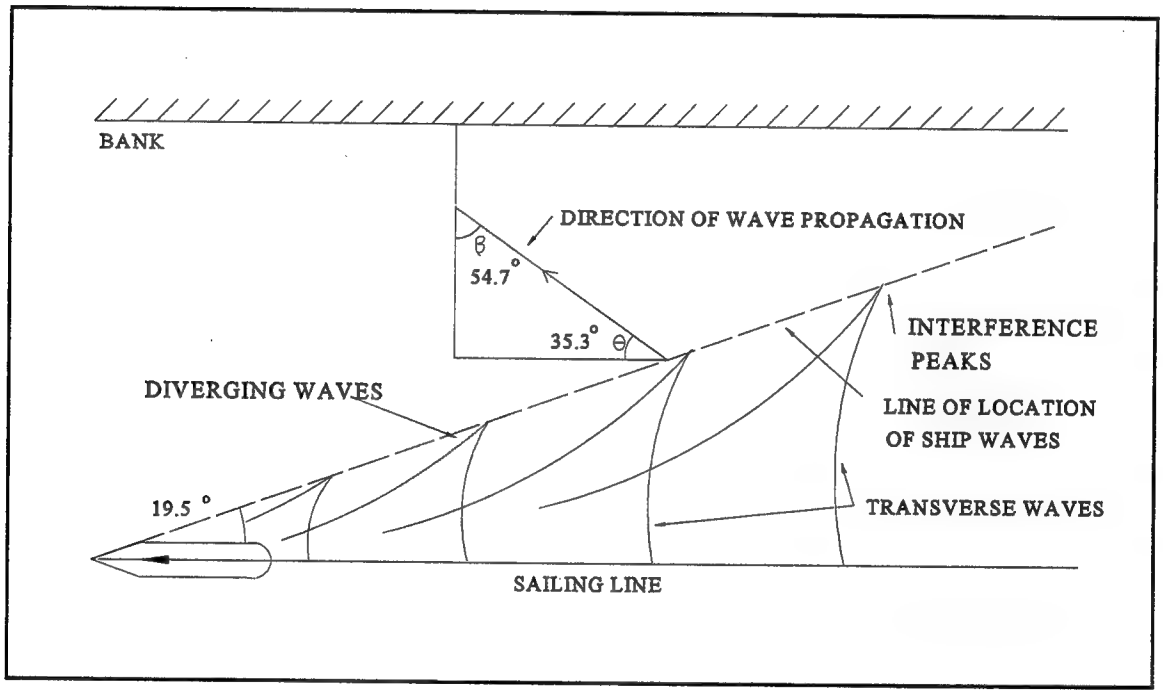

Figure 2. Ship wave angles and definition sketch

A commercial tow is generally powered by twin propellers each having diameters of 5 to 8 ft (1.5 to 2.4 m). Propeller jet forces can impact the channel bed and the lower portion of the bank slope if the tow is navigating within close proximity of the bank. Bank failure due to propeller jets could occur in areas where direct impingement is inevitable as in a tight bend, maneuvering into a lock, or mooring near a bank.

Since components of the displacement forces and the secondary waves have the most impact on the stability of channel banks, no further discussion is given to propeller jet forces or velocities beneath the vessel. Terms related to navigation effects are found in Appendix A.

Displacement motion

The general physics related to displacement of a tow moving through a channel can be represented by applying the principles of energy or momentum and continuity. These theories are represented in existing analytical equations regarding prediction of these forces particularly in the determination of return current and drawdown. Equations for return current and drawdown can be derived by applying the Bernoulli principle for energy and conservation of mass, an approach used by Jansen and Schijf (1953). Bouwmeester et al. (1977) used the momentum equation rather than the energy approach. Equating the energy along a streamline using a point mid-length of the tow and one in the undisturbed channel, and assuming superposition, the following results:

$$z_{ave} = \frac{(V_s + u_r)^2 - V_s^2}{2g} \tag{1}$$

where

z_{ave} = average drawdown, ft (m)

V_s = speed of tow relative to earth, fps (mps)

u_r = return current, fps (mps)

g = gravitational constant = 32.2 ft/s^2 (9.81 m/s^2)

Based on continuity, the equation follows:

$$V_s A_c = (V_s + u_r) A_w \tag{2}$$

where

A_c = channel cross-sectional area before drawdown, ft^2 (m^2)

A_w = wetted cross-sectional area of channel at mid-ship of the barges, ft^2 (m^2)

and

$$A_w = \frac{A_c(h - z_{ave}) - A_b h}{h} \tag{3}$$

A_b = cross-sectional area of the submerged barges, ft^2 (m^2)

h = depth of undisturbed water level, ft (m)

This standard method for estimating drawdown and return current is called the Schijf approach or method. It gives the "average" drop in water surface and return current near mid-ship. Development of these equations was based on the following assumptions:

a. uniform cross section

b. uniform return current

c. uniform water level drawdown

d. no friction

e. negligible ambient current

f. centerline placement of the vessel

The drawdown and return current are primarily a function of vessel speed and blockage ratio, n , defined as the ratio of A_c over A_b. The limiting speed, V_L, defined as the maximum or critical vessel speed, was determined by differentiating Equations 1 and 2 (Jansen and Schijf 1953). This speed is the maximum speed a vessel can reach in a confined channel of specified blockage ratio regardless of vessel horsepower.

Numerous researchers have used variations of this approach that introduce coefficients and/or modifications to the equations that account for parameters such as off-center sailing, irregularity of channel section, friction, etc. These methods were based on model studies and/or field data. Maynord (1990) presented a thorough review of the many methods for determining displacement and return velocities. The Permanent International Association of Navigation Congresses (PIANC) published guidelines for predicting navigation-induced forces (PIANC 1987). Equations in these guidelines are composites of previous researchers' efforts, particularly those from the Delft Hydraulics Laboratory, the Netherlands. Figure 3 defines some channel and vessel parameters used in the following methods for calculating physical forces.

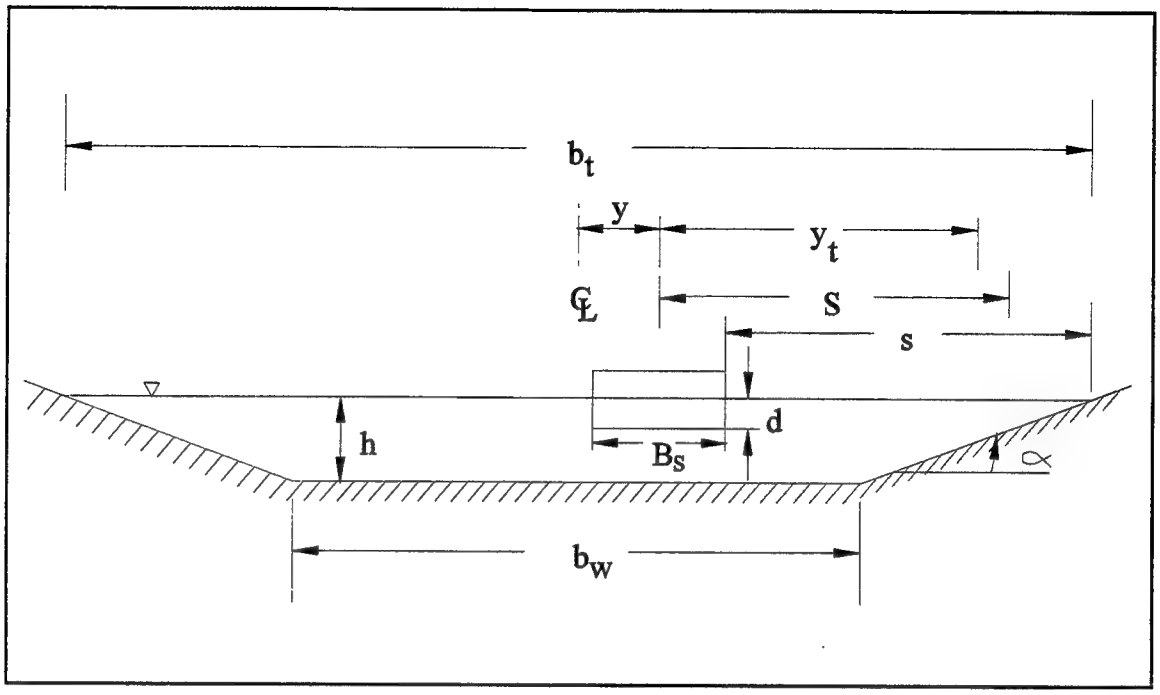

Figure 3. Definition of geometric terms used in predictive equations

PIANC (1987) recommended the average return current, u_r, and drawdown, z_{ave}, be estimated using the Schijf equations. The method is valid for waterway topwidths, b_t, to vessel beam widths, B_s, between 2 and 12. They also recommended adding an empirical coefficient, a_1, that is a function of the ratio of V_s to V_L, to the energy equation.

Rewriting Equation 1 to include a_1 gives

$$Z_{ave} = \frac{V_s^2}{2g}\left[a_1\left(\frac{A_c}{A_w}\right)^2 - 1\right] \tag{4}$$

Bouwmeester et al. (1977) describes the maximum depression of the water level as "the combined effect of the primary wave and the secondary wave system." The deepest trough occurs between the bow and stern. They define the transverse stern wave as "the slope of the water surface due to deceleration of the return flow at the stern." They observed that as the water level depression increased, the transverse stern wave had the appearance of a moving hydraulic jump. Furthermore, "under certain conditions the stern transverse wave was intensified by secondary waves," particularly when the cusp line of the secondary waves intersected with the crest of the transverse stern wave.

The transversal stern wave, z_{max}, was empirically determined as a function of the drawdown in PIANC (1987) and is defined by Figure 4 as the maximum drawdown. It can be determined for a push-tow unit (towboat and barge unit) by

$$z_{max} = c\, z_{ave} \tag{5}$$

where

$$c = 1.2 + 5 \times 10^{-4} F_h \frac{b_t}{y_t} \frac{L_s^2}{h\sqrt{A_b}} \tag{6}$$

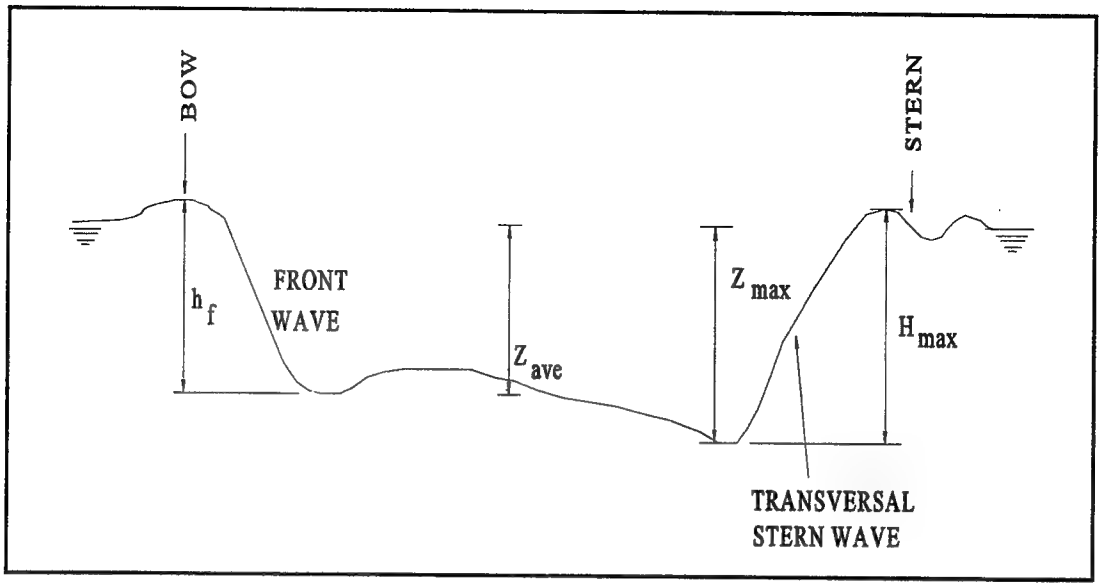

Figure 4. Definition sketch of water level terms for displacement motion

The vessel Froude number, F_h, is defined as

$$F_h = \frac{V_s}{\sqrt{gh}} \tag{7}$$

and y_t is defined as

$$y_t = 0.5 b_t - y - 0.5 h \cot \alpha \tag{8}$$

b_t = top width of channel, ft (m)

y = distance from centerline channel to centerline tow, ft (m)

L_s = length of ship at waterline, ft (m)

α = angle slope makes with horizontal

The depth, h , in a trapezoidal or irregular channel can be approximated using A_c/b_t . From a graphical solution in Blaauw et al. (1984) the following linear relationship was obtained for z_{max} as a function of y (the eccentricity), topwidth, and average drawdown.

$$z_{max} = z_{ave}\left(2.4\frac{y}{b_t} + 1.2\right) \tag{9}$$

Based on a multivariate regression of prototype data collected on the Illinois River, Bhowmik, Demissie, and Guo (1982), developed two empirical formulas for predicting wave heights as a function of tow speed. The equation for drawdown, z , was based on the following:

$$\frac{z}{Y^*} = 0.478 F_{Y^*}{}^{0.5}\left(\frac{A_b}{A_c}\right)^{0.81}\left(\frac{L_s}{S}\right)^{0.26} \tag{10}$$

where

$$Y^* = \frac{A_c}{b_t} - d \tag{11}$$

$$F_{Y^*} = \frac{V_s}{\sqrt{gY^*}} \tag{12}$$

The variable, S , is the distance from the wave gage to the sailing line and d is the draft of the barges (Figure 3). The tow speeds measured for this analysis varied from 4 to 20 fps (1.2 to 6.1 mps), and blockage ratios were quite variable as well, from 15 to 230. The maximum measured drawdown was 0.7 ft (0.2 m).

The front wave, h_f, is the total peak to following trough of the wave crest preceding the bow to the trough or drawdown (Figure 4). The relationship given in PIANC (1987) for computing this value is

$$h_f = 0.1\, z_{ave} + z_{max} \tag{13}$$

From a graphical solution in Blaauw et al. (1984), the following linear relationship was obtained

$$h_f = z_{ave}\left(4\frac{y}{b_t} + 1.2 \right) \tag{14}$$

Fuehrer, Romisch, and Engelke (1981) gave equations for calculating the maximum change in water level for vessels traveling less than critical speed and for those traveling

greater than critical speed. They stated that the primary wave system plays the dominant role in the subcritical vessel speed range. As the vessel increases its speed beyond this critical level, the secondary wave motion becomes important. Their wave height equation for vessels in the subcritical range actually represented the front wave and drawdown, such that

$$h_f = C V_s^{3.5} \tag{15}$$

The constant, C, is a function of channel parameters including blockage ratio, channel depth, and channel width.

Based on model data collected at WES and the Delft, and field studies conducted by the Louisville District, Maynord and Siemsen (1991) recommended a modified Schijf approach that introduces not only an asymmetric sailing line, but also provides a mathematical decay function for return currents in channels with higher blockage ratios. It was concluded that in confined channels where blockage ratios are small, a uniform distribution of return currents is a reasonable assumption. Even when the tow is sailing off the channel's center line, the lateral distributions are uniform even if the relative magnitudes are different on one side of the channel versus the other. In larger rivers the strength of the return current decays with distance from the tow (Maynord and Siemsen 1990). Based on his recent analysis of model and prototype data, Maynord (1996)

presented a method for calculating maximum return current, u_{rm}, and maximum drawdown, z_{max}, as a function of distance from the vessel for blockage ratios up to 52.

The composite field of currents formed from displacement motion include bow currents, lateral currents, return currents, flow beneath the vessel, and slope supply currents. The return current and slope supply flow have the most impact on the bank.

The average maximum return current in a channel, u_{rm}, is defined by Maynord (1996) as a function of the Schijf return current, u_r, and a ratio of the vessel speed to limiting speed such that

$$u_{rm} = u_r \left(1.9 - 1.29 \frac{V_s}{V_L} \right) \tag{16}$$

PIANC (1987) defined the maximum return current velocity, u_{rm}, as

$$u_{rm} = c\, u_r \tag{17}$$

The coefficient, c, according to PIANC (1987) is defined by Equation 6. From a graphical solution in Blaauw et al. (1984), a similar linear relationship existed for return current, Equation 9, and drawdown, such that

$$u_{rm} = u_r\left(2.4\frac{y}{b_t} + 1.4\right) \tag{18}$$

According to Bouwmeester et al. (1977), when ships are traveling at high speeds near the bank, a translatory wave or moving bore is formed and propagates at a speed relative to the water equal to the sum of the return current and ship's speed. They called the high velocities near the banks, which resulted from water being restored, the "slope-supply flow."

According to Blaauw et al. (1984), the maximum currents in the stern wave, or slope supply current can be estimated by

$$u_{max} = 0.1 \text{ to } 0.2\ V_s, \quad \text{if } \frac{z_{max}}{\Delta \cdot D_{50}} < 1 \tag{19}$$

$$u_{max} = \left(1 - \frac{\Delta D_{50}}{z_{max}}\right) V_s, \quad \text{if } \frac{z_{max}}{\Delta D_{50}} \geq 1 \tag{20}$$

where

$$\Delta = \frac{\gamma_r}{\gamma_w} - 1 \tag{21}$$

γ_r = specific weight of stone, lb/ft^3 (kg/m^3)

γ_w = specific weight of water, lb/ft^3 (kg/m^3)

D_{50} = diameter of stone protection for which 50 percent is lighter by weight, ft (m)

Gradients

Gradients in the front and transversal waves generate external load factors causing internal loadings. According to Blaauw et al. (1984), the gradient in the longitudinal (x) direction was of minor significance to the relationship between internal load and strength. In the case of revetment blocks, the gradients in the transverse (y) direction can be important in designing filter layers and the gradients in the z direction can cause uplift.

Internal hydraulic gradients in the y direction can be represented by the product of the external load from the height of the front wave, gradient of the front wave, i_f, and ship speed as follows

$$h_f \cdot \frac{\partial h}{\partial t} = h_f \cdot \frac{\partial h}{\partial x} \cdot \frac{\partial x}{\partial t} = h_f \cdot i_f \cdot V_s \tag{22}$$

The gradient, i_{max}, of the transversal stern wave is defined as

$$i_{max} = \left(\frac{z_{max}}{z_0} \right)^2 \tag{23}$$

The value of i_{max} has a limiting value of 0.1 to 0.15. The factor z_0 is a function of channel top width, b_t, and eccentricity, y, such that

$$\frac{z_0}{b_t} = 0.04 - 0.158 \frac{y}{b_t} \tag{24}$$

Secondary waves

Boat waves can be classified according to criteria in the *Shore Protection Manual* (1984). Drawdown will almost certainly be classified as a shallow water wave; whereas secondary waves, with periods of one to five seconds, can approach a deep water classification and may be either. Based on the same criteria, the waves formed by tows in channels, whether short period or long period, are generally nonbreaking, except in shallow near-shore areas.

Figure 5 contains time-history schematics of the waves generated by a moving vessel in a confined reach. The first response contains the unfiltered long and short period waves; the second, the filtered long period wave or drawdown; and the third, the filtered short period or secondary waves.

It has been observed by the author and others (Fuehrer, Romisch, and Engelke 1981) that secondary waves are negligible at low vessel speeds and high blockage ratios. At faster vessel speeds, secondary waves can become more significant and their magnitude approach or exceed the magnitude of the maximum drawdown. Generally, secondary

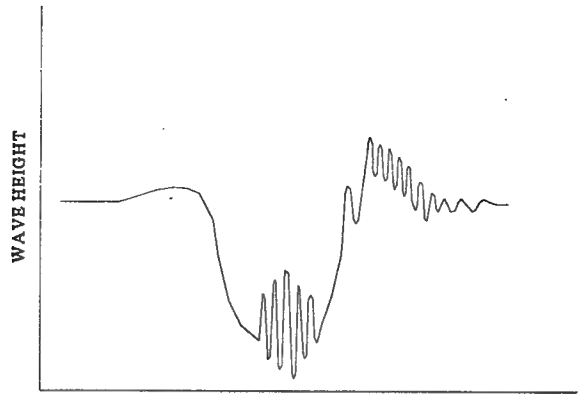

a. Total wave response, unfiltered.

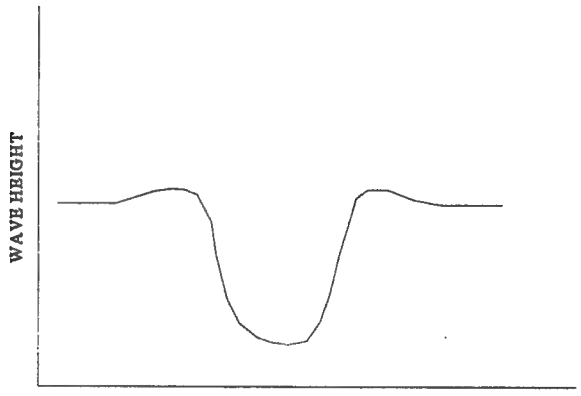

b. Long period wave response, drawdown.

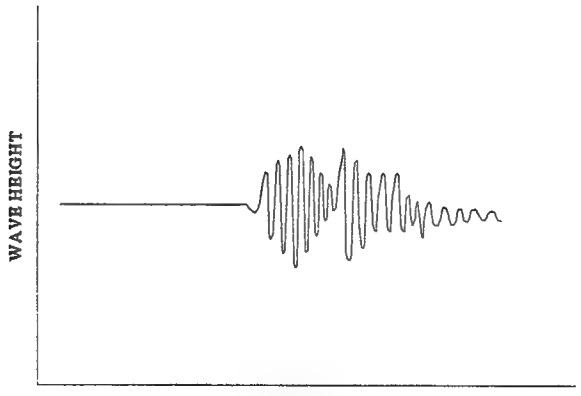

c. Short period wave response, secondary waves.

Figure 5. Typical time-history wave response for a tow in a confined channel

waves have higher frequency, lower amplitude, and last longer than the shallow water drawdown effects. For vessels in larger channels and recreational craft, the diverging coincidental peaks can dominate the wave spectrum.

Verhey and Bogaerts (1989) presented a predictive equation for secondary waves that related the wave height to the sailing line, vessel speed, and water depth. The coefficient, α_1, regards the type of vessel and its draft. The equation for estimating maximum secondary wave height, H_i, for the incidental wave peak is

$$H_i = \alpha_1 h \left(\frac{s}{h}\right)^{-0.33} F_h^{\alpha_2} \tag{25}$$

where:

α_1 = coefficient regarding hull type and draft

α_2 = coefficient experimentally determined to be 4.0

s = distance between ship's side and water's edge, ft (m)

Values of α_1 were determined experimentally as follows:

α_1 = 1.0 for loaded conventional inland motor vessels

α_1 = 0.35 for empty conventional motor vessels

α_1 = 0.5 empty European barges

Verhey and Bogaerts (1989) did not provide a value of α_1 for loaded barges stating that the wave heights for this type were negligible. Blaauw et al. (1984) used the same

equation, experimentally determining values of α_1 and α_2 for loaded push-tows of 0.80 and 2.67, respectively. In PIANC (1987) and Boeters, van der Knaap, and Verheij (1995) the coefficients for α_1 and α_2 were 1.0 and 4.0, respectively.

Equation 25 is valid for nonbreaking waves with H_i/h less than approximately 0.6 and vessel Froude numbers less than 0.7 (Verhey and Bogaerts 1989). For vessels in this Froude number range, the angle of wave propagation normal to the bank, β, is given by PIANC (1987), Verhey and Bogaerts (1989), Sorensen (1986), and others as 54.7 deg. The companion angle, θ, between the direction of propagation and the vessel sailing line is 35.3 deg. Figure 2 shows these angles.

From deep water wave theory, Verhey and Bogaerts (1989), Sorensen (1986), and others suggested that the following average wave period, T_i, and wave length, L_{wi}, correspond to H_i.

$$T_i = 2\pi(\cos\theta)\frac{V_s}{g} \tag{26}$$

$$L_{wi} = g\frac{T_i^2}{2\pi} = 2\pi(\cos^2\theta)\frac{V_s^2}{g} \tag{27}$$

As vessel Froude numbers approach 1.0 the transverse wave dominates the diverging waves so that the wave energy is concentrated in a single wave near the stern. As the Froude number increases above approximately 0.7, θ decreases from 35 deg to 0 deg

(Sorensen 1986). This phenomenon is demonstrated when the transversal stern wave moves as a hydraulic jump traveling perpendicular to the bank.

Weggle and Sorensen (1986) studied secondary waves and developed a wave height prediction model as a function of the vessel speed, distance from the sailing line, the water depth, and the vessel displacement. There were two general equations (a) one for vessel Froude numbers less than 0.55 and (b) one for Froude numbers greater than 0.55. The equations required empirical coefficients for each specific hull form.

Based on the same prototype data collected on the Illinois River for determination of an equation for drawdown, Bhowmik, Demissie, and Guo (1982) also developed an empirical formula for predicting the maximum wave height, H_i, of the secondary waves. It is given as

$$\frac{H_i}{d} = 0.133\, F_d \tag{28}$$

The draft Froude number, F_d, is defined as

$$F_d = \frac{V_s}{\sqrt{gd}} \tag{29}$$

The maximum measured wave height was 1.1 ft (0.3 m).

Current Riprap Design Criteria

Numerous equations have been developed that relate velocity, shear stress, or wave height to a stable riprap design. This study regards specifically the design of stone slope protection for tow-induced forces which, as described above, is a complex combination of waves and currents. A detailed literature review follows highlighting the most pertinent formulations, including general wave-based equations, vessel-related equations, and formulations based on shear and/or velocity.

Forces on stone slope

Van Gent (1995) and Kobayashi and Greenwald (1988) both described three basic forces that are applied to the slope under wave attack: the drag force, F_D, acting parallel to the bank in the direction of the velocity; the inertia force, F_I, acting parallel to the bank; and the lift force, F_L, acting normal to the slope. The forces were balanced against the buoyant weight of the stone, W_B. They are defined as

$$F_D = 0.5 \gamma_w C_D k_2 D^2 u^2 \tag{30}$$

$$F_I = \gamma_w C_I k_I D^3 \frac{\partial u}{\partial t} \tag{31}$$

$$F_L = 0.5\,\gamma_w C_L k_2 D^2 u^2 \tag{32}$$

$$W_B = k_1(\gamma_r - \gamma_w)D^3 \tag{33}$$

k_1 = volume shape factor, $\pi/6$ for spheres

k_2 = area shape factor, $\pi/4$ for spheres

C_D = drag coefficient

C_I = inertia coefficient

C_L = lift coefficient

D = diameter of stone, ft (m)

u = directional velocity, fps (mps)

$\frac{\partial u}{\partial t}$ = acceleration

For stability, the sum of the forces parallel, F_P , to the bank over the sum of the forces normal, F_N, to the bank are balanced against the internal friction of the slope, such that

$$\frac{\sum F_P}{\sum F_N} \leq \tan\phi \tag{34}$$

where

ϕ = natural angle of repose

and

$$\sum F_P = F_D + F_I - W_B \sin\alpha \tag{35}$$

$$\sum F_N = W_B \cos\alpha - F_L \tag{36}$$

Figure 6 is a force diagram showing the major force components and angles.

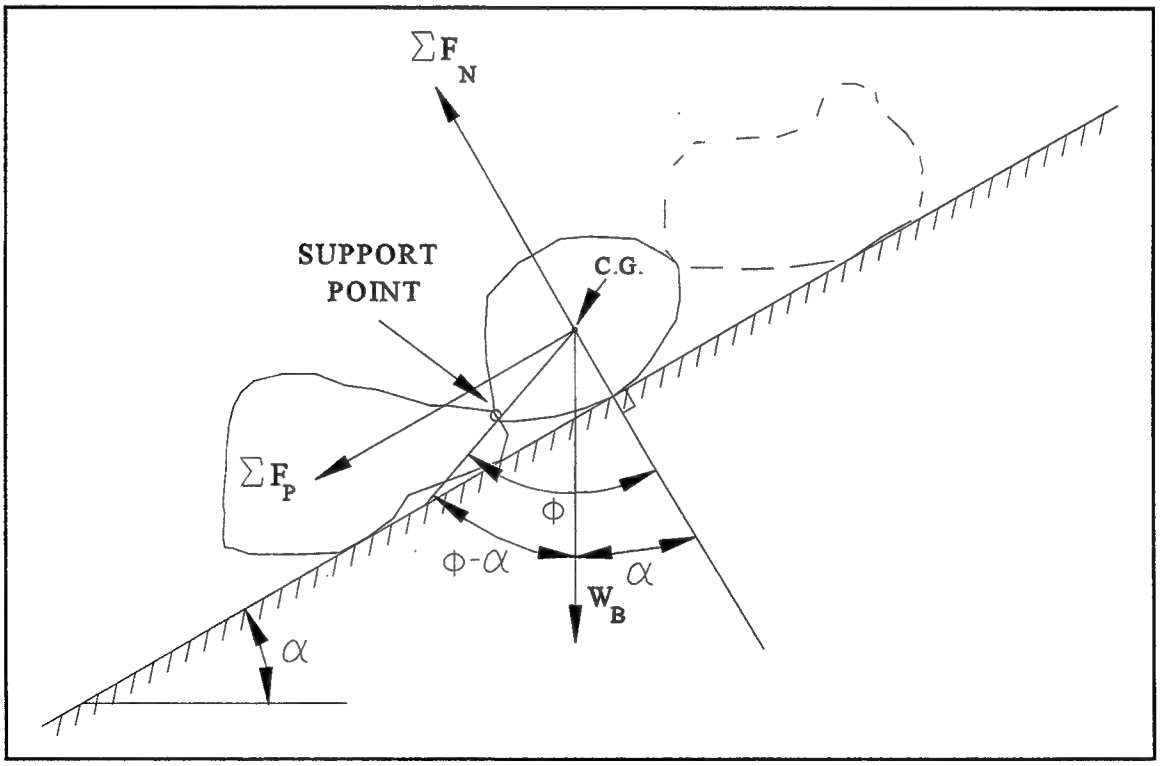

Figure 6. Forces on surface layer of riprap embankment

Kobayashi and Greenwald (1988) evaluated graded stone on an impermeable slope and Van Gent (1995) on a permeable breakwater. Van Gent (1995) described an additional force at the wave front resulting from the pressure gradient related to the free surface slope. This force determines the direction of stone motion.

Iribarren (1948) balanced the drag and lift forces against the internal friction such that

$$\frac{R}{(N - P_1)} \leq \tan\phi \tag{37}$$

where

R = parallel force resisting motion

N = normal force resisting motion

P_1 = normal force lifting stone

The resistant and normal forces, respectively, are

$$R = W_B \sin\alpha \tag{38}$$

$$N = W_B \cos\alpha \tag{39}$$

$$P_1 = k_1 \gamma_w D^2 H \tag{40}$$

where

H = height of attacking wave

k_1 = coefficient

Substituting into Equation 37 yields

$$\frac{W_B \sin\alpha}{W_B \cos\alpha - k_1 \gamma_w D^2 H} \leq \tan\phi \tag{41}$$

Due to the complexity of the acceleration term in the inertia force, Hudson (1957) combined it with the drag force resulting in a total force, F_q. Hudson dismissed the internal friction stating:

> For breakwaters constructed by dumping or placing armor units essentially pell-mell, the forces resisting displacement are the buoyant weight of the individual units and the friction between units. Except for isolated instances where wedging action is involved, friction between armor units can be neglected, and the principal resisting force for pell-mell-constructed cover layers can be assumed to be W_B.

Then for stability of a rubble-mound breakwater subjected to breaking waves Hudson (1957) used,

$$F_q \leq W_B \tag{42}$$

$$F_q = C_q \gamma_w D^2 H \tag{43}$$

where

C_q = total force coefficient

Though Hudson's equation was based on breaking waves, he states,

> The forces that tend to displace armor units from breakwater slopes when the waves do not break, or break only partially, are not the same as those forces that result from breaking waves, nor do they act in the same directions. However, the order of magnitude of the non-breaking wave forces, and the effects of these forces on the stability of rubble-mound breakwaters, should be approximately the same as those caused by breaking waves.

Hedar (1960) added a moment to his force diagram applying the resultant hydrodynamic force, F_T, at some distance from the stone's center of gravity. The angle, β, determined the direction of the force. Hedar distinguished between uprushing waves and downrushing waves in his theoretical development of the forces, such that for uprushing

$$W_B \geq F_T \frac{\cos\beta + \tan\phi \sin\beta + \frac{c \cos\beta}{\cos\phi}}{\tan\phi \cos\alpha + \sin\alpha} \tag{44}$$

The coefficient, c , relates to the distance from the center of gravity the force, F_T , is applied; if c is assumed to be 1, the force is applied to the outer edge of the stone. The total force terms can be replaced with components along the slope and normal to it such that

$$F_P = F_T \cos\beta \tag{45}$$

$$F_N = F_T \sin\beta \tag{46}$$

Substituting these equalities into Equation 44, assuming c = 1, and rearranging terms according to parallel and normal forces, yields

$$\frac{\left(1 + \frac{1}{\cos\phi}\right) F_P - W_B \sin\alpha}{W_B \cos\alpha - F_N} \leq \tan\phi \tag{47}$$

From this formulation, it can be shown that Hedar's equation for uprushing waves is comparable to Equation 34, except that the parallel force component includes a coefficient that is a function of ϕ .

A similar equation for downrushing waves can be formulated from Hedar's work such that

$$\frac{\left(1 + \frac{1}{\cos\phi}\right) F_P + W_B \sin\alpha}{W_B \cos\alpha - F_N} \leq \tan\phi \tag{48}$$

For open channel environments, the critical shear stress for noncohesive sediments was obtained by equating moments of the gravity and drag forces about the support point. Though considered important, the lift force is often neglected and assumed to be accounted for implicitly in the formulation (American Society of Civil Engineers (ASCE) 1977).

The critical shear stress, τ_c, on a sloping bed was given as

$$\tau_c = c_1(\gamma_r - \gamma_w) D \cos\alpha(\tan\phi - \tan\alpha) \tag{49}$$

For a horizontal bed, this becomes

$$\tau_c = c_1(\gamma_r - \gamma_w) D \tan\phi \tag{50}$$

where

c_1 = coefficient

Use of this in a dimensionless shear stress form, plotted against a critical Reynolds value results in the well-known Shields diagram (ASCE 1977).

Wind wave equations

Many riprap sizing methods for protection from waves are based on analytical methods supported by laboratory and field studies in which wave height is related to stone size (Hudson 1957; Iribarren 1948; Ahrens 1989; and others). Van Gent (1995) and Kobayashi and Greenwald (1988) both used numerical approaches to calculate wave forces and slope stability, and compared their results to laboratory scale tests.

Many empirical wave based equations use a dimensionless variable first defined by Hudson (1958) as the stability number, N_s. Depending on the assumptions used by the researcher for a particular application, the stability number can be a function of a number of variables. The stability number is

$$N_s = \frac{H}{\Delta D} \tag{51}$$

The weight of the stone, W_r, is related to the diameter as follows:

$$W_r = k_1 D^3 \gamma_r \tag{52}$$

Where, k_1, defined above as the volume shape factor is $\pi/6$ for spherical stones and 1 for cubic stones. The stability number as a function of W_r is defined as

$$N_s = \frac{\gamma_r^{1/3} H}{\Delta W_r^{1/3}} \tag{53}$$

Iribarren's formula (1948) for incipient motion of stone, including the friction angle and based on the balance of forces in Equation 41, yields

$$W_r = \frac{K \gamma_r \tan\phi^3 H^3}{(\tan\phi \cos \alpha - \sin \alpha)^3 \left(\frac{\gamma_r}{\gamma_w} - 1 \right)^3} \tag{54}$$

Then, the stability coefficient, N_s, for Iribarren's formula is

$$N_s = \frac{\tan\phi \cos\alpha - \sin\alpha}{(K)^{1/3} \tan\phi} \tag{55}$$

According to a graphical representation given in Hudson (1957), values of Iribarren's coefficient K are approximately 0.013 for a 2H:1V slope and 0.030 for a 3H:1V slope. For a tan ϕ of 1, this results in values of N_s of 1.9 and 2.0, respectively.

Hudson felt that the formulation of Iribarren's equation placed too much emphasis on the friction force. This meant that for steeper slopes, small variations in tan ϕ caused

DTIC COULD NOT GET MISSING

PAGE FROM CONTRIBUTOR

35

For a 2H:1V slope, N_s for nonbreaking waves on a rubble-mound breakwater is approximately 1.86 and for a 3H:1V slope, it is 2.13.

Hedar (1960) expanded on Iribarren's and Hudson's work concluding that the stability formula should include more variables. Hedar agreed with Hudson that wave period does not effect stability and for non-breaking waves, depth of water in front of the structure is not significant. From experimental results to obtain empirical coefficients related to the force balances in Equations 47 and 48, the final stability formulas were developed for uprushing and downrushing waves. The stable stone size was determined to be a function of the angle of repose, angle of attack, and the application point of the shear stress. For uprushing breaking waves

$$D = \frac{K_{up}(d_b + H)}{\Delta \frac{\pi}{6} \cdot 32 \left(\log \frac{14.83\,H}{D} \right)^2 (\tan\phi\cos\alpha + \sin\alpha)} \tag{57}$$

Hedar stated for impervious slopes the coefficient, K_{up}, was 18.0 and the depth of the breaking wave, d_b, is assumed to be approximately 1.3 times H. The stability number becomes

$$N_s = \frac{\pi}{6} \cdot 0.89 \left(\log \frac{14.83\,H}{D} \right)^2 (\tan\phi\cos\alpha + \sin\alpha) \tag{58}$$

For downrushing waves at reflection and at breaking

$$N_s = \frac{\frac{\pi}{6} \cdot 32 (\tan\phi \cos\alpha - \sin\alpha)}{K_{down}} \tag{59}$$

The coefficient, K_{down}, was given as a function of ϕ minus α and was graphically presented in Hedar's paper (1960) for both pervious and impervious slopes.

Bhowmik (1976) conducted a field investigation on the stability of existing shore protection on Carlyle and Rend Lakes in Illinois from wind waves. From his review of the literature, Bhowmik's recommended design equation is

$$W_{50} = \frac{K \gamma_r H^3}{\gamma_w^3 (\cos\alpha - \sin\alpha)^3 \Delta^3} \tag{60}$$

where

W_{50} = stone weight which is 50 percent lighter by weight, lb (kg)

K = coefficient

An "average" coefficient was selected as follows:

$$\frac{K}{\gamma_w^2} = 0.388 \tag{61}$$

Reformulating in terms of the stability number, this becomes

$$N_s = 5.438\,(\cos\alpha - \sin\alpha) \tag{62}$$

Ahrens (1989) also presented a formulation relating the stability number to the significant wave height, H_s. To account for instabilities that may result from waves in excess of the significant wave height, a safety factor was employed such that

$$N_s = 1.14\,(\cot\alpha)^{1/6} \tag{63}$$

This resulted in a zero damage stability number of 1.28 for a 2H:1V slope and 1.37 for a 3H:1V slope. Since this formulation resulted in too conservative rock sizes, he ultimately adopted an approach which incorporated a surf parameter (Van der Meer and Pilarczyk 1984).

The Delft Hydraulics Laboratory has published numerous articles and reports regarding the design of bank protection. Van der Meer and Pilarczyk (1984) conducted over 200 model tests on rubble mound slopes under random wave attack to determine the importance of the number of waves, wave period, stone grading, and core permeability. Their tests showed that erosion damage was definitely dependent upon wave period. This result was contrary to other author's results (Hudson 1957; Hedar 1960; and Broderick

and Ahrens 1982). Van der Meer and Pilarzyck (1984) developed the following relationships for N_s that included the surf similarity parameter, ξ, and the damage level, S.

The surf similarity parameter at zero damage, ξ_z, is defined as follows:

$$\xi_z = \frac{\tan\alpha}{\left(\frac{2\pi H_s}{g T_z^2}\right)^{1/2}} \tag{64}$$

T_z is the wave period associated with "no damage," and, according to Ahrens (1989), is generally taken to be when S is between 1 and 3 stones eroded. "Failure" is defined as S between 8 and 17.

Where

$$S = \frac{A}{D_{50}^2} \tag{65}$$

A is the area eroded on the profile in Figure 7. Both permeable and impermeable slopes were tested. Soundings and a profiler were used to determine S.

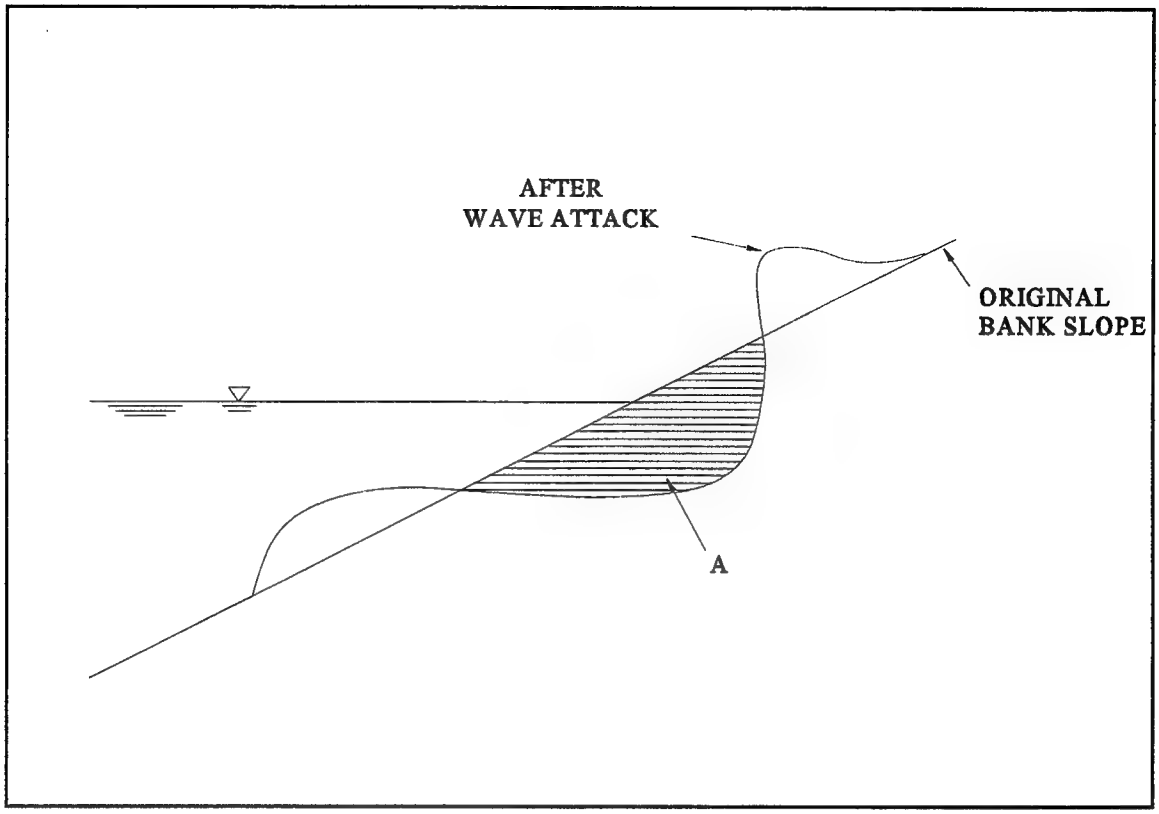

Figure 7. Profile of bankline eroded by wave action

Then the following stability formulae were used for impermeable slopes:

For breaking waves with $\xi_z < 2.5 - 3.5$,

$$N_s = \frac{H_s}{\Delta D_{50}} = 4.4 \left(\frac{S}{\sqrt{N}} \right)^{0.22} \xi_z^{-0.54} \qquad (66)$$

where

N = number of waves

For nonbreaking waves with $\xi_z > 2.5 - 3.5$ and $\cot \alpha \leq 3$

$$N_s = 1.25 \sqrt{\cot \alpha} \left(\frac{S}{\sqrt{N}} \right)^{1/6} \xi_z^{0.1} \tag{67}$$

For nonbreaking waves with $\xi_z > 2.5 - 3.5$ and $\cot \alpha \geq 3$

$$N_s = 1.25 \sqrt{3} \left(\frac{S}{\sqrt{N}} \right)^{1/6} \xi_z^{0.1} \tag{68}$$

In these equations, the stones were assumed to be cubic not spherical. Figure 8 schematically represents the surf similarity parameter for riprap slopes as defined by PIANC (1987).

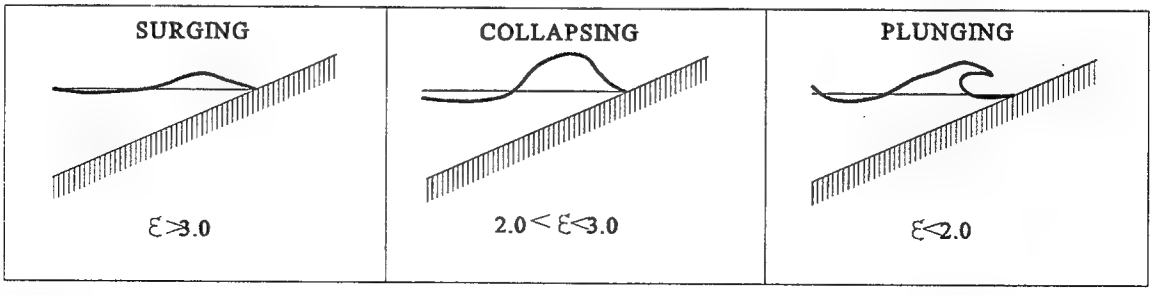

Figure 8. Approximate values of the surf similarity parameter as defined in PIANC (1987)

The stability formula given for wind waves in PIANC (1987) in terms of the dimensionless stability number is

$$\frac{H_s}{\Delta D_{50}} \leq 2.25\,\xi^{-0.5} \tag{69}$$

Vessel equations

Fuehrer, Romisch, and Engelke (1981) conducted extensive tests regarding bank and bottom protection against vessel waves and propeller jets. They determined that return current was only important on the lower portion of the slopes particularly on unprotected banks. For riprap stability in a trapezoidal navigation canal, they recommended protection from the primary wave system, particularly the front wave. For initiation of motion, the stability number is

$$N_s = 3.2\,(\cot\alpha)^{1/3} \tag{70}$$

The authors felt a safety factor was necessary, so recommended

$$N_s = 1.05\,(\cot\alpha)^{1/3} \tag{71}$$

Additionally, the authors found that relative scour was a function of the number of runs (vessels passing the embankment) and after approximately 100 runs, a quasi-steady state condition was reached.

Blaauw et al. (1984) presented a total methodology including formulas for drawdown, secondary waves, and return current, as well as guidance on the design of riprap due to vessel motion. Tests were carried out at prototype and at reduced scales mainly concerning push tows in canals having a bank slope of 4H:1V and for riprap on a granular filter. Details regarding the prototype testing on the Hartel Canal can be found in Pilarczyk (1984). Blaauw et al. (1984) conducted their study specifically to address tow-induced motion and riprap design.

Blaauw et al. (1984) discussed navigation-induced effects in three primary categories of water motion already described. They stated that the upper bank revetment is affected by the secondary waves and transversal stern wave, while the lower slope and channel bottom are affected by the propeller jet and return current. The subsoil is effected by pore pressure variations due to the front wave, drawdown, and secondary waves.

The authors evaluated effects of return current using two approaches. The first, a shear stress approach, stated that the maximum shear stress, τ_m, occurs at maximum return current, u_{rm}, such that

$$\tau_m = \frac{1}{2} C_{fr} \rho u_{rm}2 \qquad (72)$$

where

ρ = density of water, slug/ft^3 (kg/m^3)

The equation for the coefficient of drag, C_{fr}, is given according to the Schlicting formula for rough plates (Schlichting 1979).

$$C_{fr} = \left(2.87 + 1.58 \log \frac{x}{k_s} \right)^{-2.5} \tag{73}$$

where

$$x = \frac{u_r}{u_r + V_s} L_s \tag{74}$$

and

$$k_s = 4 D_{50} \tag{75}$$

The bottom roughness, k_s, is defined as an "average" value using the multiple of four to account for surface irregularities. The velocity, u_r, is the average return current, L_s is the total ship's length and x is the distance a water particle moves due to u_r. According to the authors, the maximum return current occurs at 0.25 to 0.35 of the ship's length from the bow.

Using Shield's criteria for stable rock design and taking advantage of the shear stress formula in Equation 72, Blaauw et al. (1984) uses the flow parameter, ψ, given as

$$\psi = \frac{\tau_m}{\rho g \Delta D_{50}} \cdot \frac{1}{k_d} \tag{76}$$

where

$$k_d = \cos\alpha \sqrt{1 - \frac{\tan^2\alpha}{\tan^2\phi}} \tag{77}$$

Riprap stability criteria for this method was given as

$\psi \leq 0.03$ = no transport of riprap

$\psi \leq 0.06$ = small transport of riprap

$\psi > 0.06$ = transport increases

For their recommended design for return current, the authors used the well-known Isbash equation.

$$D_{50} \geq \frac{u_c^2}{k_1^2 \Delta g} \tag{78}$$

Using the return current near the bank, u_c, if known, the slope was stable for values of k_1 from 1.2 to 1.5.

An equation was given for zero damage (initiation of motion) against the transversal stern wave for a push tow sailing near a bank based on a stability number called the "characteristic stern wave parameter" by Blaauw et al. (1984).

$$N_s = \frac{z_{max}}{\Delta D_{50}} \leq 2.3 \tag{79}$$

This equation is valid for a 4H:1V slope and assumes cubic stones.

Blaauw et al. (1984) found during testing that no material was transported due to secondary waves for the following condition, where the cot $\alpha = 4$ and $\beta = 55$ deg.

$$\frac{H_i}{\Delta D_{50}} \leq 3.0 \tag{80}$$

The use of gradients and slope supply flow was only applied when trying to predict transport of the stones. Blaauw et al. (1984) gave equations for determining the lowest level of transport below the undisturbed water by the stern wave and the secondary waves. In this manner, they recommended a duel riprap cover design protection (upper for waves, lower for return current).

In their study of ship waves and slope protection, Verhey and Bogaerts (1989) examined the validity of the Hudson approach to ship waves. They stated that ship waves, propeller jet, return current, and water level depression attacked the banks. Verhey and Bogaerts distinguished ship waves from secondary waves as the interference peaks of the diverging and transverse waves and should be determined by Equation 25. Adjusting the wave height, H_i, by the waves' angle of incidence normal to the slope, β, model studies indicated that riprap protection was stable for

$$N_s \leq \frac{H_i \cos\beta^{0.5}}{\Delta D_{50}} \leq 1.8 \text{ to } 2.3 \tag{81}$$

However, their recommended equation incorporated the surf similarity parameter, ξ, to account for wave length, such that

$$N_s \leq \frac{H_i \cos\beta^{0.5}}{\Delta D_{50}} \leq \frac{2.25(\cos\alpha + \sin\alpha)}{\xi^{0.5}} \tag{82}$$

Here the surf similarity parameter is given as a function of incidental wave length, L_{wi}, instead of period as in Equation 64.

$$\xi = \frac{\tan\alpha}{\left(\frac{H_i}{L_{wi}}\right)^{0.5}} \tag{83}$$

Furthermore, the relationship is only valid for

$$\xi < (0.05 \cot\alpha)^{-0.5} \tag{84}$$

and was only confirmed for a slope of 4H:1V. The authors stated, "the equation seems too optimistic" for a slope of 3H:1V. Based on a graphical representation for full-scale tests on 2H:1V and 3H:1V slopes, values of N_s (H_i not adjusted by angle of attack) between 1.6 to 2.0 resulted in only a small displacement of stones.

Verhey and Bogaerts (1989) presented both deterministic and probabilistic design criteria. These studies, similar to those conducted by Blaauw et al. (1984) at the Delft Hydraulics Laboratory, presented design methodologies for bank protection based on both approaches. According to the authors,

> In the deterministic approach a dominant design condition is selected. On the basis of this condition the dimensions of the protection and filter layer are determined for the criterion of "initiation of motion" (no or slight displacement of individual stone of a riprap top layer can be accepted.)

Conversely, a probabilistic approach calculates total damage during a time period based on number of stones transported.

A generalized form of Equation 79 was found in PIANC (1987) for the transversal stern wave. That equation is

$$N_s \leq \frac{z_{max}}{\Delta D_{50}} \leq 1.5\,(\cot\alpha)^{1/3} \tag{85}$$

At $\cot\alpha = 4$, $N_s = 2.38$, making it similar to that found above for a 4:1 slope. They stated that the water level depression can be considered a "truncated form of a long period wave." Water level depression causes excess pore water pressure because the soil in the banks cannot respond immediately to the change.

The secondary wave height, H_i, of the interference peaks at the revetment is estimated using Equation 25. The stable riprap size was determined as

$$\frac{H_i}{\Delta D_{50}} \leq 1.8\,(\cos\beta)^{-0.5} \tag{86}$$

Again, the angle of incidence, β, is assumed to be 55 deg.

PIANC (1987) also used the Isbash approach to evaluate return current protection. The equation presented is similar to that given by Blaauw et al. (1984) in Equation 76 but uses different coefficients and the maximum return current, u_{rm},

$$D_{50} \geq \frac{0.7\,u_{rm}^{\,2}}{g\Delta k_d} \tag{87}$$

The coefficient, k_d, is defined by Equation 77 and the angle of repose, ϕ, is assumed to be between 40 and 45 deg. This reference stated, "Current attack will affect the entire

wetted zone of the bank. However, wave attack is more likely to be the dominant effect in the zone near the water line."

Sorensen (1986) recommended using the Hudson equation with a stability coefficient using the incident wave height, H_i, as follows:

$$N_s = 1.37(\cot\alpha)^{1/3} \tag{88}$$

He suggested this approach "until further insight is gained on the impact of a group of vessel waves on a riprap armor layer." He further suggested that layer thickness and gradation designs be obtained from *Engineering Manual* 1110-2-1614 (Headquarters, U.S. Army Corps of Engineers (HQUSACE) 1985).

Other studies

Maynord (1984) conducted a site specific study of the Sacramento ship channel because existing channel protection was experiencing extensive channel maintenance due to the extremely small blockage ratios (typically around 4). The model section tested had a trapezoidal channel with a shallow berm. The study results found that with small increases in vessel speed, otherwise stable rock failed due to large increases in drawdown, which was due to the small blockage ratio.

Prototype gradations of W_{50} of 90 lb and 340 lb (40.8 kg and 154.2 kg) were tested in this model. Failure of the small stone was observed for two blockage ratios, 4.3 and

6.1. Vessel speeds for initiation of motion respectively, were approximately 8 mph and 8.5 mph (12.9 km/h and 13.7 km/h) . The drawdown associated with a 6 ft (1.8 m) depth over the test berm was approximately 2 ft (0.6 m) for these conditions. An increase in channel area of 20 percent only affected the maximum speed by an increase of less than 1 mph (1.6 km/h). The larger gradation was only stable for increases in ship speeds of approximately 1 mph (1.6 km/h).

A physical model study was conducted for the U.S. Army Engineer District, Mobile by WES regarding riprap stability on the Tennessee-Tombigbee Waterway. The main objective of this study was to find optimum tow speeds for existing riprap (Maynord and Oswalt 1986). Two gradations, W_{50} of 27 and 13 lb (12.2 and 5.9 kg), smaller than the existing stone, and W_{50} of 68 lb (30.8 kg), were tested in a 1:20 model study by driving a free-moving vessel past the embankment under various tow speeds, water depths, and sailing lines. A general equation was not developed, but incipient motion data verified that the Hudson equation (Equation 56) would be safe. The conclusion stated that operating tow speeds less than 80 to 90 percent of the limiting speed would be sufficient to prevent failure of the existing stone due to tow waves. However, it was concluded that propeller jets directed toward the stone could easily fail the stone. Observations indicated that incipient motion of the smaller stone did not occur for wave heights less than 2 ft (0.6 m).

In a preliminary evaluation of results to date from data collected for navigation research and from several site-specific studies, including the Tennessee-Tombigbee data, Martin (1992) observed in channels with blockage ratios (generally from 6 to 10) that

stone having a W_{50} of 13 lb (5.9 kg) was stable for tows traveling at speeds of approximately 6 to 8 mph (9.7 to 12.9 km/h). It was also observed that the slope protection on the 3H:1V slope could withstand higher vessel-induced forces than the 2H:1V slope.

Gelencser's (1977) conclusions from studies of the Welland Canal, both prototype and model investigations, stated the following:

a. At vessel speeds of 14 to 15 mph (22.5 to 24.1 km/h), a 730-ft (222.6-m) vessel failed riprap having a maximum diameter of 5 ft (1.5 m).

b. Reducing the speed to 10 mph (16.1 km/h) resulted in riprap protection with practically no damage for stones having a maximum diameter of 30 in. (0.76 m).

c. Bank protection could be accomplished with two stone sizes due to the concentration of erosive forces on the upper slope near the water line.

In the prototype data, blockage ratios for displacement-type vessels ranged from 5.3 to 22, vessel speed (relative to water) from approximately 8.8 to 17 mph (14.2 to 27.4 km/h) with a maximum recorded drawdown of 2.78 ft (0.85 m).

Balanin and Bykov (1965) stated in their introduction, "Selection of rational bank protection is the most complicated problem to be solved under navigable canal conditions..." The philosophy employed in design of navigation canals in the previous USSR balanced costs of bank protection with increasing canal size. They did not give specific criteria for designing riprap protections but stated that riprap protection was a practical and economical solution for navigation canals. Balanin and Bykov also suggested that lower slopes can have lesser protection than upper slopes.

Tenaud (1977) conducted a number of model tests specifically designed to determine riprap protection from tow induced impacts. Tenaud's stone size recommendations were as follows:

a. 2H:1V slope, 66.2 lbs (30 kg) at 24 in. (0.6 m) thickness for the entire slope.

b. 3H:1V slope, 44.1 lbs (20 kg) at 20 in. (0.5 m) thickness for 4.9 ft (1.5 m) of slope.

This "design" was based on a ship with a 3.2-ft (0.98-m) draft navigating near the limit speed of 8.7 mph (14 km/h) in a channel section with a cross-sectional area of 2,152 ft^2 (200 m^2). The ship beam was approximately 37.4 ft (11.4 m), making the blockage ratio approximately 17.

Tenaud differentiated between drawdown and the "attacking wave" saying the attacking waves (secondary waves) can be larger for lighter drafts. He stated, "empty or light laden boats, as well as service boats, travel at high speed, and this contributes the most to bank erosion." According to Tenaud, the attacking wave rather than the water level drop has the greatest erosion effect on the bank.

Bouwmeester et al. (1977) conducted a 1:25-scale model test to observe the behavior of bank protection and measure the primary and secondary waves. They concluded that the transverse stern wave, the transition from the water level depression alongside the ship and the region behind the ship, was likely the cause of rock displacements. Slope supply flow contributed to the transport and the depressed water level caused ground water flow. Stones were displaced no higher (vertically) than 1.6 ft (0.5 m) and no lower than 6.6 ft (2 m) below the still water level. They stated,

> Summarizing, it can be said that the sum total of the water motions described above gives rise to pressure gradients in and above the banks, and erosive currents, which may result in:
> a. loss of stability inside the slope because resistance to sliding is reduced;
> b. loss of stability of individual particles in and near the surface of the bank.

Pilarczyk's (1984) paper supported general conclusions of research conducted by both the Delft and WES. The prototype tests on the Hartel Canal were conducted with gravel on geotextiles and sandy subsoil. Riprap sizes on one embankment were 1.2- to 3.2-in. (30- to 80-mm) gravel and 3.2- to 7.9-in. (80- to 200-mm) gravel on another. The canal had a 246-ft (75- m) bottom width and was approximately 23 ft (7 m) deep. The banks had 4H:1V slopes. By comparison the Tennessee-Tombigbee had a 280-ft (85.4-m) bottom width and was 14 to 22 ft (4.3 to 6.7 m) deep. Boat speeds were not given, but the push tows had 4,500 hp and 5,400 hp. Each barge was 250 ft long by 39 ft wide by 9.8 ft draft (76.5 by 11.8 by 3 m). The configurations were 3 by 2 and 2 by 3. Blockage ratios for these tests were generally less than 10.

The studies concluded, "High gravel transports were only observed when push-tows and tugs sailed at high speeds near the bank." Also, small vessels near the bank appeared to cause a high transport of fine gravel. For riprap 11 to 88 lbs (5 to 40 kg) on geotextile, Pilarcyzk (1984) observed:

> For this class riprap, the beginning of movement was rather exceptional. It has been observed to occur mainly due to secondary waves induced by empty barges and tugs sailing very close to the bank (at the toe of the slope). It can be concluded that in the most practical cases this, or a little higher class of riprap would be satisfactory for the normal inland fairways. In the Netherlands the stone classes used normally for bank protection of channels with high shipping-intensity (incl. push-tow) are of the 10-60 kg and/or 60-300 kg types.

Variability in riprap size resulting from equations

The wide array of form and parameters in the coefficient N_s produces a design rock weight that can vary considerably. Table 1 summarizes typical values of N_s developed for waves. These formulas represent different interpretations of the force balance, stability criteria, assumptions regarding nominal diameter (cubic or spherical stones), design wave height, and waves characteristics such as the surf parameter and angle of attack. Figure 9 shows the relationship between three different wave heights and the nominal stone diameter using the definition of stability number in Equation 51. The specific weight of the stone is $\gamma_r = 165$ lb/ft^3 (2.12 kg/m^3).

The stability coefficients determined from these formulations resulted in highly variable stable rock designs. Even among the formulas developed for vessel waves, the range of N_s is from 1.32 from the Fuehrer, Romisch, and Engelke (1981) formulation to 2.38 in the PIANC (1987) criteria for a 2H:1V slope. Going to Figure 9, the resulting design stone diameter for a 2-ft (0.6-m) wave height can range from approximately 11 to 6 in. (0.3 to 0.15 m). Then resulting stone weights are from 129 to 22 lb (58.5 to 10 kg), respectively. At a wave height of 3 ft (0.9 m), the stone weights vary from 436 to 74 lb (197.7 to 33.6 kg).

The existing stability equations produced a wide variation in stable riprap size, and with the exception of the Tennessee-Tombigbee study (Maynord and Oswalt 1986) and the Hartel Canal study (Pilarczyk 1984), few have been specifically verified at full-scale

Table 1
Values of the Stability Number, N_s, Based on Different Formulations

Source[1]	Equation #	cot α = 2	cot α = 3	cot α = 4
Wind Wave Equations				
Iribarren (1948)	55	1.9	2.0	--
Hudson (1957)	56	1.86	2.13	2.34
Hedar[2] (1960)	59	1.04	1.16	1.34
Bhowmik (1976)	62	2.43	3.44	3.96
Ahrens (1989)	63	1.28	1.37	1.44
Van der Meer and Pilarczyk (1984)	67	1.25	1.53	--
PIANC (1987)	69	1.3	1.3	1.3
Vessel Equations				
Maximum Front Wave				
Fuehrer, Romisch, and Engelke (1981)	71	1.32	1.51	1.67
Transversal Stern Wave				
Blaauw et. al. (1984)	79	--	--	2.3
PIANC (1987)	85	1.89	2.16	2.38
Secondary Waves				
Blaauw et. al. (1984)	80	--	--	3.0
Verhey and Bogaerts (1989)	82	2.3	2.2	2.1
PIANC (1987)	86	2.38	2.38	2.38
Sorensen (1986)	88	1.73	1.98	2.17

[1] To obtain values of N_s the following assumptions were used depending on the formula: $\phi = 45°$; $\beta = 55°$; $\xi = 3$; $N = 1000$; $S = 2$.
[2] K_{down} was obtained for each slope from a graph in Hedar (1960).

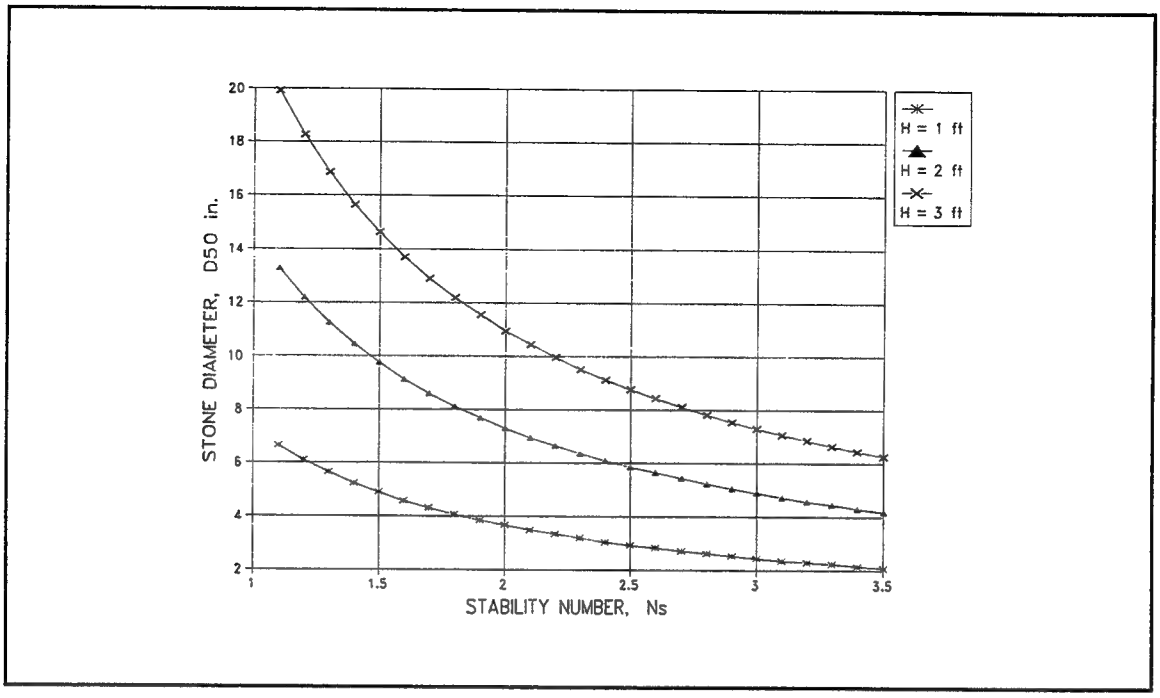

Figure 9. Relationship between N_s and D_{50}

for commercial tow traffic. Determination of a generalized equation would minimize the need for site-specific studies and maximize the safe and economical design of riprap in United States inland navigable waterways.

Scale Effects in Physical Modeling

Physical model scales should be carefully selected to preserve similarity between the model and the prototype. Hydraulic models usually are geometrically similar (have the same length ratios from prototype to model). To ensure dynamic similarity, either the Froude number or the Reynolds number must be the same in model and prototype. The Froude number approach accurately scales gravitational effects and the Reynolds number

accounts for viscous effects. Since no fluid exists to satisfy both criteria simultaneously, Froude criteria is generally used and often an empirical adjustment is made to the forces affected by viscosity (Sharp 1981). A model scale is selected such that Reynolds numbers are sufficiently high to minimize these effects (Yalin 1989).

In the study of ship dynamics, wave dynamics, stone slope protection, and navigation effects, researchers have employed many different physical model scales. The selection of scale is based on a combination of Reynolds numbers and on experience. When scale effects can affect the measured outcome of the parameter of interest, the method for compensation of the effects is a function of the researcher and the techniques used by the researcher's laboratory.

Model scale and Reynolds values

Vessel models. Ship modeling presents some scaling challenges related to boundary conditions. As a vessel moves through the water, it develops a boundary layer on the bottom of the channel and the bottom of the vessel (Gates and Herbich 1977). Because the boundary layer is a function of Reynolds number and viscosity, this value can be different in the model and prototype. The boundary layer problem is compounded in the model due to low Reynolds numbers which causes a greater influence due to displacement thickness than actually occurs in the prototype. In other words, the smaller the model scale, the greater the viscous forces and the displacement thickness; consequently, the effective size of the tow is larger than reality. The shape of the lead barges can cause flow separation both in the horizontal and vertical planes. In the vertical

plane this further complicates the issue of boundary layer development beneath the tow and influences its effective draft. In the horizontal plane, this separation pushes the flow field away from the sides of the barges, effectively increasing its width. This violates the assumptions in the theoretical approach presented by Jansen and Schijf (1953).

Sorensen (1966) found that viscous effects can cause damping of very short waves. He conducted a series of scale effect tests to determine the circumstances affected by viscous damping for ship studies in deep water. He concluded that some scale effects were present at low Froude numbers (less than 0.5) and with vessel speeds of less than 1.8 fps (0.5 mps). He recommended avoiding the smallest model tested.

In the computation of drag coefficients in towing tank tests, Sharp (1981) recommends using velocities based on Froudian criteria and adjusting the drag forces by an empirical calculation of the viscous forces. He further stated the model scale can be increased to make the differences between prototype and model negligible.

At WES, model scales from as large as 1:10 to as small as 1:120 have been used to evaluate navigation effects. The tests at 1:70 and smaller were influenced by the scale effects and the studies provided qualitative results at best. A 1:37.5 scale model has been used on several occasions due to lack of adequate space to evaluate return currents in large river sections, but it was recognized that the absolute magnitude of the answers require adjustment. Maynord (1984) has also modeled ships and tows at 1:10, 1:20, and 1:30.

The boundary layer and separation problems can cause the effective size of the vessel to change in the model. In a study conducted at a 1:37.5 scale by WES for the

U.S. Army Engineer District, Louisville, a comparison was made between model data and prototype data. It was found that for the channel modeled, the effective draft of the tow was actually on the order of 10.8 ft not 9 ft (3.3 m not 2.74 m). Also in a recent 1:25-scale model study for the Upper Mississippi River System where model values were compared to actual field data, the model draft was lightened from a prototype draft of 9 ft (2.74 m) to approximately 7.5 ft (2.29 m) to reproduce field data (Maynord and Martin 1996).

Based on Reynolds numbers related to vessel length, the rudder, and the propeller, Novak and Cabelka (1981) recommended that self-propelled vessels be reduced at most to a 1:15 scale. Bouwmeester et al. (1977) conducted their experiments with a free moving vessel at a 1:25 scale. Verhey (1983) conducted studies primarily regarding effects of propeller jets on channel bottom and banks and assumed scale effects were insignificant at a 1:25 scale.

Koster (1975) did a scale effects study using 1:10.5, 1:25, and 1:40; ultimately recommending the use of a 1:25-scale model. In his tests, the scale effects to the rudder action and drift angle seemed to counteract each other, making it difficult to isolate and compare them to prototype values.

Scale effects due to frictional resistance are sometimes compensated by increasing the propeller speed. At the Netherlands Ship Model Basin, a 10 percent increase in propeller speed was used over the Froude scaling criteria (Kooman 1973). These studies were conducted at a 1:25 scale. Instead of adjusting propeller speed, tests conducted at WES to evaluate propeller effects are related to the pushing force, or bollard push. Force

measurements were made on the model tow at various propeller speeds and scaled to prototype values according to Froude criteria (Toutant 1982).

Riprap and wave models. Hudson (1975) suggested the model Reynolds number, R_D, be greater than 3×10^4 for conducting riprap stability tests under wave activity. Reynolds is defined in terms of the model wave height, H, and stone size, according to

$$R_D = \frac{\sqrt{g\,H}\,(W_r/\gamma_r)^{1/3}}{\nu} \tag{89}$$

where

ν = kinematic viscosity of water, ft^2/s (m^2/s)

Parameters in Hudson's (1957) small-scale tests to evaluate non-breaking waves on pervious breakwaters that resulted in Equation 56 were as follows: wave heights from 0.28 to 0.69 ft (0.09 to 0.21 m) with periods of 0.88 to 2.65 sec; water depth from 1.26 to 2.00 ft (0.38 to 0.6 m); quarry stone sizes from 0.09 to 0.31 lb (0.04 to 0.14 kg); and seven breakwater slopes from cot α of 1.25 to 5.

O'Loughlin et al. (1970) discussed scale effects on rock due to jets. They stated that scour rate is "practically independent of Reynolds number at values above 2.5×10^3..." The authors define the particle Reynolds number, R_D, as:

$$R_D = \frac{VD}{\nu} \tag{90}$$

where

V = jet efflux velocity, fps (mp/s)

D = particle diameter, ft (m)

In their experiments, data corresponding to small beads (3 mm) fell out of sync with data from larger diameter beads (6 mm to 15 mm) indicating a scale effects problem. Verhey (1983) in his studies of the effects of propeller jets on the channel bottom and banks, also recommends using the particle Reynolds number and that the model have values greater than 3,000.

Hedar (1960) conducted his experiments in a wave tank at a water depth of 1.8 ft (0.5 m) with crushed stone on an impermeable sheet of plywood. Bank slopes varied from 1.125H:1V to 4.5H:1V. The median diameter of the stone was 1.87 in. (47.5 mm). Wave period was 2 sec and wave heights were from 0.25 to 0.75 ft (80 to 230 mm). The scale was 1:10 and 1:20. There was no discussion of scale effects or Reynolds criteria.

Dai and Kamel (1969) performed tests to evaluate the stability of rough quarry stone from nonbreaking waves on a pervious rubblemound breakwater. Two small rock sizes were tested and compared to a prototype size stone. According to them, the friction force is directly proportional to the product of the coefficient of friction and the weight of the armor unit. They found appreciable scale effects in tests conducted at the smallest scale.

Dai and Kamel attribute these effects to the relatively high value of the drag coefficient for the small model versus the large model. The higher the coefficient the less stable the cover layers. Viscous forces were predominant and the drag coefficient decreased with increasing values of the Reynolds number until it reached a critical value of 3×10^4. The Reynolds number was given as

$$R_D = \frac{V_R D}{\nu} \tag{91}$$

where

V_R = value of water particle velocity parallel to breakwater side slope at a distance R equal D/2.

The smallest stone had a weight of 0.048 lb (0.02 kg) with a diameter of 0.20 in. (5 mm). Water velocities in the wave near the breakwater slope, V_R, were from 1.58 to 2.8 fps (0.48 to 0.85 mps) and zero damage wave heights were 0.14 to 0.22 ft (0.04 to 0.07 m). The next size rock had a weight of 0.38 lb (0.17 kg) and a diameter of 0.57 in. (14.5 mm). Zero damage wave heights were from 0.35 to 0.44 ft (0.11 to 0.13 m) and velocities were from 2.6 to 3.0 fps (0.8 to 0.9 mps).

Madsen and White (1975) conducted tests for reflection coefficients on rough impermeable slopes. The theoretical assumptions are (a) relatively long, normally incident waves (linear long wave theory) and (b) energy dissipation on a rough impermeable slope is a function of bottom frictional effects. Their experiments were

considered valid for fully rough turbulent flow as defined by the following wave Reynolds number, R_e, relationship developed by Jonsson (1966):

$$R_e = \frac{|A|^2 \omega}{\nu \tan^2 \alpha} > 10^4 \qquad (92)$$

where

A = representative wave amplitude or the runup

ω = radian frequency ($2\pi/T$)

The conditions tested by Madsen and White (1975) on an impermeable slope were: wave periods of 2, 1.8, and 1.6 sec; a water depth of 1 ft (0.3 m); d_{50} of 0.5 in. (12.7 mm), 1.0 in. (25.4 mm), 1.5 in. (38.1 mm), and 2.0 in. (50.8 mm); and wave heights varied from 0.05 to 0.17 ft (0.02 to 0.05 m).

Broderick conducted small-scale tests in the laboratory and compared them to large wave tank tests conducted by Ahrens, essentially representing full-scale field conditions (Broderick and Ahrens 1982). Failure of stone was defined as "the riprap being shifted enough to expose part of the filter layer which was removed by the wave action." The authors measured volume of erosion by profiling the slope between tests.

Broderick and Ahrens (1982) also found evidence that at higher Reynolds values, scale effects diminished. They calculated Reynolds values using two different equations. The first was a variation of Equation 92 used by Madsen and White (1975). Fully

turbulent flow was defined by R_E as a function of wave period, zero-damage runup, and slope angle such that

$$R_E = \frac{R_z\left(1 + \cot^2\alpha\right)\left(\frac{2\pi}{T}\right)}{\nu} \tag{93}$$

where

R_z = the wave runup associated with the zero-damage wave height, ft (m)

T = the wave period, sec

α = the slope angle

The critical values of R_E were defined by a graph, where R_E was given as a function of a roughness term. According to this criteria, the authors stated that both small-scale and prototype tests were in the rough turbulent flow regime.

A Reynolds number, R_N was also computed using Equation 89, but replacing H with the zero damage wave height, H_z, and W_r with W_{50}.

$$R_N = \frac{(gH_z)^{1/2}\left(\frac{W_{50}}{\gamma_r}\right)^{1/3}}{\nu} \tag{94}$$

According to a figure given in their paper, scale effects were less evident at an R_N greater than 10^5. The authors evaluated results from other sources and found that where low values of R_N were observed, N_s was as much as 40 percent lower than prototype values. Whereas, in the tests Broderick conducted, the stability numbers of the small scale tests were observed to be only about 20 percent lower than full-scale values.

Broderick conducted her studies at a 1:10 scale. The median weight of the model riprap was 0.075 lb (0.03 kg) on a bank slope of 3.5H:1V. The cover layer had a specific gravity of 2.71 and was laid on a granular filter on top of a compacted sand core. The still water depth in the flume was 1.5 ft (0.46 m), and the wave heights varied from 2 to 3 in. (50.8 to 76.2 mm). Number of waves varied from 340 for long period waves to 1,050 for short period waves. Wave periods in the model were from about 0.9 to 3.6 sec.

In conclusion this reference stated, "Tests at 1:10 Froude scale yield zero-damage stability numbers about 20 percent lower than prototype tests... Scale effects were less severe at high levels of damage than at zero-damage level." Since both small-scale and large-scale tests were considered to be in the rough turbulent regime, the 20 percent difference is still unexplained! Other conclusions are as follows: runup at zero damage is 20 percent higher in the small scale tests; damage profiles are the same in model and prototype; and wave period had little influence in the small-scale tests.

Van der Meer and Pilarczyk (1984) used broken stone with the following characteristics: W_{50} = 0.27 lb (0.12 kg); D_{50} =1.42 in. (36.1 mm); layer thickness = 3.15 in. (80 mm); and filter layer thickness = 0.79 in. (20.1 mm). The slope was constructed of mortar when an impermeable core was being tested. A total of 3,000

waves ranging from a height of 0.16 to 0.85 ft (0.05 to 0.26 m), periods of 1.3 to 3.2 sec, a water depth of 2.62 ft (0.8 m), and slope angles from cot α of 2 to 6 were tested. Scale effects were not mentioned.

Breakwater studies have been conducted at variable scales as well. Jensen (1989) suggested that typical breakwater studies are conducted at a 1:30 scale. To maintain similarity in the cover layer and the core, the core of the structure should be built of larger stones than required by geometric similitude. Jensen (1989) recommended a lower value of the critical particle Reynolds number (6,000 to 7,000) for the cover layer than Dai and Kamel (1969). Jensen calculated the Reynolds number using Equation 90 and found a high degree of variability in the minimum or critical Reynolds criteria.

Oumeraci (1984) reevaluated test results conducted by Hudson (1957), Broderick and Ahrens (1982), Dai and Kamel (1969), and others to determine the critical Reynolds values to minimize scale effects. Oumeraci found a wide variation in reported critical values of Reynolds with Dai and Kamel's representation at a value of 3×10^4 being the most reasonable. He plotted the stability number against the Reynolds value and suggested a method for adjusting the stability numbers in the model if the scale was not sufficient to meet the Reynolds criteria. Oumeraci also recommended a minimum wave height in the model of 0.33 to 0.49 ft (0.1 to 0.15 m) and unit weights of stone of 0.22 to 0.33 lb (0.1 to 0.15 kg). Like Jensen, Oumeraci recommended that core materials be geometrically larger in the model to minimize pressures inside the structure.

Koyabashi and Greenwald (1988) conducted wave tests in a flume on an impermeable 3H:1V slope for calibrating a numerical model. Using one gradation of model gravel

with a median diameter of 0.83 in. (21 mm), they measured values of the specific weight, friction angle, and volume coefficient of stone for input to their numerical model equations. Results were not compared to another larger model gradation or to the prototype. Experimental error on the order of 10 percent was discussed, but error due to scale effects was not.

Riprap and vessel models. In studies where both navigation effects and riprap stability were tested, there have also been several size scales used. Tenaud (1977) used a scale of 1:20 in a flume 262.5 ft (80 m) long. Blockage ratios varied from 5.6 to 33.7. Model barges were 10.25 ft (3.1 m) long by 1.87 ft (0.6 m) wide and drafted from 0.08 to 0.49 ft (0.02 to 0.15 m). Model grains sizes ranged from 0.16 to 0.87 in. (4 to 22 mm) for riprap and 0.2 to 2 mm sand. Slope angles included 3H:1V and 2H:1V. Scale effects were not discussed for this model but were determined to be significant for a 1:50-scale model.

Gelencser (1977) conducted tests at a 1:60 and 1:80 scale to determine drawdown in a restricted ship canal. The blockage ratio for these studies was 5 to 7. The maximum prototype vessel speed of 14 to 15 mph (22.5 to 24.1 km/h) was assumed to be the limiting speed due to the vessel touching the bottom. Bank slopes were 2.75H:1V and 2.25H:1V. No details were given regarding the materials used in the bank stability studies.

Fuehrer, Romisch, and Engelke (1981) conducted extensive tests regarding bank and bottom protection against vessel waves and propeller jets. These tests were conducted at low Reynolds numbers and with small grain sizes. Their scale model testing found that

the limiting stability coefficient was a function of the Reynolds number, R_D. They defined the Reynolds number as a function of the front wave height (Equation 15) by

$$R_D = \frac{D_{50}\sqrt{g h_f}}{\nu} \tag{95}$$

Fuehrer, Romisch, and Engelke plotted the stability number versus Reynolds number and concluded that N_s at initiation of motion was constant above a value of 1,000. They described the Shield's type graph stating,

> The coefficients of the limiting stability, determined for the different grain sizes and loading situations of the canal slopes by the ship in the case of normal navigation can be fitted by a reference curve, of which the functional course corresponds to the Shield limiting tractive force relationship for the beginning of bedload movement in flows.

Fuehrer, Romisch, and Engelke (1981) used a 1:60-scale model with model grain sizes from 0.019 to 0.106 in. (0.48 to 2.7 mm). Water depths were from 0.69 to 1.08 ft (0.21 to 0.33 m) with draft to depth ratios from 1.45 to 1.98. Blockage ratios were from approximately 22 to 28 on 3H:1V slopes.

Maynord and Oswalt (1986) used a 1:20-scale model for the riprap stability studies on the Tennessee-Tombigbee Waterway. Blockage ratios varied from 4.6 to 16.4 in a model trapezoidal channel with a 2H:1V side slope. Median diameter stone sizes tested ranged from 0.32 to 0.56 in. (8.1 to 14.2 mm). Water depths varied from 0.7 to 1.1 ft (0.21 to

0.34 m). A free-moving model tow and barges at two drafts and several configurations were used during testing. Model Reynolds values were computed to be on the order of 10^4 and determined to be in the fully rough turbulent regimen according to the criteria by Madsen and White.

Angle of Repose

In the literature discussions of scale effects, little information is given regarding how the natural angle of repose affects model test results. While the angle of repose is built into all the stability equations presented in this paper, except the Hudson formula, this value is generally assumed to be constant over the range of stone materials tested in the model and/or used in the prototype. The natural angle of repose is most likely not a constant over the range of sizes tested in both model and prototype; therefore, a potential source of error exists in scaling up results.

Ulrich (1987) contended that there are two different angles of repose, one for resistance to sliding and one for resistance to wrenching. The resistance to sliding is met if the ratio of parallel forces to normal forces is less than the tangent of the support layer's angle of friction, as presented in Equation 34. Ulrich slightly modified the balance of forces assuming, for downslope, the hydrostatic pressure is normal to the slope. The resulting modified coefficient for "steady, uniform, fully-turbulent, downslope flow in the absence of seepage and wave forces," is

$$K = \cos\alpha \left(1 - \frac{\gamma_r}{\gamma_r - \gamma_w} \frac{\tan\alpha}{\tan\phi} \right) \tag{96}$$

He also stated that the material's natural angle of repose, based on dumping the stone, was not the appropriate angle for the angle of friction. Ulrich recommended a method for determining the value by raising a layer of materials on a tilting surface and observing motion. From Ulrich's experiments, he suggested using a constant bearing angle of 75 deg making the effects of this angle negligible in the force equations. However, this value was determined experimentally over a very short length of slope, L , (two stone diameters), even though he determined that the angle decreases as the L/D_{50} increases.

Using a similar experimental procedure as Ulrich, Maynord (1988) determined the angle of repose was 53 deg. He concluded that the angle of repose was not always equal to the material's bulk angle of repose and that the angle was affected by the height of the revetment, thickness, and placement. As L/D_{50} increases, the angle decreases. Maynord deals with the variability of the angle empirically as Hudson did in his experiments.

Hudson (1957) abandoned correlations using the angle of repose in his stability formula due to the wide variation of experimental results when attempting to measure this value. From Hudson's tests to determine the friction coefficient, defined as $\tan\phi$, and from tabular data in his report, the average value of the friction coefficient of stone

dumped in water and stone stacked in water for 0.1, 0.3, and 0.62 lb (0.05, 0.14, and 0.28 kg) quarry stone was 1.06, 1.09, and 1.20, respectively.

Froelich and Ogden (1994) concluded from field studies of dumped stone, that angle of repose was more correlated to angularity and gradation rather than median stone size. They qualify their conclusion with the following: "A discernible relation between ϕ_R and D_{50} is not apparent... However, more data with a larger range of particle sizes might be needed to detect such a trend."

Based on other researcher's testing, however, there is clearly an increase in the angle of repose with increasing grain size, and even in Hudson's testing, the average experimental values increased with rock size. In data provided by Froehlich and Ogden (1994), the measured value of angle of repose for small stones in the less-than-50-mm range varied from approximately 35.5 to 40 deg.

Several references were consulted to determine the angle of repose values for different stone sizes as compared to Hudson's tests. Figure 10 shows a composite of this research. Data for this graph were taken from Chow (1959), ASCE (1977), Henderson (1966), Hedar (1960), and Maynord (1988). In Chow (1959), points were obtained from a graph developed from Bureau of Reclamation data for very angular stones. Values by White and Chepil for sand were obtained from the ASCE manual. The value from Hedar for ϕ, obtained experimentally, was 48 deg. Since the reference does not clearly state the stone size he used for the tests, an average stone diameter was assumed based on the

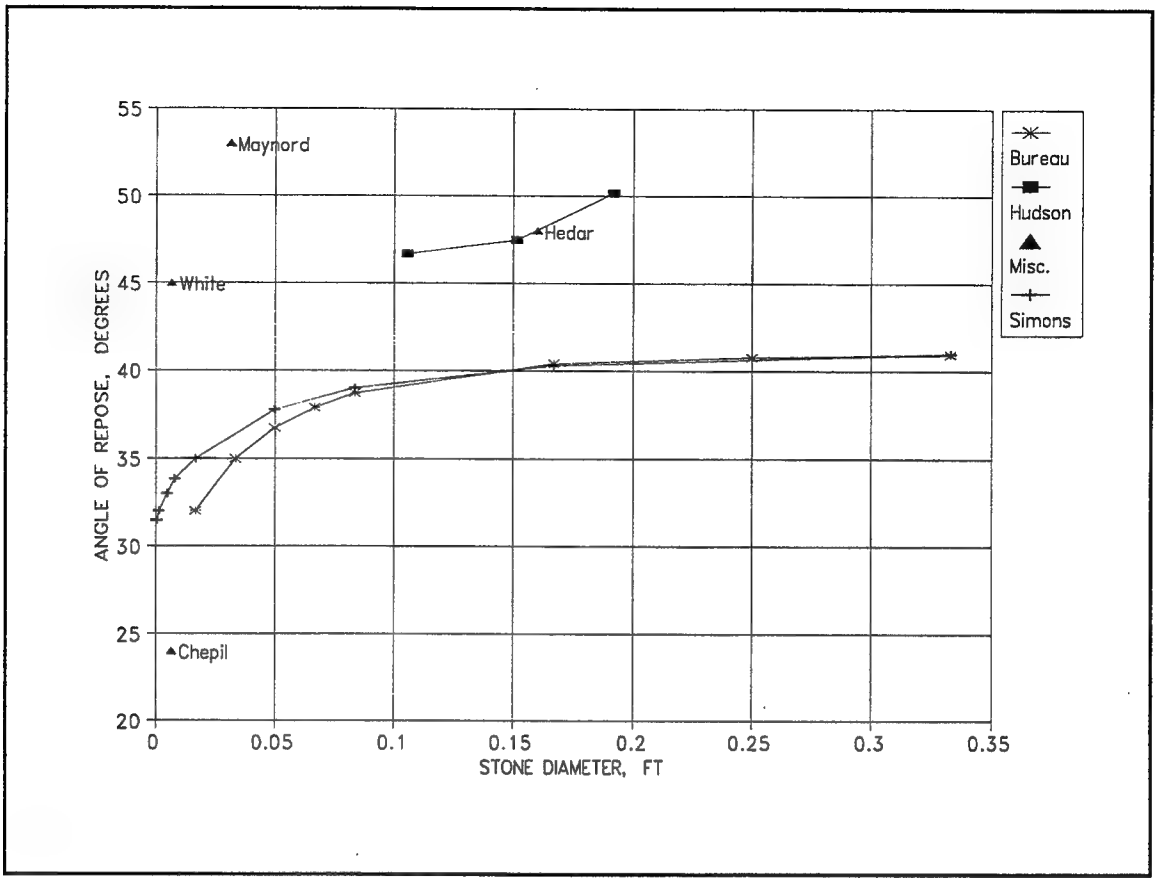

Figure 10. Comparison of angle of repose from various sources

range of model stones he tested (125 to 175 grams). The data labeled "Simons" came from a graph in Henderson's *Open Channel Hydraulics* (1966) and was after research by Simons and Albertson.

In the curves developed by the Bureau of Reclamation and Simons, it can be seen that at diameters greater than approximately 0.15 ft (0.05 m) the angle of repose has an almost constant value. Certainly all prototype stones would fall in this range on the graph and some model stone. However, for small diameter stones, particularly less than approximately 0.1 ft (30.5 mm), the angle of repose has a very nonlinear relationship to diameter.

Iribarren's original formula for the weight of armor units in rubblemound breakwaters that retained the coefficient of friction as a variable was given in Equation 54. If we let k_ϕ represent terms related to the internal friction, such that

$$k_\phi = \frac{(\tan\phi)}{(\tan\phi\cos\alpha - \sin\alpha)} \tag{97}$$

then, stone weight is a function of k_ϕ cubed, and stone diameter, D, is directly related to k_ϕ as

$$D = K^{1/3}\frac{k_\phi H}{\Delta} \tag{98}$$

Using Hudson's experimental values for ϕ, Iribarren's formulation of k_ϕ is calculated in Table 2.

Table 2
Calculation of k_ϕ Using Hudson's Experimental Data

W_r, lb	ϕ	tan ϕ	α	tan α	k_ϕ
0.10	46.7	1.06	26.6	2	2.12
0.30	47.5	1.09	26.6	2	2.07
0.62	50.2	1.20	26.6	2	1.92
0.10	46.7	1.06	18.4	3	1.58
0.30	47.5	1.09	18.4	3	1.52
0.62	50.2	1.20	18.4	3	1.46
0.10	46.7	1.06	14.0	4	1.35
0.30	47.5	1.09	14.0	4	1.34
0.62	50.2	1.20	14.0	4	1.30

Since the stable diameter, D , is a direct function of k_ϕ, it can be seen that for smaller angles of repose, k_ϕ increases; therefore, a larger stone size is required. As the angle of repose approaches the slope angle, k_ϕ is more influenced by the angle of repose. According to Equations 55 and 98, N_s is inversely proportional to k_ϕ, so as k_ϕ increases, N_s decreases.

Another example using the shear stress approach, Equation 76 and 77, requires the factor, k_d, that is also dependent upon the angle of repose, ϕ. The relationship is such that as ϕ gets smaller so does k_d. Furthermore, the required stable stone size is inversely proportional to k_d resulting in larger stone sizes for smaller coefficients.

Ignoring variations in the angle of repose could account for more observed failures in the model at small stone sizes than previously observed in the prototype for equivalent riprap sizes. In several papers where small model stones were used in testing, the amount of stone movement and degree of failure were in disagreement with observations for equivalent larger stone. Recall in Broderick and Ahrens (1982) that even though the flow regime for the smaller stone was considered to be fully turbulent, stability numbers for the small stone were as much as 20 percent lower than the equivalent prototype values. They had no explanation for this difference.

Van Gent (1995) used small-scale modeling to calibrate a numerical approach for predicting geomorphic reshaping of permeable breakwaters due to wave action. He first adjusted the lift coefficient in his numerical model to match results of physical model tests using a small diameter stone, 0.43 in. (10.9 mm), then attempted to use the same coefficients to predict the geomorphic response with a larger material, 1 in. (25.4 mm).

The lifting process appeared to be underestimated, meaning the lift coefficient, c_L, is larger for larger stones. To maintain a balance between the lift forces and the internal friction, c_L would have to go up if $\tan \phi$ went up. Dai and Kamel (1969) observed similar discrepancies with the smallest stones they tested and concluded that the drag coefficient, c_D must be higher with the smaller stones. Again, to maintain a balance between internal friction and drag, c_D would have to increase as the $\tan \phi$ decreased. In these examples, the resulting observations could as easily be explained by inaccurate representation of the friction angle, that is assuming a constant value, as errors in the drag or lift coefficients.

The absolute value of the angle of repose is questionable and determined by many means, but assuming that for small experimental stones a factor could exist regarding this effect, an effort has been made to quantify such. Clearly many scaling problems are directly attributed to the Reynolds number, while some are a function of the angle of repose.

3 Methodology-Physical Model Tests

Physical model approaches are often used in navigation effects studies due to the highly 3-D effects near the vessel, the complexity of the phenomena, and the lack of verified numerical solutions. Physical modeling cannot answer all questions regarding the forces, nor can it address the manner in which nature couples these forces, but it is a viable means of systematically evaluating them. Simple analytical approaches based largely on empiricism are slowly evolving into more complex and intricate solutions as modeling capabilities regarding instrumentation are improved and as the need increases to define more precisely the interaction of these forces with the surrounding environment.

Similitude

Ideally Reynolds values would dictate model size, but often available space and cost govern the selection. Testing conducted for this study varied from a 1:37.5 to 1:20 model scale based on (a) the literature review, (b) results of previous navigation effects studies, and (c) the size of the available flume. This study used previous riprap stability data collected for the Tennessee-Tombigbee study at a 1:20 scale. Additional stability data were collected at a 1:25 scale. Hydrodynamic data were collected and analyzed from three different model scales: 1:37.5, 1:25, and 1:20.

The equations of hydraulic similitude for Froude number scaling are provided in Table 3.

Table 3
Similitude Relationships

Characteristic	Dimension	Scale Relations Model : Prototype		
Length	$L_r=L$	1:20	1:25	1:37.5
Area	$A_r=L_r^2$	1:400	1:625	1:1,406.3
Velocity	$V_r=L_r^{1/2}$	1:4.472	1:5.000	1:6.124
Time	$T_r=L_r^{1/2}$	1:4.472	1:5.000	1:6.124
Discharge	$Q_r=L_r^{5/2}$	1:1,788.9	1:3,125.0	1:8,611.5
Weight	$W_r=L_r^3$	1:8,000	1:15,625	1:52,734
Roughness Coefficient	$N_r=L_r^{1/6}$	1:1.648	1:1.710	1:1.830

Physical Model Tests

Riprap stability tests

Data regarding riprap stability came from four physical model studies conducted at WES, the Tennessee-Tombigbee Waterway (Maynord and Oswalt 1986), the Gallipolis Lock approach study for the U.S. Army Engineer District, Huntington, and two separate data sets from research sponsored by the Headquarters U.S. Army Corps of Engineers, Washington, DC, in 1990 and 1993. The primary objective of these tests was to identify

the most severe operational conditions in which a specific gradation of riprap remained stable. Secondarily, a relationship was sought to link these operations (sailing speed and blockage ratio) to their effects (the return current and/or waves).

The testing program covered a range of conditions. Underway test conditions represented normal navigation operations and assessed the stability of stone slope protection in a confined channel for tows traveling at various speeds, drafts, and distances from the bank. All tests were conducted under quiescent pool conditions; therefore all flow disturbances were those created by the movement of the tow. A summary of details regarding the Tennessee-Tombigbee, Gallipolis, and the 1990 data set are found in Martin (1992).

In general, various combinations of the following prototype conditions were tested as follows:

a. Depth of pool: 14 to 22 ft (4.3 to 6.7 m).

b. Sailing line (distance from tow C/L to toe of slope): 52.5 to 300 ft (16.0 to 91.4 m).

c. Speed of tow: 5 to 15 fps (1.5 to 4.6 mps).

d. Configuration of barges: 2- and 3-barge widths, 1- to 5-barge lengths.

e. Lead barges: raked and square.

f. Bank slopes: 2H:1V, 3H:1V.

g. Equivalent spherical diameter of stone for which 50 percent is lighter by weight, D_{50} : 3.25 to 13 in. (1.3 to 5.1 cm).

h. Weight of stone for which 50 percent is lighter by weight, W_{50}: 1.7 to 111 lb (0.8 to 50.3 kg)..

The cross sections in each test series and other pertinent geometric data in prototype dimensions are shown in Figures 11-14 for the Tennessee-Tombigbee, the Gallipolis, and two sets of navigation research studies, respectively. The data sets are identified as: NR93 for navigation research conducted in fiscal year 1993; NR90 for navigation

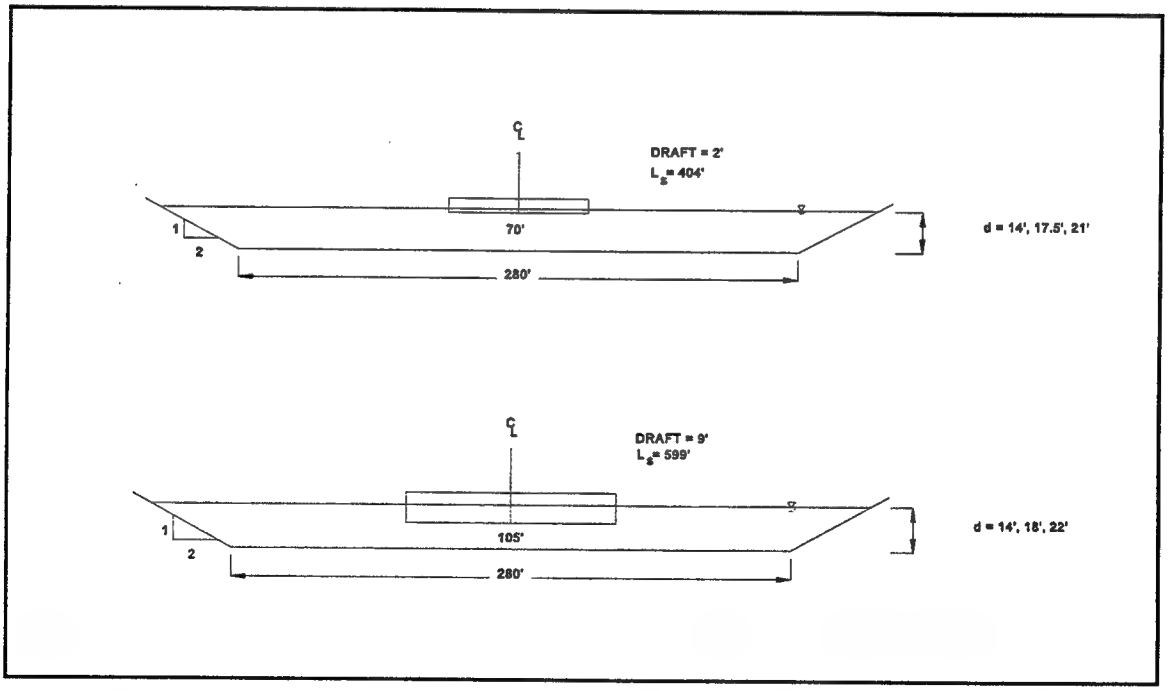

Figure 11. Pertinent cross-section and test data, Tennessee-Tombigbee study

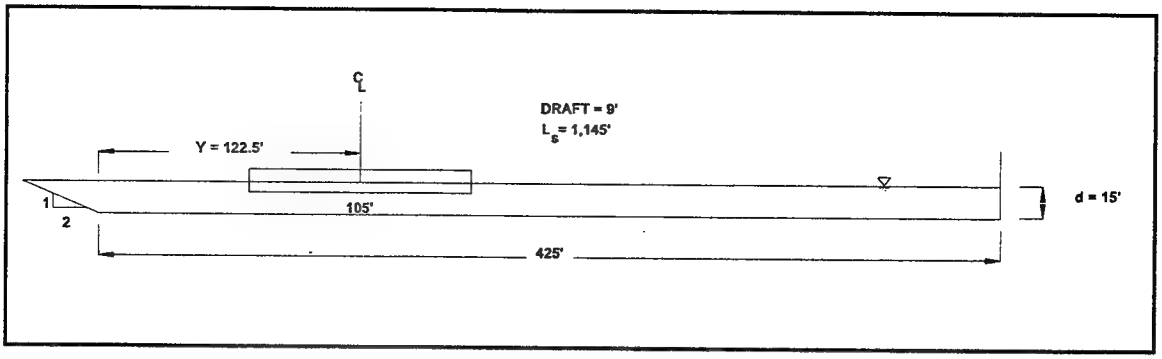

Figure 12. Pertinent cross-section and test data, Gallipolis study

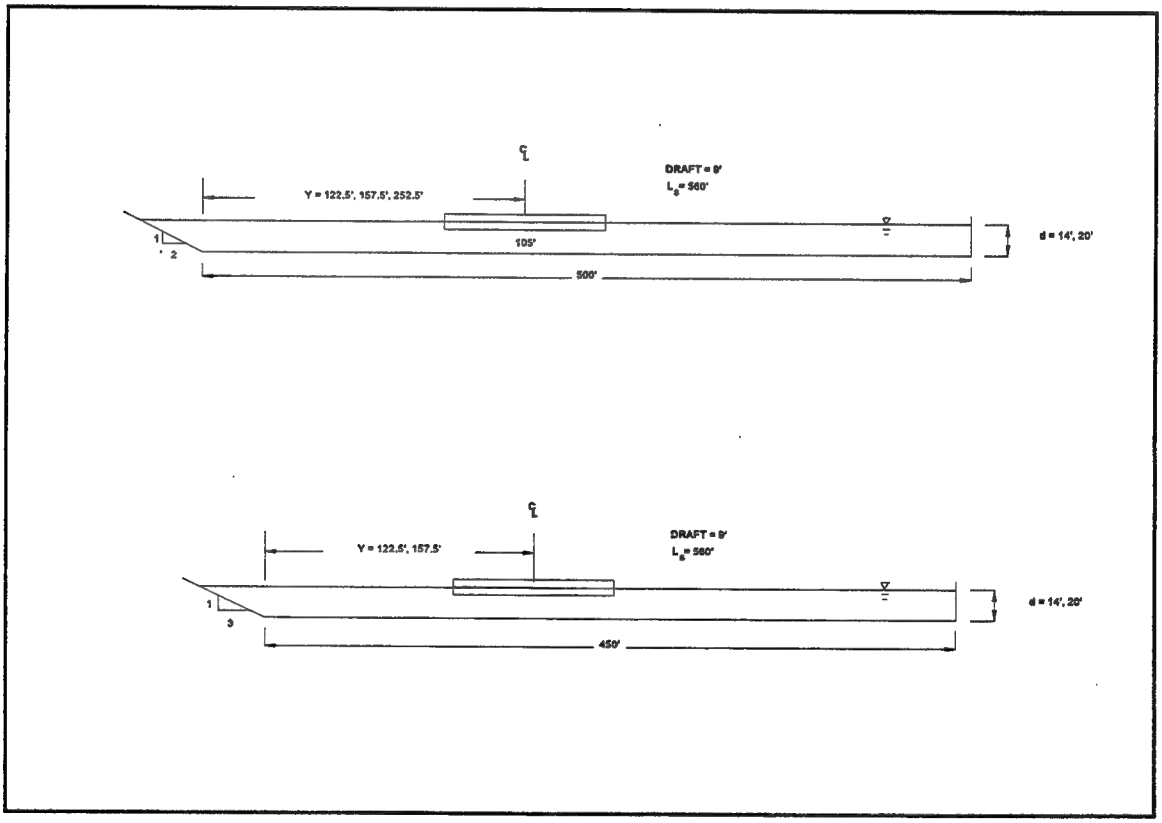

Figure 13. Pertinent cross-section and test data, navigation research, FY90

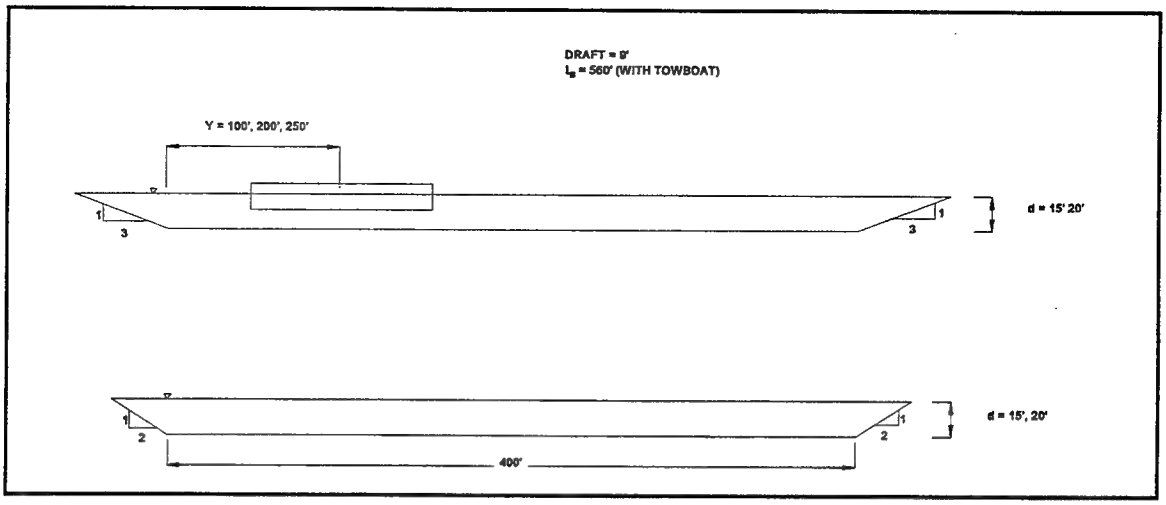

Figure 14. Pertinent cross-section and test data, navigation research, FY93

research conducted in fiscal year 1990; GAL for Gallipolis lock approach studies; and TT for Tennessee-Tombigbee model studies. Eight different gradations of riprap were tested. Tables 4-7 contain the prototype gradations tested in all the studies. Table 8 provides a summary of the model dimensions for the eight gradations.

A nonporous slope condition was modeled so no seepage could occur. The model riprap was placed on filter fabric at a thickness of approximately D_{100}. Model stone sizes were selected based on gradations recommended in the *Engineering Technical Letter (ETL) 120-2-120*, (HQUSACE 1971). Actual model gradations in relationship to the ETL guidance are shown in Figures 15-18.

Table 4
Gradations for the Tennessee-Tombigbee Study

	Type II Gradation		Type X Gradation		Type Y Gradation	
Thickness, in.	18.0		15.0		10.0	
D_{50}, in. γ_r = 166 pcf	11.1		8.1		6.4	
Percent Finer by Weight	Type II		Type X		Type Y	
	Weight, lb	Size* in.	Weight lb	Size in.	Weight lb	Size in.
100	360.0	19.3	170.0	15.0	50.0	10.0
80	170.0	15.0	75.0	11.4	28.0	8.2
60	92.0	12.2	37.0	9.0	16.0	6.8
50	68.0	11.1	27.0	8.1	13.0	6.4
40	50.0	10.0	21.0	7.5	10.0	5.8
30	33.0	8.7	13.5	6.4	7.9	5.4
20	21.0	7.5	8.8	5.6	6.0	4.9
10	9.0	5.6	5.6	4.8	4.8	4.6
0	3.6	4.2	3.6	4.2	3.6	4.2

* Equivalent spherical stone diameter using Equation 52.

Table 5
Gradations for the Gallipolis Study

	Original		Proposed	
Thickness, in.	24.0		12.0	
D_{50}, in. γ_R = 167 pcf	13.0		6.0	
Percent Finer by Weight	Original		Proposed	
	Weight, lb	Size, in.	Weight, lb	Size, in.
100	347.0	19.0	41.7	9.4
80	217.0	16.3	25.0	7.9
60	139.0	14.0	14.0	6.5
50	111.0	13.0	10.9	6.0
40	87.0	12.0	8.3	5.5
30	64.0	10.8	6.2	5.0
20	40.0	9.2	4.8	4.6
10	25.0	7.9	-----	-----
0	10.9	6.0	0.6	2.3

Table 6
Gradations for the Navigation Research, FY90

	Type 1		Type 2		Type 3	
Thickness, in.	9.0		9.0		12.0	
D_{50}, in. γ_r = 167 pcf	3.3		5.0		5.8	
Percent Finer by Weight	Type 1		Type 2		Type 3	
	Weight lb	Size in.	Weight lb	Size in.	Weight lb	Size in.
100	5.4	4.8	12.4	6.3	41.7	9.4
80	3.5	4.1	9.5	5.7	23.0	7.7
60	2.2	3.5	7.1	5.2	12.4	6.3
50	1.7	3.3	6.3	5.0	10.0	5.8
40	------	------	5.4	4.8	8.2	5.5
30	------	------	3.1	3.9	6.7	5.1
20	------	------	1.7	3.3	5.4	4.8
10	------	------	------	------	------	------
0	0.6	2.3	0.6	2.3	0.6	2.3

Table 7
Gradations for the Navigation Research, FY 93

	G1		G2		G3		G4	
Thickness, in.	9		12		15		18	
D_{50} γ_r = 167 pcf	3.25		5.8		8.1		11.1	
Percent Finer by Weight	G1		G2		G3		G4	
	Weight lb	Size in.	Weight lb	Size in.	Weight lb	Size in.	Weight lb	Size in.
100	5.4	4.75	41.7	9.4	170.0	15.0	360.0	18.0
80	3.5	4.1	23.0	7.7	75.0	11.4	170.0	15.0
60	2.2	3.5	12.4	6.3	37.0	9.0	92.0	12.2
50	1.7	3.25	10.0	5.8	27.0	8.1	68.0	11.1
40	------	------	8.2	5.5	21.0	7.5	50.0	10.0
30	------	------	6.7	5.1	13.5	6.4	33.0	8.7
20	------	------	5.4	4.8	8.8	5.6	21.0	7.5
10	------	------	------	------	5.6	4.8	9.0	5.6
0	0.6	2.3	0.6	2.3	3.6	4.2	3.6	4.2

Table 8
Characteristics of Model Riprap

Model Study	Type Name	γ_r lb/ft^3	D_{50} ft	W_{50} lb	Thickness ft
NR90	1	167	0.011	1.2×10^{-4}	0.03
NR90	2	167	0.017	4.3×10^{-4}	0.03
NR90	3	167	0.019	5.99×10^{-4}	0.04
GAL	orig	167	0.043	6.95×10^{-3}	0.08
GAL	prop	167	0.020	6.99×10^{-4}	0.04
TT	II	166	0.047	9×10^{-3}	0.075
TT	X	166	0.034	3.4×10^{-3}	0.063
TT	Y	166	0.027	1.7×10^{-3}	0.042
NR93	G1	167	0.011	1.2×10^{-4}	0.03
NR93	G2	167	0.019	5.99×10^{-4}	0.04
NR93	G3	167	0.027	1.7×10^{-3}	0.05
NR93	G4	167	0.037	4.4×10^{-3}	0.06

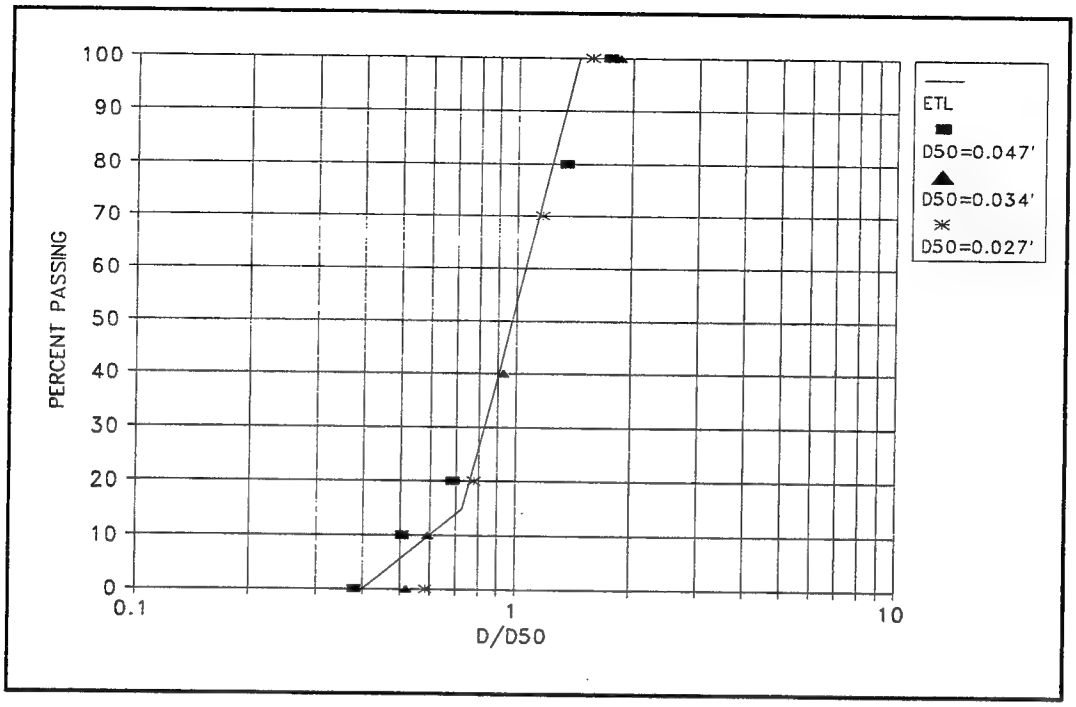

Figure 15. Model stone gradations used in Tennessee-Tombigbee study

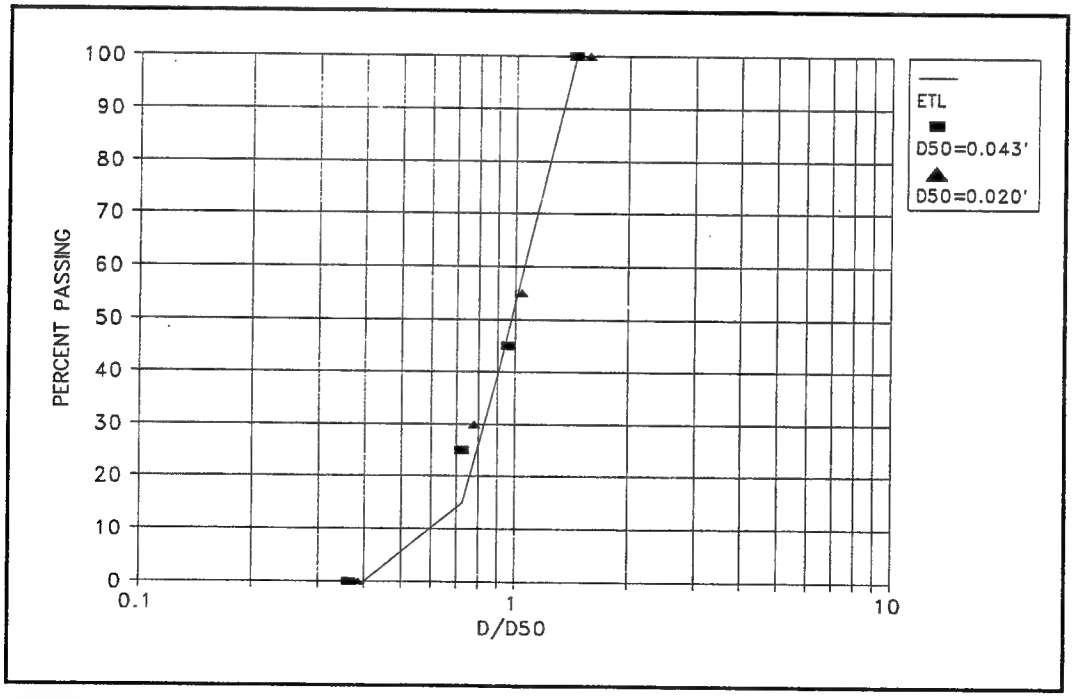

Figure 16. Model stone gradations used in Gallipolis lock approach study

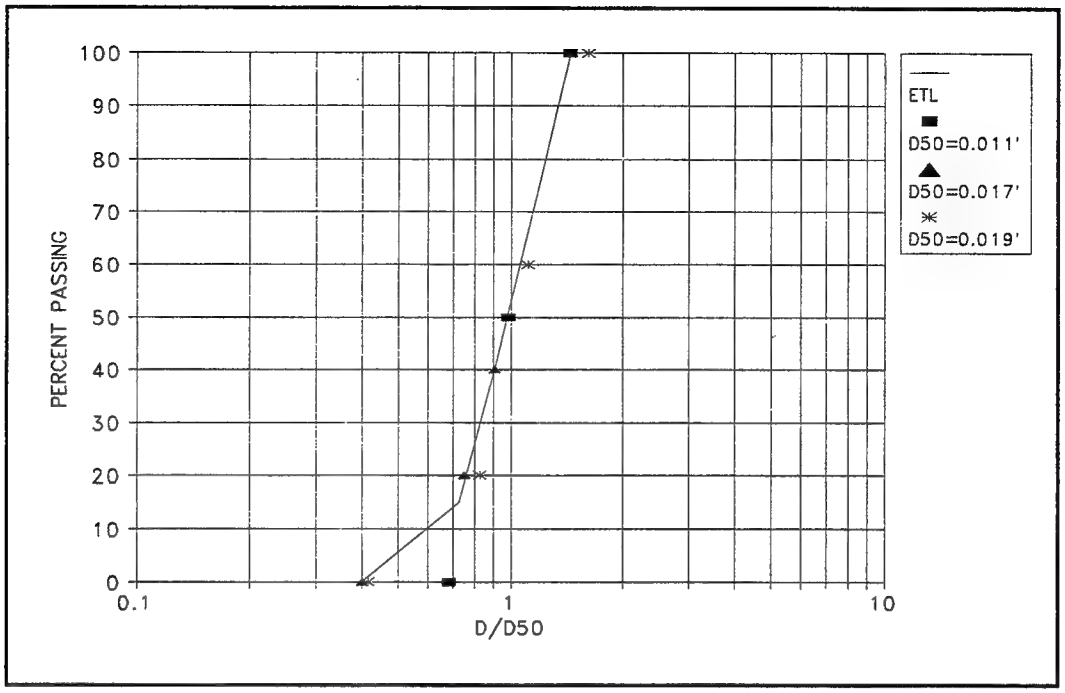

Figure 17. Model stone gradations used in navigation research testing, FY90

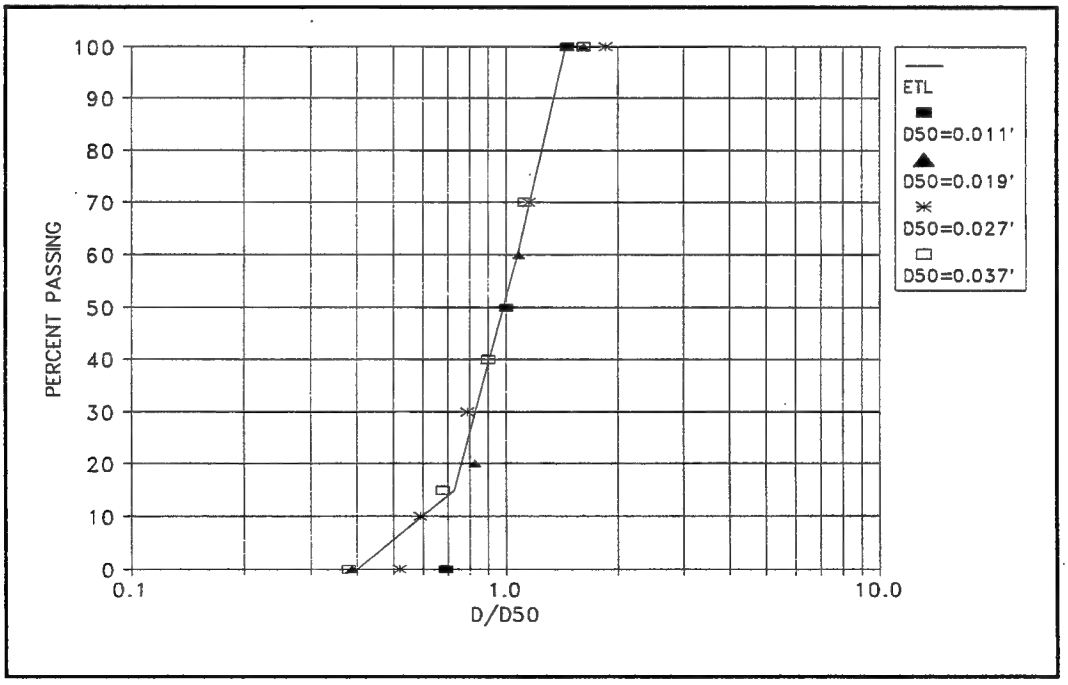

Figure 18. Model stone gradations used in navigation research, FY93

The stability tests were conducted by setting up the stone slope protection in a specific channel cross section and water depth. The tow was then configured and "driven" or towed past the slope protection at a specific sailing line and speed. Stability of the stone was observed after numerous passages of the tow at these conditions. In fact, each test series was repeated generally 100 times unless failure occurred prior to completion of the repetitions. Conducting this number of tests was recommended by Fuehrer, Romisch, and Engelke (1981) in their slope stability studies to fully expose the riprap to a sufficient number of waves. This finding corresponded with coastal studies of breakwaters where a minimum of 1,000 waves to a maximum of 7,000 are used during testing. The wave train accompanying and following the boat had multiple waves depending on vessel length and energy, making the number of waves impacting the slope after 100 vessel passages the same order of magnitude as in coastal studies. This implied that a minimum of 100 tests were required to establish one data point in the analysis of stable riprap.

Test conditions for the riprap stability studies are found in Appendix B. Each line represents a set of conditions including barge characteristics, channel characteristics, bank slope, stone size, and the vessel speed at which the model riprap embankment was repeatedly passed by the vessel. Stability is determined through observation of the stone on the embankment during testing. Failure (F), also called incipient failure, is defined, in this study and others, as the condition in which the filter cloth is exposed (Maynord, Ruff, and Abt 1989). Stable (S) indicates that while some individual stones may have overturned or moved, the general thickness of the riprap was not affected. A category,

marginal (M), was added for the research work unit. During these tests, relatively small and previously untested stone sizes were used. Although the filter fabric was not exposed, the riprap thickness showed signs of thinning in the zone of wave action. A safety factor will be added back into the stone size for stable design conditions.

Other tests

In addition to the tests conducted for stability, large amounts of hydrodynamic data were collected to determine suitable predictive equations for the navigation effects. In addition to data collected for the Tennessee-Tombigbee and the Gallipolis study, wave and velocity data collected included the following:

a. Tests were conducted for a prototype rectangular channel, 400 ft (122 m) wide and 20 ft (6.1 m) deep, at three different model scales (1:37.5, 1:25, 1:20) to determine associated problems with smaller scales. Figure 19 is a schematic of the prototype dimensions tested in the model. Wave and velocity data were collected for variable boat speeds at approximately three lateral locations. Velocity data were also collected in three vertical positions. Hydrodynamic data included boat speed, lateral location of the measurement from the bank, vertical location of the measurement from the bottom, the absolute value of the maximum return current (x-direction), the absolute values of the lateral peak velocities at bow and stern, and the maximum drawdown. This test series is referred to as the scale tests (SCT).

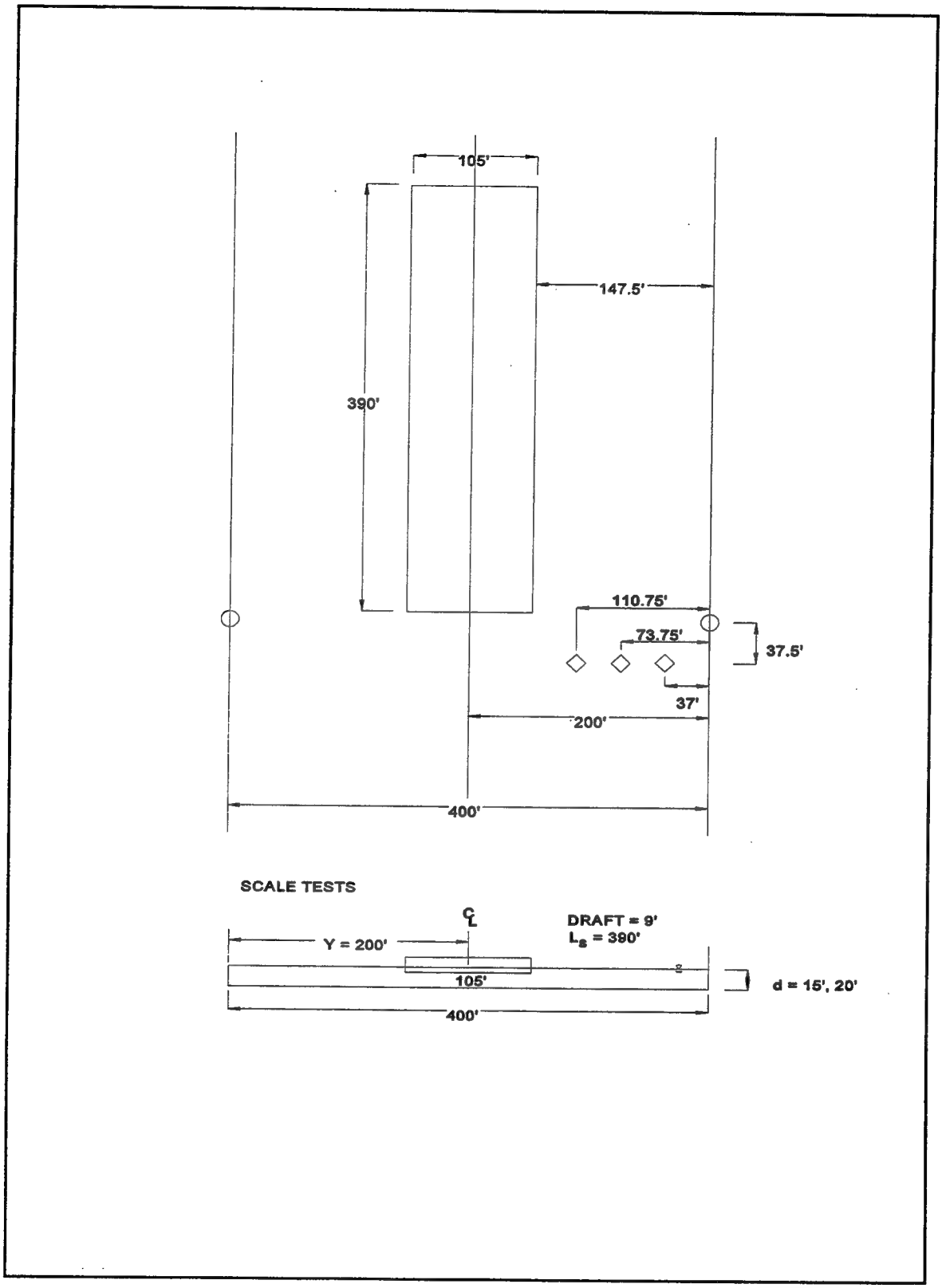

Figure 19. Plan and cross section of prototype conditions tested in scale models

b. In the fiscal year 1993 navigation research program, wave and velocity data were collected for most conditions in which riprap stability were evaluated, and for some conditions (different boat draft, depth, etc.) not relevant to actual stability tests. These data were used to develop regression equations for obtaining drawdown and return current values for each test scenario in the stability analysis. Further details will follow in the next chapter.

Model Description and Appurtenances

The model flume dimensions for all tests except the Tennessee-Tombigbee tests are shown in Figure 20. The maximum water depth that could be tested in the flume was 1 ft. Data were collected in an approximately 100-ft- (30.5-m-) long area where the floor was level. The flume was not equipped with a recirculating system; therefore, all tests were conducted in quiescent conditions. The flume was equipped with a winch and pulley system for the fiscal year 93 navigation tests. The sailing line was adjusted by moving the winch and cable assembly across the width of the usable flume area. In some cases, the location of columns in the facility limited the number of sailing lines that could be tested.

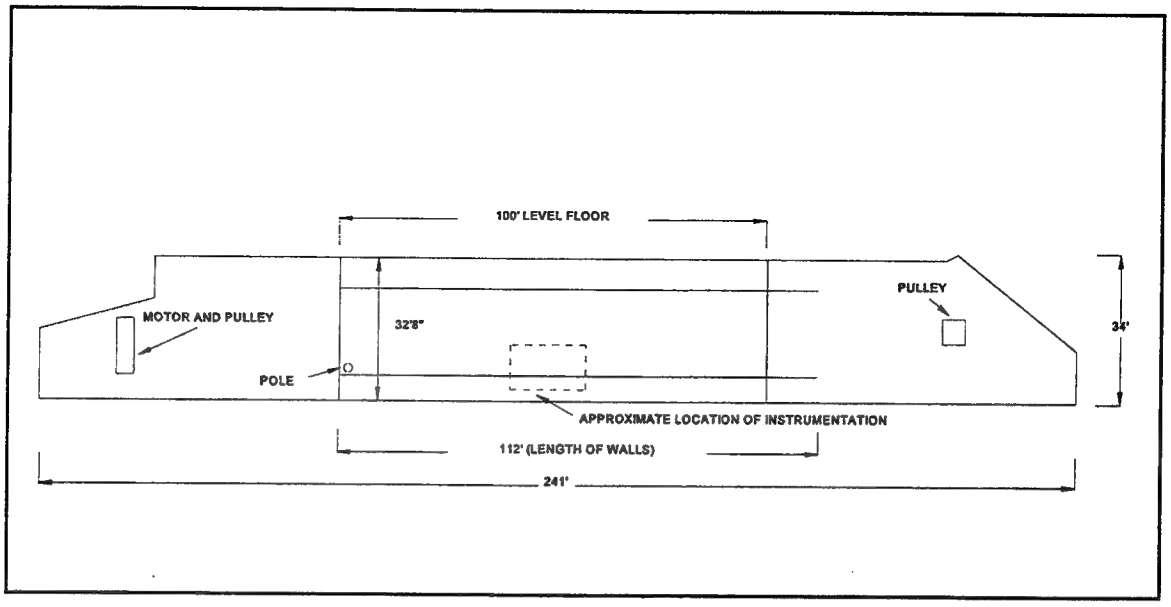

Figure 20. Dimensions of model flume area for navigation effects testing, plan view

Riprap stability

The riprap gradations used in the 1993 tests, were based on previous tests and observed failure characteristics. Four gradations were selected ranging in model size from a D_{50} of 0.0108 to 0.0370 ft (3.3 to 11.3 mm) with corresponding prototype gradations as specified in Table 7. A layer of sand was placed on the slope and covered with filter fabric. The scaled riprap was placed at the specified thickness from the toe of the slope to well above the waterline. Observations of movement were recorded for areas unaffected by boundary edges. Figure 21 shows the layout of the slopes and gradations observed for this test series in model dimensions. The riprap was lightly painted after placement to help identify the direction of motion and the origin of displaced stones.

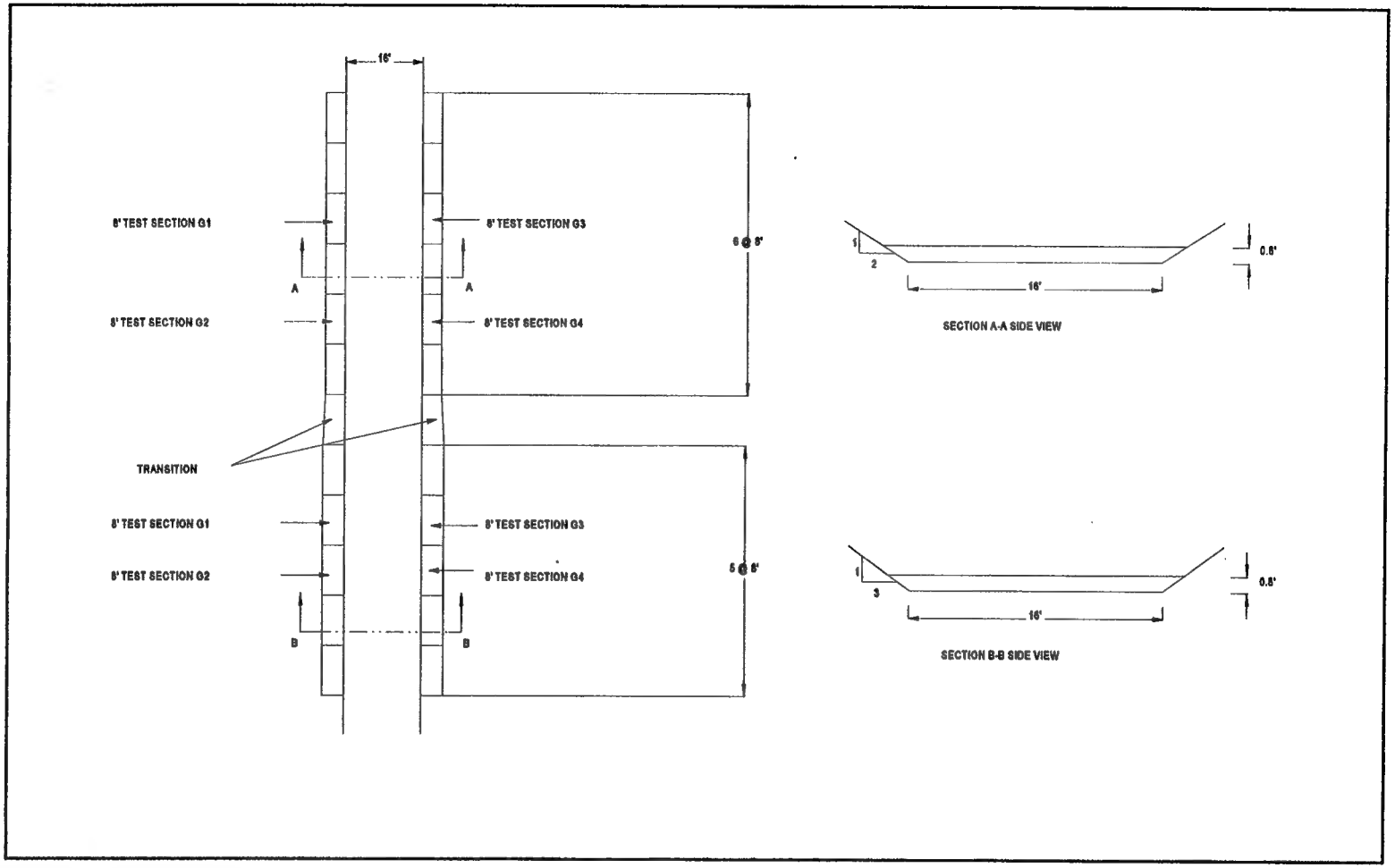

Figure 21. Model dimensions and layout of stability tests

Hydrodynamic data

Data collected for this study included the tow's speed, the water-surface movement, and the water velocity at various locations adjacent to the tow. All analog data were collected, converted, and saved digitally on DOS-based personal computers. The tow speed was monitored through the test section by interrupting a retro-reflective light beam with 1-ft panels attached to the top of the moving barges. All wave data were collected using capacitance wave rods. No more than two rods were used at once. Sampling frequency was generally 25 hz. The location of the instruments varied with testing. Velocity data over the course of these studies have been collected with a variety of instruments. An electromagnetic meter measured return currents in the Tennessee-Tombigbee study. An impeller type probe was used in the Gallipolis study to pick up a few velocity measurements. Recent testing for the Navigation Hydraulics program included using a two-dimensional (2-D) laser doppler velocimeter (LDV) and, near the end of testing, newly developed 3-D acoustic doppler velocity (ADV) probes. The location and depth of velocity measurements were varied during testing.

The vessel

The tests conducted for the Tennessee-Tombigbee, the Gallipolis, and the first set of navigation research tests used a free moving model tow. The tow in the Tennessee-Tombigbee model was a 1:20-scale self-powered vessel operated by a technician on board; in the Gallipolis and NR90 studies, it was a 1:25-scale radio-operated tow. For the

NR93 tests, a towing cable and winch pulled the tow model through the test section. This included pulling the barges (three wide by two long) and the model towboat while operating the propellers during the stability tests.

The operation of the propellers was based on tow thrust calculated as a percentage of a boat's bollard push. Toutant (1982) defines bollard push as the dock or zero-speed force of the vessel and presented formulas for calculating this force as a function of horsepower. The equations presented by Toutant were used to determine an appropriate bollard push for the prototype towboat being modeled. To obtain a maximum bollard push, the prototype was assumed to have 5,600 hp; therefore, the maximum bollard push was 105,500 lb (4.7×10^5 N) or 6.75 lb (30 N) in the model. The model towboat was built as a replica of the U.S. Army Engineer District, Vicksburg, working boat, the *Benyaurd*. According to conversations with personnel at the U.S. Army Engineer District, Huntington, and the pilot of the *Benyaurd*, maximum rpm's for this size towboat is 200 to 220 which equals approximately 1,000 to 1,100 rpm's in the model. Based on the same conversations with the Huntington District, operators in open river use approximately 75 to 80 percent throttle. Then at maximum operation, the bollard push should be approximately $0.75 \times 6.75 = 5.1$ lb (23 N). From graphs obtained from testing the force produced by the tow at various rpm's, the corresponding operation for the model boat should be approximately 860 rpm (172 rpm prototype). Likewise at 50 percent throttle, the bollard push would be 3.38 lb (15 N), and the corresponding rpm is 720 (144 prototype). Operation of the model tow using the prescribed method for determining the appropriate rpm, resulted in tow speeds that were too slow due to viscous effects in the

model. Operating the free moving towboat and barges using only the boat's self propulsion resulted in the prototype values of boat speed shown in Table 9.

Table 9
Vessel Thrust and Force

Thrust %	Force lb	Tachometer rpm	Boat Speed fps
10	10,625	74	2.50
25	26,250	112	4.25
50	52,813	152	6.00
75	79,688	172	7.00

To achieve the testing program objectives, vessel speeds needed to approach their limiting speed. In the fiscal year 1993 test channel at a 20-ft (6.1-m) prototype water depth, the prototype limit velocity is approximately 14.9 fps (4.5 mps). All propeller speeds were set proportional to the vessel speed used in testing. To overcome the viscous effects and get the vessel to operate closer to the higher speeds, the towing cable assembly was used for the following two basic reasons:

a. It improved the repeatability of the testing particularly regarding the sailing line. Also, it helped maintain a constant tow speed that was not influenced by depleting battery supplies, interference in radio transmitted tachometer signals, and the like.

b. It allowed a wider range of tow speed operations without unduly overpowering the propulsion from the propellers.

The propellers were operated to insure that any influence of propeller turbulence was not disregarded as pertains to slope stability. As it turns out, the primary area where the propellers could influence the bank stability is when the tow's edge operates over the toe of the slope. In this area, the turbulence from the propellers has a localized influence on stone movement at the slope bottom due to the proximity of the jet to the channel bottom and the potential for steering maneuvers to keep away from the bank. However, under most sailing line conditions, the hull displacement generates the critical forces.

Barges for all studies were made of sheet metal, ballast with weights, and connected with C-clamps. Each barge used in the 1:20-scale Tennessee-Tombigbee study and for the scale tests was 9.75 ft (3.0 m) long by 1.75 ft (0.8 m) wide and had a curved rake at the bow. Two different configurations were used in the Tennessee-Tombigbee study; a two-wide-by-one long unloaded and a three-wide-by-two-long loaded configuration. The configuration for all the scale tests was three wide by two long. The rakes on these barges varied according to the scale barges used. Barges used at the 1:37.5 scale had a configuration of three wide by two long with a rake that made an angle of 26.5 deg with the horizontal. Barges in the Gallipolis study had a square bow and stern, and the configurations varied from a three wide by two long to a three wide by five long. Barges in the 1:25-scale riprap tests were 7.8 ft (2.4 m) long by 1.4 ft (0.4 m) wide. The configuration used for these tests was three wide by two long. The lead barges had a rake that made a 45 deg angle with the horizontal. The rear barges had square ends.

4 Analysis and Results

Data Collection and Uncertainty

Problems inherent to physical model testing include scale-effects phenomena, difficulties with the flume itself, accuracy of the instrumentation, location of the instrumentation, and whether the tow is free-moving or towed, etc. The variabilities that arise from these problems can cause uncertainties in the data collection. Every effort was made to correct for these problems and minimize their effects.

Flume limitations

The length of the test facility (Figure 20) used in the NR93 testing limited the tow size that could be modeled, the length of time available to capture the event, and the ability to get the vessel operating at full speed. The maximum length of tow modeled was two barge lengths. As the tow starts, particularly when towed, a celerity wave is generated that reflects off the ends of the flume. The travel time of this wave can interfere with the time history of the data collection since it is a function of the vessel speed and water depth. The startup time and distance to testing apparatus was evaluated for each test condition so that the longest time history response could be obtained prior to the bow passing the instrument and following the stern. Interference due to reflective

waves was unavoidable in some conditions. Data were collected near the center of the flume where the vessel was operating at a relatively uniform speed to minimize potential accelerations and decelerations of the vessel.

Bow wave phenomena

The amplitude of the bow wave could be effected by both the timing of the celerity wave and the influence of the towing system. In the examination of wave data, the reflective wave and the bow wave were often indistinguishable. The tow travel time and starting position were adjusted when possible so that the celerity wave could be easily distinguished from the bow wave. In Tenaud's testing (1977) conducted at a 1:20 scale, the tow was attached to a "tractor," or mechanical wheel on the floor that guided the boat along the sailing line, and was pulled by a cable. He observed a substantial wave at the bow, also observed in subsequent studies conducted at WES using both a towing cable and a towing carriage. This is likely an artifact of the rigidity of the towing system and its acceleration. It is also likely in Fuehrer, Romisch, and Engelke's (1981) testing that the towing apparatus in their 1:60 scale model caused an exaggeration of the bow wave. In fact, their stability equation was based on this phenomena. Conversely, bow waves in tests of free-running model tows, such as that used on the Tennessee-Tombigbee study (Maynord and Oswalt 1986), and prototype data collected on the Illinois River and Upper Mississippi River indicate that a rise preceding drawdown at the bow is imperceptible.

Drawdown discrepancies

When Tenaud (1977) compared his measurements of drawdown to Schijf theory (Jansen and Schijf 1953), he found them close for boat speeds less than 90 percent of the limiting speed. For higher speeds and drafts, the water level drops that were measured were lower than those calculated. A similar observation was made during scale testing at WES. At the 1:25 scale and 1:37.5 scale, model data were higher than Schijf values and at the 1:20 scale, values were lower at higher speeds. Without any other reasonable explanation, the towing cable and assembly may be responsible for this discrepancy. Tenaud also observed that measured values are greater than the estimated values for all tests using a lighter draft.

Variability of data scatter

Variability in the data can occur for multiple reasons; therefore, quality control was exercised to minimize those variabilities. One quality control method is to replicate tests. To improve consistency of results and evaluate variability, tests were replicated during the collection of wave and velocity data at each measuring point. Figures 22 and 23 show typical scatters of return currents and drawdowns for multiple boat speeds and repetitions collected during the NR93 testing. The prototype test conditions for these measurements were tow sailing on the centerline of the channel, depth of water, 20 ft (6.1 m), and a 2H:1V bank slope. Another method to insure repeatability of tow passage for both the vessel speed and sailing line is to use the towing cable. In spite of efforts to

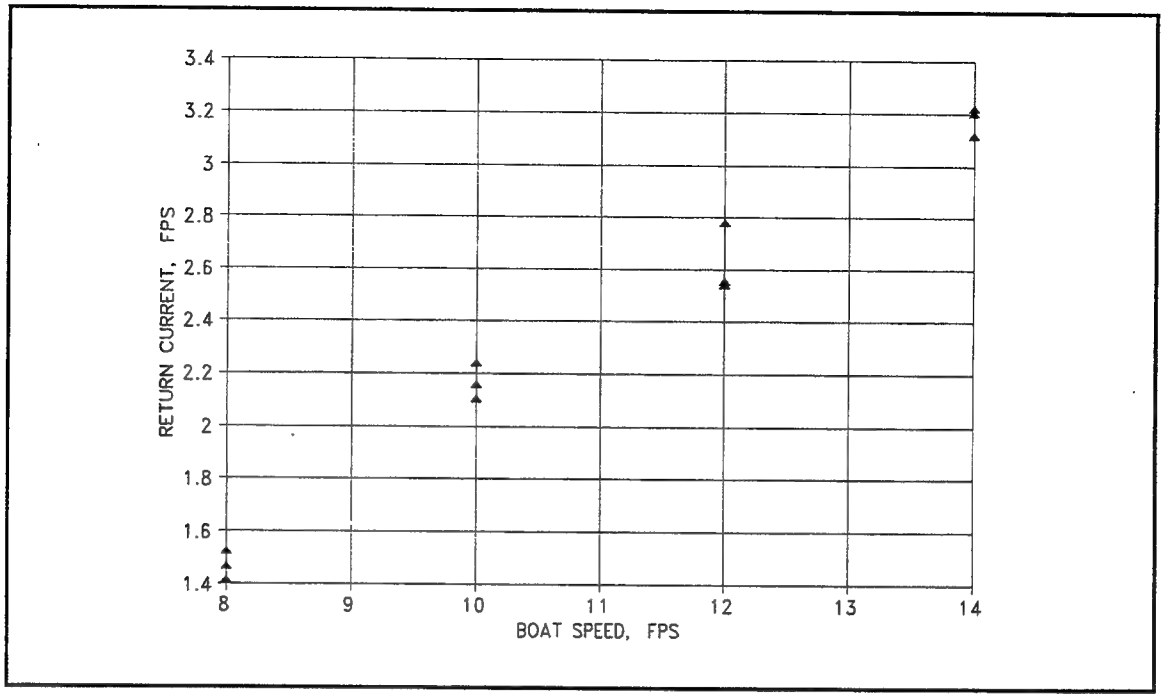

Figure 22. Variability in measuring return currents in model

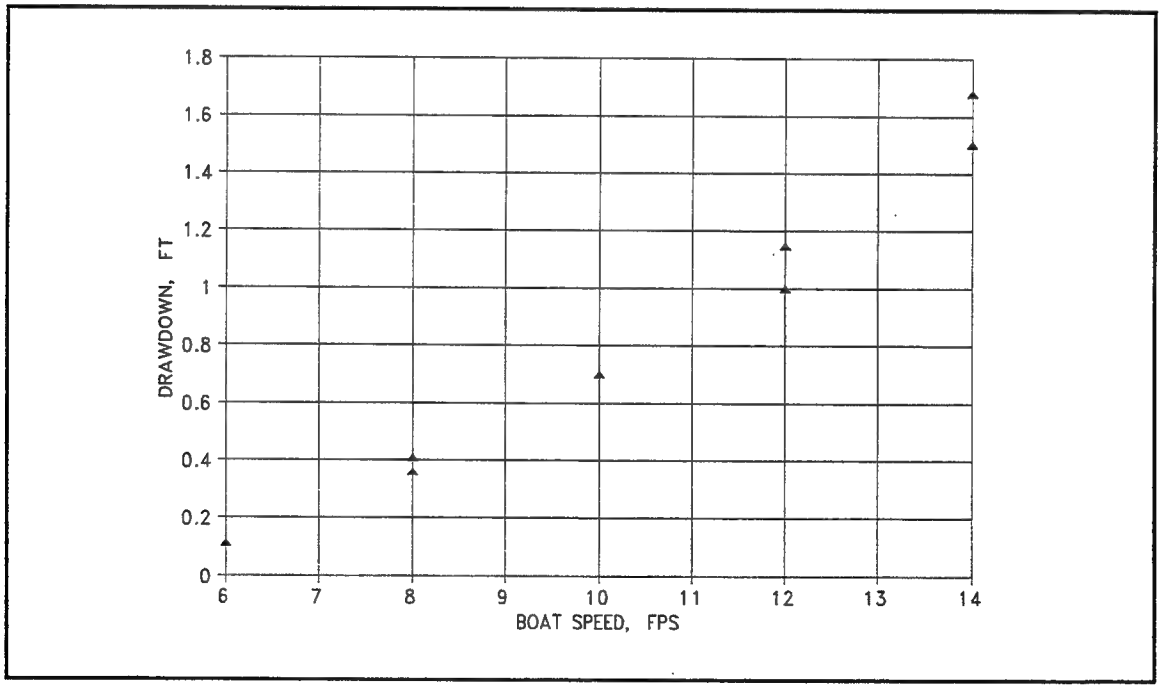

Figure 23. Variability in measuring drawdown in model

minimize irregularities between vessel passage, some problems still occurred with tension on the cable, motor speed controllability, operator variations, etc. Since velocity measurements were taken with different instruments over the course of the testing program, the data results were compared and found favorable. Figure 24 shows the comparison of values taken for the same test conditions as Figure 22 using both the LDV and ADV to measure velocity. Although propeller influence was determined to be minimal unless the sailing line is very close to the toe of the slope, the propellers were operated, whenever possible, to more closely represent the actual vessel passage.

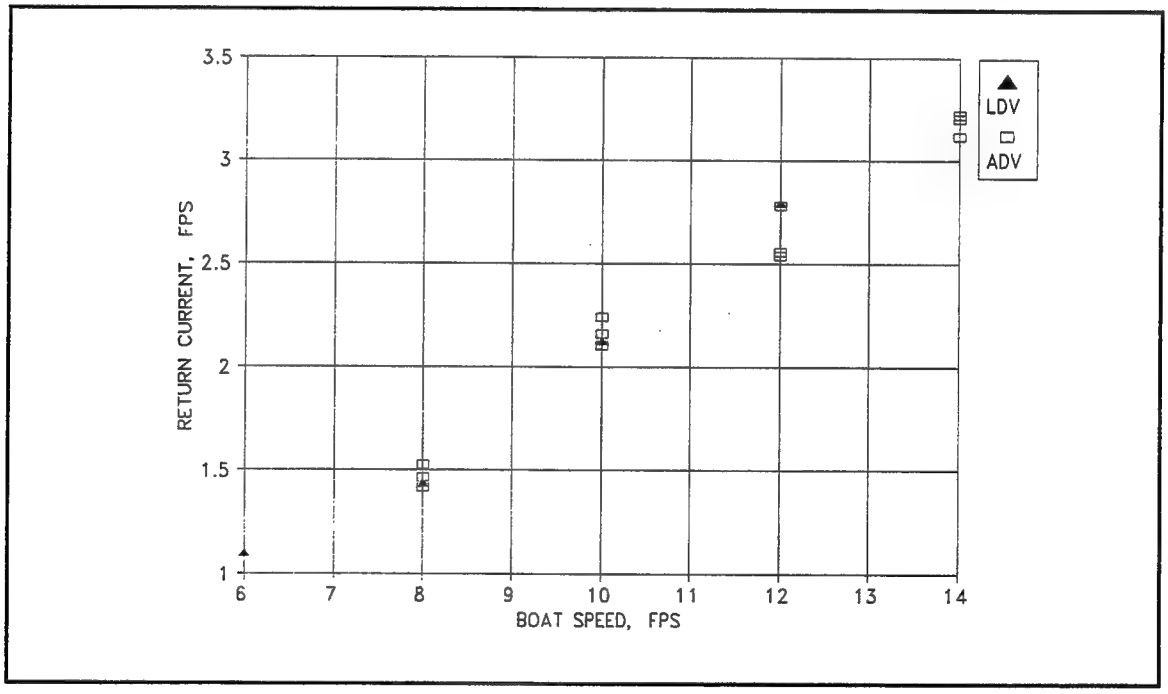

Figure 24. Comparison of measurements taken with LDV and ADV

Lateral variability of drawdown and return current

Return current and drawdown data were collected halfway between the edge of the tow and the toe of the slope. It was assumed that these variables were laterally uniform from the vessel to the shore. Recall, this is true for uniform channels of small blockage ratios (Jansen and Schijf 1953). Since riprap is generally placed in uniform channels such as narrow canals or lock approaches, this assumption is valid. Tenaud (1977) also confirmed this assumption stating that measured wave heights at several locations gave "practically identical results." Results of hydrodynamic data collected at the three lateral locations shown in Figure 19 during the 1:20-scale tests (SCT) support this assumption. The data collected at 110.75 ft (33.76 m), 73.75 ft (22.48 m), and 37 ft (11.28 m) in prototype dimensions from the vertical wall of the channel are referred to as "near tow," "mid-channel," and "near bank," respectively. In Figures 25 and 26, where boat speed is plotted against return current and drawdown, respectively, data scatter does not appear to follow any particular trend related to the three locations between the vessel and the bank.

Vertical variability of velocity

An assumption typically made regarding return currents is that the velocity profile is uniform over the depth of the water column. This is more pronounced since the boundary layer has not fully developed. Figure 27 shows velocities taken at three vertical locations in a 20-ft (6.1-m) prototype channel during the 1:25-scale testing. More data are currently being collected to verify this assumption particularly in nonuniform channels.

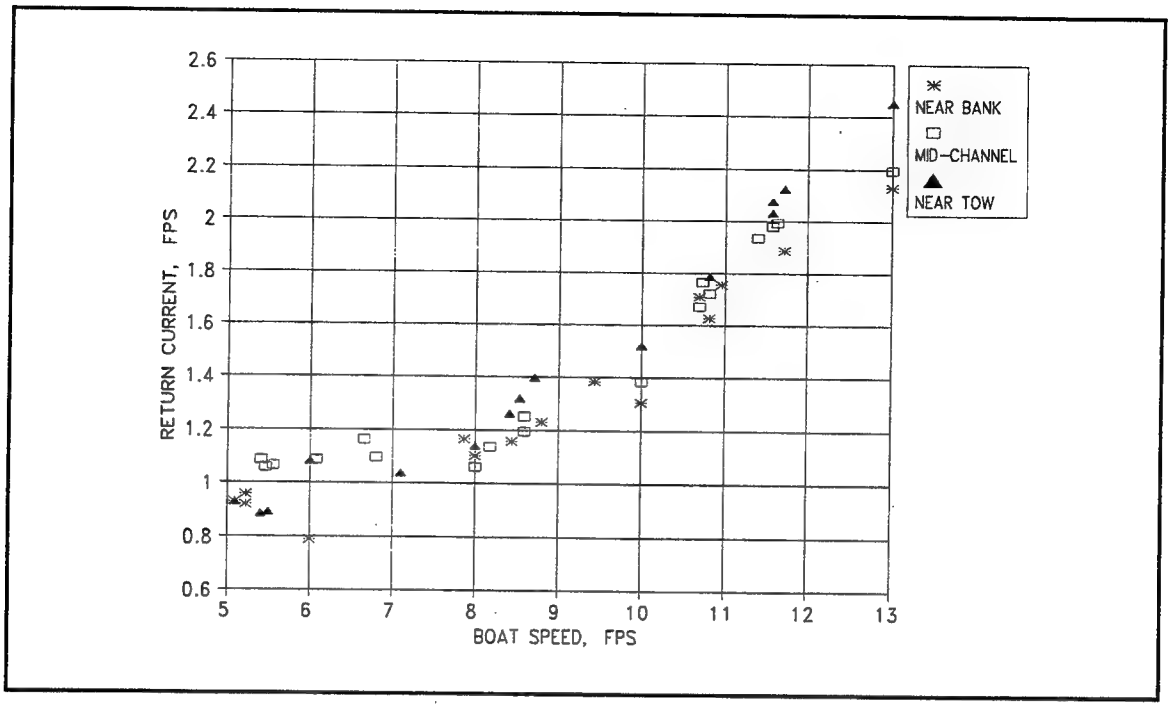

Figure 25. Variability in the lateral distribution of return currents

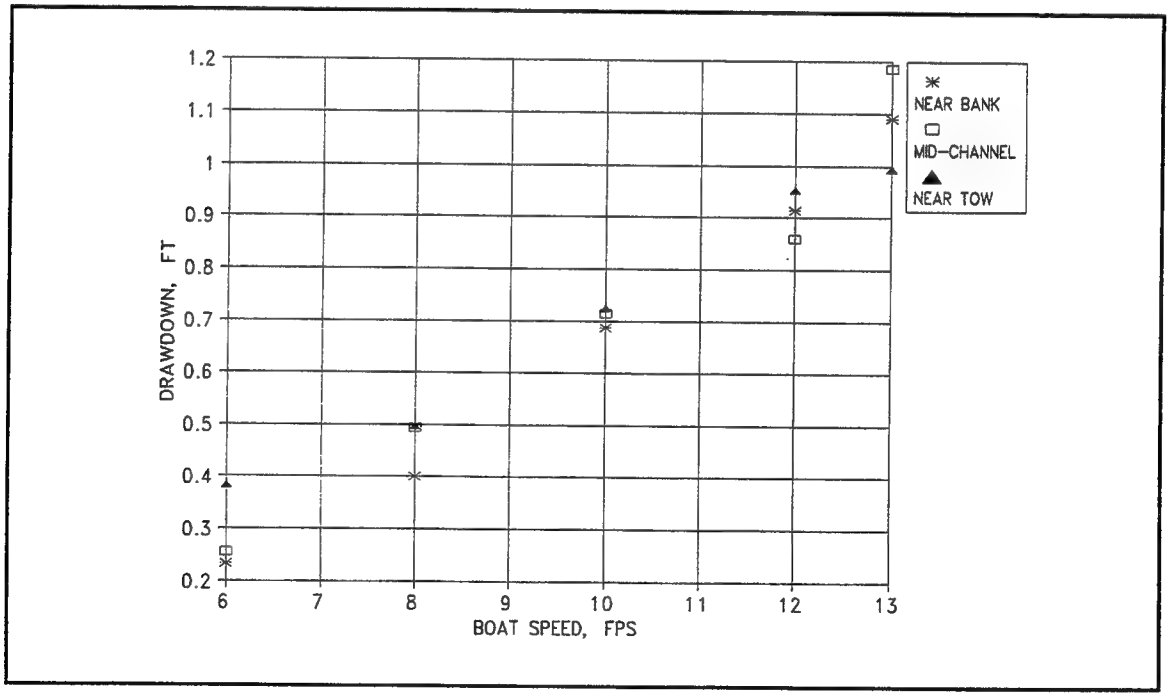

Figure 26. Variability in lateral distribution of drawdown

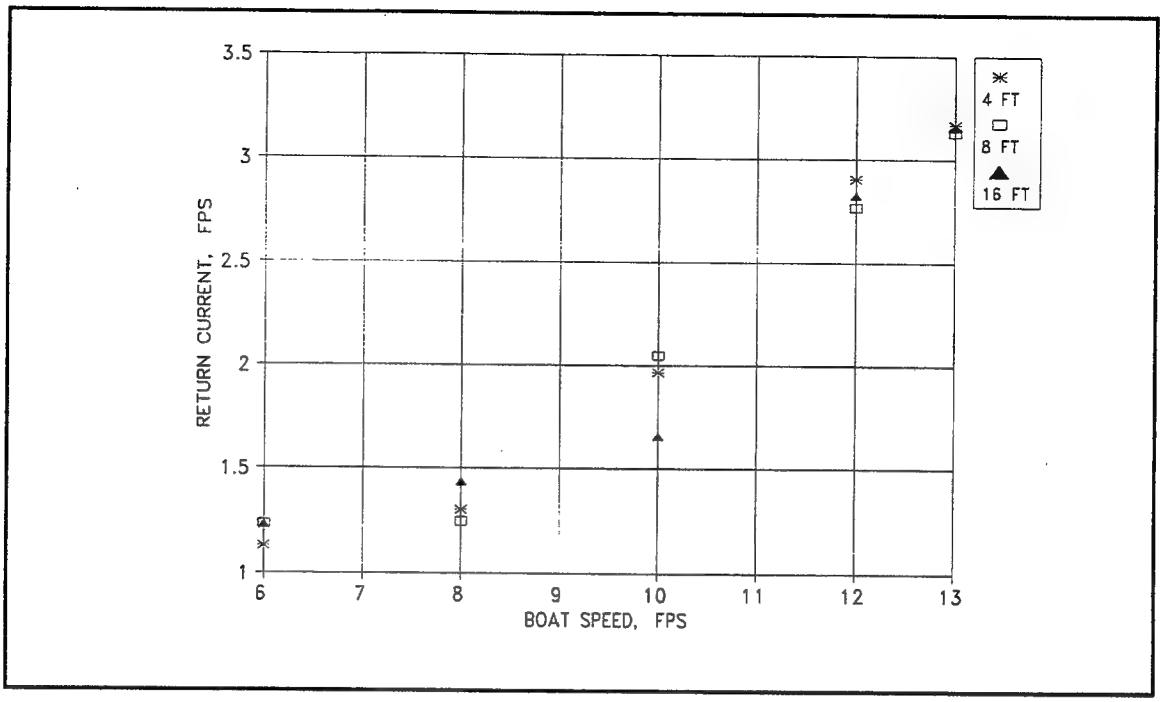

Figure 27. Vertical variability in return currents, mid-channel, depths are from bottom

Hydrodynamic Data Analysis

Selection of peak values

Time history hydrodynamic data of waves and currents collected during navigation effects testing were analyzed and peak values were extracted. The test conditions, peak velocity, and wave data are found in Appendixes C and D for velocities and waves, respectively. They contain the test series, model scale, channel dimensions, sailing line, vessel width, draft, speed, location of measurements, and all peak data.

The maximum return current, u_{rm}, in the x-direction velocity was taken from the data and is defined according to the definition in the literature given by PIANC (1987) and Maynord (1996). A comparison of calculated values of return current using the Schijf approach with a coefficient, a_1, of 1 to measured values of u_{rm} from the SCT and NR93 data sets is found in Figure 28. Schijf values are included in the summary table in Appendix C. Comparisons of TT velocity data to theory are found in Maynord and Oswalt (1986).

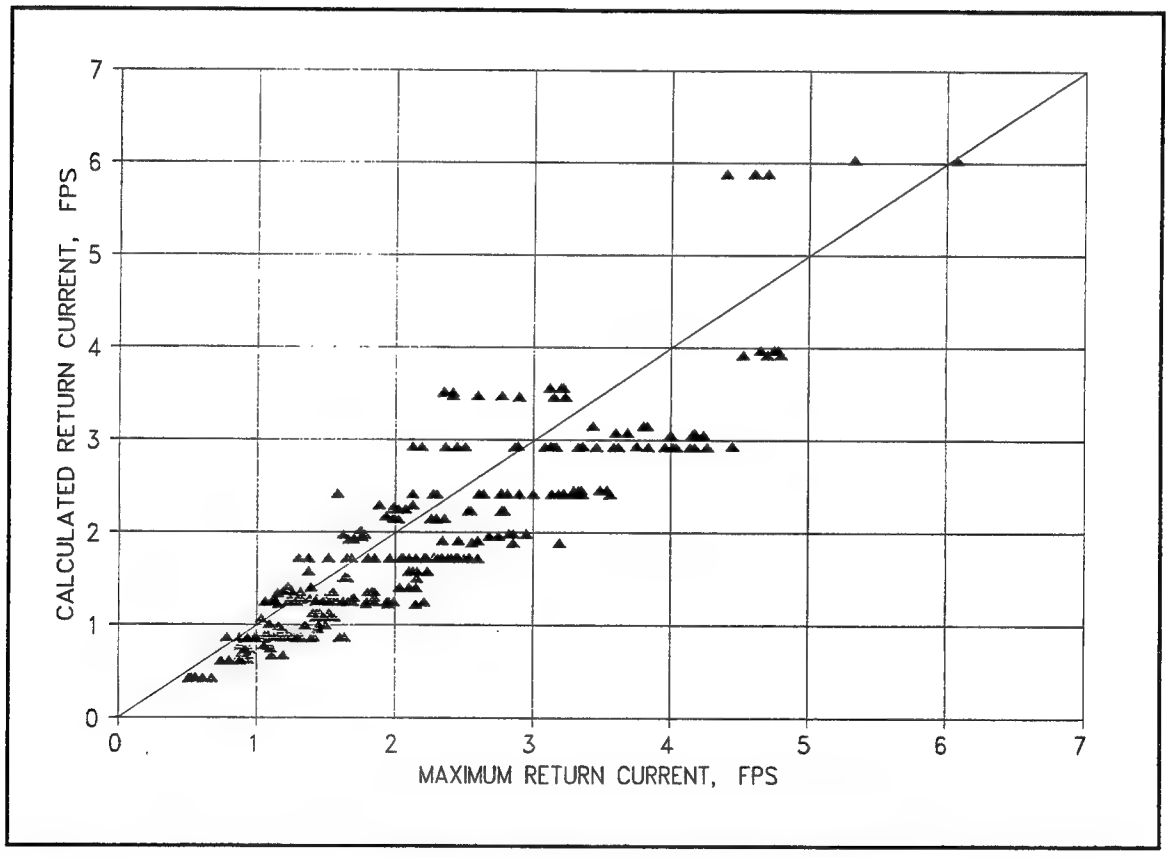

Figure 28. Comparison of measured values of return current to computed values using the Schijf approach

Since velocities were collected in two dimensions, plan view, in the NR93 and SCT data, the maximum lateral velocities were also recorded. An absolute peak value away from the bow, u_{yb}, and one toward the stern, u_{ys}, are included in Appendix C in prototype dimensions. The magnitude of these velocities is small relative to the peak return current as shown in Figure 29.

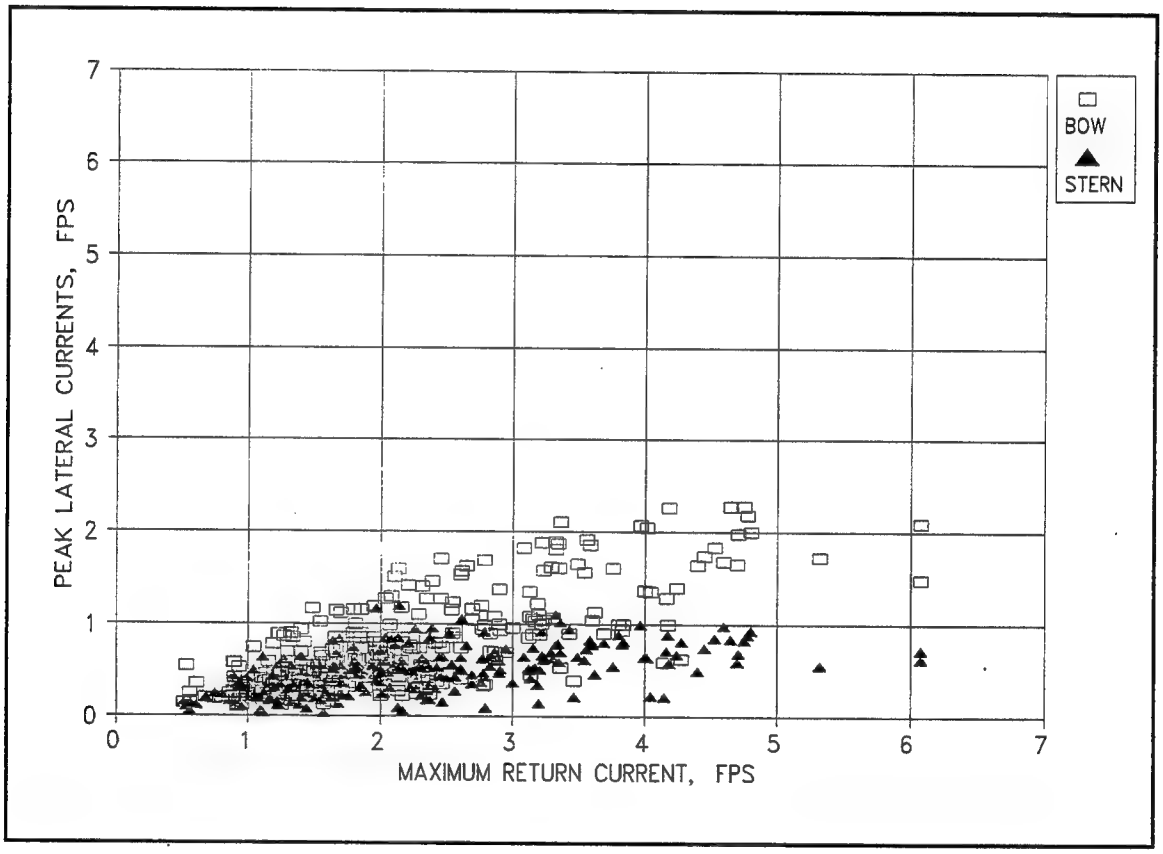

Figure 29. Comparison of longitudinal currents to lateral currents produced by tow

Four different pieces of peak wave data were extracted from the time history plots, the bow wave, h_f, the maximum drawdown, z_{max}, the maximum peak of the secondary

waves, H_i, and a variation of the transversal stern wave, H_{max} (defined as the trough to following peak of the transversal stern wave). H_{max} differs slightly from z_{max} in that it represents the actual height of the wave at the stern rather than the height of the trough of the water level depression back to the still water level, as shown in Figure 4. The bow wave data were not used in any of the analysis due to the potential error, already discussed, imposed by the towing cable and assembly.

To separate long period responses from the NR93 time history data, a moving average was used to filter out the high frequency response of the short period waves. The maximum drawdown, z_{max}, and maximum wave height at the stern of the vessel, H_{max}, were determined from plots of the smoothed time histories. Short period waves were obtained using a Fourier transform method. Essentially, the data are transformed from the time domain to the frequency domain; low frequency data are filtered out; and the remaining high frequency data are converted back to the time domain (Press et al. 1986). H_i is the maximum short period response in the high frequency wave spectrum. Figure 5 shows typical filtered and unfiltered wave responses. The TT data set was not filtered, and H_{max} actually represented either the maximum trough to following peak of the transversal stern wave, if present, or a maximum secondary wave.

Figure 30 shows how the secondary waves from the NR93 data and the maximum wave data for all data sets relate to the maximum measured drawdown. As can be seen, both the secondary wave and the maximum wave are dispersed on either side of the line of perfect agreement with slightly more points below the line. This graph tends to show that the value of z_{max} conservatively represents the peak wave in the wave spectrum for

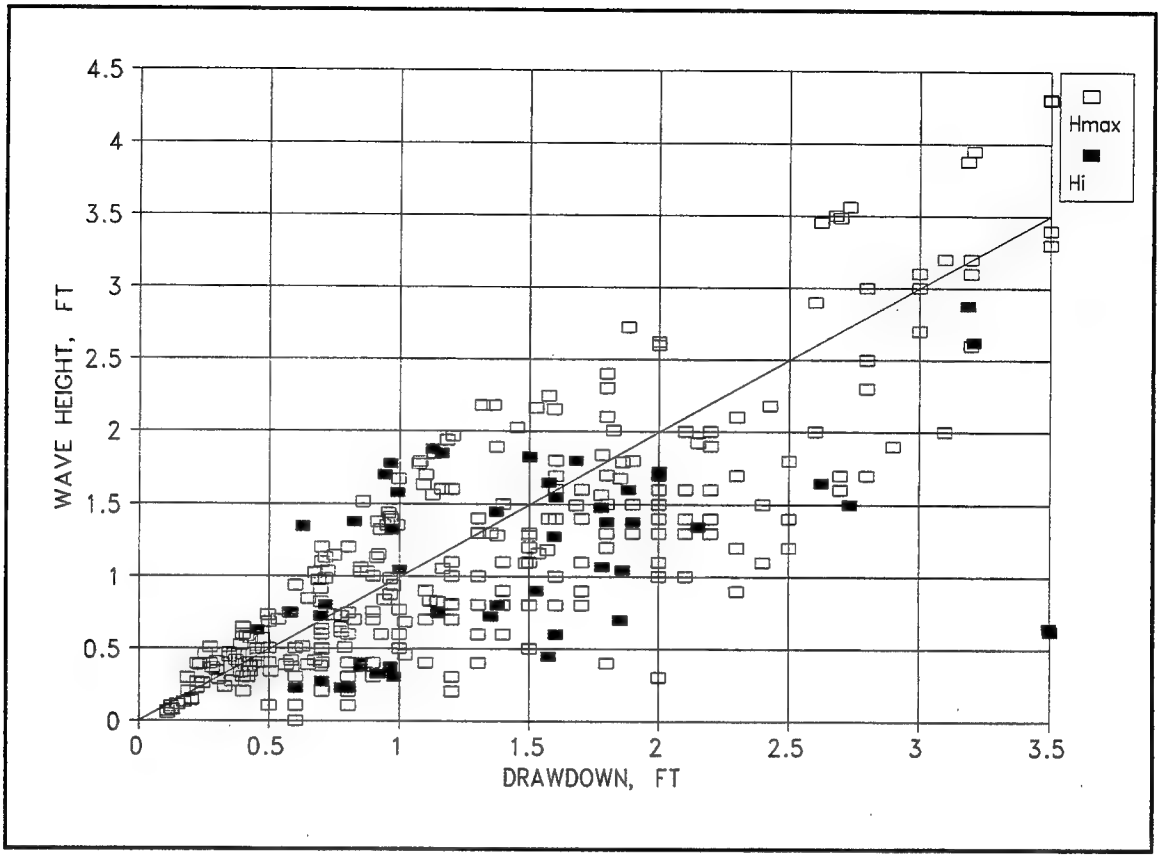

Figure 30. Relationship between secondary waves, maximum wave, and maximum drawdown

commercial tows in confined channels with blockage ratios less than approximately 16. For low vessel speeds, less than approximately 8 fps (2.4 mps), H_i was negligible. In an unconfined channel, for vessels traveling at high speeds, the secondary or hull-formed waves would dominate the wave spectrum.

The measured maximum drawdown for the SCT and NR93 data is compared to values obtained by the Schijf method, again using an a_1 of 1, in Figure 31. Comparisons of TT wave data to theory are found in Maynord and Oswalt (1986). The measured secondary waves are compared to calculated values based on Equation 25 in Figure 32.

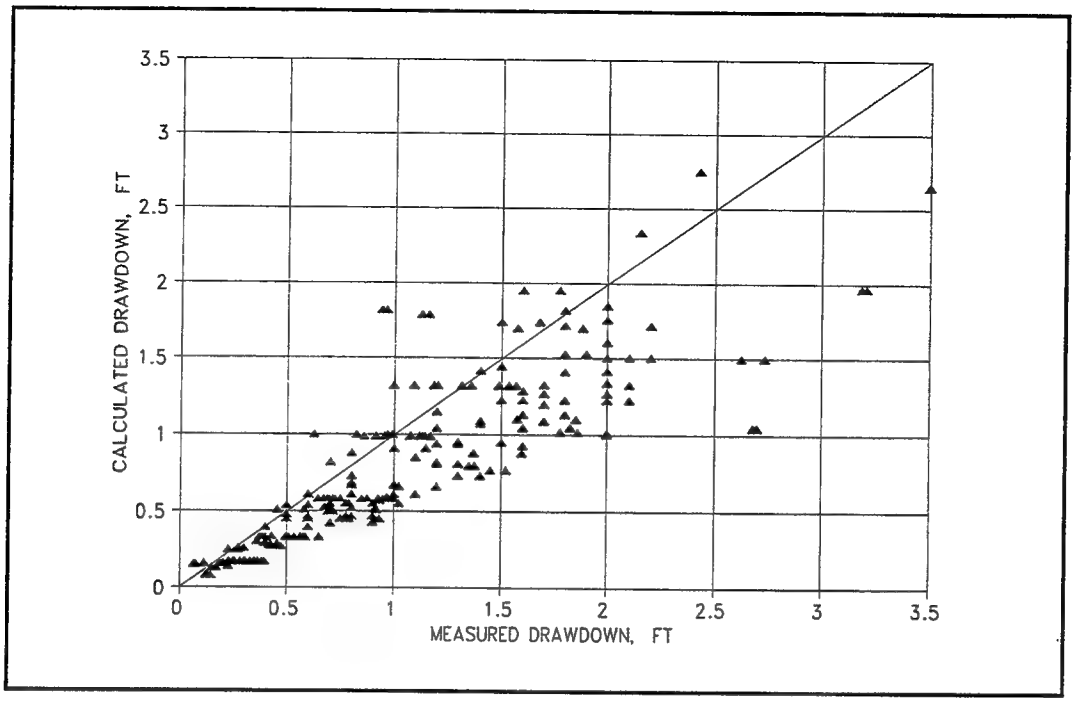

Figure 31. Comparison of measured values of z_{max} to computed values of drawdown using the Schijf approach

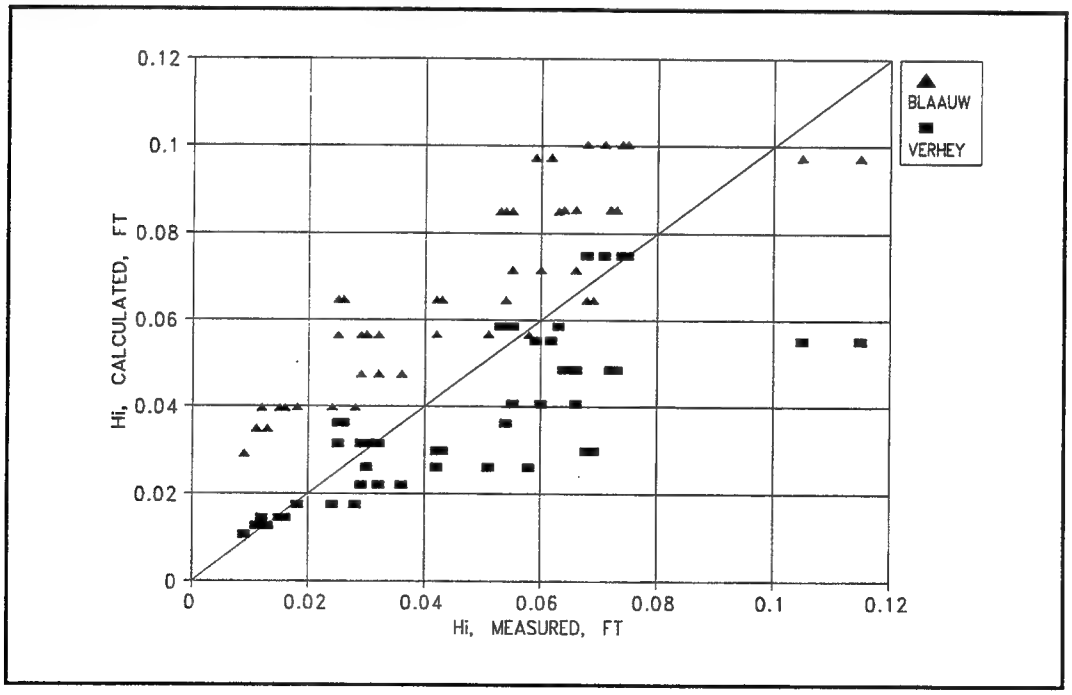

Figure 32. Comparison of measured values of H_i to computed values

The coefficients α_1 and α_2, respectively, taken from Blaauw et al. (1984) are 0.8 and 2.67, and from Verhey and Bogaerts (1989) are 1.0 and 4.0. Appendix D contains the test conditions and peak wave data from these tests and Schijf values of drawdown.

Mapping hydrodynamic data to stability tests

Each set of stability tests was conducted by operating the vessel at a constant speed for up to 100 passes. Since wave heights and velocities were not measured for each of these passes, a representative value corresponding to that test series was needed to analyze the relationship between navigation forces and bank stability. The hydrodynamic data provided in Appendixes C and D had to be mapped to the test conditions presented for the stability tests in Appendix B.

For most of the data, regression analysis was conducted with the hydrodynamic data to relate model tow speed to return current and drawdown. A return current and drawdown were determined from the regression corresponding to the channel conditions, sailing line, configuration, and boat speed used during each set of stability tests. The maximum return current, drawdown, maximum wave, and secondary wave for each test series were determined as follows:

a. If actual measurements were taken for fixed conditions of water depth, channel section, and sailing line, a regression analysis was done of boat speed versus each parameter. The best correlations were found with second order regressions and values corresponding to the test were taken from the regression. Where the curves

had low regression constants, engineering judgment was used to select the best estimate of these values corresponding to the data.

b. For certain sailing lines and depths, data were not collected on both sides of the tow. Actual measured values were weighted according to distributions from Schijf equations with skew coefficients (Maynord 1990).

c. Not many velocities or wave heights were collected for the 1990 navigation research data nor the Gallipolis study. Values of return current and drawdown for these tests were based on the Schijf equations. The values resulting from this method are low (as discussed in scale effects). Due to the inadequacies of these measurements, data points were not used in the stability analysis from the NR90 and GAL data sets.

d. In the Tennessee-Tombigbee study, maximum wave height, H_{max}, was given corresponding to failure or stability. Boat speed data were not given for those points but were backed out from graphs in the report relating boat speed to wave height (Maynord and Oswalt 1986). Drawdown values corresponding to each boat speed and test condition were extracted from curves through actual measurements.

The peak hydrodynamic data corresponding to each set of stability tests are summarized in Appendix B. These data are used in the original stability analysis to determine relationships between stone failure and hydrodynamic characteristics such as waves and currents.

Dimensional Analysis

Dimensional analysis is often used in experimental studies to develop predictive equations not easily described by the laws of nature. When coupled with experimental data, the analysis can provide quantitative results in the form of predictive equations. The complexity of the problem presented in this study leads to many dimensionless parameters. Riprap design for tow-induced forces is based on essentially three sets of variables: those related to ship waves, displacement motion of the tow, and stability of the stone on the slope embankments.

Sorensen and Weggle (1984) used dimensional analysis to develop four dimensionless parameters related to ship waves. The dimensionless variables were:

(1) The vessel Froude number , already defined as $V_s/\sqrt{(gh)}$

(2) The dimensionless wave height, $H/\forall^{(1/3)}$, dependent variable

(3) Dimensionless distance from sailing line, $S/\forall^{(1/3)}$

(4) Dimensionless depth, $h/\forall^{(1/3)}$

where $\forall$ is the displacement volume of the ship, and S is the distance from the sailing line to the point where the wave height is measured.

Using dimensional analysis, the author derived the following terms for vessel displacement motion based on the variables in the Schijf equations.

(1) $(Hg)/V_s^2$, dependent variable

(2) $V_s/\sqrt{(gh)}$, vessel Froude number

(3) A_c/A_b, blockage ratio

Hudson (1957) stated in his analysis of pervious breakwaters, where λ is wave length,

> Characteristics of the motion of water particles when short-period wind waves encounter a rubble-mound breakwater are determined by the wave steepness (H/λ), the relative depth (h/λ), the relative height (H/h), the depth at the breakwater slope (h), the angle of the beach slope seaward of the breakwater, angle of seaside slope of the breakwater with the horizontal (α), the angle of obliquity of the attacking waves (β), and the shape, thickness, and porosity of the cover layer and underlayer materials.

Hudson presented his dimensional analysis of rubble-mound structures in Hudson (1979). As a result of both the analysis of the problem dynamics and the dimensional analysis, and based on several assumptions, he reduced the basic equation to the following:

$$\frac{\gamma_r^{1/3} H}{\left(\frac{\gamma_r}{\gamma_w} - 1\right) W_r^{1/3}} = f\left(\frac{H}{\lambda}, \frac{h}{\lambda}, \alpha, \text{shape, placement, \% damage}\right) \qquad (99)$$

The left side of the equation is the already defined dimensionless parameter, the stability number, N_s. Hudson assumed variations of H/h and the Reynolds number to be minimal during testing and did not include them in his analysis. He dismissed the use of repose angle altogether for reasons already discussed.

Other dimensionless variables included in studies of stone stability and vessel effects were the repose angle, surf similarity parameter, and draft vessel Froude number. In this study the stability number was plotted against many dimensionless variables. The Reynolds number, repose angle, and bank slope were determined to influence the stability number.

Scale Effects Analysis

Scale effects can exist both in the ability to reproduce the tow-induced forces and in modeling the graded stone. Boundary layer problems, low Reynolds values, and the angle of repose are addressed in an attempt to minimize scale effects and make model adjustments. Corrections to Reynolds or angle of repose would leave fewer dimensionless variables to analyze for stability.

Boundary layer effects

It has been discovered through recent navigation effects modeling at WES, that as a result of the misrepresentation of viscous forces at the model scale, the moving tow actually behaves as a larger tow. Due to the boundary layer growth, model tows have apparent drafts much larger than their equivalent prototype tows. Therefore, prototype vessels going the same respective speed as the Froudian-scaled model boat will produce lesser effects; i.e., the prototype return current and drawdown will be smaller for the same given tow configuration and speed. Results of scale effects testing revealed differences in model data, best shown graphically in Figures 33 and 34, by comparing peak return current and drawdown data between three model scales. For equivalent prototype vessel speeds, the maximum variation in return current between a 1:37.5-scale model data and 1:20-scale model data was as much as 1.5 fps (0.46 mps). For drawdown, the variation was as high as 0.57 ft (0.17 m). One would expect these scale effects to be even greater when extrapolating from say a 1:20 scale to a 1:1 scale (prototype).

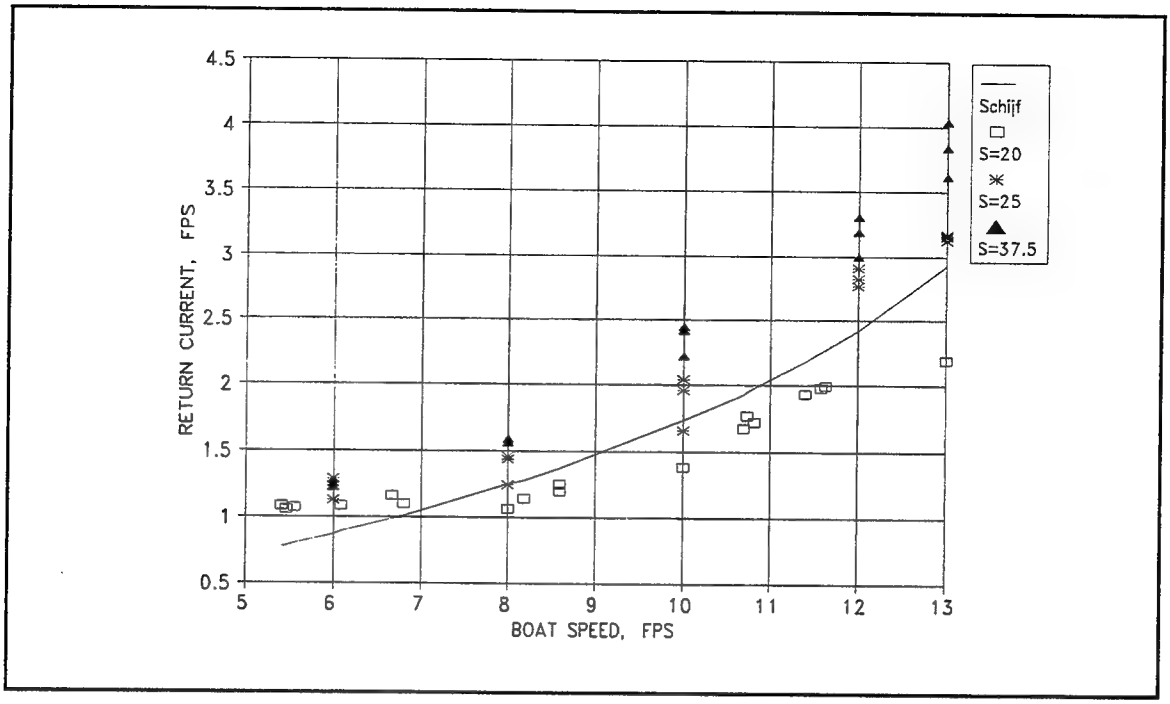

Figure 33. Results of scale effects testing, return current

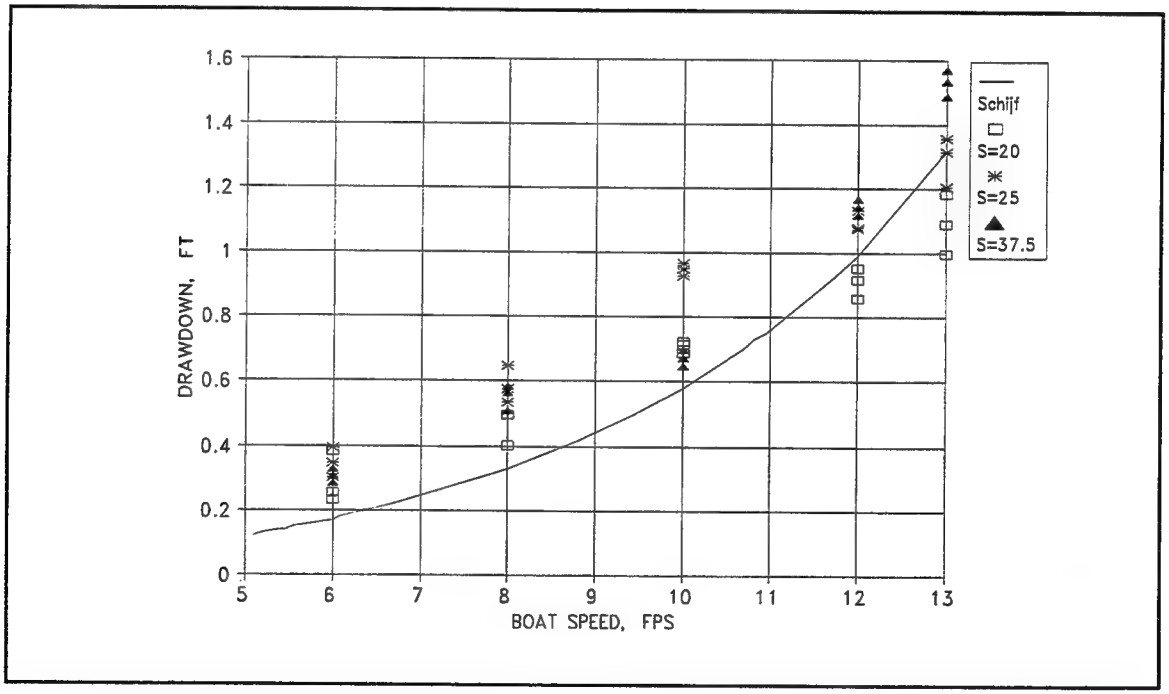

Figure 34. Results of scale effects testing, drawdown

For the navigation research, vessel speeds in the model varied approximately from 0.6 fps (0.18 mps) to 2.8 fps (0.85 mps), and for the Tennessee-Tombigbee study, 1.3 fps (0.40 mps) to 3.6 fps (1.10 mps). According to Sorensen (1966), only boat speeds greater than approximately 1.8 fps (0.5 mps) should be tested to minimize scale effects.

As a result of these discrepancies, design guidance regarding riprap stability as a direct function of boat speed has been avoided in this analysis. Relationships in the analysis were primarily sought relating the actual model values of tow-induced currents and waves to stability. Boundary layer scale effects also prohibited attaining limiting or critical prototype vessel speeds in the model; thus making it essentially impossible to create conditions that would fail the larger stones.

Reynolds criteria

Assuming that stone size is a function of wave height cubed, as in the literature formulations, implies that the stability number, N_s, is essentially constant for a given slope. Some authors included the angle of repose, surf similarity parameter, or the number of waves but most suggest a constant value of N_s. Observations during the NR93 testing suggested smaller stone sizes exhibited greater instabilities, consequently smaller stability numbers. These observations may be attributed in part to low model Reynolds values. Fuehrer, Romisch, and Engelke (1981) also found N_s to vary with Reynolds, while conducting tests with very small diameter stones for vessel-induced wave heights. Oumeraci (1984) determined N_s to be smaller at low Reynolds and recommended adjusting values of N_s to compensate.

One way of evaluating low Reynolds values is to compare computed numbers in the model to recommended values from the literature. In summary, recommended critical values of particle Reynolds numbers in a wave environment varied according to the source as follows:

a. Fuehrer, Romisch, Engelke (1981) : 1000

b. Jensen (1989): 6000 - 7000

c. Dai and Kamel (1969): 3×10^4

d. Hudson (1957): 3×10^4

e. Oumeraci (1984): 3×10^4

f. Broderick and Ahrens (1982): 10^5

Particle Reynolds values for maximum and minimum stone sizes and wave heights were computed based on Equation 89 for a kinematic viscosity of water at 60° F (16° C). The equation is presented in several forms in Chapter 2, and Table 10 presents these computation results. The largest computed Reynolds value for model stone and wave height was used in the Tennessee-Tombigbee study. With a model diameter of 0.046 ft (0.014 m) and a maximum model wave height of 0.175 ft (0.046 m), the computed Reynolds value is 9×10^3. The smallest Reynolds value was less than 400. According to these calculations, none of the data would meet Dai and Kamel's (1969), Hudson's (1957) or Broderick and Ahren's (1982) criteria. To meet Jensen's criteria, the minimum model wave height for the smallest stone would have to be 1.42 ft (0.43 m)! All data, except wave heights less than 0.04 ft (0.01 m) imposed on the smallest model stone, have Reynolds values exceeding 1,000.

Table 10
Computed Values of Model Particle Reynolds

D_{50} Prototype in.	D_{50} Model ft	H_{max} Model ft	R Model
Navigation Research			
3.25	0.011	0.005	3.6×10^2
3.25	0.011	0.160	1.9×10^3
5.8	0.019	0.005	6.3×10^2
5.8	0.019	0.160	3.5×10^3
8.1	0.027	0.005	1.5×10^3
8.1	0.027	0.160	5.0×10^3
11.1	0.037	0.005	1.2×10^2
11.1	0.037	0.160	6.9×10^3
Tennessee-Tombigbee Study			
6.3	0.026	0.005	8.6×10^2
6.3	0.026	0.175	5.1×10^3
8.1	0.034	0.005	4.0×10^3
8.1	0.034	0.175	6.6×10^3
11.1	0.046	0.005	1.5×10^3
11.1	0.046	0.175	8.9×10^3

Reynolds values can be computed independent of particle size. Using Equation 92 developed by Jonsson (1966), the Reynolds values related to wave runup should be greater than 10^4. Varying the model time periods, from 0.5 to 2 seconds, and solving

Equation 92 for A, Table 11 gives the minimum model values of runup according to this criteria. The actual wave periods measured in the model ranged from about 0.5 to 0.8 seconds. Computed minimum values of runup for these periods on a 2H:1V or 3H:1V slopes are from 0.033 ft (0.01 m) to 0.062 ft (0.019 m). As an approximation, runup is on the order of 3.0 times the actual wave height. The *Shore Protection Manual* (1984) and Broderick's tabular data (Broderick and Ahren 1982) suggest that this multiplier is appropriate. Calculations regarding wave runup will be discussed later. Therefore, the minimum acceptable range for wave heights in the model is from 0.011 to 0.02 ft (0.003 to 0.006 m). The equivalent prototype runup conditions considered valid in the model, according to this criteria, for a 3-second prototype wave period are:

a. Tennessee-Tombigbee - For 2H:1V slope, H > 1.16 ft (0.35 m).

b. Navigation Research - For 2H:1V slope, H > 1.35 ft (0.41 m) and for 3H:1V slope, H > 0.89 ft (0.27 m).

Table 11
Minimum Values of Model Wave Runup to Satisfy Reynolds Criteria

Model Wave Period, seconds	Runup, ft for cot $\alpha = 2$	Runup, ft for cot $\alpha = 3$	Runup, ft for cot $\alpha = 4$
0.5	0.049	0.033	0.025
0.6	0.054	0.036	0.027
0.7	0.058	0.039	0.029
0.8	0.062	0.042	0.031
0.9	0.066	0.044	0.033
1.0	0.070	0.046	0.035
1.2	0.076	0.051	0.038
1.5	0.085	0.057	0.043
2.0	0.098	0.066	0.049

Since recommended critical values of Reynolds numbers range from 1,000 to 100,000, a minimum value was sought using the model data as it relates to the stability number. N_s was computed using the maximum wave height, H_{max}, observed during each stability test. The graph in Figure 35 shows the computed values of particle Reynolds numbers for all TT and NR93 stability data for a 2H:1V slope.

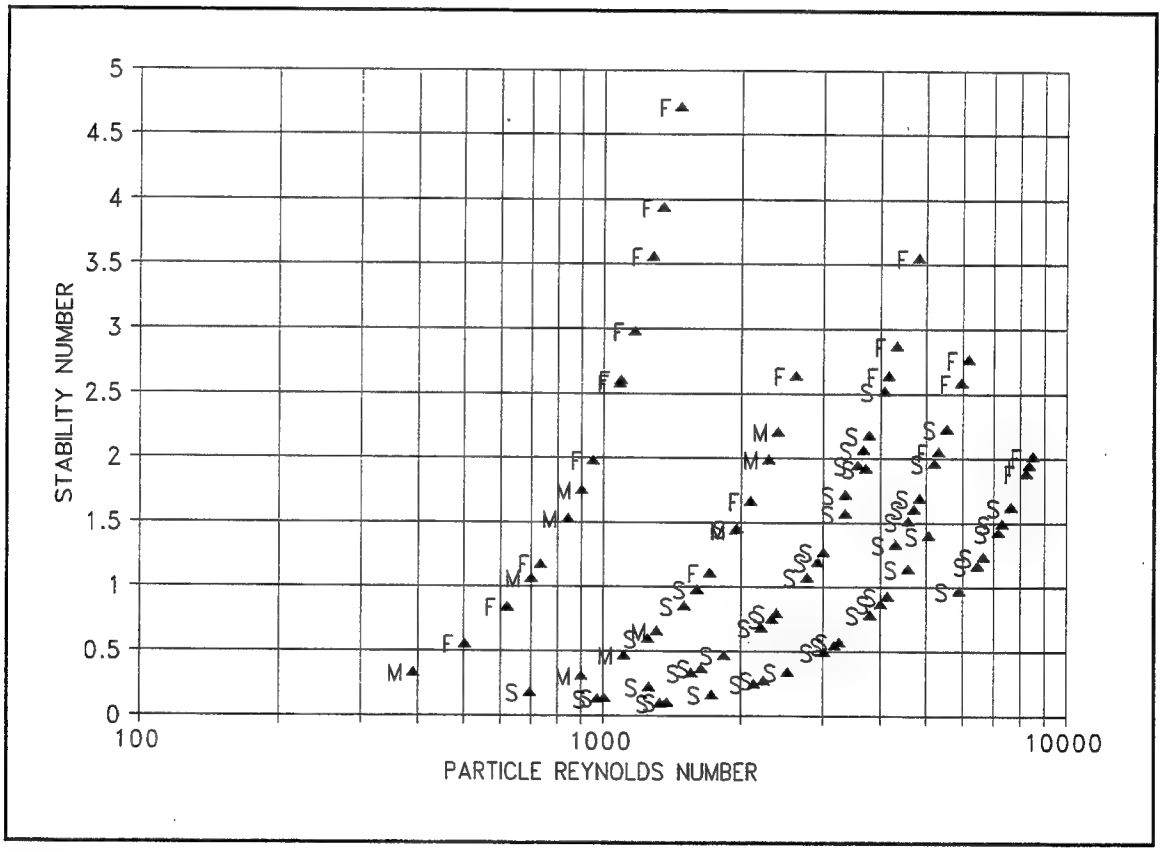

Figure 35. Stability number as a function of particle Reynolds number, 2H:1V slope

N_s is plotted as a function of the wave Reynolds number in Figure 36. On both graphs, more failed points are observed at lower Reynolds values. On either graph a clear relationship does not appear, such that N_s could be adjusted based on a Reynolds value as Oumeraci (1984) suggested.

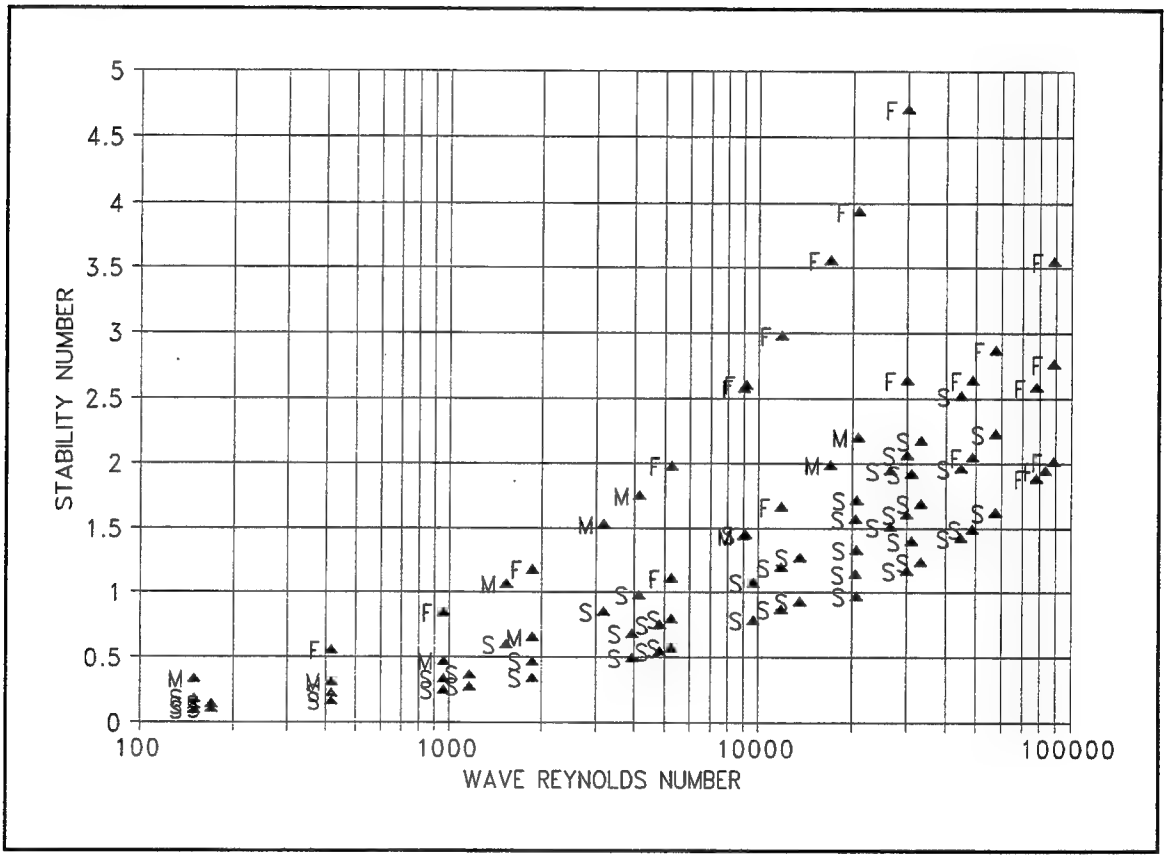

Figure 36. Stability number as a function of wave Reynolds number, 2H:1V slope

Angle of repose

According to the literature, the angle of repose decreases for small stone sizes and as the relative height of the revetment, L/D_{50}, increases, particularly for those less than approximately 2 in. The average diameter, D_{50}, of the model stone sizes ranged from

0.13 to 0.56 in. (3.3 to 14 mm), and for full range of gradations the sizes were as small as 0.092 in. (2.3 mm) and as large as 1.0 in. (25.4 mm). These variations equate to differences in ϕ from the smallest to largest model stones of 3 to 5 deg based on either the "Bureau" or "Simons" curve in Figure 10. Differences from model to prototype could be as high as 10 deg.

The actual length of the model slope ranged from approximately 1.6 to 2.4 ft (0.5 to 0.7 m). This resulted in relative revetment heights in the model of approximately 35 to 220. According to a figure relating angle of repose to this ratio in Maynord (1988), the angle of repose value at L/D_{50} equal to 35 was 45 deg and decreased to a minimum datum of 38.4 deg. Values were not given for ranges of L/D_{50} greater than approximately 42.

The variation in ϕ between the largest and smallest gradations, from either perspective, equates to potential impacts from the angle of repose on stone slope stability. To evaluate these impacts, a value of ϕ was assigned to each model stone gradation based on the "Simons" curve in Figure 10. The prototype diameter, model diameter and corresponding angle ϕ are found in Table 12.

The stability number was evaluated as a function of the angle of repose, in the same manner as the Reynolds number. Figure 37 shows the angle of repose for each respective model gradation versus the stability number calculated using H_{max} for a 2H:1V slope. As can be seen, the smaller angle of repose values shows more failed points at lower stability numbers. A clear delineation or relationship between ϕ and N_s cannot be developed without more data.

Table 12
Model Angle of Repose

Study	D_{50} prototype, in.	D_{50} model, ft	ϕ deg
TT	11.1	0.0463	37.5
NR	11.1	0.0370	36.6
TT	8.1	0.0338	36.4
NR	8.1	0.0270	35.9
TT	6.3	0.0263	35.8
NR	6.3	0.0210	35.6
GAL	6.0	0.0200	35.4
NR	5.8	0.0193	35.2
NR	3.25	0.0108	34.2

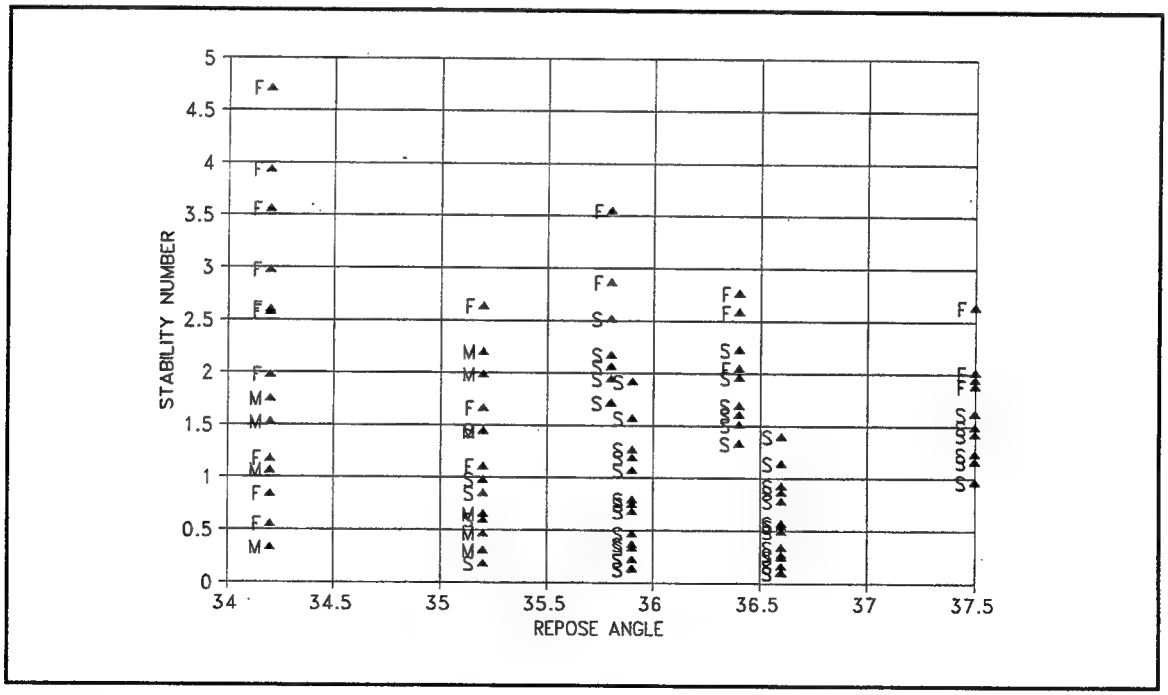

Figure 37. Stability number as a function of the angle of repose, 2H:1V slope

Three methods were evaluated to calculate a factor for adjusting the stone diameter based on the angle of repose variations between gradations in the model stone. Method 1 is based on the shear approach presented in Equation 76 from Blaauw et al. (1984), where the diameter is a function of k_d. In method 2, the coefficient is based on Hedar's formulation for a downrushing wave, Equation 59, where D is a function of K_{down}, $\tan\phi$, and α. Finally, method 3 employs a coefficient from Iribarren's formulation in Equations 97 and 98 containing ϕ. These methods are used to determine if an adjustment can or should be made to the model stone diameters.

In the shear approach used in Method 1, K_1 is assumed to equal k_d, and computed according to Equation 77. The stone diameter, D, is related to K_1 as

$$D \propto \frac{1}{K_1} \tag{100}$$

In method 2 for a downrushing wave on an impervious straight slope, the stable stone size was related to K_{down} as

$$D = \frac{H}{\left(\frac{\gamma_r}{\gamma_w} - 1\right)} \cdot \frac{1}{\frac{16\pi}{3}} \cdot \frac{K_{down}}{(\tan\phi\cos\alpha - \sin\alpha)} \tag{101}$$

Values for K_{down} were taken from Figure 65.3 in Hedar (1960).

Letting

$$K_2 = \frac{K_{down}}{(\tan\phi \cos\alpha - \sin\alpha)} \tag{102}$$

then,

$$D \propto K_2 \tag{103}$$

In method 3, letting K_3 equal k_ϕ in Equation 97, then

$$D \propto K_3 \tag{104}$$

Table 13 contains calculated values for each K coefficient at two slope angles and for a range of repose angles between 30 to 50 deg. Generally, the K factor increases with decreasing angles of repose and increasing bank slope. Since these values are presented as directly proportional to stone diameter, one can conclude that regardless of method, the angle of repose can impact effective diameter. It is also shown that there are larger differences in the K coefficients at smaller angles of repose, for example between 30 and 35 deg, than at higher angles, 45 to 50 deg. Variations in K are smaller for flatter bank slopes than for steeper slopes. It can also be seen that the shear-stress-related

Table 13
Calculation of K Values for Wide Variation in Repose Angle

cot α	ϕ	K_1^{-1}	K_2	K_3
2	30	2.247	52.57	8.431
2	35	1.600	26.92	3.926
2	40	1.394	19.83	2.774
2	45	1.292	16.13	2.240
2	50	1.233	13.60	1.929
3	30	1.289	24.12	2.487
3	35	1.187	19.21	2.008
3	40	1.148	16.44	1.746
3	45	1.118	14.37	1.579
3	50	1.098	11.04	1.462

factors are smaller than the factors from the wave-related methods. Then for the experiments where ϕ varies between approximately 34 and 38 deg, and particularly for the 2H:1V slope, the angle of repose should be considered as contributing to the effective diameter of the model stone, and consequently, to its stability.

Of the three methods, it was assumed that methods 2 and 3 would be more valid since waves were considered the dominating force in these tests. In evaluating the factors based on Hedar's formulation (method 2), the factors did not give intuitive results. For instance, for angles of repose from 45 to 50 deg, the difference in K values for a 2H:1V slope were smaller than for a 3H:1V slope. The steeper slope should experience more instabilities than the flatter slope for the same change in ϕ. Therefore, Iribarren's

formulation (method 3) was assumed appropriate for this application. Table 14 contains computed values of K_3 for each model gradation and slope tested.

Table 14
Values of K_3 for Each Model Condition

Study	D_{act}	ϕ	K_3 cot α= 2	K_3 cot α = 3
TT	0.0463	37.5	3.22	1.86
NR	0.0370	36.6	3.43	1.91
TT	0.0338	36.4	3.49	1.92
NR	0.0270	35.9	3.63	1.95
TT	0.0263	35.8	3.66	1.96
NR	0.0210	35.6	3.72	1.97
GAL	0.0200	35.4	3.79	1.98
NR	0.0193	35.2	3.86	1.99
NR	0.0108	34.2	4.26	2.06

To compensate for differences resulting from the angle of repose, the model diameters were normalized based on an adjustment factor related to the computed values of K_3. Two different factors were generated, one for adjusting the model rock sizes to the largest model size and one for adjusting all model sizes to an approximate prototype size. Model diameters were adjusted according to

$$D_{eq} = \frac{K_{max}}{K_{act}} \times D_{act} \qquad (105)$$

where

D_{eq} = equivalent stone diameter, ft (m)

K_{max} = maximum K_3 value for normalizing data

K_{act} = actual K_3 value corresponding to each model test condition

D_{act} = actual stone diameter used in each model test, ft (m)

The equivalent prototype diameters normalized to the largest model stone are represented in the Table 15. K_{max} corresponds to a 37.5-deg angle of repose. The actual diameters, column 2, represent the geometrically scaled gradations used in the model tests. The factors in columns 4 and 5 are the ratio K_{max}/K_{act} where K_{max} for a 2H:1V slope at ϕ equals 37.5 deg is 3.22, and for a 3H:1V slope is 1.86. Values for K_{max} and K_{act} are calculated based on values of K_3 in Table 14. Equivalent diameters, columns 6 and 7, are normalized by multiplying column 2 by columns 4 or 5, respectively, for a 2H:1V slope or 3H:1V slope.

Table 16 represents adjusted values of the D_{50} stone diameters to prototype stone size based on an assumed 42-deg angle of repose. The values in this table are obtained using the K_3 formulation and adjusting the values accordingly as in Table 15. K_{max} for a 2H:1V slope at ϕ equals 42 deg is 2.52, and for a 3H:1V slope is 1.671.

Table 15
Equivalent Prototype D_{50} Normalized Based on ϕ of 37.5 deg

1 Study	2 D_{act} prototype, in.	3 ϕ deg.	4 K_{max} /K_{act} 2H:1V	5 K_{max} /K_{act} 3H:1V	6 D_{eq} 2H:1V in.	7 D_{eq} 3H:1V in.
TT	11.1	37.5	1.00	1.00	11.1	--
NR	11.1	36.6	0.94	0.97	10.43	10.77
TT	8.1	36.4	0.92	0.97	7.45	--
NR	8.1	35.9	0.89	0.95	7.21	7.70
TT	6.3	35.8	0.88	0.95	5.54	--
NR	6.3	35.6	0.87	0.94	5.45	5.95
GAL	6.0	35.4	0.85	0.94	--	5.64
NR	5.8	35.2	0.83	0.93	4.81	5.39
NR	3.25	34.2	0.76	0.90	2.47	2.93

Table 16
Equivalent Prototype D_{50} Normalized Based on ϕ of 42 deg

1 Study	2 D_{act} prototype, in.	3 ϕ deg.	4 K_{max} /K_{act} 2H:1V	5 K_{max} /K_{act} 3H:1V	6 D_{eq} 2H:1V in.	7 D_{eq} 3H:1V in.
--	--	42.0	1.00	1.00	--	--
TT	11.1	37.5	0.78	0.90	8.66	--
NR	11.1	36.6	0.73	0.87	8.10	9.66
TT	8.1	36.4	0.72	0.87	5.83	--
NR	8.1	35.9	0.69	0.86	5.59	6.97
TT	6.3	35.8	0.69	0.85	4.35	--
NR	6.3	35.6	0.68	0.85	4.28	5.36
GAL	6.0	35.4	0.66	0.84	--	5.04
NR	5.8	35.2	0.65	0.84	3.77	4.87
NR	3.25	34.2	0.59	0.81	1.92	2.63

Final criteria for adjustment of model data

Several approaches could be taken to compensate for the angle of repose variations, Reynolds effects, and/or boundary layer problems. They are as follows:

a. Data could be eliminated below a critical Reynolds criteria.

b. Data associated with the smallest model stone gradation could merely be thrown out.

c. Model stone sizes could be normalized to either the largest model size or to an approximate prototype size.

d. The model stone sizes could be adjusted and then a Reynolds criteria applied.

Based on the investigation of Reynolds criteria, it is obvious that a wide range of criteria exist for evaluation of model scale effects due to low Reynolds values. Without doubt, the larger scales result in larger particle Reynolds numbers and wave Reynolds numbers. Like Broderick and Ahrens (1982), in this research, N_s was found to be lower at small wave heights and rock sizes. Since Reynolds criteria did not explain all the 20 percent differences observed in their testing and was uncertain in this testing, this method was not considered effective by itself to compensate for scale effects.

Removing the smallest stone has a two-fold advantage. It leaves larger stones that have higher angles of repose (closer to prototype) and retains threshold points in the data that are subject to higher Reynolds numbers. Remember that the smallest diameter model stones were not valid for many test conditions using any of the Reynolds criteria.

However, simply removing the small rock data does not eliminate scale effects for larger model rock sizes and removes some data points that meet Reynolds criteria.

Normalizing diameters to the maximum model size indicates that observations of failure in the model tests provide conservative solutions. Furthermore, diameters normalized to a "prototype" value would indicate that the size of the prototype stones could be as much as 40 percent smaller than their model counterparts. Due to insufficient data regarding model to prototype, differences in the angle of repose were not adjusted to "prototype" values. This means that the actual stones sizes are still conservatively represented in the model. Adjusting the model diameters alone, does not eliminate potential Reynolds effects, it simply compensates for a property of the material that is not generally a factor at the prototype scale.

The final method was adopted for compensation of scale effects. First, the stone diameters were normalized to the maximum model stone size as in Table 15 and second, a wave Reynolds criteria was applied to all the data. All stability tests that corresponded to z_{max}, H_{max}, and H_i with magnitudes approximately less than 0.6 in. (1.5 cm) in the model were discarded. If any of the three model wave heights met the criteria, they were kept in the data set. Table 17 contains the final adjusted data set, in prototype dimensions, used in the stability analysis for the 2H:1V slope. Table 18 contains the final adjusted data set for the 3H:1V slope.

Table 17
Final Data Set for 2H:1V Slope in Prototype Dimensions

Data Set	Water depth, h ft	Vessel Speed, V_s fps	Adjusted D_{50} in.	W_{50} lbs	Stability F/M/S	z_{max} ft	H_{max} ft	H_i ft	u_r fps
NR93	15	10	2.47	0.76	F	1.3	1.17	0.47	3.49
NR93	20	10	2.47	0.76	F	1.19	1.16	0.41	3.07
NR93	15	10	4.81	5.60	S	1.3	1.17	0.47	3.49
NR93	20	10	4.81	5.60	M	1.19	1.16	0.41	3.07
NR93	15	10	7.21	18.85	S	1.58	1.43	0.58	4.15
NR93	15	10	10.43	57.07	S	1.58	1.43	0.58	4.15
NR93	20	12	2.47	0.76	F	1.71	1.6	1.29	4.16
NR93	15	12	2.47	0.76	F	2	1.77	1.11	4.87
NR93	15	12	4.81	5.60	M	2	1.77	1.11	4.87
NR93	20	12	4.81	5.60	M	1.71	1.6	1.29	4.16
NR93	20	12	7.21	18.85	S	1.3	1.21	0.76	2.84
NR93	15	12	7.21	18.85	S	2.44	2.16	1.35	5.8
NR93	20	12	10.43	57.07	S	1.09	0.89	0.9	2.63
NR93	15	12	10.43	57.07	S	2.44	2.16	1.35	5.8

(Sheet 1 of 4)

Table 17 (Continued)

Data Set	Water depth, h ft	Vessel Speed, V_s fps	Adjusted D_{50} in.	W_{50} lbs	Stability F/M/S	z_{max} ft	H_{max} ft	H_i ft	u_r fps
NR93	20	12	10.43	57.07	S	1.3	1.21	0.76	2.84
NR93	20	14	2.47	0.76	F	1.59	1.34	1.81	3.24
NR93	20	14	2.47	0.76	F	2.32	2.12	1.83	5.4
NR93	20	14	4.81	5.60	F	2.32	2.12	1.83	5.4
NR93	20	14	4.81	5.60	F	1.59	1.34	1.81	3.24
NR93	20	14	7.21	18.85	S	1.87	1.76	1.375	3.71
NR93	20	14	7.21	18.85	S	1.59	1.34	1.81	3.24
NR93	20	14	10.43	57.07	S	1.87	1.76	1.375	3.71
NR93	20	14	10.43	57.07	S	1.59	1.34	1.81	3.24
TT	14	8.6	5.54	8.55	S	1.9	1.5		4.25
TT	14	8.6	7.45	20.80	S	1.9	1.5		4.25
TT	14	8.6	11.1	68.79	S	1.9	1.5		4.25
TT	18	10.6	5.54	8.55	S	1.85	1.5		
TT	18	10.6	7.45	20.80	S	1.85	1.5		
TT	18	10.6	11.1	68.79	S	1.85	1.5		

(Sheet 2 of 4)

Table 17 (Continued)

Data Set	Water depth, h ft	Vessel Speed, V_s fps	Adjusted D_{50} in.	W_{50} lbs	Stability F/M/S	z_{max} ft	H_{max} ft	H_i ft	u_r fps
TT	18	11.2	5.54	8.55	S	2.1	1.8		
TT	18	11.2	7.45	20.80	S	2.1	1.8		
TT	18	11.2	11.1	68.79	S	2.1	1.8		
TT	22	12.1	5.54	8.55	S	1.7	1.9		
TT	22	12.1	7.45	20.80	S	1.7	1.9		
TT	22	12.1	11.1	68.79	S	1.7	1.9		
TT	22	12.8	5.54	8.55	S	1.9	2.2		
TT	22	12.8	7.45	20.80	S	1.9	2.2		
TT	22	12.8	11.1	68.79	S	1.9	2.2		
TT	14	13	5.54	8.55	S	2.2	1.5		
TT	14	13	7.45	20.80	S	2.2	1.5		
TT	14	13	11.1	68.79	S	2.2	1.5		
TT	14	13.3	5.54	8.55	F	2.9	3.1		
TT	14	13.3	7.45	20.80	F	2.9	3.1		
TT	14	13.3	11.1	68.79	F	2.9	3.1		

Table 17 (Concluded)

Data Set	Water depth, h ft	Vessel Speed, V_s fps	Adjusted D_{50} in.	W_{50} lbs	Stability F/M/S	z_{max} ft	H_{max} ft	H_i ft	u_r fps
TT	17.5	14.7	5.54	8.55	S	1.7	1.7		7.17
TT	17.5	14.7	7.45	20.80	S	1.7	1.7		7.17
TT	17.5	15	5.54	8.55	F	2.3	2.3		7.44
TT	17.5	15	7.45	20.80	F	2.3	2.3		7.44
TT	17.5	15	11.1	68.79	S	2.3	2.3		7.44
TT	17.5	15.3	11.1	68.79	F	3	3		7.72
TT	21	15.6	5.54	8.55	S	1.5	1.7		5.1
TT	21	16.4	5.54	8.55	F	2.15	2.5		5.4
TT	21	16.4	7.45	20.80	S	2.15	2.5		5.4
TT	21	16.4	11.1	68.79	S	2.15	2.5		5.4
TT	21	16.7	7.45	20.80	F	2.8	2.9		5.5
TT	21	16.7	11.1	68.79	F	2.8	2.9		5.5

(Sheet 4 of 4)

Table 18
Final Data Set for 3H:1V Slope in Prototype Dimensions

Data Set	Water depth, h ft	Vessel Speed, V_s fps	Adjusted D_{50} in.	W_{50} lbs	Stability F/M/S	z_{max} ft	H_{max} ft	H_i ft	u_r fps
NR93	20	10	2.93	1.27	F	1.21	1.45	0.45	2.91
NR93	15	10	2.93	1.27	M	1.75	2.15	0.5	3.04
NR93	20	10	5.39	7.88	M	1.21	1.45	0.45	2.91
NR93	15	10	5.39	7.88	S	1.75	2.15	0.5	3.04
NR93	15	10	7.7	22.96	S	2.11	2.59	0.6	3.62
NR93	15	10	10.77	62.84	S	2.11	2.59	0.6	3.62
NR93	15	12	2.93	1.27	F	3.01	3.68	0.53	3.77
NR93	20	12	2.93	1.27	F	1.31	1.78	1.36	2.38
NR93	20	12	2.93	1.27	F	2.27	2.78	1.99	3.98
NR93	20	12	5.39	7.88	M	2.27	2.78	1.99	3.98
NR93	20	12	5.39	7.88	M	1.31	1.78	1.36	2.38
NR93	15	12	5.39	7.88	M	3.01	3.68	0.53	3.77
NR93	20	12	7.7	22.96	S	1.31	1.78	1.36	2.38
NR93	20	12	7.7	22.96	S	1.6	2.17	0.9	2.7
NR93	15	12	7.7	22.96	S	3.63	4.43	0.64	4.49

(Continued)

Table 18 (Concluded)

Data Set	Water depth, h ft	Vessel Speed, V_s fps	Adjusted D_{50} in.	W_{50} lbs	Stability F/M/S	z_{max} ft	H_{max} ft	H_i ft	u_r fps
NR93	20	12	10.77	62.84	S	1.31	1.78	1.36	2.38
NR93	15	12	10.77	62.84	S	3.63	4.43	0.64	4.49
NR93	20	12	10.77	62.84	S	1.6	2.17	0.9	2.7
NR93	20	14	2.93	1.27	F	1.87	2.66	1.625	2.95
NR93	20	14	2.93	1.27	F	3.59	4.45	3.19	5.22
NR93	20	14	5.39	7.88	M	1.87	2.66	1.625	2.95
NR93	20	14	5.39	7.88	F	3.59	4.45	3.19	5.22
NR93	20	14	7.7	22.96	S	1.87	2.66	1.625	2.95
NR93	20	14	7.7	22.96	S	2.54	3.4	1.575	3.58
NR93	20	14	10.77	62.84	S	2.54	3.4	1.575	3.58
NR93	20	14	10.77	62.84	S	1.87	2.66	1.625	2.95

Stability Analysis

Much effort has been made to minimize scale effects due to both low Reynolds values and repose angle of the model stone. It is important to emphasize in the deterministic design of bank protection for tow-induced impacts that the critical design parameters lie on the upper bound of impacts. Model data used for analysis in that range of impacts are the least effected by any scale problem. Based on the critical examination of scale effects and the adjustments made accordingly, this data set is believed to be valid for evaluating stone slope stability due to tow-induced impacts.

The experimental approach adopted for this study of riprap protection for tow-induced forces leads us to an integrated solution. That is, the stable bank protection observed from this testing is exposed to the total energy imparted by the passing vessel including pore water pressures due to drawdown, shear stresses due to velocities, and lift and drag forces due to waves. The issue then becomes what general equation for riprap design can be used considering all the different causal mechanisms acting on the bank?

There are basically three approaches one could take in devising a methodology for the design stone slope protection from the integrated testing. First, considering that the indirect causes of bank failure are the vessel speed, its hull form, the shape of the channel, and the sailing line, the stability of stone slope protection could be directly related to these mechanisms. The advantage of this approach is that it is an absolutely integrated solution. The effects are related to characteristics of the waterway that are essentially

given. There is no added error due to prediction of measurement of forces or in coupling the causal mechanisms. The problem with this approach is that considerably more data are needed to develop relationships between stability and say blockage ratio or boat speed. This approach would also be more empirically based and is not an accepted methodology like the Hudson or Isbash equations. Second, an integrated solution could be developed such that the total energy of the direct causal mechanisms (front wave, gradients, drawdown, stern wave, return current, secondary waves, etc.) is related to the stability of the stone. Each force could be predicted or measured and plugged into a single stability equation. The disadvantages of this approach include not knowing the relative contributions to riprap failure of each force component, the inability to account for the spatial and temporal application of these forces on the slope, and the variability in the equations for predicting each of the forces. The form of this equation is not known, but it is probably not an accepted or standard solution. The third approach for development of a general equation for riprap stability is to use the most dominant or characteristic force or forces in an existing stability equation with empirical coefficients designed for each mechanism. This is essentially the approach taken in the PIANC (1987) guidance. Evaluating the stone size from either a return current, stern wave, or secondary wave equation not only reduces the bias of looking at one solution, but adds a degree of safety by giving the designer the option of picking the most conservative answer. The approach is relatively simple. Conversely, the results or empirical coefficients developed from the integrated data sets are likely biased because the parameters are not truly separated. Furthermore, the approach may oversimplify the problem. In a

related approach, one or more variables that best represent an integrated solution can be selected. Blauuw et al. chose a "characteristic stern wave" for his solution. More than one characteristic parameter could be used in this approach.

The third method of stability analysis was adopted. Since existing methods for designing riprap are based on either a shear stress approach, velocity, or waves, the stability analysis included an evaluation of these approaches with several dominant mechanisms.

Return current

An attempt was made to use the shear stress approach presented by Blaauw et al. (1984) in Equations 72-77 with data collected from this research. Observations in the model did not comply to the suggested stability criteria. However, this may be due to the evaluation of the drag coefficient. Based on information from Schlicting (1979), the equation used for the drag coefficient may not be appropriate for gravel and riprap size materials. And since the drag coefficient is a function of Reynolds number, it may not be valid for the conditions tested in the model.

Both Blaauw et al. (1984) and PIANC (1987) ultimately recommend the use of an Isbash type approach for evaluating return currents. The observed data are compared to Equation 78 in Figure 38, where the stone size is related to the maximum return currents. An average value of the coefficient, k_1, of 1.35 was selected for the analysis. The line represents the suggested failure threshold. Points above the line should be stable and below, failed. As seen by the figure, all observations did not adhere to the criteria. That

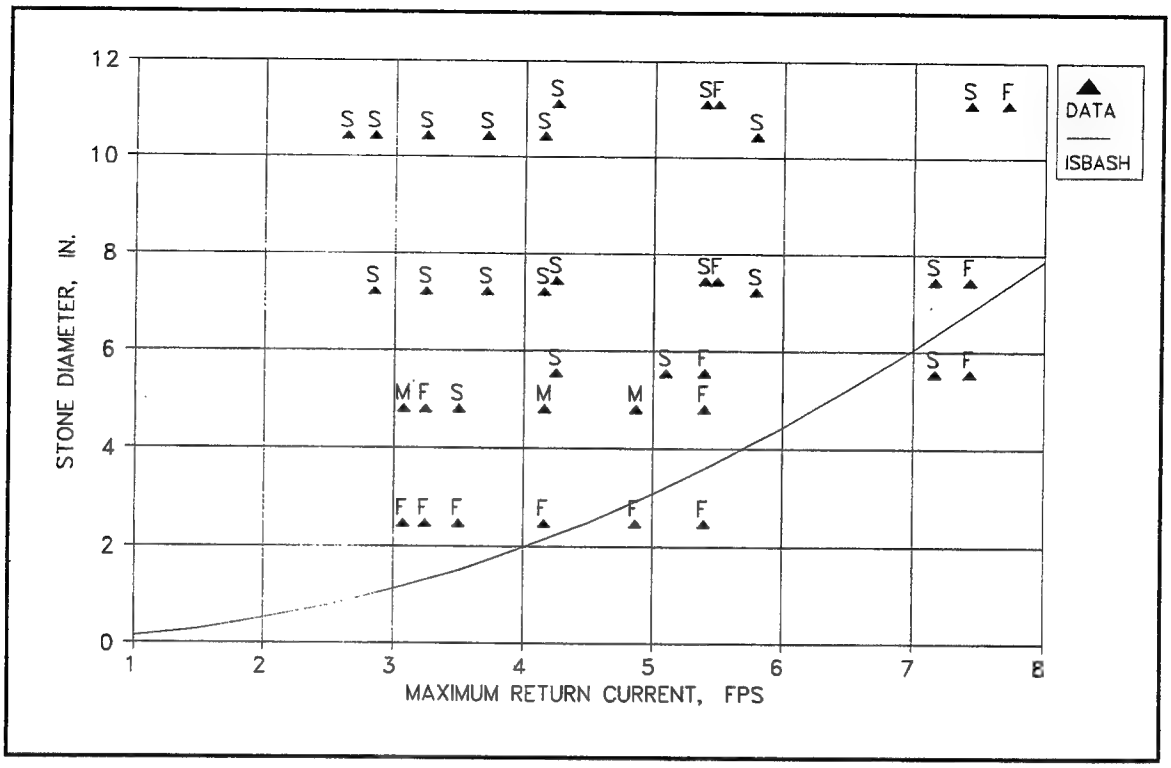

Figure 38. Analysis of return current using Isbash approach, 2H:1V

is, many failure points were observed above the Isbash failure threshold. This is probably due to the fact that the return current does not cause failure of the stone on the upper bank. Other mechanisms are involved in the failure process that are not captured in this approach.

Waves

Three characteristic waves were chosen to analyze using the wave-based stability approach presented by Iribarren, Hudson, and others. They were the maximum

drawdown at the stern, z_{max} ; the maximum secondary wave, H_i ; and the maximum stern wave, H_{max} . Figures 39 and 40 show how the final adjusted data for D_{50} and z_{max} , compare to Hudson's equation with stability coefficients of 1.86 and 2.13 for 2H:1V and 3H:1V, respectively. Data below Hudson's threshold would indicate potential failure of the stone, while data above it are within the safe threshold. All the observed failure points fall on or below Hudson's safe threshold.

In Figures 41 and 42 , the peak secondary waves associated with observed data points are compared to Hudson's equation. There were few values for H_i , and consequently, few data points to delineate a failure threshold. Recall, secondary wave data were not available for the TT data. Also, if any wave height exceeded the minimum required to meet the Reynolds criteria, all data pertaining to that data set were retained in the plots. Ignoring values of H_i less than approximately 1 ft, the failure points remaining were still below the threshold.

Since the actual height of the stern wave can differ from z_{max} , H_{max} was chosen as an alternative for a characteristic parameter associated with the stern wave. However, both secondary waves and the maximum stern wave showed a strong relationship to z_{max} as was shown in Figure 30. Figures 43 and 44 show the relationship of the observed data to Hudson's equation. As in Figures 39 and 40, the separation of failed and stable points adhered to the Hudson criteria. Hudson's equation. As in Figures 39 and 40, the separation of failed and stable points adhered to the Hudson criteria.

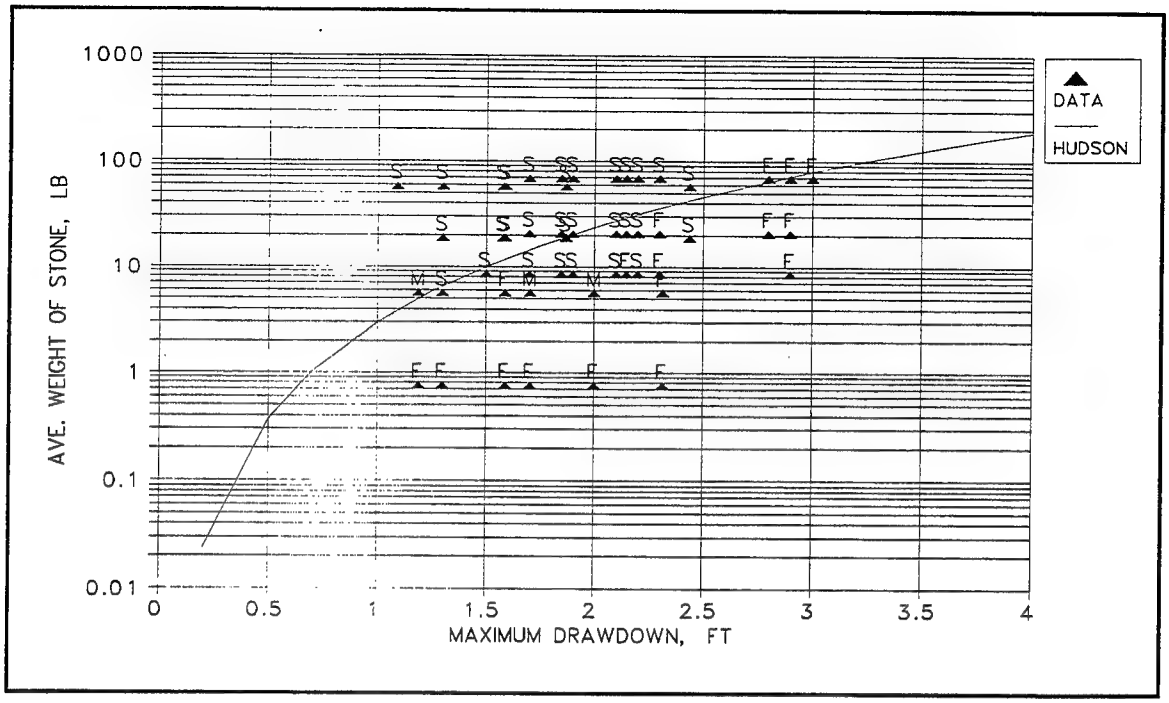

Figure 39. Analysis of z_{max} using Hudson approach, 2H:1V

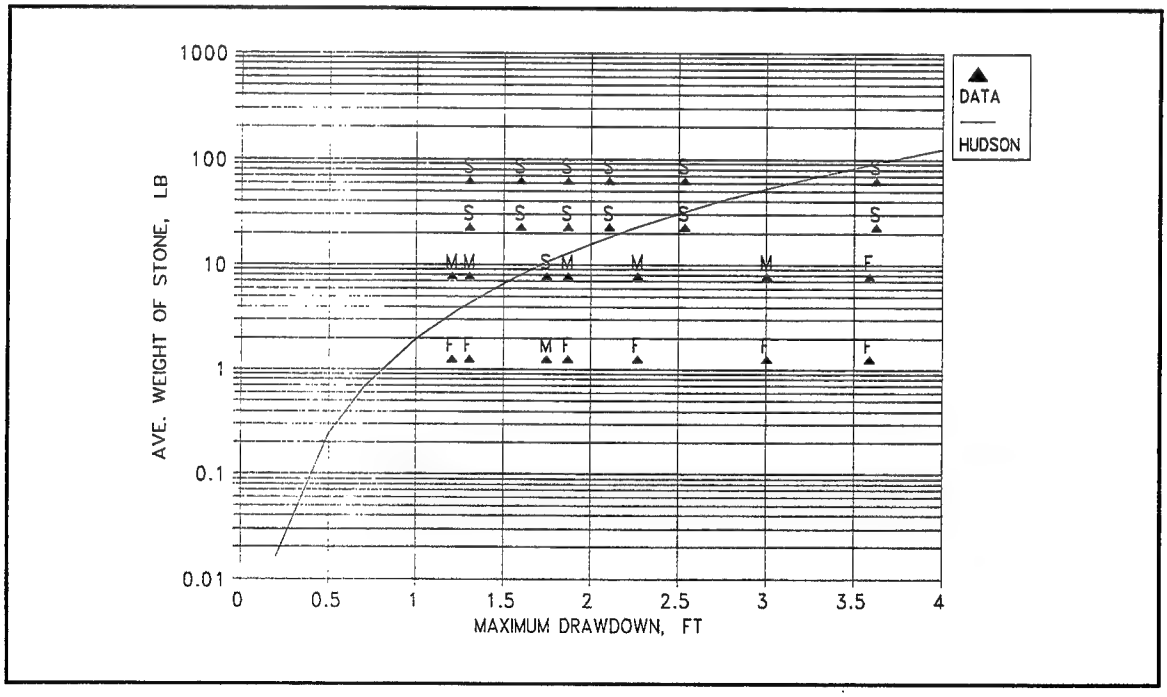

Figure 40. Analysis of z_{max} using Hudson approach, 3H:1V

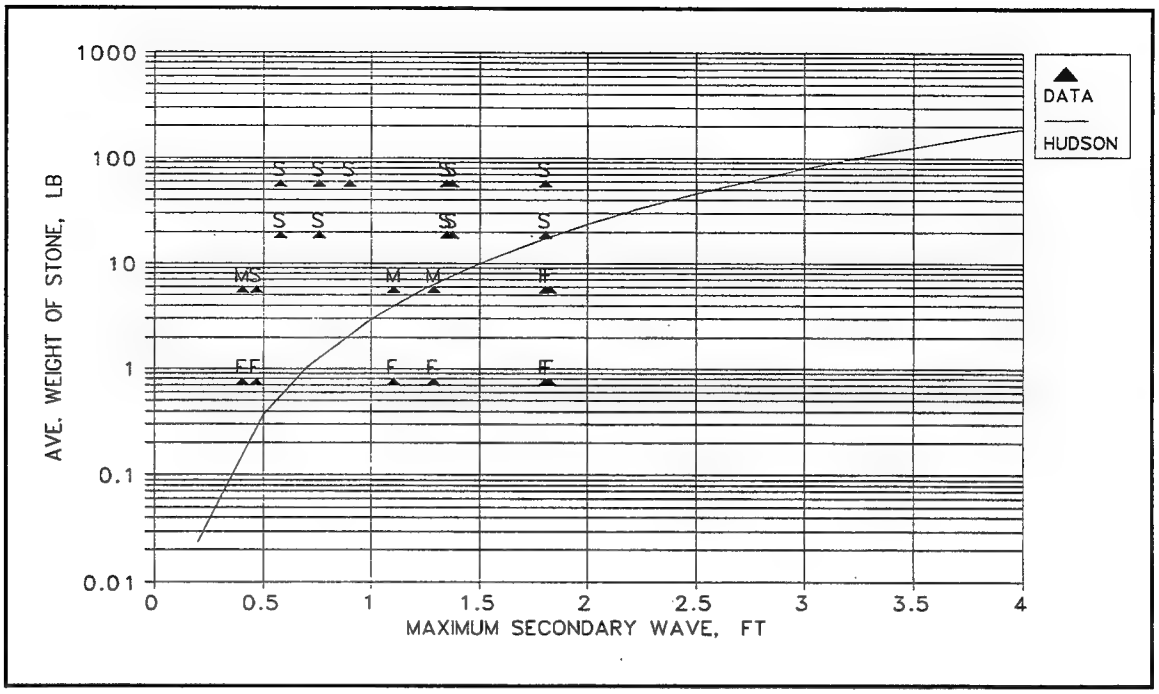

Figure 41. Analysis of H_i using Hudson approach, 2H:1V

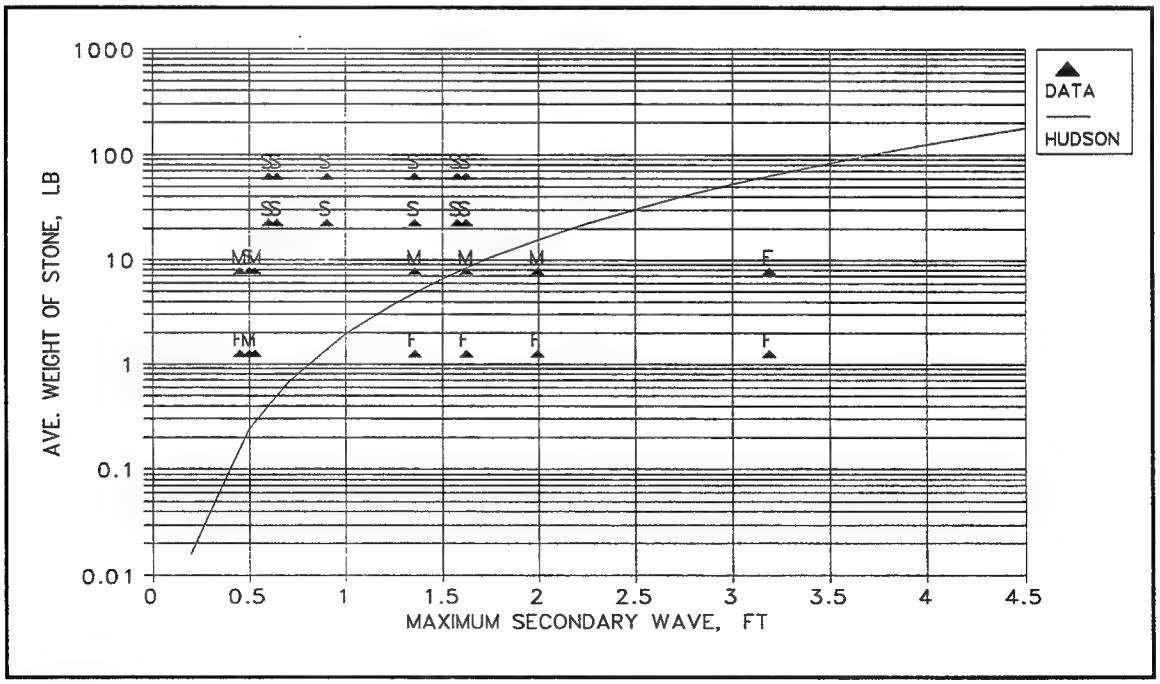

Figure 42. Analysis of H_i using Hudson approach, 3H:1V

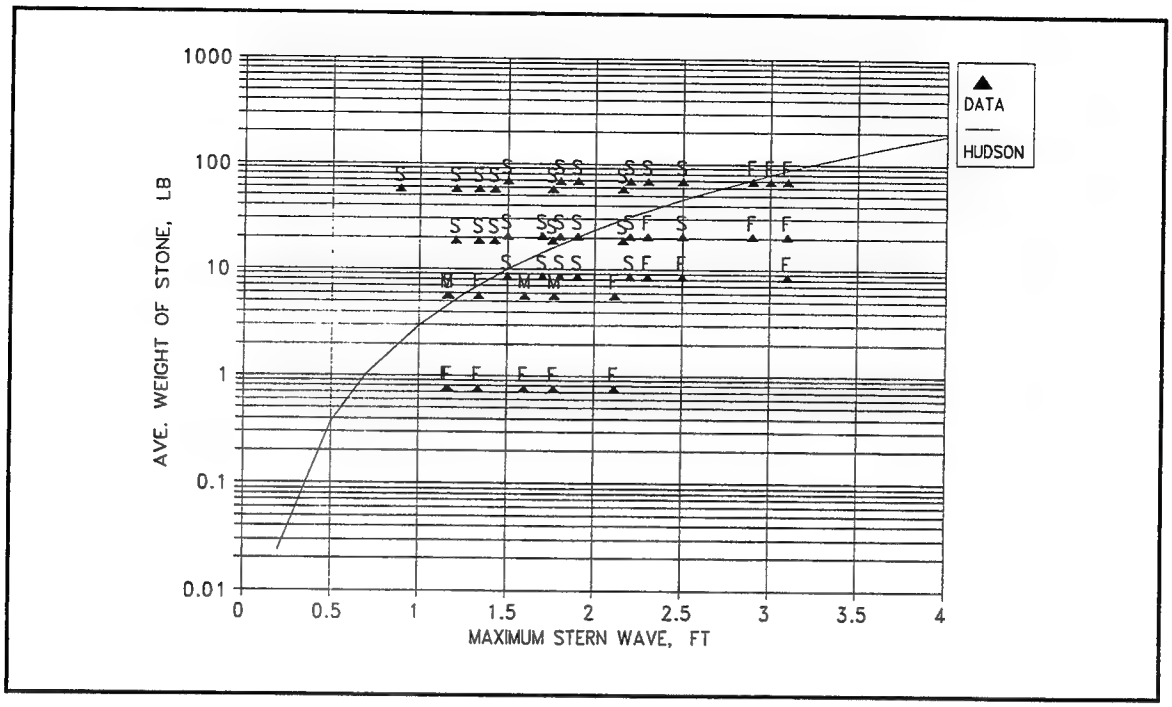

Figure 43. Analysis of H_{max} using Hudson approach, 2H:1V.

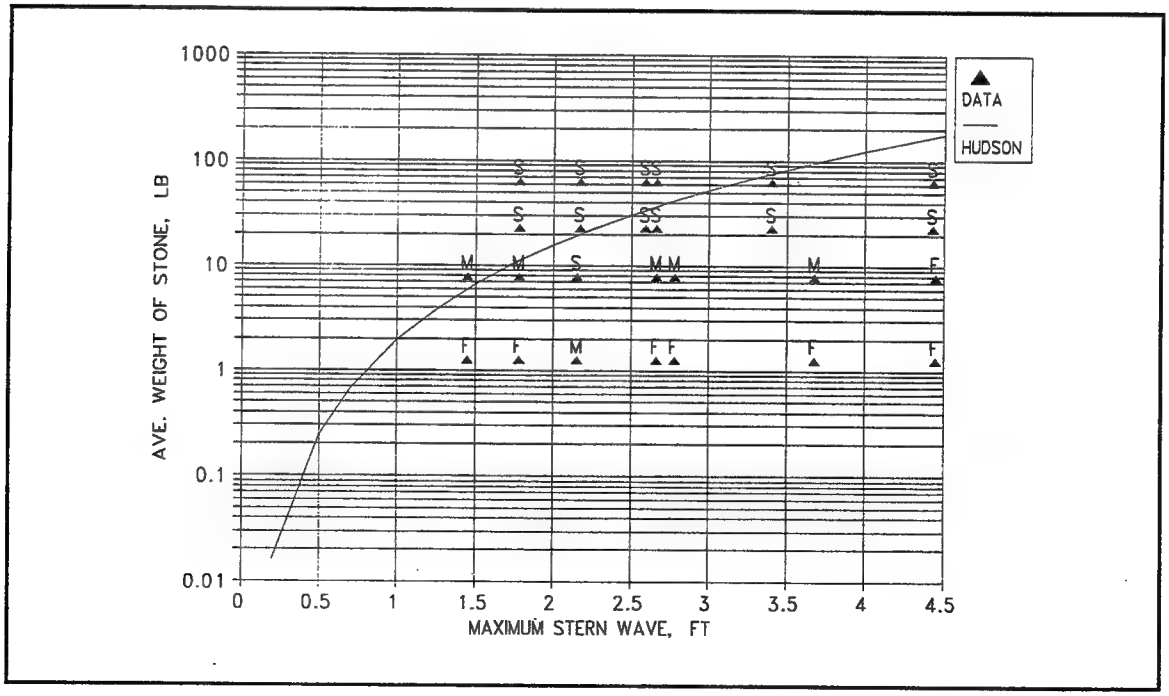

Figure 44. Analysis of H_{max} using Hudson approach, 3H:1V

In an attempt to couple tow-induced forces, drawdown and return current were evaluated as a total head term, H_T, such that

$$H_T = z_{max} + \frac{U_{rm}^2}{2g} \tag{106}$$

Replacing wave height with H_T and comparing the values for N_s from Hudson (1957), Figures 45 and 46 show the relationship between W_{50} and H_T for each slope, respectively. Since the velocity head due to return current is small relative to the drawdown, little, if anything, is gained in using this method. Separation of failed and stable points does not appear to fit the cubic relationship of the Hudson curve any better than using drawdown alone.

Selection of N_s

The next step in the analysis is to determine the failure threshold for the data given. Return current formulations and coupled approaches were dismissed from the analysis based on the results above. Failure thresholds were analyzed as a function of z_{max}, H_{max},

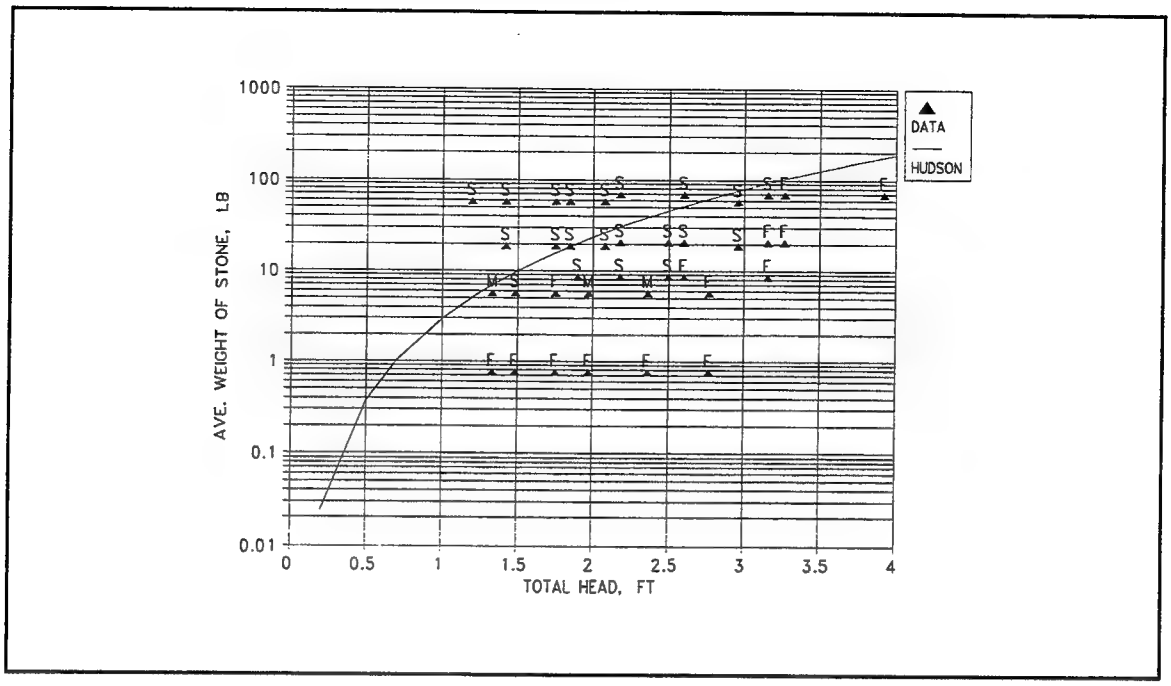

Figure 45. Combined analysis of u_{rm} and z_{max} using Hudson approach, 2H:1V

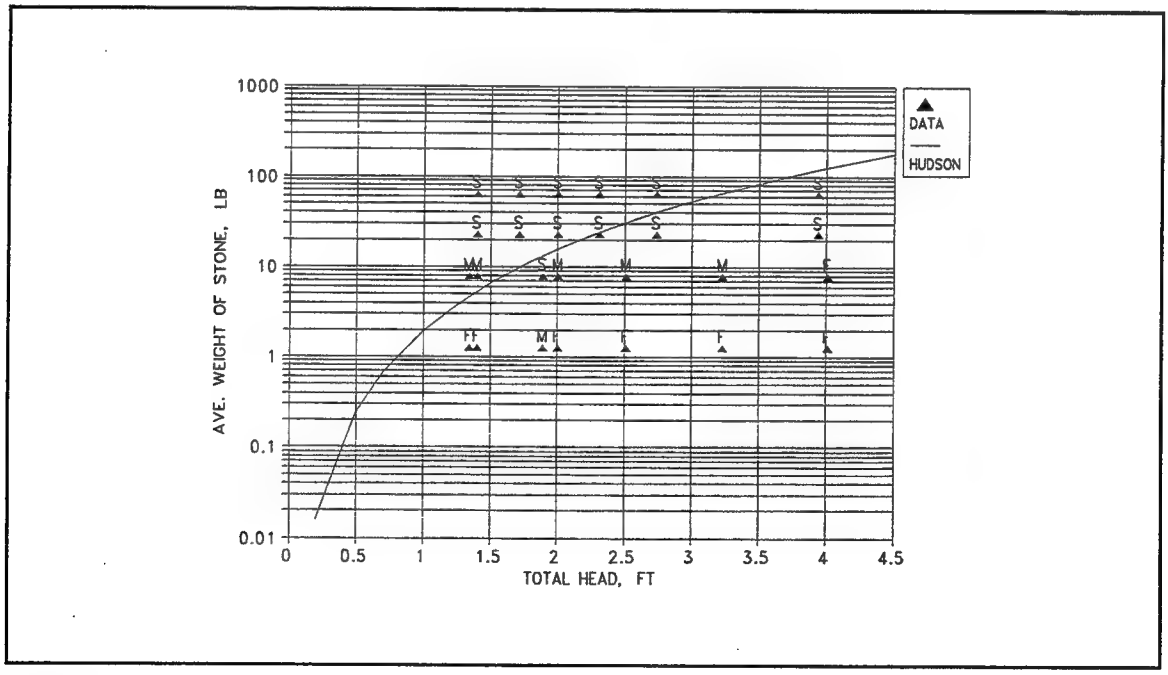

Figure 46. Combined analysis of u_{rm} and z_{max} using Hudson approach, 3H:1V

and H_i. Values of N_s were adjusted in each of the plots of stone weight versus wave height, such that the curve passed through the highest failure point. That is, every point at and below the failure threshold is assumed to fail. As N_s increases, the threshold shifts downward, indicating that the required stable stone size is smaller. Figures 47-52 show failure thresholds through these data for z_{max}, H_i, and H_{max}, respectively. Data points below the Reynolds criteria were not considered in the selection of the thresholds.

These values of N_s do not represent a safe design. There are several ways to incorporate safety into the equation. Ahren's work (Ahrens 1982) resulted in such conservative results that he ultimately recommended a method using the damage criteria where zero damage is defined as the conditions in which one to two stones are moved. Broderick and Ahrens (1982) use the same approach, where zero damage is based on the movement of two to three stones. Hudson (1957) likewise used a similar approach for zero damage plus varied the significant wave height to determine sensitivity. If there were many failure points along the threshold, a best fit line can be used to determine the failure curve and safety could be incorporated by shifting this curve through the outliers. This method was used by Abt et al. (1991) in the design of riprap grade control structures. The recommended safety factor resulting from that methodology and for a subsequent model study at the WES regarding grade control structures (Martin, Knight, and Murphy 1994) was 1.25 times D_{50}. In fact, safety factors increasing D_{50} have been used by a number of researchers. Fuehrer, Romische and Engelke (1981) increase the stable stone size from their tests by a factor of 3. Maynord's recommendations in *Engineering Manual 1110-2-1601* (HQUSACE 1991) was a multiple of 1.1.

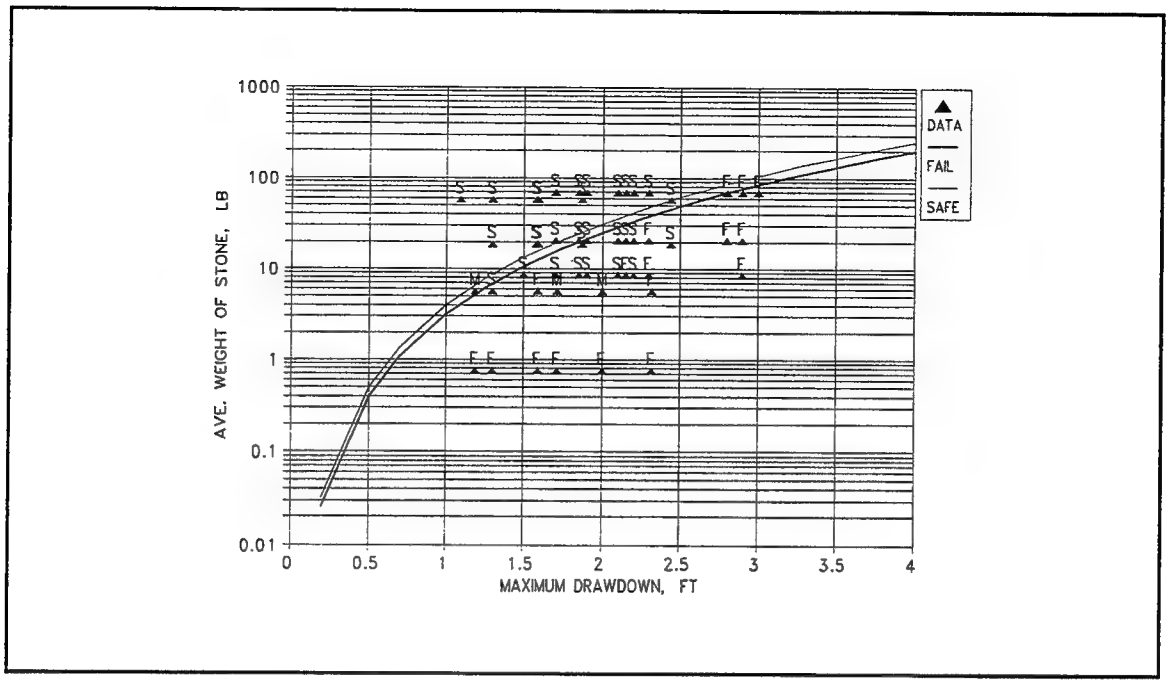

Figure 47. Determination of N_s for z_{max}, 2H:1V

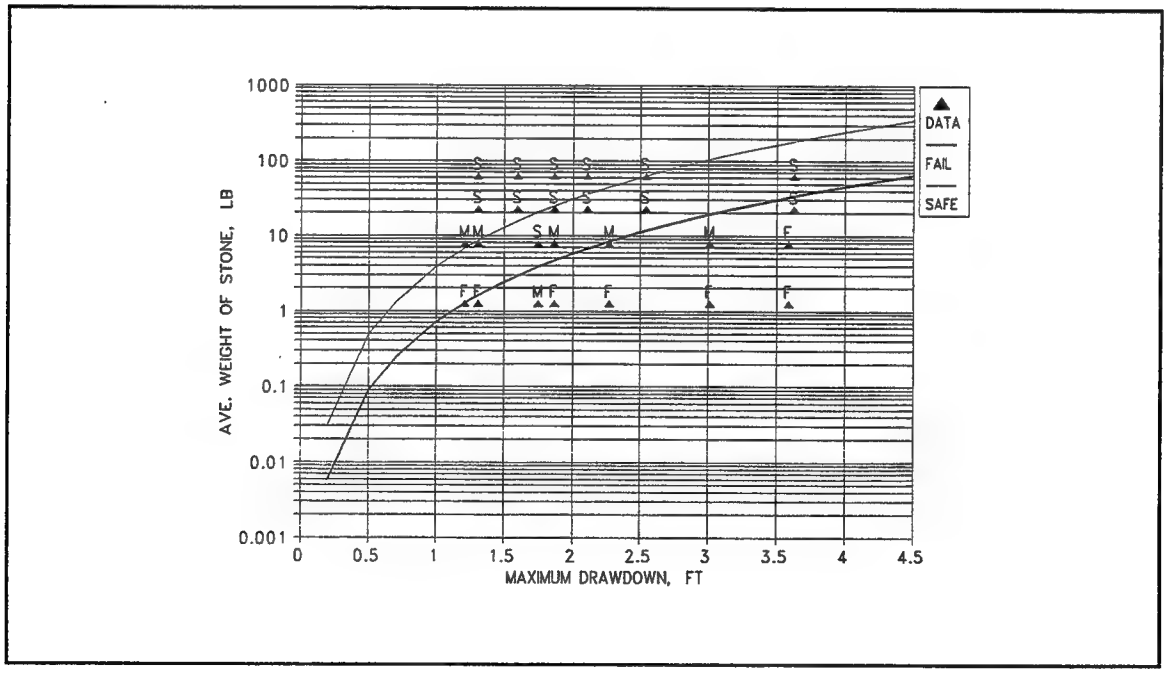

Figure 48. Determination of N_s for z_{max}, 3H:1V

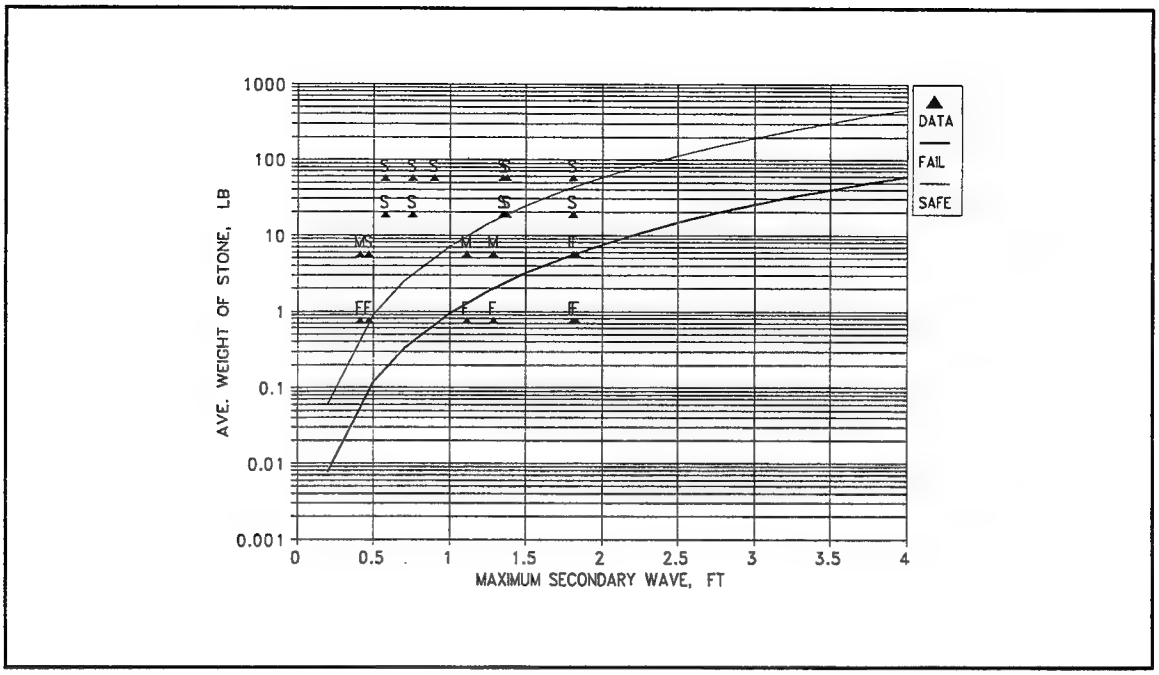

Figure 49. Determination of N_s for H_i, 2H:1V

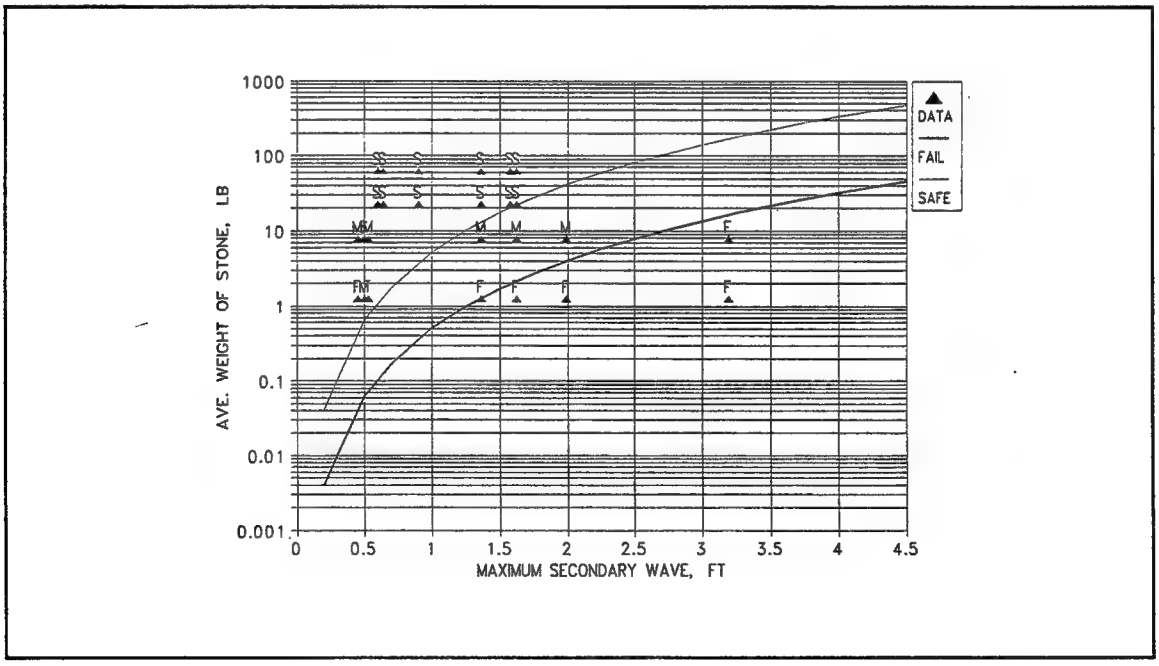

Figure 50. Determination of N_s for H_i, 3H:1V

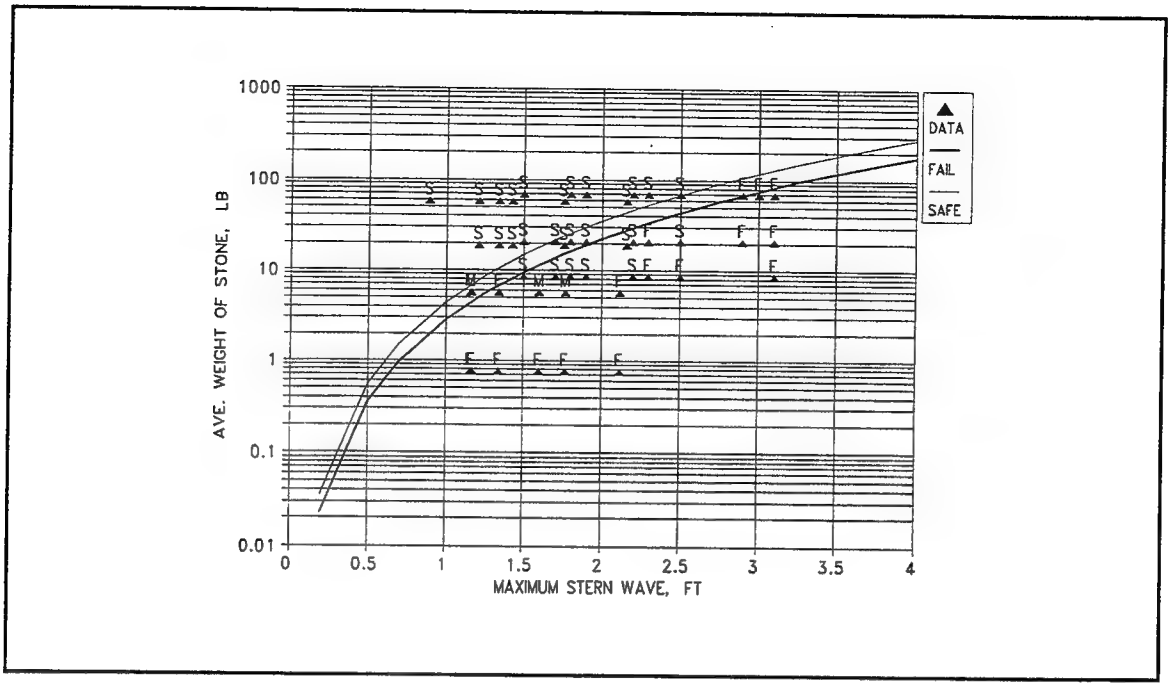

Figure 51. Determination of N_s for H_{max}, 2H:1V

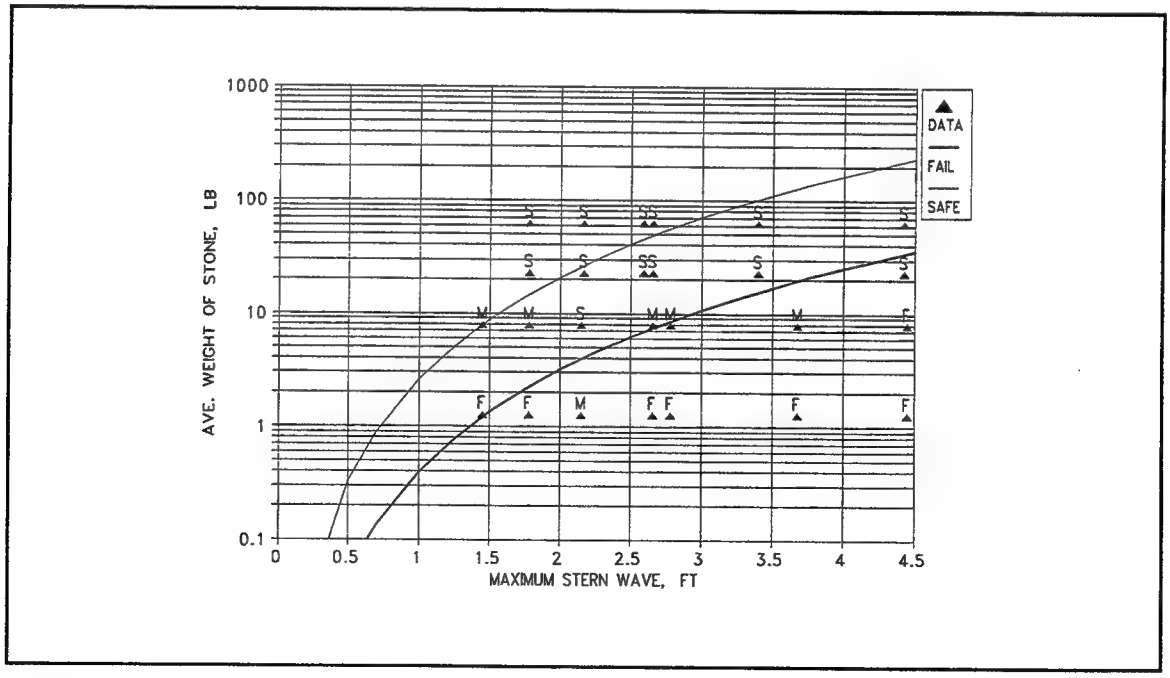

Figure 52. Determination of N_s for H_{max}, 3H:1V

An approach similar to the Hudson approach, wherein zero damage was observed, was used in this analysis. Values of the zero damage stability number, N_{sz}, were selected such that all data points along and above the line were stable. Observations of "marginal" had to fall on or below the stable threshold. The curves shifted through the stable points are also shown in Figures 47-52. The safety factor, S_f, resulting from this analysis can be calculated by the ratio of N_s/N_{sz}. Values of N_s at the failure threshold, N_{sz} at zero damage and S_f, the safety factor for each parameter as shown in Table 19.

Table 19
Final Determination of Stability Coefficients

	N_s 2H:1V	N_{sz} 2H:1V	S_f 2H:1V	N_s 3H:1V	N_{sz} 3H:1V	S_f 3H:1V
z_{max}	1.82	1.69	1.08	2.98	1.71	1.74
H_i	2.72	1.38	1.97	3.35	1.54	2.16
H_{max}	1.89	1.63	1.16	3.63	1.94	1.87

Computed safety factors ranged from 1.08 to 2.16. Safety factors used in open channel flow environments can be typically be lower than in breakwater areas or near structures since human safety or loss of property would be minimal in these areas. The safety factors resulting from this analysis are acceptable for this application.

For the 2H:1V slopes where there are many points related to H_{max} and z_{max}, the values of N_s, N_{sz} and S_f are similar. This is not a surprise since both parameters are characteristic terms for the stern wave. These results also follow trends in the

hydrodynamic analysis suggesting strong correlations between the two parameters, as was shown in Figure 30. In fact, it follows that either parameter could be selected to characterize the primary wave system described by many authors as the dominant mechanism for failure. The 3H:1V curves did not have as many points as the 2H:1V curves since no TT data were taken on that slope angle. For H_{max} and z_{max}, however, there were data points over a broad range of wave heights. Stability coefficients in the literature (Table 1) for z_{max} ranged from 1.89 to 2.3. The zero damage stability coefficients from this analysis for z_{max} and H_{max} were from 1.69 to 1.94. Due to the similarities between z_{max} and H_{max}, values of N_{sz} were averaged for each slope yielding, 1.66 and 1.83 for the 2H:1V and 3H:1V slopes, respectively.

The values of N_{sz} related to the secondary waves were 1.38 and 1.54 for the 2H:1V and 3H:1V slopes, respectively. Values in the literature recommended for secondary waves ranged from 1.73 from Sorensen (1986) to 2.4 from PIANC (1987). Only Blaauw et al. (1984) and PIANC (1987) presented formulations for both z_{max} and H_i. Comparing those values of stability numbers given in Table 1, both authors suggest that secondary waves have higher, not lower, stability numbers than the stern wave. The stability numbers related to H_i were dropped from the analysis based on the following:

a. There were few data points to delineate the thresholds.

b. The secondary waves were implicitly represented by the stern wave parameters, since secondary waves accompany the primary wave system in confined reaches where this design methodology will be applied.

c. analysis has already shown the strong correlations between these parameters.

d. The highest measured value of wave height was less than 2 ft for the 2H:1V slope.

f. Safe values of the stability numbers in this analysis do not trend in the same direction as the literature suggests.

Slope Angle Relationship

The relationship used by Hudson (1957) for relating stability number to slope angle, in a general form is

$$N_s = a\,(\cot\alpha)^{1/3} \tag{107}$$

Hudson's stable value of **a** is 1.47. He states in his paper that the best-fit line was drawn through the data points with a slope of one-third to simplify the formula and so that it could be plotted as a straight line on log-log paper. He obtained this value experimentally using seven different slope angles between cot α = 1.25 and 5. PIANC (1987) uses this formulation and the coefficient, **a**, is 1.5.

Solving this equation for **a** yields

$$a = \frac{N_{sz}}{(\cot\alpha)^{1/3}} \tag{108}$$

Then calculating **a** based on values of N_{sz} associated with z_{max} and H_{max} results in an average **a** of 1.30.

Figure 53 shows the relationship between the stability coefficient and the slope angle for coefficients of **a** from Hudson, PIANC and this study.

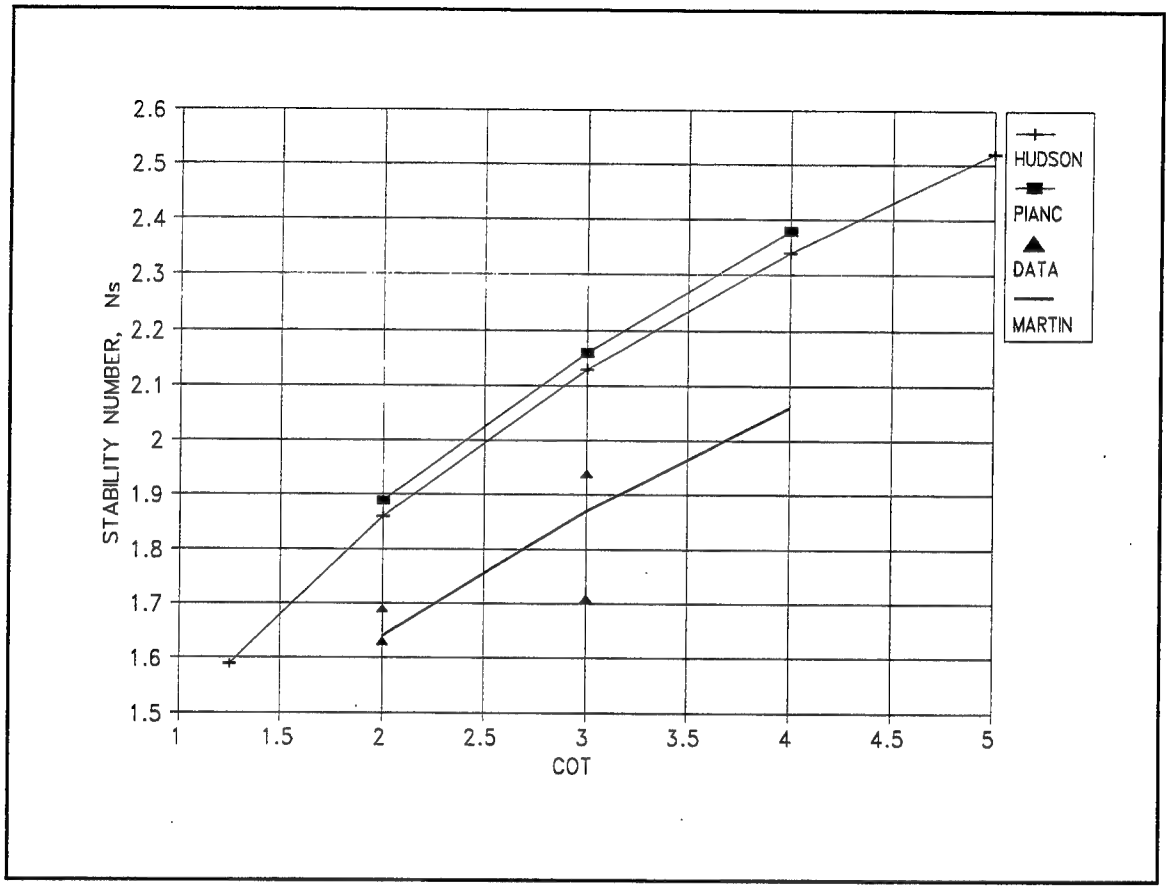

Figure 53. Relationship between slope angle and the zero damage stability number

Since tests were only conducted at two bank slopes in this study and since the data points shown in Figure 53 follow a similar slope to Hudson's, the zero damage stability number for this analysis is given by

$$N_{sz} = 1.30\,(\cot\alpha)^{\frac{1}{3}} \qquad (109)$$

Runup

From the *Shore Protection Manual* (1984), the runup is defined by Figure 54.

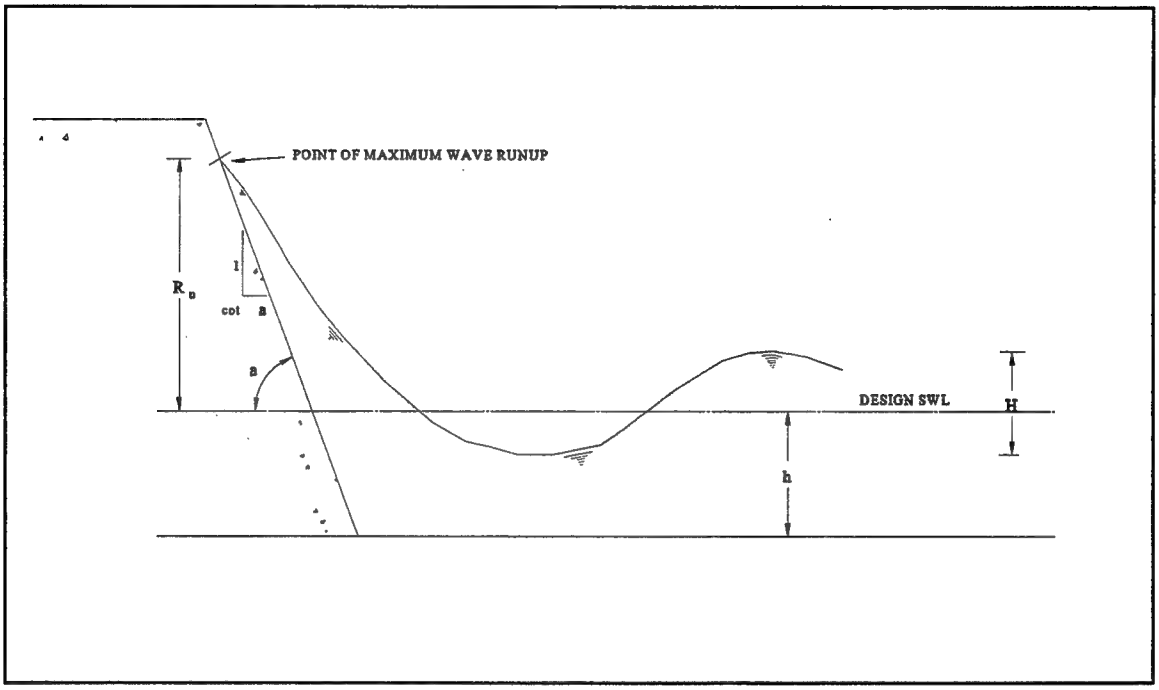

Figure 54. Definition sketch of wave runup

The manual provides a method for calculating runup on smooth surfaces, making corrections for scale effects. When model tests for riprapped structures are not available for quantification of runup, the manual also provides an adjustment for riprap from the smooth surface estimate.

In subsequent work regarding runup, Ahrens and Heimbaugh (1988) present an equation for runup as a function of the surf parameter and slope angle based on two

laboratory studies on riprap. Their equations provide a simple method for the prediction of runup based on empirical data. Their recommended formulae are:

$$\xi_L = \frac{\tan \alpha}{\left(\frac{H_{mo}}{L_p} \right)^{1/2}} \tag{110}$$

$$\frac{R_{max}}{H_{mo}} = \frac{1.154\, \xi_L}{1.0 + 0.202\, \xi_L} \tag{111}$$

where:

ξ_L is the surf similarity parameter using local wavelength. R_{max} is the maximum wave runup. H_{mo} is the energy-based, zero-moment wave height. L_p is the Airy wavelength calculated using T_p, the period of peak wave energy density of incident wave spectrum.

Broderick and Ahrens (1982) definition for runup is: "Runup was visually defined as the average point of maximum wave uprush on the riprap surface near the center of the wave tank." Small-scale test results at the zero-damage level gave more conservative estimates of both the stability number and the runup. In fact, they conclude that runup in the small-scale tests is approximately 20 percent higher than prototype measurements. From their tables, it appeared that the magnitude of runup was on the order of three times the zero damage wave height.

Blauuw et al. (1984) define the upper boundary or limit of riprap protection from the undisturbed water surface with the wave run-up, R_u, formula

$$\frac{R_u}{H} = 2c\left(\frac{H}{L_{wi}}\right)^{-0.5}\tan\alpha \qquad (112)$$

where H represents secondary waves, L_{wi} is the wave length, and c is a coefficient. They also give a formula to determine the lowest level of protection from secondary waves below the undisturbed water level.

5 Summary and Conclusions

Existing methodologies for designing stone slope protection for navigation-induced forces produced a wide variation of resulting stone sizes. A generalized equation for the design of stone protection for inland navigable waterways in the U.S. for commercial tow traffic is needed to optimize safety and minimize cost. This research verifies the use of the Hudson approach to riprap design for waves with specific recommendations for the zero damage stability coefficient, N_{sz}, for tow-induced forces based on a characteristic parameter of the primary wave system, maximum drawdown.

Furthermore, lessons learned during extensive physical model testing of navigation effects have led to recommendations for future model studies particularly regarding the scale effects at low Reynolds values and related to the stability of small model stones due to their angle of repose.

Recommendations for Physical Model Testing

A few recommendations are suggested regarding physical model testing of riprap in view of the findings of this research regarding scale effects at low Reynolds numbers and

for small stone sizes. Wave Reynolds values should be approximately greater than 10^4. This conservatively results in model wave heights in excess of approximately 0.6 in. (1.5 cm).

Extremely small rock sizes should be avoided unless tests can be conducted to determine not only the relative differences in angle of repose between gradations, but also the importance the angle of repose has on the friction coefficient in the balance of forces. If small sizes are necessary, adhere to the method prescribed for adjusting model sizes. Preferably, angle of repose should be measured for the specific model gradation tested. More research is also needed to verify the importance of the friction angle in the balance of forces.

Finally, regarding navigation effects scale testing, adjustments should be made to the tow model to compensate for boundary layer problems. Recommendations regarding model adjustments can be found in Maynord and Martin (1996) based on the most recent comparisons between scale testing and field measurements.

Design Methodology for Sizing Riprap for Tow-induced Forces

The completed analysis revealed that the stern wave is the dominant force produced by the tow, particularly in the small blockage ratios studied here. Secondary waves are small or negligible for slow-moving vessels and are of the same order magnitude as the stern wave for laden vessels. There were no tests where only secondary waves were present. In the case where tows are drafting light and traveling fast, secondary waves can

be of greater order magnitude than the primary wave. Since this analysis integrates these waves with the primary wave system, the recommended equation conservatively provides a stable rock design.

The following methodology is recommended for sizing riprap in navigation channels with blockage ratios less than approximately 20 and for slopes from 2H:1V to 4H:1V:

(1) Determine channel dimensions and sailing line.

(2) Select the critical tow dimensions (the largest primary wave will be associated with the smallest blockage ratio). The largest secondary waves will be associated with the highest vessel speed and perhaps the lightest vessel draft.

(3) Using the modified Schijf equations presented in Maynord (1996), calculate the vessels limiting speed given these waterway and tow characteristics.

(4) If an actual maximum vessel speed is not known for this channel reach, select a vessel speed of approximately 95 percent of the limiting speed to calculate the stern wave parameter, z_{max} , using the methods in Maynord (1996) or PIANC (1987).

(5) Calculate the secondary wave height, H_i , using the methods in PIANC (1987) or in Verhey and Bogaerts (1989).

(6) Select a bank slope. Use the following equation to determine N_{sz} for that slope

$$N_{sz} = 1.30 (\cot \alpha)^{1/3} \quad (113)$$

(7) Compare z_{max} to H_i and select the largest value for design. Using the maximum wave, H, calculate the stone size as follows:

$$D_{50} = \frac{H}{N_{sz}\left(\frac{\gamma_r}{\gamma_w} - 1\right)} \tag{114}$$

(8) Determine stone weight, W_{50}, based on a spherical stone diameter such that

$$W_{50} = \frac{\pi}{6} \gamma_r D_{50}^3 \tag{115}$$

Other Design Considerations

There are other considerations in the design of riprap in addition to its size. Existing guidance should be used to determine quality, gradation, placement, and limits of bank protection.

The stability of the riprap is dependent upon the gradation, placement, and thickness of the stone. Stone should be well graded, and the thickness should not be less than D_{100}. Specific guidance for determination of these parameters and others can be found in *Engineering Manual 1110-2-1601* (HQUSACE 1991).

In a riverine situation, pool fluctuations and/or flood stages may dictate the upper limit of bank protection. However, if the waterway is being designed for tow-induced

waves, then the upper extents of stone protection should reflect the maximum navigable pool or stage plus the maximum potential wave runup. Generally, protection will extend from this upper limit to the toe of the slope. Runup should be calculated using guidance in the *Shore Protection Manual* or with Ahren's equations until further research verifies runup values appropriate for boat waves in shallow water in navigable waterways.

As was discussed in the literature review, some researchers suggest that different size stone protection may be used for upper and lower banks along the waterway. In that case, the upper bank protection for tow-induced waves should extend from the upper limit of protection to below the water level at the lowest expected navigable conditions, taking into account the maximum expected drawdown. If stone protection is required for the upper slope, the lower portion of slope should not be left unprotected. Studies conducted at the WES for Huntington District suggest that unprotected lower slopes could experience failure due to tow-induced currents, particularly if tows travel close to the bank. More research is needed regarding placement of different rock sizes on upper and lower slope.

Location of the protection should be considered when selecting the hydrodynamic conditions. In lock approaches, it is highly unlikely that tows will travel near the limiting speed. Reasonable operating conditions should dictate design methodologies in these areas. In the case of long, narrow reaches of natural rivers or man-made canals where vessels underway can approach the limiting speed, critical hydraulic loadings based on approximately 95-percent limiting speed, should be selected for bank protection design. If wind waves, ambient currents, or propeller jets could potentially impact the bank,

hydrodynamic forces should be estimated for each of the conditions using available literature (the PIANC guidelines provide an acceptable start) and stone sizes should be estimated using riprap equations developed for those conditions. If the analysis produces different stone sizes, the maximum stone protection should be selected.

In design of the waterway, attention should be given to expected and potential mooring locations. Observations by the author during a bank erosion field survey on the Upper Mississippi and Illinois Rivers suggested that the integrity of the bank can be jeopardized at locations where barge mooring occurs. Once a nick point has been made in the bank protection (whether rock or vegetation), the bank becomes subject to further unraveling from other mechanisms. This can result in dynamically eroding reaches of bank along the waterway. Care should be taken to either prohibit mooring in critical reaches, design specific areas for mooring of barges, and/or be prepared to repair areas of failure through routine maintenance.

6 Current and Future Studies in Navigation Effects

Navigation Effects Studies

The WES is currently funded to investigate the physical effects due to projected incremental increases in navigation on the Upper Mississippi River System - Illinois Waterway (UMRS) as a part of the environmental portion of a feasibility navigation study. The environmental concerns for this project regard the impacts of navigation on adult fish, fish larvae, aquatic vegetation, and benthic organisms. Of primary concern is the resuspension and transport of sediments into critical biological areas such as backwaters or side channels adjacent to the main channel waterways. Also important are the hydrodynamic forces in the main channel that potentially could disturb the biota, including the mixing due to tow passage, the propeller jet forces, the wave energy, and the current reversals.

A new funding start from HQUSACE in fiscal year 1995 allowed the research and testing to continue into the more complex phenomena regarding navigation effects. This work has focused on the engineering aspects of this subject, and its research is directed toward design of channel protection in navigation channels. Particular emphasis for the research overlaps the objectives of the UMRS study including the development of

predictive methods for return currents and wave heights in irregular channels with ambient current conditions. Design guidance regarding stable riprap will also be developed for propeller jets and maneuvering tows. A tow-induced sediment resuspension algorithm will be investigated for both studies and its potential inclusion in a 2-D sediment transport model.

Developing Technologies

All the navigation effects studies will benefit from better physical model facilities, relatively new technologies in instrumentation, and the development of numerical codes that can model the tow movement. Both physical and numerical model output will be used for visualization of the physics of the problem and to provide a better understanding of the effects of navigation.

A new flume for the UMRS Navigation Effects Study provides ample length and width to conduct experiments that were otherwise not possible in the old facility. The flume is 400 ft (122 m) long by 70 ft (21.3 m) wide by 4 ft (1.2 m) deep, is equipped with a towing carriage, and has a flow capacity of 50 cfs (1.4 cms). Channels with irregular cross sections and ambient currents can be modeled in the facility.

State-of-the-art data acquisition and instrumentation are available on this model. It is equipped with ten acoustic doppler velocity probes that are capable of taking non-intrusive 3-D velocities, a 2-D laser doppler velocimeter, and wave capacitance rods for water surface measurements.

Recent numerical model modifications of an existing hydrodynamic code, HIVEL2D (Stockstill and Berger 1992), have resulted in a product that can be used to simulate tow movement through a channel. This code has been verified with physical model data so that it can be used as the hydrodynamic driver for the sediment transport studies and as a tool for predicting velocities and drawdown due to incremental increases in navigation in reaches of the UMRS (Stockstill, Martin, and Berger 1995). Because it is a 2-D model, it is only valid for evaluating far-field effects, areas away from the boundaries of the tow.

The products of these studies will be a family of tools that will predict forces produced by navigation and provide design guidance for channel protection in navigable waterways. These studies will help in the avoidance and mitigation of environmental impacts due to commercial traffic on inland waterways. These studies have already and will continue to advance the state of knowledge regarding navigation effects.

REFERENCES

References

Abt, S. R., Watson, C. C., Johns, D. D., Hamilton, G. B., Garton, A. D., Flerentin, C. B., and Thornton, C. I. (1991). "Riprap sizing criteria for ARS-type drop structures," prepared by the Department of Civil Engineering, Colorado State University, Fort Collins, CO, for U.S. Army Engineer Waterways Experiment Station, Vicksburg, Ms.

Ahrens, J. P. (1982). "Design of riprap revetments for protection against wave attack," Technical Paper No. 81-5, Coastal Engineering Research Center, Fort Belvoir, VA.

Ahrens, J. P. (1989). "Recommendations for updating EM 1110-2-1614, design of coastal revetments, seawalls, and bulkheads," Draft.

Ahrens, J. P., and Heimbaugh, M. S. (1988). "Irregular wave runup on riprap revetments," *Journal of waterway, port, coastal, and ocean engineering*, American Society of Civil Engineers, 114(4), 524-530.

American Society of Civil Engineers. (1977). *Sedimentation engineering.* ASCE Manuals and Reports on Engineering Practice—No. 54, Vito Vanoni, ed., New York.

Balanin, V. V., and Bykov, L. S. (1965). "Selection of leading dimensions of navigation canal sections and modern methods of bank protection." *21st International Navigation Congress,* Stockholm, Sweden. Permanent International Association of Navigation Congresses, Section 1-4, 151-170.

Bhowmik, N. G. (1976). "Development of criteria for shore protection against wind-generated waves for lakes and ponds in Illinois," Research Report No. 107 (UILU-WRC-76-0107), Illinois State Water Survey, Champaign, Illinois.

Bhowmik, N. G., Demissie, M., and Guo, C. Y. (1982). "Waves generated by river traffic and wind on the Illinois and Mississippi Rivers," Research Report No. 167 (UILU-WRC-82-0167), Illinois State Water Survey, Champaign, Illinois.

Blaauw, H. G., van der Knaap, F. C., de Groot, M. T., and Pilarczyk, K. W. (1984). "Design of bank protection of inland navigation fairways," Delft Hydraulics Laboratory Publication No. 320, Delft, The Netherlands, presented at the International Conference on Flexible Armoured Revetments Incorporating Geotextiles, London, England.

Boeters, R. E. A. M, van der Knaap, F. C. M., and Verheij, H. J. (1995). "Behavior of armour layers of riprap bank protections along navigation channels." *River, coastal and shoreline protection, erosion control using riprap and armourstone*. C. Thorne, S. Abt, F. Barends, S. Maynord, and K. Pilarczyk, ed., John Wiley, Chichester, England, 163-176.

Bouwmeester, J., van de Kaa, E. J., Nuhoff, H. A., and van Orden, R. G. (1977). *24th International Navigation Congress*, Leningrad, Russia. Permanent International Association of Navigation Congresses, Brussels, Belgium, Section I-Subject 3, 139-158.

Broderick, L. L., and Ahrens, J. P. (1982). "Riprap stability scale effects," Technical Paper No. 82-3, U.S. Army Corps of Engineers Coastal Engineering Research Center, Fort Belvoir, Va.

Chow, V. T. (1959). *Open-channel hydraulics,* McGraw-Hill, New York.

Dai, Y. B., and Kamel, A. M. (1969). "Scale effect tests for rubble-mound breakwaters," Research Report H-69-2, U.S. Army Engineer Waterways Experiment Station, Vicksburg, Ms.

Froehlich, D. C., and Ogden, J. T. "Angle of repose of dumped coarse open-graded stone," (unpublished draft), submitted to *Journal of Materials in Civil Engineering,* American Society of Civil Engineers.

Fuehrer, M., Romisch, K., and Engelke, G. (1981). "Criteria for dimensioning the bottom and slope protections and for applying the new methods of protecting navigation canals." *Proceedings of the 25th International Navigation Congress,* Edinburgh. Permanent International Association of Navigation Congresses, Section 1, 29-50.

Gates, E. T., and Herbich, J. B. 1977. "Mathematical model to predict the behavior of deep-draft vessels in restricted waterways," TAMU-SG-77-206, Texas A&M Ocean Engineering Program, College Station, TX.

Gelencser, G. J. (1977). "Drawdown surge and slope protection" *Proceedings of the 24th International Navigation Congress,* Leningrad, Russia. Permanent International Association of Navigation Congresses, Brussels, Belgium, Section I-3, 21-41.

Headquarters, U.S. Army Corps of Engineers. (1971). "Additional guidance for riprap channel protection," Engineer Technical Letter 1110-2-120, U.S. Government Printing Office, Washington, D.C.

Headquarters, U.S. Army Corps of Engineers. (1985). "Design of coastal revetments, seawalls, bulkheads," Engineer Manual 1110-2-1614, U.S. Government Printing Office, Washington, D.C.

Headquarters, U.S. Army Corps of Engineers. (1991). "Hydraulic design of flood control channels," Engineer Manual 1110-2-1601, U.S. Government Printing Office, Washington, D.C.

Hedar, P. A. (1960). "Stability of rock-fill breakwaters," University of Technology, Scandinavian University Books, Goteborg.

Henderson, F. M. (1966). *Open channel flow.* Macmillan, New York.

Hudson, R. Y. (1957). "Laboratory investigation of rubble-mound breakwaters," Presented at the June 1957 Meeting of the American Society of Civil Engineers, Buffalo, NY.

Hudson, R. Y. (1975). "Scale effects in rubble-mound breakwater stability models caused by variations in the specific gravity of the armor units and underlayer stones," Miscellaneous Paper H-75-4, U.S. Army Engineer Waterways Experiment Station, Vicksburg, MS.

Hudson, R. Y. (1979). "Stability of coastal structures." *Coastal hydraulic models.* Special Report No. 5, R. Y. Hudson, F. A. Herrmann, Jr., R. A. Sager, R. W. Whalin, G. H. Keulegan, C. E. Chatham, Jr., and L. Z. Hales, authors. U.S. Army Corps of Engineers, Coastal Engineering Research Center, Fort Belvoir, VA, 314-452.

Iribarren, C. R. (1948). "A formula for the calculation of rock-fill dikes," Technical Report HE-116-295, translated from Spanish by D. Heinrich, University of California, Navy Department-Bureau of Ships, Berkeley, Ca.

Jansen, P. Ph., and Schijf, J. B. (1953). *Eighteenth International Navigation Congress,* Rome. Permanent International Association of Navigation Congresses, Brussels, Belgium, Section 1, Communication 1, 175-197.

Jensen, O. J. (1989). "Dynamic action on breakwaters." *Recent Advances in Hydraulic Physical Modelling, Proceedings of the NATO Advanced Study Institute,* Lisbon, Portugal. Rui Martins, ed., Kluwer Academic Publishers, The Netherlands, 503-539.

Jonsson, I. G. (1966). "Wave boundary layers and friction factors," *Proceedings 10th Conference on Coastal Engineering.* American Society of Civil Engineers, New York, 127-148.

Kooman, IR. C. (1973). "Navigation locks for push tows," Rijkswaterstaat Communications No. 16, The Hague, The Netherlands.

Koster, IR. J. (1975). "Push tows in canals," Rijkswaterstaat Communications No. 21, Government Publications Office, The Hague, The Netherlands.

Kobayashi, N. and Greenwald, J. (1988). "Waterline oscillation and riprap movement," *Journal of Waterway, Port, Coastal, and Ocean Engineering*, American Society of Civil Engineers, 114(3), Paper No. 22426, 281-296.

Madsen, O. S., and White, S. M. (1975). "Reflection and transmission characteristics of porous rubble mound breakwaters," Report No. 207, Ralph M. Parsons Laboratory for Water Resources and Hydrodynamics, Department of Civil Engineering, Massachusetts Institute of Technology, Cambridge, MA, for U.S. Army Coastal Engineering Research Center, Fort Belvoir, VA.

Martin, S. K. (1992). "Riprap design for towboat-induced forces in lock approaches," Miscellaneous Paper HL-92-3, U.S. Army Engineer Waterways Experiment Station, Vicksburg, MS.

Martin, S. K. (1989). "Gallipolis Locks and Dam, hydraulic model investigation to determine stone slope protection requirements," Memorandum for Record, available through author at CEWES-HN-E, U.S. Army Engineer Waterways Experiment Station, 3909 Halls Ferry Road, Vicksburg, MS 39180-6199.

Martin, S. K., Knight, S. F., Murphy, T. E. (1994). "Demonstration Erosion Control Monitoring Program, fiscal year 1993 report; Volume VI: Appendix E, model study of the Demonstration Erosion Control 10-ft riprap drop grade control structure," Technical Report HL-94-1, U.S. Army Engineer Waterways Experiment Station, Vicksburg, MS.

Maynord, S. T. (1996). "Return velocity and drawdown in navigable waterways" (in preparation), U.S. Army Engineer Waterways Experiment Station, Vicksburg, MS.

Maynord, S. T. (1990). "Velocities induced by commercial navigation," Technical Report HL-90-15, U.S. Army Engineer Waterways Experiment Station, Vicksburg, MS.

Maynord, S. T. (1989). "Letter report on model testing of riprap in the approaches of the proposed Point Marion Lock and Dam, Pennsylvania," Memorandum for U.S. Army Engineer Division, Ohio River, prepared by U.S. Army Engineer Waterways Experiment Station, Vicksburg, MS.

Maynord, S. T. (1988). "Stable riprap size for open channel flows," Technical Report HL-88-4, U.S. Army Engineer Waterways Experiment Station, Vicksburg, MS.

Maynord, S. T. (1984). "Riprap Protection on Navigable Waterways," Technical Report HL-84-3, U.S. Army Engineer Waterways Experiment Station, Vicksburg, MS.

Maynord, S. T., and Martin, S. K. (1996). "Upper Mississippi River system physical forces study, Kampsville, Illinois waterway" (in preparation), U.S. Army Engineer Waterways Experiment Station, Vicksburg, MS.

Maynord, S. T., and Oswalt, N. R. (1986). "Riprap stability and navigation tests for the divide-cut section, Tennessee-Tombigbee Waterway," Technical Report HL-86-3, U.S. Army Engineer Waterways Experiment Station, Vicksburg, MS.

Maynord, S., Ruff, J., and Abt, S. (1989). "Riprap design," *Journal of Hydraulic Engineering*, American Society of Civil Engineers, Paper No. 23686, 115(7), 937-949.

Maynord, S., and Siemsen, T. (1991). "Return velocities induced by shallow-draft navigation." *Hydraulic engineering: Proceedings of the 1991 National Conference.* R. M. Shane, ed., American Society of Civil Engineers, New York, 894-899.

Maynord, S., and Siemsen, T. (1990). "Flow field near an inland navigation tow." *Hydraulic engineering: Proceedings of the 1990 National Conference,* San Diego, CA, July 30-August 3, 1990. Howard H. Chang and Joseph C. Hill, ed., American Society of Civil Engineers, New York, 610-615.

Novak, P., and Cabelka, J. (1981). *Models in Hydraulic Engineering*, Pitman Advanced Publishing Program, Boston.

O'Loughlin, E. M., Mehrotra, S. C., Chang, Y. C., and Kennedy, J. F. (1970). "Scale effects in hydraulic model tests of rock protected structures," IIHR Report No. 124, Iowa Institute of Hydraulic Research, The University of Iowa, Iowa City, IA.

Oumeraci, H. (1984). "Scale effects in coastal hydraulic models." *Proceedings of the Symposium on scale effects in modelling hydraulic structures.* H. Kobus, ed., International Association for Hydraulic Research and Deutscher Verband fur Wasserwirtschaft und Kulturbau e.V., Neckar, Germany, 7.10-1 - 7.10-6.

Permanent International Association of Navigation Congresses. (1987). "Guidelines for the design and construction of flexible revetments incorporating geotextiles for inland waterways," Report of Working Group 4 of the Permanent Technical Committee, Supplement to Bulletin No. 57, par. 3.3, "Determination of Hydraulic Load."

DTIC COULD NOT GET MISSING

PAGE FROM CONTRIBUTOR

177

Ulrich, T. (1987). "Stability of rock protection on slopes," *Journal of Hydraulic Engineering*, American Society of Civil Engineers, 113(7), 879-891.

Van der Meer, J., and Pilarczyk, K. (1984). "Stability of rubble mound slopes under random wave attack," Delft Hydraulics Publication No. 332, Delft, The Netherlands, Presented at 19th International Conference on Coastal Engineering, Houston, TX.

Van Gent, M. (1995). "Wave interaction with berm breakwaters," *Journal of waterway, port, coastal, and ocean engineering*, American Society of Civil Engineers, Paper No. 8434, 121(5), 229-238.

Verhey, H. J. (1983). "The stability of bottom and banks subject to the velocities in the propeller jet behind ships," Publication No. 303, Delft Hydraulics Laboratory, The Netherlands, Presented at the 8th International Harbour Congress, Antwerp, Belgium.

Verhey, H. J., and Bogaerts, M. P. (1989). "Ship waves and the stability of armor layers protecting slopes," Publication No. 428, Delft Hydraulics Laboratory, The Netherlands.

Yalin, M. S. (1989). "Fundamentals of hydraulic physical modelling." *Recent advances in hydraulic physical modelling, proceedings of the NATO Advanced Study Institute*, Lisbon, Portugal. Rui Martins, ed., Kluwer Academic Publishers, Norwell, MA, The Netherlands, 1-38.

Weggle, J., and Sorensen, R. (1986). "Ship wave prediction for port and channel design." *Ports '86, Proceedings of a Specialty Conference on Innovations in Port Engineering and Development in the 1990's,* Oakland, CA, May 19-21, 1986. Paul H. Sorensen, ed., American Society of Civil Engineers, New York, 797-814.

Appendix A
Definitions

Ambient current: The river current undisturbed by the presence of a vessel.

Blockage ratio: The ratio of the channel cross-sectional area to the submerged cross-sectional area of the vessel.

Bottom displacement current: The current beneath the vessel acting in the opposite direction to the movement of the vessel.

Bow current: The current moving ahead of the vessel in general direction of the vessel.

Bow wave: The wave generated at the bow of the vessel.

Drawdown: The water level depression that forms as the vessel moves forward and water is displaced from bow to stern. Drawdown is a function of vessel speed, vessel size, and channel geometry.

Limiting speed: The maximum attainable speed of a vessel in a confined waterway or its critical speed. This speed is limited by the blockage ratio not the vessel horsepower.

Primary waves: The long period disturbance caused by the displacement of water from a vessel moving through the waterway. This disturbance includes the front wave, drawdown, return current, and transversal stern wave.

Propeller jet: The highly three-dimensional currents associated with propeller jets which cause localized disturbances to the flow field.

Return current: The current adjacent to the vessel that accompanies the drawdown as the water moves from bow to stern during the forward motion of the vessel. This current acts in the direction opposite of tow movement and generally parallel to the bank.

Sailing line: The path of the vessel in the navigation channel. Usually stated as its distance from the bankline.

Secondary waves: The waves generated by a moving pressure disturbance in deep water. Transverse and diverging waves intersect to form interference peaks or ship waves.

Slope supply flow: The current produced as water fills in behind the stern to replace the water displaced as the vessel moves forward.

Transversal stern wave: The transition at the stern of the vessel from the drawdown to the normal water level following the vessel.

Appendix B

Stability Test Parameters and Data

Appendix B
Stability Test Parameters and Data

Data Set	Barge Length L_s, ft	Barge Width B_s, ft	Barge Draft d, ft	Water Depth h, ft	Total Channel Data: Bottom Width b_w, ft	Total Channel Data: Cross-Section Area, ft^2	Total Channel Data: Blockage Ratio	Parameters Nearest to Rock Bank: Bank Slope (cot α)	Parameters Nearest to Rock Bank: Cross-Section Area, ft^2	Parameters Nearest to Rock Bank: Tow Position S, ft	Parameters Nearest to Rock Bank: Boat Speed V_s, fps	D_{50} in.	W_{50} lbs	Stability F/M/S	z_{max}, ft	H_{max}, ft	H_i, ft	u_r, fps
NR93	390	105	9	15	400	6,450	6.83	2	2,475	180	8	8.1	27	S	0.9	0.85		2.78
NR93	390	105	9	15	400	6,450	6.83	2	2,475	180	8	11.1	68	S	0.9	0.85		2.78
NR93	390	105	9	15	400	6,450	6.83	2	2,475	180	10	8.1	27	S	1.58	1.43	0.58	4.15
NR93	390	105	9	15	400	6,450	6.83	2	2,475	180	10	11.1	68	S	1.58	1.43	0.58	4.15
NR93	390	105	9	15	400	6,450	6.83	2	2,475	180	12	8.1	27	S	2.44	2.16	1.35	5.8
NR93	390	105	9	15	400	6,450	6.83	2	2,475	180	12	11.1	68	S	2.44	2.16	1.35	5.8
NR93	390	105	9	15	400	6,450	6.83	2	3,975	280	8	3.25	1.7	M	0.74	0.69		2.33
NR93	390	105	9	15	400	6,450	6.83	2	3,975	280	8	5.8	10	S	0.74	0.69		2.33
NR93	390	105	9	15	400	6,450	6.83	2	3,975	280	10	3.25	1.7	F	1.3	1.17	0.47	3.49
NR93	390	105	9	15	400	6,450	6.83	2	3,975	280	10	5.8	10	S	1.3	1.17	0.47	3.49
NR93	390	105	9	15	400	6,450	6.83	2	3,975	280	12	3.25	1.7	F	2	1.77	1.11	4.87
NR93	390	105	9	15	400	6450	6.83	2	3975	280	12	5.8	10	M	2	1.77	1.11	4.87
NR93	390	105	9	15	400	6675	7.06	3	2587.5	195	8	8.1	27	S	0.95	1.19		2.8
NR93	390	105	9	15	400	6675	7.06	3	2587.5	195	8	11.1	68	S	0.95	1.19		2.8
NR93	390	105	9	15	400	6,675	7.06	3	2,587.5	195	10	8.1	27	S	2.11	2.59	0.6	3.62
NR93	390	105	9	15	400	6,675	7.06	3	2,587.5	195	10	11.1	68	S	2.11	2.59	0.6	3.62

Appendix B
Stability Test Parameters and Data

Data Set	Barge Length L_s, ft	Barge Width B_s, ft	Barge Draft d, ft	Water Depth h, ft	Total Channel Data: Bottom Width b_w, ft	Total Channel Data: Cross-Section Area, ft^2	Total Channel Data: Blockage Ratio	Parameters Nearest to Rock Bank: Bank Slope (cot α)	Parameters Nearest to Rock Bank: Cross-Section Area, ft^2	Parameters Nearest to Rock Bank: Tow Position S, ft	Parameters Nearest to Rock Bank: Boat Speed V_s, fps	D_{50} in.	W_{50} lbs	Stability F/M/S	z_{max}, ft	H_{max}, ft	H_j, ft	u_r, fps
NR93	390	105	9	15	400	6,675	7.06	3	2,587.5	195	12	8.1	27	S	3.63	4.43	0.64	4.49
NR93	390	105	9	15	400	6,675	7.06	3	2,587.5	195	12	11.1	68	S	3.63	4.43	0.64	4.49
NR93	390	105	9	15	400	6,675	7.06	3	4,087.5	295	8	3.25	1.7	S	0.79	0.99		2.35
NR93	390	105	9	15	400	6,675	7.06	3	4,087.5	295	8	5.8	10	S	0.79	0.99		2.35
NR93	390	105	9	15	400	6,675	7.06	3	4,087.5	295	10	3.25	1.7	M	1.75	2.15	0.5	3.04
NR93	390	105	9	15	400	6,675	7.06	3	4,087.5	295	10	5.8	10	S	1.75	2.15	0.5	3.04
NR93	390	105	9	15	400	6,675	7.06	3	4,087.5	295	12	3.25	1.7	F	3.01	3.68	0.53	3.77
NR93	390	105	9	15	400	6,675	7.06	3	4,087.5	295	12	5.8	10	M	3.01	3.68	0.53	3.77
NR93	390	105	9	20	400	8,800	9.31	2	2,400	140	6	3.25	1.7	M	0.43	0.48		1.37
NR93	390	105	9	20	400	8,800	9.31	2	2,400	140	6	5.8	10	S	0.43	0.48		1.37
NR93	390	105	9	20	400	8,800	9.31	2	2,400	140	8	3.25	1.7	M	0.76	0.79		2.14
NR93	390	105	9	20	400	8,800	9.31	2	2,400	140	8	5.8	10	S	0.76	0.79		2.14
NR93	390	105	9	20	400	8,800	9.31	2	2,400	140	10	3.25	1.7	F	1.19	1.16	0.41	3.07
NR93	390	105	9	20	400	8,800	9.31	2	2,400	140	10	5.8	10	M	1.19	1.16	0.41	3.07
NR93	390	105	9	20	400	8,800	9.31	2	2,400	140	12	3.25	1.7	F	1.71	1.6	1.29	4.16
NR93	390	105	9	20	400	8,800	9.31	2	2,400	140	12	5.8	10	M	1.71	1.6	1.29	4.16

Appendix B
Stability Test Parameters and Data

Data Set	Barge Length L_s, ft	Barge Width B_s, ft	Barge Draft d, ft	Water Depth h, ft	Total Channel Data: Bottom Width b_w, ft	Total Channel Data: Cross-Section Area, ft^2	Total Channel Data: Blockage Ratio	Parameters Nearest to Rock Bank: Bank Slope (cot α)	Parameters Nearest to Rock Bank: Cross-Section Area, ft^2	Parameters Nearest to Rock Bank: Tow Position S, ft	Parameters Nearest to Rock Bank: Boat Speed V_s, fps	D_{50} in.	W_{50} lbs	Stability F/M/S	z_{max}, ft	H_{max}, ft	H_j, ft	u_r, fps
NR93	390	105	9	20	400	8,800	9.31	2	2,400	140	14	3.25	1.7	F	2.32	2.12	1.83	5.4
NR93	390	105	9	20	400	8,800	9.31	2	2,400	140	14	5.8	10	F	2.32	2.12	1.83	5.4
NR93	390	105	9	20	400	8,800	9.31	2	4,400	240	3	3.25	1.7	S				0.49
NR93	390	105	9	20	400	8,800	9.31	2	4,400	240	3	5.8	10	S				0.49
NR93	390	105	9	20	400	8,800	9.31	2	4,400	240	3	8.1	27	S				0.49
NR93	390	105	9	20	400	8,800	9.31	2	4,400	240	3	11.1	68	S				0.49
NR93	390	105	9	20	400	8,800	9.31	2	4,400	240	5	3.25	1.7	S	0.06			0.88
NR93	390	105	9	20	400	8,800	9.31	2	4,400	240	5	5.8	10	S	0.06			0.88
NR93	390	105	9	20	400	8,800	9.31	2	4,400	240	5	8.1	27	S	0.06			0.88
NR93	390	105	9	20	400	8,800	9.31	2	4,400	240	5	11.1	68	S	0.06			0.88
NR93	390	105	9	20	400	8,800	9.31	2	4,400	240	7	3.25	1.7	M	0.24	0.15		1.32
NR93	390	105	9	20	400	8,800	9.31	2	4,400	240	7	5.8	10	S	0.24	0.15		1.32
NR93	390	105	9	20	400	8,800	9.31	2	4,400	240	7	8.1	27	S	0.24	0.15		1.32
NR93	390	105	9	20	400	8,800	9.31	2	4,400	240	7	11.1	68	S	0.24	0.15		1.32
NR93	390	105	9	20	400	8,800	9.31	2	4,400	240	8	3.25	1.7	F	0.37	0.25		1.56
NR93	390	105	9	20	400	8,800	9.31	2	4,400	240	8	5.8	10	M	0.37	0.25		1.56

Appendix B
Stability Test Parameters and Data

Data Set	Barge Length L_s, ft	Barge Width B_s, ft	Barge Draft d, ft	Water Depth h, ft	Total Channel Data			Parameters Nearest to Rock Bank				D_{50} in.	W_{50} lbs	Stability F/M/S	z_{max}, ft	H_{max}, ft	H_i, ft	u_r, fps
					Bottom Width b_w, ft	Cross-Section Area, ft^2	Blockage Ratio	Bank Slope (cot α)	Cross-Section Area, ft^2	Tow Position S, ft	Boat Speed V_s, fps							
NR93	390	105	9	20	400	8,800	9.31	2	4,400	240	8	8.1	27	S	0.37	0.25		1.56
NR93	390	105	9	20	400	8,800	9.31	2	4,400	240	8	11.1	68	S	0.37	0.25		1.56
NR93	390	105	9	20	400	8,800	9.31	2	4,400	240	9	3.25	1.7	F	0.51	0.38		1.81
NR93	390	105	9	20	400	8,800	9.31	2	4,400	240	9	5.8	10	M	0.51	0.38		1.81
NR93	390	105	9	20	400	8,800	9.31	2	4,400	240	9	8.1	27	S	0.51	0.38		1.81
NR93	390	105	9	20	400	8,800	9.31	2	4,400	240	9	11.1	68	S	0.51	0.38		1.81
NR93	390	105	9	20	400	8,800	9.31	2	4,400	240	10	3.25	1.7	F	0.68	0.53	0.275	2.07
NR93	390	105	9	20	400	8,800	9.31	2	4,400	240	10	5.8	10	M	0.68	0.53	0.275	2.07
NR93	390	105	9	20	400	8,800	9.31	2	4,400	240	10	8.1	27	S	0.68	0.53	0.275	2.07
NR93	390	105	9	20	400	8,800	9.31	2	4,400	240	10	11.1	68	S	0.68	0.53	0.275	2.07
NR93	390	105	9	20	400	8,800	9.31	2	4,400	240	12	3.25	1.7	F	1.09	0.89	0.9	2.63
NR93	390	105	9	20	400	8,800	9.31	2	4,400	240	12	5.8	10	F	1.09	0.89	0.9	2.63
NR93	390	105	9	20	400	8,800	9.31	2	4,400	240	12	8.1	27	S	1.09	0.89	0.9	2.63
NR93	390	105	9	20	400	8,800	9.31	2	4,400	240	12	11.1	68	S	1.09	0.89	0.9	2.63
NR93	390	105	9	20	400	8,800	9.31	2	4,400	240	14	3.25	1.7	F	1.59	1.34	1.81	3.24
NR93	390	105	9	20	400	8,800	9.31	2	4,400	240	14	5.8	10	F	1.59	1.34	1.81	3.24

Appendix B
Stability Test Parameters and Data

Data Set	Barge Length L_s, ft	Barge Width B_s, ft	Barge Draft d, ft	Water Depth h, ft	Total Channel Data: Bottom Width b_w, ft	Total Channel Data: Cross-Section Area, ft^2	Total Channel Data: Blockage Ratio	Parameters Nearest to Rock Bank: Bank Slope (cot α)	Parameters Nearest to Rock Bank: Cross-Section Area, ft^2	Parameters Nearest to Rock Bank: Tow Position S, ft	Parameters Nearest to Rock Bank: Boat Speed V_s, fps	D_{50} in.	W_{50} lbs	Stability F/M/S	z_{max}, ft	H_{max}, ft	H_i, ft	u_r, fps
NR93	390	105	9	20	400	8,800	9.31	2	4,400	240	14	8.1	27	S	1.59	1.34	1.81	3.24
NR93	390	105	9	20	400	8,800	9.31	2	4,400	240	14	11.1	68	S	1.59	1.34	1.81	3.24
NR93	390	105	9	20	400	8,800	9.31	2	6,400	340	6	8.1	27	S	0.19	0.16		0.91
NR93	390	105	9	20	400	8,800	9.31	2	6,400	340	6	11.1	68	S	0.19	0.16		0.91
NR93	390	105	9	20	400	8,800	9.31	2	6,400	340	8	8.1	27	S	0.46	0.42		1.44
NR93	390	105	9	20	400	8,800	9.31	2	6,400	340	8	11.1	68	S	0.46	0.42		1.44
NR93	390	105	9	20	400	8,800	9.31	2	6,400	340	10	8.1	27	S	0.83	0.77	0.225	2.09
NR93	390	105	9	20	400	8,800	9.31	2	6,400	340	10	11.1	68	S	0.83	0.77	0.225	2.09
NR93	390	105	9	20	400	8,800	9.31	2	6,400	340	12	8.1	27	S	1.3	1.21	0.76	2.84
NR93	390	105	9	20	400	8,800	9.31	2	6,400	340	12	11.1	68	S	1.3	1.21	0.76	2.84
NR93	390	105	9	20	400	8,800	9.31	2	6,400	340	14	8.1	27	S	1.87	1.76	1.375	3.71
NR93	390	105	9	20	400	8,800	9.31	2	6,400	340	14	11.1	68	S	1.87	1.76	1.375	3.71
NR93	390	105	9	20	400	9,200	9.74	3	2,600	160	6	3.25	1.7	M				1.25
NR93	390	105	9	20	400	9,200	9.74	3	2,600	160	6	5.8	10	S				1.25
NR93	390	105	9	20	400	9,200	9.74	3	2,600	160	8	3.25	1.7	M	0.43	0.47		2
NR93	390	105	9	20	400	9,200	9.74	3	2,600	160	8	5.8	10	S	0.43	0.47		2

Appendix B
Stability Test Parameters and Data

Data Set	Barge Length L_s, ft	Barge Width B_s, ft	Barge Draft d, ft	Water Depth h, ft	Total Channel Data			Parameters Nearest to Rock Bank				D_{50} in.	W_{50} lbs	Stability F/M/S	z_{max}, ft	H_{max}, ft	H_j, ft	u_r, fps
					Bottom Width b_w, ft	Cross-Section Area, ft^2	Blockage Ratio	Bank Slope (cot α)	Cross-Section Area, ft^2	Tow Position S, ft	Boat Speed V_s, fps							
NR93	390	105	9	20	400	9,200	9.74	3	2,600	160	10	3.25	1.7	F	1.21	1.45	0.45	2.91
NR93	390	105	9	20	400	9,200	9.74	3	2,600	160	10	5.8	10	M	1.21	1.45	0.45	2.91
NR93	390	105	9	20	400	9,200	9.74	3	2,600	160	12	3.25	1.7	F	2.27	2.78	1.99	3.98
NR93	390	105	9	20	400	9,200	9.74	3	2,600	160	12	5.8	10	M	2.27	2.78	1.99	3.98
NR93	390	105	9	20	400	9,200	9.74	3	2,600	160	14	3.25	1.7	F	3.59	4.45	3.19	5.22
NR93	390	105	9	20	400	9,200	9.74	3	2,600	160	14	5.8	10	F	3.59	4.45	3.19	5.22
NR93	390	105	9	20	400	9,200	9.74	3	4,600	260	3	3.25	1.7	S				0.43
NR93	390	105	9	20	400	9,200	9.74	3	4,600	260	3	5.8	10	S				0.43
NR93	390	105	9	20	400	9,200	9.74	3	4,600	260	3	8.1	27	S				0.43
NR93	390	105	9	20	400	9,200	9.74	3	4,600	260	3	11.1	68	S				0.43
NR93	390	105	9	20	400	9,200	9.74	3	4,600	260	5	3.25	1.7	S				0.78
NR93	390	105	9	20	400	9,200	9.74	3	4,600	260	5	5.8	10	S				0.78
NR93	390	105	9	20	400	9,200	9.74	3	4,600	260	5	8.1	27	S				0.78
NR93	390	105	9	20	400	9,200	9.74	3	4,600	260	5	11.1	68	S				0.78
NR93	390	105	9	20	400	9,200	9.74	3	4,600	260	7	3.25	1.7	M	0.33	0.31		1.18
NR93	390	105	9	20	400	9,200	9.74	3	4,600	260	7	5.8	10	S	0.33	0.31		1.18

Appendix B
Stability Test Parameters and Data

Data Set	Barge Length L_s, ft	Barge Width B_s, ft	Barge Draft d, ft	Water Depth h, ft	Total Channel Data: Bottom Width b_w, ft	Total Channel Data: Cross-Section Area, ft^2	Total Channel Data: Blockage Ratio	Parameters Nearest to Rock Bank: Bank Slope (cot α)	Parameters Nearest to Rock Bank: Cross-Section Area, ft^2	Parameters Nearest to Rock Bank: Tow Position S, ft	Parameters Nearest to Rock Bank: Boat Speed V_s, fps	D_{50} in.	W_{50} lbs	Stability F/M/S	z_{max}, ft	H_{max}, ft	H_i, ft	u_r, fps
NR93	390	105	9	20	400	9,200	9.74	3	4,600	260	7	8.1	27	S	0.33	0.31		1.18
NR93	390	105	9	20	400	9,200	9.74	3	4,600	260	7	11.1	68	S	0.33	0.31		1.18
NR93	390	105	9	20	400	9,200	9.74	3	4,600	260	8	3.25	1.7	F	0.51	0.52		1.39
NR93	390	105	9	20	400	9,200	9.74	3	4,600	260	8	5.8	10	M	0.51	0.52		1.39
NR93	390	105	9	20	400	9,200	9.74	3	4,600	260	8	8.1	27	S	0.51	0.52		1.39
NR93	390	105	9	20	400	9,200	9.74	3	4,600	260	8	11.1	68	S	0.51	0.52		1.39
NR93	390	105	9	20	400	9,200	9.74	3	4,600	260	9	3.25	1.7	F	0.65	0.77		1.62
NR93	390	105	9	20	400	9,200	9.74	3	4,600	260	9	5.8	10	M	0.65	0.77		1.62
NR93	390	105	9	20	400	9,200	9.74	3	4,600	260	9	8.1	27	S	0.65	0.77		1.62
NR93	390	105	9	20	400	9,200	9.74	3	4,600	260	9	11.1	68	S	0.65	0.77		1.62
NR93	390	105	9	20	400	9,200	9.74	3	4,600	260	10	3.25	1.7	F	0.84	1.07	0.33	1.87
NR93	390	105	9	20	400	9,200	9.74	3	4,600	260	10	5.8	10	M	0.84	1.07	0.33	1.87
NR93	390	105	9	20	400	9,200	9.74	3	4,600	260	10	8.1	27	S	0.84	1.07	0.33	1.87
NR93	390	105	9	20	400	9,200	9.74	3	4,600	260	10	11.1	68	S	0.84	1.07	0.33	1.87
NR93	390	105	9	20	400	9,200	9.74	3	4,600	260	12	3.25	1.7	F	1.31	1.78	1.36	2.38

Appendix B
Stability Test Parameters and Data

					Total Channel Data			Parameters Nearest to Rock Bank										
Data Set	Barge Length L_s, ft	Barge Width B_s, ft	Barge Draft d, ft	Water Depth h, ft	Bottom Width b_w, ft	Cross-Section Area, ft^2	Block-age Ratio	Bank Slope (cot α)	Cross-Section Area, ft^2	Tow Position S, ft	Boat Speed V_s, fps	D_{50} in.	W_{50} lbs	Stab-ility F/M/S	z_{max}, ft	H_{max}, ft	H_i, ft	u_r, fps
NR93	390	105	9	20	400	9,200	9.74	3	4,600	260	12	5.8	10	M	1.31	1.78	1.36	2.38
NR93	390	105	9	20	400	9,200	9.74	3	4,600	260	12	8.1	27	S	1.31	1.78	1.36	2.38
NR93	390	105	9	20	400	9,200	9.74	3	4,600	260	12	11.1	68	S	1.31	1.78	1.36	2.38
NR93	390	105	9	20	400	9,200	9.74	3	4,600	260	14	3.25	1.7	F	1.87	2.66	1.63	2.95
NR93	390	105	9	20	400	9,200	9.74	3	4,600	260	14	5.8	10	M	1.87	2.66	1.63	2.95
NR93	390	105	9	20	400	9,200	9.74	3	4,600	260	14	8.1	27	S	1.87	2.66	1.63	2.95
NR93	390	105	9	20	400	9,200	9.74	3	4,600	260	14	11.1	68	S	1.87	2.66	1.63	2.95
NR93	390	105	9	20	400	9,200	9.74	3	6,600	360	6	8.1	27	S	0.13	0.1		0.79
NR93	390	105	9	20	400	9,200	9.74	3	6,600	360	6	11.1	68	S	0.13	0.1		0.79
NR93	390	105	9	20	400	9,200	9.74	3	6,600	360	8	8.1	27	S	0.29	0.45		1.3
NR93	390	105	9	20	400	9,200	9.74	3	6,600	360	8	11.1	68	S	0.29	0.45		1.3
NR93	390	105	9	20	400	9,200	9.74	3	6,600	360	10	8.1	27	S	0.85	1.19	0.23	1.94
NR93	390	105	9	20	400	9,200	9.74	3	6,600	360	10	11.1	68	S	0.85	1.19	0.23	1.94
NR93	390	105	9	20	400	9,200	9.74	3	6,600	360	12	8.1	27	S	1.6	2.17	0.9	2.7
NR93	390	105	9	20	400	9,200	9.74	3	6,600	360	12	11.1	68	S	1.6	2.17	0.9	2.7
NR93	390	105	9	20	400	9,200	9.74	3	6,600	360	14	8.1	27	S	2.54	3.4	1.58	3.58

Appendix B
Stability Test Parameters and Data

Data Set	Barge Length L_s, ft	Barge Width B_s, ft	Barge Draft d, ft	Water Depth h, ft	Total Channel Data: Bottom Width b_w, ft	Total Channel Data: Cross-Section Area, ft^2	Total Channel Data: Blockage Ratio	Parameters Nearest to Rock Bank: Bank Slope (cot α)	Parameters Nearest to Rock Bank: Cross-Section Area, ft^2	Parameters Nearest to Rock Bank: Tow Position S, ft	Parameters Nearest to Rock Bank: Boat Speed V_s, fps	D_{50} in.	W_{50} lbs	Stability F/M/S	z_{max}, ft	H_{max}, ft	H_i, ft	u_r, fps
NR93	390	105	9	20	400	9,200	9.74	3	6,600	360	14	11.1	68	S	2.54	3.4	1.58	3.58
NR90	390	105	9	14	450	6,594	6.98	3	2,009	164.5	5.4	3.25	1.7	S	0.26			1.36
NR90	390	105	9	14	450	6,594	6.98	3	2,009	164.5	5.4	5	6.3	S	0.26			1.36
NR90	390	105	9	14	450	6,594	6.98	3	2,009	164.5	5.4	5.8	10	S	0.26			1.36
NR90	390	105	9	14	450	6,594	6.98	3	2,499	199.5	5.4	3.25	1.7	S	0.23			1.23
NR90	390	105	9	14	450	6,594	6.98	3	2,499	199.5	5.4	5	6.3	S	0.23			1.23
NR90	390	105	9	14	450	6,594	6.98	3	2,499	199.5	5.4	5.8	10	S	0.23			1.23
NR90	390	105	9	14	500	7,196	7.61	2	1,911	150.5	5.4	3.25	1.7	F	0.25			1.31
NR90	390	105	9	14	500	7,196	7.61	2	1,911	150.5	5.4	5	6.3	F	0.25			1.31
NR90	390	105	9	14	500	7,196	7.61	2	1,911	150.5	5.4	5.8	10	M	0.25			1.31
NR90	390	105	9	14	500	7,196	7.61	2	2,401	185.5	5.4	3.25	1.7	F	0.22			1.17
NR90	390	105	9	14	500	7,196	7.61	2	2,401	185.5	5.4	5	6.3	M	0.22			1.17
NR90	390	105	9	14	500	7,196	7.61	2	2,401	185.5	5.4	5.8	10	S	0.22			1.17
NR90	390	105	9	20	450	9,600	10.16	3	3,750	217.5	7.2	3.25	1.7	S	0.26			1.07
NR90	390	105	9	20	450	9,600	10.16	3	3,750	217.5	7.2	5	6.3	S	0.26			1.07
NR90	390	105	9	20	450	9,600	10.16	3	3,750	217.5	7.2	5.8	10	S	0.26			1.07

Appendix B
Stability Test Parameters and Data

Data Set	Barge Length L_s, ft	Barge Width B_s, ft	Barge Draft d, ft	Water Depth h, ft	Total Channel Data: Bottom Width b_w, ft	Total Channel Data: Cross-Section Area, ft^2	Total Channel Data: Blockage Ratio	Parameters Nearest to Rock Bank: Bank Slope (cot α)	Parameters Nearest to Rock Bank: Cross-Section Area, ft^2	Parameters Nearest to Rock Bank: Tow Position S, ft	Parameters Nearest to Rock Bank: Boat Speed V_s, fps	D_{50} in.	W_{50} lbs	Stability F/M/S	z_{max}, ft	H_{max}, ft	H_i, ft	u_r, fps
NR90	390	105	9	20	450	9,600	10.16	3	3,750	217.5	9.9	3.25	1.7	S	0.56			1.68
NR90	390	105	9	20	450	9,600	10.16	3	3,750	217.5	9.9	5	6.3	S	0.56			1.68
NR90	390	105	9	20	450	9,600	10.16	3	3,750	217.5	9.9	5.8	10	S	0.56			1.68
NR90	390	105	9	20	500	10,400	11.01	2	3,550	197.5	7.2	3.25	1.7	F	0.25			1.04
NR90	390	105	9	20	500	10,400	11.01	2	3,550	197.5	7.2	5	6.3	F	0.25			1.04
NR90	390	105	9	20	500	10,400	11.01	2	3,550	197.5	7.2	5.8	10	M	0.25			1.04
NR90	390	105	9	20	500	10,400	11.01	2	3,550	197.5	9.9	3.25	1.7	F	0.53			1.61
NR90	390	105	9	20	500	10,400	11.01	2	3,550	197.5	9.9	5	6.3	F	0.53			1.61
NR90	390	105	9	20	500	10,400	11.01	2	3,550	197.5	9.9	5.8	10	M	0.53			1.61
TT	390	105	9	14	280	4,312	4.56	2	2,156	168	8.6	11.1	68	S	1.9	1.5		4.25
TT	390	105	9	14	280	4,312	4.56	2	2,156	168	8.6	8.1	27	S	1.9	1.5		4.25
TT	390	105	9	14	280	4,312	4.56	2	2,156	168	8.6	6.3	13	S	1.9	1.5		4.25
TT	195	70	2	14	280	4,312	10.50	2	2,156	168	13.3	11.1	68	F	2.9	3.1		
TT	195	70	2	14	280	4,312	10.50	2	2,156	168	13.3	8.1	27	F	2.9	3.1		
TT	195	70	2	14	280	4,312	10.50	2	2,156	168	13.3	6.3	13	F	2.9	3.1		
TT	195	70	2	14	280	4,312	10.50	2	2,156	168	13	11.1	68	S	2.2	1.5		

Appendix B
Stability Test Parameters and Data

Data Set	Barge Length L_s, ft	Barge Width B_s, ft	Barge Draft d, ft	Water Depth h, ft	Total Channel Data			Parameters Nearest to Rock Bank				D_{50} in.	W_{50} lbs	Stability F/M/S	z_{max}, ft	H_{max}, ft	H_i, ft	u_r, fps
					Bottom Width b_w, ft	Cross-Section Area, ft^2	Blockage Ratio	Bank Slope (cot α)	Cross-Section Area, ft^2	Tow Position S, ft	Boat Speed V_s, fps							
TT	195	70	2	14	280	4,312	10.50	2	2,156	168	13	8.1	27	S	2.2	1.5		
TT	195	70	2	14	280	4,312	10.50	2	2,156	168	13	6.3	13	S	2.2	1.5		
TT	195	70	2	17.5	280	5,513	13.40	2	2756.3	175	15.3	11.1	68	F	3	3		7.72
TT	195	70	2	17.5	280	5,513	13.40	2	2,756.3	175	15	8.1	27	F	2.3	2.3		7.44
TT	195	70	2	17.5	280	5,513	13.40	2	2,756.3	175	15	6.3	13	F	2.3	2.3		7.44
TT	195	70	2	17.5	280	5,513	13.40	2	2,756.3	175	15	11.1	68	S	2.3	2.3		7.44
TT	195	70	2	17.5	280	5,513	13.40	2	2,756.3	175	14.7	8.1	27	S	1.7	1.7		7.17
TT	195	70	2	17.5	280	5,513	13.40	2	2,756.3	175	14.7	6.3	13	S	1.7	1.7		7.17
TT	390	105	9	18	280	5,688	6.02	2	2,844	176	11.2	11.1	68	S	2.1	1.8		
TT	390	105	9	18	280	5,688	6.02	2	2,844	176	11.2	8.1	27	S	2.1	1.8		
TT	390	105	9	18	280	5,688	6.02	2	2,844	176	11.2	6.3	13	S	2.1	1.8		
TT	390	105	9	18	280	5,688	6.02	2	2,844	176	10.6	11.1	68	S	1.85	1.5		
TT	390	105	9	18	280	5,688	6.02	2	2,844	176	10.6	8.1	27	S	1.85	1.5		
TT	390	105	9	18	280	5,688	6.02	2	2,844	176	10.6	6.3	13	S	1.85	1.5		
TT	195	70	2	21	280	6,762	16.40	2	3,381	182	16.7	11.1	68	F	2.8	2.9		5.5
TT	195	70	2	21	280	6,762	16.40	2	3,381	182	16.7	8.1	27	F	2.8	2.9		5.5

Appendix B
Stability Test Parameters and Data

Data Set	Barge Length L_a, ft	Barge Width B_a, ft	Barge Draft d, ft	Water Depth h, ft	Total Channel Data			Parameters Nearest to Rock Bank				D_{50} in.	W_{50} lbs	Stability F/M/S	z_{max}, ft	H_{max}, ft	H_j, ft	u_r, fps
					Bottom Width b_w, ft	Cross-Section Area, ft^2	Blockage Ratio	Bank Slope (cot α)	Cross-Section Area, ft^2	Tow Position S, ft	Boat Speed V_s, fps							
TT	195	70	2	21	280	6,762	16.40	2	3,381	182	16.4	6.3	13	F	2.15	2.5		5.4
TT	195	70	2	21	280	6,762	16.40	2	3,381	182	16.4	11.1	68	S	2.15	2.5		5.4
TT	195	70	2	21	280	6,762	16.40	2	3,381	182	16.4	8.1	27	S	2.15	2.5		5.4
TT	195	70	2	21	280	6,762	16.40	2	3,381	182	15.6	6.3	13	S	1.5	1.7		5.1
TT	390	105	9	22	280	7,128	7.54	2	3,564	184	12.8	11.1	68	S	1.9	2.2		
TT	390	105	9	22	280	7,128	7.54	2	3,564	184	12.8	8.1	27	S	1.9	2.2		
TT	390	105	9	22	280	7,128	7.54	2	3,564	184	12.8	6.3	13	S	1.9	2.2		
TT	390	105	9	22	280	7,128	7.54	2	3,564	184	12.1	11.1	68	S	1.7	1.9		
TT	390	105	9	22	280	7,128	7.54	2	3,564	184	12.1	8.1	27	S	1.7	1.9		
TT	390	105	9	22	280	7,128	7.54	2	3,564	184	12.1	6.3	13	S	1.7	1.9		
GAL	975	105	9	15	425	6,712.5	7.10	3	2,175	167.5	7.9	6	10.9	S	0.88			1.7

(Concluded)

Appendix C
All Data Related to Velocities From Hydrodynamic Tests

Appendix C
All Data Related to Velocities from Hydrodynamic Tests

Test Series	Bottom Width b_w, ft	Water Depth h, ft	Left Bank cot α	Tow Position, S, ft	Barge Width B_s, ft	Barge Draft d, ft	Boat Speed V_s, fps	Inst. Dist. from Left Bank, ft	Inst. Depth from Bottom ft	Velocity Data Measured				Blockage Ratio, Left Side, n	Schijf Calculated	
										x-vel		y-vel				
										Return Current u_r, fps	Bow Current u_b, fps	Max away from Bow u_{yb}, fps	Max to Stern u_{ys}, fps		Limit Speed V_L, fps	Left Side u_r, fps
TT	280	14	2	168	105	9	6.03	14	3	1.84				4.56	9.2	2.06
TT	280	14	2	168	105	9	6.34	14	3	2.13				4.56	9.2	2.22
TT	280	14	2	168	105	9	6.67	14	3	2.18				4.56	9.2	2.41
TT	280	14	2	168	105	9	6.72	14	3	2.37				4.56	9.2	2.44
TT	280	14	2	168	105	9	6.95	14	3	2.72				4.56	9.2	2.58
TT	280	14	2	168	105	9	7.07	14	3	2.84				4.56	9.2	2.66
TT	280	14	2	168	105	9	7.38	14	3	2.89				4.56	9.2	2.88
TT	280	14	2	168	105	9	7.47	14	3	3.08				4.56	9.2	2.95
TT	280	14	2	168	105	9	7.58	14	3	3.26				4.56	9.2	3.04
TT	280	14	2	168	105	9	7.7	14	3	3.37				4.56	9.2	3.14
TT	280	14	2	168	105	9	7.95	14	3	3.5				4.56	9.2	3.37
TT	280	14	2	168	105	9	8.11	14	3	3.68				4.56	9.2	3.37
TT	280	14	2	168	105	9	8.19	14	3	3.79				4.56	9.2	3.54

Appendix C
All Data Related to Velocities from Hydrodynamic Tests

Test Series	Bottom Width b_w, ft	Water Depth h, ft	Left Bank cot α	Tow Position, S, ft	Barge Width B_s, ft	Barge Draft d, ft	Boat Speed V_s, fps	Inst. Dist. from Left Bank, ft	Inst. Depth from Bottom ft	Velocity Data Measured				Blockage Ratio, Left Side, n	Schijf Calculated	
										x-vel		y-vel			Limit Speed V_L, fps	Left Side u_r, fps
										Return Current u_r, fps	Bow Current u_b, fps	Max away from Bow u_{yb}, fps	Max to Stern u_{ys}, fps			
TT	280	14	2	168	105	9	8.3	14	3	3.95				4.56	9.2	3.76
TT	280	14	2	168	105	9	8.49	14	3	4.16				4.56	9.2	4.02
TT	280	14	2	168	105	9	8.57	14	3	4.25				4.56	9.2	4.15
TT	280	14	2	168	105	9	8.96	14	3	4.5				4.56	9.2	4.99
TT	280	17.5	2	175	70	2	5.21	17.5	4.75	1.37				13.40		
TT	280	17.5	2	175	70	2	6.85	17.5	4.75	2.17				13.40		
TT	280	17.5	2	175	70	2	8.57	17.5	4.75	2.17				13.40		
TT	280	17.5	2	175	70	2	9.73	17.5	4.75	3.14				13.40		
TT	280	17.5	2	175	70	2	10.42	17.5	4.75	3.53				13.40		
TT	280	17.5	2	175	70	2	10.65	17.5	4.75	3.95				13.40		
TT	280	17.5	2	175	70	2	11.18	17.5	4.75	4.92				13.40		
TT	280	21	2	182	70	2	5.09	21	6.5	1.1				16.40		
TT	280	21	2	182	70	2	5.63	21	6.5	1.76				16.40		

Appendix C
All Data Related to Velocities from Hydrodynamic Tests

Test Series	Bottom Width b_w, ft	Water Depth h, ft	Left Bank cot α	Tow Position, S, ft	Barge Width B_s, ft	Barge Draft d, ft	Boat Speed V_s, fps	Inst. Dist. from Left Bank, ft	Inst. Depth from Bottom ft	Velocity Data Measured				Blockage Ratio, Left Side, n	Schijf Calculated	
										x-vel		y-vel			Limit Speed V_L, fps	Left Side u_r, fps
										Return Current u_r, fps	Bow Current u_b, fps	Max away from Bow u_{yb}, fps	Max to Stern u_{ys}, fps			
TT	280	21	2	182	70	2	6.84	21	6.5	1.76				16.40		
TT	280	21	2	182	70	2	7.1	21	6.5	1.79				16.40		
TT	280	21	2	182	70	2	8.64	21	6.5	2.67				16.40		
TT	280	21	2	182	70	2	11.15	21	6.5	3.58				16.40		
TT	280	21	2	182	70	2	11.97	21	6.5	3.58				16.40		
TT	280	21	2	182	70	2	11.97	21	6.5	4.47				16.40		
TT	280	21	2	182	70	2	13.39	21	6.5	3.58				16.40		
GAL	425	15	3	167.5	105	9	7.92	30	2	2				4.60	12	1.97
GAL	425	15	3	167.5	105	9	7.92	30	2	1.4				4.60	12	1.97
GAL	425	15	3	167.5	105	9	7.92	30	2	1.8				4.60	12	1.97
GAL	425	15	3	167.5	105	9	7.92	30	2	1.9				4.60	12	1.97
GAL	425	15	3	167.5	105	9	7.92	30	2	1.5				4.60	12	1.97
SCT	400	20	0	200	105	9	5.55	73.75	10	1.067		0.309	0.186	8.47	15	0.8

Appendix C
All Data Related to Velocities from Hydrodynamic Tests

Test Series	Bottom Width b_w, ft	Water Depth h, ft	Left Bank cot α	Tow Position, S, ft	Barge Width B_s, ft	Barge Draft d, ft	Boat Speed V_s, fps	Inst. Dist. from Left Bank, ft	Inst. Depth from Bottom ft	Velocity Data Measured				Blockage Ratio, Left Side, n	Schijf Calculated	
										x-vel		y-vel			Limit Speed V_L, fps	Left Side u_r, fps
										Return Current u_r, fps	Bow Current u_b, fps	Max away from Bow u_{yb}, fps	Max to Stern u_{ys}, fps			
SCT	400	20	0	200	105	9	5.41	73.75	10	1.085		0.306	0.183	8.47	15	0.77
SCT	400	20	0	200	105	9	5.46	73.75	10	1.058		0.326	0.2	8.47	15	0.78
SCT	400	20	0	200	105	9	6.66	73.75	10	1.161	0.135	0.389	0.287	8.47	15	0.99
SCT	400	20	0	200	105	9	6.08	73.75	10	1.085	0.105	0.375	0.24	8.47	15	0.89
SCT	400	20	0	200	105	9	6.8	73.75	10	1.098	0.108	0.395	0.252	8.47	15	1.01
SCT	400	20	0	200	105	9	8	73.75	8	1.061	0.594			8.47	15	1.25
SCT	400	20	0	200	105	9	8.18	73.75	10	1.139	0.439	0.461	0.267	8.47	15	1.28
SCT	400	20	0	200	105	9	8.59	73.75	10	1.195	0.427	0.478	0.316	8.47	15	1.37
SCT	400	20	0	200	105	9	8.59	73.75	10	1.25	0.331	0.472	0.317	8.47	15	1.37
SCT	400	20	0	200	105	9	10	73.75	8	1.382	0.667			8.47	15	1.73
SCT	400	20	0	200	105	9	10.82	73.75	10	1.722	0.695	0.592	0.435	8.47	15	1.98
SCT	400	20	0	200	105	9	10.73	73.75	10	1.765	0.67	0.615	0.496	8.47	15	1.95
SCT	400	20	0	200	105	9	10.69	73.75	10	1.67	0.663	0.61	0.449	8.47	15	1.93

Appendix C
All Data Related to Velocities from Hydrodynamic Tests

Test Series	Bottom Width b_w, ft	Water Depth h, ft	Left Bank cot α	Tow Position, S, ft	Barge Width B_s, ft	Barge Draft d, ft	Boat Speed V_s, fps	Inst. Dist. from Left Bank, ft	Inst. Depth from Bottom ft	Velocity Data Measured				Blockage Ratio, Left Side, n	Schijf Calculated	
										x-vel		y-vel			Limit Speed V_L, fps	Left Side u_r, fps
										Return Current u_r, fps	Bow Current u_b, fps	Max away from Bow u_{yb}, fps	Max to Stern u_{ys}, fps			
SCT	400	20	0	200	105	9	11.4	73.75	10	1.935	0.782	0.63	0.544	8.47	15	2.18
SCT	400	20	0	200	105	9	11.63	73.75	10	1.995	0.82	0.663	0.499	8.47	15	2.27
SCT	400	20	0	200	105	9	11.58	73.75	10	1.979	0.7714	0.663	0.533	8.47	15	2.25
SCT	400	20	0	200	105	9	13	73.75	8	2.196	1.217			8.47	15	2.93
SCT	400	20	0	200	105	9	5.23	36.88	10	0.919		0.107	0.141	8.47	15	0.74
SCT	400	20	0	200	105	9	5.23	36.88	10	0.957	0.032	0.111	0.089	8.47	15	0.74
SCT	400	20	0	200	105	9	5.1	36.88	10	0.93	0.057	0.118	0.096	8.47	15	0.72
SCT	400	20	0	200	105	9	6	36.88	8	0.788	0.402			8.47	15	0.87
SCT	400	20	0	200	105	9	7.87	36.88	10	1.165	0.325	0.2	0.16	8.47	15	1.22
SCT	400	20	0	200	105	9	8	36.88	8	1.105	0.495			8.47	15	1.25
SCT	400	20	0	200	105	9	9.44	36.88	10	1.382	0.444	0.325	0.112	8.47	15	1.58
SCT	400	20	0	200	105	9	8.81	36.88	10	1.228	0.4445	0.23	0.175	8.47	15	1.42
SCT	400	20	0	200	105	9	8.45	36.88	10	1.157	0.437	0.21	0.173	8.47	15	1.34

Appendix C
All Data Related to Velocities from Hydrodynamic Tests

Test Series	Bottom Width b_w, ft	Water Depth h, ft	Left Bank cot α	Tow Position, S, ft	Barge Width B_s, ft	Barge Draft d, ft	Boat Speed V_s, fps	Inst. Dist. from Left Bank, ft	Inst. Depth from Bottom ft	Velocity Data Measured				Blockage Ratio, Left Side, n	Schijf Calculated	
										x-vel		y-vel			Limit Speed V_L, fps	Left Side u_r, fps
										Return Current u_r, fps	Bow Current u_b, fps	Max away from Bow u_{yb}, fps	Max to Stern u_{ys}, fps			
SCT	400	20	0	200	105	9	10	36.88	8	1.305	0.739			8.47	15	1.73
SCT	400	20	0	200	105	9	10.69	36.88	10	1.708	0.66	0.284	0.208	8.47	15	1.93
SCT	400	20	0	200	105	9	10.82	36.88	10	1.626	0.933	0.291	0.2	8.47	15	1.98
SCT	400	20	0	200	105	9	10.96	36.88	10	1.755	0.774	0.312	0.208	8.47	15	2.02
SCT	400	20	0	200	105	9	11.72	36.88	10	1.887	0.717	0.303	0.255	8.47	15	2.3
SCT	400	20	0	200	105	9	13	36.88	8	2.13	1.095			8.47	15	2.93
SCT	400	20	0	200	105	9	5.5	110.63	10	0.891	0.337	0.578	0.405	8.47	15	0.79
SCT	400	20	0	200	105	9	5.41	110.63	10	0.885	0.313	0.575	0.437	8.47	15	0.77
SCT	400	20	0	200	105	9	5.1	110.63	10	0.931	0.443	0.537	0.364	8.47	15	0.72
SCT	400	20	0	200	105	9	6	110.63	8	1.084	0.368			8.47	15	0.87
SCT	400	20	0	200	105	9	7.11	110.63	10	1.038	0.392	0.747	0.491	8.47	15	1.07
SCT	400	20	0	200	105	9	8	110.63	8	1.14	0.601			8.47	15	1.25
SCT	400	20	0	200	105	9	8.54	110.63	10	1.319	0.531	0.897	0.547	8.47	15	1.36

Appendix C
All Data Related to Velocities from Hydrodynamic Tests

Test Series	Bottom Width b_w, ft	Water Depth h, ft	Left Bank cot α	Tow Position, S, ft	Barge Width B_s, ft	Barge Draft d, ft	Boat Speed V_s, fps	Inst. Dist. from Left Bank, ft	Inst. Depth from Bottom ft	Velocity Data Measured				Blockage Ratio, Left Side, n	Schijf Calculated	
										x-vel		y-vel			Limit Speed V_L, fps	Left Side u_r, fps
										Return Current u_r, fps	Bow Current u_b, fps	Max away from Bow u_{yb}, fps	Max to Stern u_{ys}, fps			
SCT	400	20	0	200	105	9	8.41	110.63	10	1.261	0.536	0.87	0.611	8.47	15	1.33
SCT	400	20	0	200	105	9	8.72	110.63	10	1.398	0.547	0.941	0.648	8.47	15	1.4
SCT	400	20	0	200	105	9	10	110.63	8	1.519	0.791			8.47	15	1.73
SCT	400	20	0	200	105	9	10.82	110.63	10	1.787	0.78	1.148	0.741	8.47	15	1.98
SCT	400	20	0	200	105	9	11.72	110.63	10	2.125	1.02	1.594	0.85	8.47	15	2.3
SCT	400	20	0	200	105	9	11.58	110.63	10	2.075	1.01	1.3	0.825	8.47	15	2.25
SCT	400	20	0	200	105	9	11.58	110.63	10	2.032	0.978	1.271	0.851	8.47	15	2.25
SCT	400	20	0	200	105	9	13	110.63	8	2.45	1.139			8.47	15	2.93
SCT	400	20	0	200	105	9	6	73.75	16	1.231	0.523	0.432	0.154	8.47	15	0.87
SCT	400	20	0	200	105	9	6	73.75	8	1.231	0.545	0.884	0.544	8.47	15	0.87
SCT	400	20	0	200	105	9	6	73.75	4	1.128	0.507	0.374	0.221	8.47	15	0.87
SCT	400	20	0	200	105	9	8	73.75	16	1.433	0.667	0.544	0.239	8.47	15	1.25
SCT	400	20	0	200	105	9	8	73.75	8	1.245	0.509			8.47	15	1.25

Appendix C
All Data Related to Velocities from Hydrodynamic Tests

Test Series	Bottom Width b_w, ft	Water Depth h, ft	Left Bank cot α	Tow Position, S, ft	Barge Width B_s, ft	Barge Draft d, ft	Boat Speed V_s, fps	Inst. Dist. from Left Bank, ft	Inst. Depth from Bottom ft	Velocity Data Measured				Blockage Ratio, Left Side, n	Schijf Calculated	
										x-vel		y-vel			Limit Speed V_L, fps	Left Side u_r, fps
										Return Current u_r, fps	Bow Current u_b, fps	Max away from Bow u_{yb}, fps	Max to Stern u_{ys}, fps			
SCT	400	20	0	200	105	9	8	73.75	4	1.298	0.638	0.522	0.275	8.47	15	1.25
SCT	400	20	0	200	105	9	10	73.75	16	1.654	0.801	0.857	0.515	8.47	15	1.73
SCT	400	20	0	200	105	9	10	73.75	8	2.047	0.992	0.686	0.466	8.47	15	1.73
SCT	400	20	0	200	105	9	10	73.75	4	1.963	1.135	0.7128	0.449	8.47	15	1.73
SCT	400	20	0	200	105	9	12	73.75	16	2.824	1.166	0.897	0.544	8.47	15	2.42
SCT	400	20	0	200	105	9	12	73.75	8	2.769	1.39	0.947	0.63	8.47	15	2.42
SCT	400	20	0	200	105	9	12	73.75	4	2.908	1.228	0.94	0.513	8.47	15	2.42
SCT	400	20	0	200	105	9	13	73.75	16	3.155	1.497	1.052	0.518	8.47	15	2.93
SCT	400	20	0	200	105	9	13	73.75	8	3.129	1.609	1.08	0.5	8.47	15	2.93
SCT	400	20	0	200	105	9	13	73.75	4	3.169	1.479	1.034	0.531	8.47	15	2.93
SCT	400	20	0	200	105	9	6	36.88	16	0.941	0.517	0.228	0.372	8.47	15	0.87
SCT	400	20	0	200	105	9	6	36.88	8	0.984	0.468	0.209	0.409	8.47	15	0.87
SCT	400	20	0	200	105	9	6	36.88	4	0.878	0.476	0.204		8.47	15	0.87

Appendix C
All Data Related to Velocities from Hydrodynamic Tests

Test Series	Bottom Width b_w, ft	Water Depth h, ft	Left Bank cot α	Tow Position, S, ft	Barge Width B_s, ft	Barge Draft d, ft	Boat Speed V_s, fps	Inst. Dist. from Left Bank, ft	Inst. Depth from Bottom ft	Velocity Data Measured				Blockage Ratio, Left Side, n	Schijf Calculated	
										x-vel		y-vel			Limit Speed V_L, fps	Left Side u_r, fps
										Return Current u_r, fps	Bow Current u_b, fps	Max away from Bow u_{yb}, fps	Max to Stern u_{ys}, fps			
SCT	400	20	0	200	105	9	8	36.88	16	1.105	0.557	0.261	0.644	8.47	15	1.25
SCT	400	20	0	200	105	9	8	36.88	8	1.254	0.729	0.29	0.46	8.47	15	1.25
SCT	400	20	0	200	105	9	8	36.88	4	1.229	0.561	0.246		8.47	15	1.25
SCT	400	20	0	200	105	9	10	36.88	16	1.966	0.94	0.543	1.164	8.47	15	1.73
SCT	400	20	0	200	105	9	10	36.88	8	1.689	0.838	0.37	0.844	8.47	15	1.73
SCT	400	20	0	200	105	9	10	36.88	4	1.805	0.826	0.3534	0.5345	8.47	15	1.73
SCT	400	20	0	200	105	9	12	36.88	16	2.279	1.177	0.477		8.47	15	2.42
SCT	400	20	0	200	105	9	12	36.88	8	2.305	1.121	0.535		8.47	15	2.42
SCT	400	20	0	200	105	9	12	36.88	4	2.133	1.047	0.419	1.198	8.47	15	2.42
SCT	400	20	0	200	105	9	13	36.88	16	2.514	1.551	0.476	0.896	8.47	15	2.93
SCT	400	20	0	200	105	9	13	36.88	8	2.872	1.557	0.614		8.47	15	2.93
SCT	400	20	0	200	105	9	13	36.88	4	2.372	1.15	0.548	0.854	8.47	15	2.93
SCT	400	20	0	200	105	9	6	110.63	16	1.174	0.555	0.29	0.428	8.47	15	0.87

Appendix C
All Data Related to Velocities from Hydrodynamic Tests

Test Series	Bottom Width b_w, ft	Water Depth h, ft	Left Bank cot α	Tow Position, S, ft	Barge Width B_s, ft	Barge Draft d, ft	Boat Speed V_s, fps	Inst. Dist. from Left Bank, ft	Inst. Depth from Bottom ft	Velocity Data Measured				Blockage Ratio, Left Side, n	Schijf Calculated	
										x-vel		y-vel			Limit Speed V_L, fps	Left Side u_r, fps
										Return Current u_r, fps	Bow Current u_b, fps	Max away from Bow u_{yb}, fps	Max to Stern u_{ys}, fps			
SCT	400	20	0	200	105	9	6	110.63	8	1.184	0.478	0.784	0.432	8.47	15	0.87
SCT	400	20	0	200	105	9	6	110.63	4	1.225	0.532	0.884	0.544	8.47	15	0.87
SCT	400	20	0	200	105	9	8	110.63	16	1.541	0.658	1.021	0.551	8.47	15	1.25
SCT	400	20	0	200	105	9	8	110.63	8	1.697	0.723	1.12	0.543	8.47	15	1.25
SCT	400	20	0	200	105	9	8	110.63	4	1.48	0.753	1.163	0.561	8.47	15	1.25
SCT	400	20	0	200	105	9	10	110.63	16	2.209	0.946	1.419	0.791	8.47	15	1.73
SCT	400	20	0	200	105	9	10	110.63	8	2.311	1.17	1.403	0.627	8.47	15	1.73
SCT	400	20	0	200	105	9	10	110.63	4	2.102	1.02	1.511	0.772	8.47	15	1.73
SCT	400	20	0	200	105	9	12	110.63	16	2.614	1.286	1.572	1.057	8.47	15	2.42
SCT	400	20	0	200	105	9	12	110.63	8	2.648	1.165	1.633	0.765	8.47	15	2.42
SCT	400	20	0	200	105	9	12	110.63	4	2.78	1.356	1.69	0.912	8.47	15	2.42
SCT	400	20	0	200	105	9	13	110.63	16	3.328	1.48	1.897	1.103	8.47	15	2.93
SCT	400	20	0	200	105	9	13	110.63	8	3.086	1.262	1.819	0.655	8.47	15	2.93

Appendix C
All Data Related to Velocities from Hydrodynamic Tests

Test Series	Bottom Width b_w, ft	Water Depth h, ft	Left Bank cot α	Tow Position, S, ft	Barge Width B_s, ft	Barge Draft d, ft	Boat Speed V_s, fps	Inst. Dist. from Left Bank, ft	Inst. Depth from Bottom ft	Velocity Data Measured				Blockage Ratio, Left Side, n	Schijf Calculated	
										x-vel		y-vel				
										Return Current u_r, fps	Bow Current u_b, fps	Max away from Bow u_{yb}, fps	Max to Stern u_{ys}, fps		Limit Speed V_L, fps	Left Side u_r, fps
SCT	400	20	0	200	105	9	13	110.63	4	3.587	1.462	1.862	0.828	8.47	15	2.93
SCT	400	20	0	200	105	9	6	73.75	16	1.223	0.561	0.433	0.312	8.47	15	0.87
SCT	400	20	0	200	105	9	6	73.75	8	1.247	0.59	0.459	0.195	8.47	15	0.87
SCT	400	20	0	200	105	9	6	73.75	4	1.277	0.692	0.426	0.224	8.47	15	0.87
SCT	400	20	0	200	105	9	8	73.75	16	1.559	0.707	0.652	0.294	8.47	15	1.25
SCT	400	20	0	200	105	9	8	73.75	8	1.584	0.638	0.585	0.254	8.47	15	1.25
SCT	400	20	0	200	105	9	8	73.75	4	1.585	0.603	0.561	0.259	8.47	15	1.25
SCT	400	20	0	200	105	9	10	73.75	16	2.442	1.13	0.812	0.637	8.47	15	1.73
SCT	400	20	0	200	105	9	10	73.75	8	2.415	1.1	0.799	0.292	8.47	15	1.73
SCT	400	20	0	200	105	9	10	73.75	4	2.226	0.922	0.75	0.309	8.47	15	1.73
SCT	400	20	0	200	105	9	12	73.75	16	3.307	1.237	1.064	0.629	8.47	15	2.42
SCT	400	20	0	200	105	9	12	73.75	8	3.000	1.529	0.965	0.364	8.47	15	2.42
SCT	400	20	0	200	105	9	12	73.75	4	3.189	1.4	1.219	0.342	8.47	15	2.42

Appendix C
All Data Related to Velocities from Hydrodynamic Tests

Test Series	Bottom Width b_w, ft	Water Depth h, ft	Left Bank cot α	Tow Position, S, ft	Barge Width B_s, ft	Barge Draft d, ft	Boat Speed V_s, fps	Inst. Dist. from Left Bank, ft	Inst. Depth from Bottom ft	Velocity Data Measured				Blockage Ratio, Left Side, n	Schijf Calculated	
										x-vel		y-vel				
										Return Current u_r, fps	Bow Current u_b, fps	Max away from Bow u_{yb}, fps	Max to Stern u_{ys}, fps		Limit Speed V_L, fps	Left Side u_r, fps
SCT	400	20	0	200	105	9	13	73.75	16	3.84	1.368	1	0.82	8.47	15	2.93
SCT	400	20	0	200	105	9	13	73.75	8	3.618	1.571	1.127	0.455	8.47	15	2.93
SCT	400	20	0	200	105	9	13	73.75	4	4.042	1.384	1.354	0.219	8.47	15	2.93
SCT	400	20	0	200	105	9	6	36.88	16	1.323	0.479	0.213	0.339	8.47	15	0.87
SCT	400	20	0	200	105	9	6	36.88	8	1.321	0.619	0.152	0.149	8.47	15	0.87
SCT	400	20	0	200	105	9	6	36.88	4	1.218	0.538	0.236	0.109	8.47	15	0.87
SCT	400	20	0	200	105	9	8	36.88	16	1.632	0.676	0.343	0.201	8.47	15	1.25
SCT	400	20	0	200	105	9	8	36.88	8	1.546	0.635	0.239	0.16	8.47	15	1.25
SCT	400	20	0	200	105	9	8	36.88	4	1.675	0.615	0.268	0.126	8.47	15	1.25
SCT	400	20	0	200	105	9	10	36.88	16	2.5	0.894	0.463	0.418	8.47	15	1.73
SCT	400	20	0	200	105	9	10	36.88	8	2.342	0.907	0.304	0.174	8.47	15	1.73
SCT	400	20	0	200	105	9	10	36.88	4	2.46	1.212	0.354	0.146	8.47	15	1.73
SCT	400	20	0	200	105	9	12	36.88	16	3.363	1.31	0.532	0.702	8.47	15	2.42

Appendix C
All Data Related to Velocities from Hydrodynamic Tests

Test Series	Bottom Width b_w, ft	Water Depth h, ft	Left Bank cot α	Tow Position, S, ft	Barge Width B_s, ft	Barge Draft d, ft	Boat Speed V_s, fps	Inst. Dist. from Left Bank, ft	Inst. Depth from Bottom ft	Velocity Data Measured				Blockage Ratio, Left Side, n	Schijf Calculated	
										x-vel		y-vel			Limit Speed V_L, fps	Left Side u_r, fps
										Return Current u_r, fps	Bow Current u_b, fps	Max away from Bow u_{yb}, fps	Max to Stern u_{ys}, fps			
SCT	400	20	0	200	105	9	12	36.88	8	1.584	0.52	0.489	0.353	8.47	15	2.42
SCT	400	20	0	200	105	9	12	36.88	4	3.14	1.333	0.452	0.417	8.47	15	2.42
SCT	400	20	0	200	105	9	13	36.88	16	4.273	1.324	0.625	0.819	8.47	15	2.93
SCT	400	20	0	200	105	9	13	36.88	8	3.463	1.426	0.388	0.213	8.47	15	2.93
SCT	400	20	0	200	105	9	13	36.88	4	4.149	1.705	0.596	0.213	8.47	15	2.93
SCT	400	20	0	200	105	9	6	110.63	16	1.639	0.454	0.726	0.813	8.47	15	0.87
SCT	400	20	0	200	105	9	6	110.63	8	1.421	0.595	0.805	0.37	8.47	15	0.87
SCT	400	20	0	200	105	9	6	110.63	4	1.33	0.389	0.858	0.345	8.47	15	0.87
SCT	400	20	0	200	105	9	8	110.63	16	1.661	0.538	1.136	0.677	8.47	15	1.25
SCT	400	20	0	200	105	9	8	110.63	8	1.949	0.566	1.194	0.449	8.47	15	1.25
SCT	400	20	0	200	105	9	8	110.63	4	1.854	1.104	1.156	0.333	8.47	15	1.25
SCT	400	20	0	200	105	9	10	110.63	16	2.387	1.145	1.466	0.966	8.47	15	1.73
SCT	400	20	0	200	105	9	10	110.63	8	2.603	0.933	1.531	0.515	8.47	15	1.73

Appendix C
All Data Related to Velocities from Hydrodynamic Tests

Test Series	Bottom Width b_w, ft	Water Depth h, ft	Left Bank cot α	Tow Position, S, ft	Barge Width B_s, ft	Barge Draft d, ft	Boat Speed V_s, fps	Inst. Dist. from Left Bank, ft	Inst. Depth from Bottom ft	Velocity Data Measured				Blockage Ratio, Left Side, n	Schijf Calculated	
										x-vel		y-vel			Limit Speed V_L, fps	Left Side u_r, fps
										Return Current u_r, fps	Bow Current u_b, fps	Max away from Bow u_{yb}, fps	Max to Stern u_{ys}, fps			
SCT	400	20	0	200	105	9	10	110.63	4	2.452	1.193	1.273	0.429	8.47	15	1.73
SCT	400	20	0	200	105	9	12	110.63	16	3.222	1.68	1.882	0.922	8.47	15	2.42
SCT	400	20	0	200	105	9	12	110.63	8	3.564	1.793	1.918	0.737	8.47	15	2.42
SCT	400	20	0	200	105	9	12	110.63	4	3.23	1.73	1.584	0.615	8.47	15	2.42
SCT	400	20	0	200	105	9	13	110.63	16	3.966	1.546	2.068	1	8.47	15	2.93
SCT	400	20	0	200	105	9	13	110.63	8	4.022	1.74	2.044	0.642	8.47	15	2.93
SCT	400	20	0	200	105	9	13	110.63	4	4.181	1.629	2.267	0.585	8.47	15	2.93
NR93	400	20	2	240	105	9	6	113.75	10	1.095	0.185	0.2	0.055	9.31	14.9	0.79
NR93	400	20	2	240	105	9	8	113.75	10	1.435	0.35	0.195	0.08	9.31	14.9	1.13
NR93	400	20	2	240	105	9	10	113.75	10	2.125	0.735	0.27	0.085	9.31	14.9	1.58
NR93	400	20	2	240	105	9	12	113.75	10	2.795	1.02	0.335	0.085	9.31	14.9	2.24
NR93	400	20	3	260	105	9	6	133.75	10	1.105	0.255	0.175	0.031	9.74	14.8	0.75
NR93	400	20	3	260	105	9	8	133.75	10	1.57	0.465	0.13	0.034	9.74	14.8	1.08

Appendix C
All Data Related to Velocities from Hydrodynamic Tests

Test Series	Bottom Width b_w, ft	Water Depth h, ft	Left Bank cot α	Tow Position, S, ft	Barge Width B_s, ft	Barge Draft d, ft	Boat Speed V_s, fps	Inst. Dist. from Left Bank, ft	Inst. Depth from Bottom ft	Velocity Data Measured				Blockage Ratio, Left Side, n	Schijf Calculated	
										x-vel		y-vel			Limit Speed V_L, fps	Left Side u_r, fps
										Return Current u_r, fps	Bow Current u_b, fps	Max away from Bow u_{yb}, fps	Max to Stern u_{ys}, fps			
NR93	400	20	3	260	105	9	10	133.75	10	2.165	0.71	0.22	0.05	9.74	14.8	1.51
NR93	400	20	3	260	105	9	12	133.75	10	2.365	0.985	0.235	0.175	9.74	14.8	2.16
NR93	400	20	2	240	105	9	8	113.75	10	1.415	0.4	0.5	0.48	9.31	14.9	1.13
NR93	400	20	2	240	105	9	8	113.75	10	1.525	0.635	0.56	0.32	9.31	14.9	1.13
NR93	400	20	2	240	105	9	8	113.75	10	1.465	0.44	0.485	0.37	9.31	14.9	1.13
NR93	400	20	2	240	105	9	10	113.75	10	2.24	0.675	0.735	0.485	9.31	14.9	1.58
NR93	400	20	2	240	105	9	10	113.75	10	2.105	0.795	0.85	0.5	9.31	14.9	1.58
NR93	400	20	2	240	105	9	10	113.75	10	2.16	0.785	0.805	0.5	9.31	14.9	1.58
NR93	400	20	2	240	105	9	12	113.75	10	2.54	1.355	0.905	0.56	9.31	14.9	2.24
NR93	400	20	2	240	105	9	12	113.75	10	2.78	1.175	0.99	0.44	9.31	14.9	2.24
NR93	400	20	2	240	105	9	12	113.75	10	2.555	0.94	0.85	0.42	9.31	14.9	2.24
NR93	400	20	2	240	105	9	14	113.75	10	3.12	1.395	0.85	0.525	9.31	14.9	3.56
NR93	400	20	2	240	105	9	14	113.75	10	3.22	1.49	1.005	0.66	9.31	14.9	3.56

Appendix C
All Data Related to Velocities from Hydrodynamic Tests

Test Series	Bottom Width b_w, ft	Water Depth h, ft	Left Bank cot α	Tow Position, S, ft	Barge Width B_s, ft	Barge Draft d, ft	Boat Speed V_s, fps	Inst. Dist. from Left Bank, ft	Inst. Depth from Bottom ft	Velocity Data Measured				Blockage Ratio, Left Side, n	Schijf Calculated	
										x-vel		y-vel				
										Return Current u_r, fps	Bow Current u_b, fps	Max away from Bow u_{yb}, fps	Max to Stern u_{ys}, fps		Limit Speed V_L, fps	Left Side u_r, fps
NR93	400	20	2	240	105	9	14	113.75	10	3.205	1.465	0.895	0.51	9.31	14.9	3.56
NR93	400	20	3	260	105	9	8	133.75	10	1.43	0.425	0.48	0.395	9.74	14.8	1.08
NR93	400	20	3	260	105	9	8	133.75	10	1.485	0.32	0.515	0.345	9.74	14.8	1.08
NR93	400	20	3	260	105	9	8	133.75	10	1.545	0.06	0.455	0.41	9.74	14.8	1.08
NR93	400	20	3	260	105	9	10	133.75	10	1.645	0.805	0.605	0.54	9.74	14.8	1.51
NR93	400	20	3	260	105	9	10	133.75	10	1.665	0.42	0.75	0.395	9.74	14.8	1.51
NR93	400	20	3	260	105	9	10	133.75	10	1.635	0.6	0.55	0.505	9.74	14.8	1.51
NR93	400	20	3	260	105	9	12	133.75	10	2.26	1.055	0.365	0.955	9.74	14.8	2.16
NR93	400	20	3	260	105	9	12	133.75	10	1.99	1.335	0.745	0.705	9.74	14.8	2.16
NR93	400	20	3	260	105	9	12	133.75	10	2.295	0.88	0.75	0.535	9.74	14.8	2.16
NR93	400	20	3	260	105	9	14	133.75	10	3.24	1.38	1.05	0.64	9.74	14.8	3.47
NR93	400	20	3	260	105	9	14	133.75	10	2.9	1.37	0.995	0.605	9.74	14.8	3.47
NR93	400	20	3	260	105	9	14	133.75	10	3.155	1.31	0.89	0.745	9.74	14.8	3.47

Appendix C
All Data Related to Velocities from Hydrodynamic Tests

Test Series	Bottom Width b_w, ft	Water Depth h, ft	Left Bank cot α	Tow Position, S, ft	Barge Width B_s, ft	Barge Draft d, ft	Boat Speed V_s, fps	Inst. Dist. from Left Bank, ft	Inst. Depth from Bottom ft	Velocity Data Measured				Blockage Ratio, Left Side, n	Schijf Calculated	
										x-vel		y-vel				
										Return Current u_r, fps	Bow Current u_b, fps	Max away from Bow u_{yb}, fps	Max to Stern u_{ys}, fps		Limit Speed V_L, fps	Left Side u_r, fps
NR93	400	20	2	340	105	9	6	163.75	10	0.905	0.345	0.355	0.305	13.54	14.9	0.7
NR93	400	20	2	340	105	9	6	163.75	10	0.895	0.15	0.41	0.3	13.54	14.9	0.7
NR93	400	20	2	340	105	9	6	163.75	10	0.9	0.2	0.36	0.3	13.54	14.9	0.7
NR93	400	20	2	340	105	9	8	163.75	10	1.5	0.39	0.5	0.45	13.54	14.9	1
NR93	400	20	2	340	105	9	8	163.75	10	1.45	0.345	0.5	0.395	13.54	14.9	1
NR93	400	20	2	340	105	9	8	163.75	10	1.35	0.245	0.45	0.35	13.54	14.9	1
NR93	400	20	2	340	105	9	10	163.75	10	2.1	0.55	0.71	0.55	13.54	14.9	1.4
NR93	400	20	2	340	105	9	10	163.75	10	2.15	0.59	0.6	0.545	13.54	14.9	1.4
NR93	400	20	2	340	105	9	10	163.75	10	2.035	0.71	0.64	0.59	13.54	14.9	1.4
NR93	400	20	2	340	105	9	12	163.75	10	2.83	0.845	0.705	0.655	13.54	14.9	1.99
NR93	400	20	2	340	105	9	12	163.75	10	2.95	0.91	0.7	0.735	13.54	14.9	1.99
NR93	400	20	2	340	105	9	12	163.75	10	2.86	1	0.695	0.695	13.54	14.9	1.99
NR93	400	20	2	340	105	9	14	163.75	10	3.825	1.4	0.94	0.795	13.54	14.9	3.16

Appendix C
All Data Related to Velocities from Hydrodynamic Tests

Test Series	Bottom Width b_w, ft	Water Depth h, ft	Left Bank cot α	Tow Position, S, ft	Barge Width B_s, ft	Barge Draft d, ft	Boat Speed V_s, fps	Inst. Dist. from Left Bank, ft	Inst. Depth from Bottom ft	Velocity Data Measured				Blockage Ratio, Left Side, n	Schijf Calculated	
										x-vel		y-vel				
										Return Current u_r, fps	Bow Current u_b, fps	Max away from Bow u_{yb}, fps	Max to Stern u_{ys}, fps		Limit Speed V_L, fps	Left Side u_r, fps
NR93	400	20	2	340	105	9	14	163.75	10	3.435	1.62	0.9	0.95	13.54	14.9	3.16
NR93	400	20	2	340	105	9	14	163.75	10	3.8	1.45	1	0.895	13.54	14.9	3.16
NR93	400	20	3	360	105	9	6	183.75	10	1.11	0.405	0.355	0.245	13.97	14.8	0.67
NR93	400	20	3	360	105	9	6	183.75	10	0.94	0.25	0.3615	0.305	13.97	14.8	0.67
NR93	400	20	3	360	105	9	6	183.75	10	1.195	0.155	0.355	0.3	13.97	14.8	0.67
NR93	400	20	3	360	105	9	8	183.75	10	1.445	0.305	0.5	0.395	13.97	14.8	0.96
NR93	400	20	3	360	105	9	8	183.75	10	1.445	0.34	0.5	0.355	13.97	14.8	0.96
NR93	400	20	3	360	105	9	8	183.75	10	1.195	0.495	0.465	0.305	13.97	14.8	0.96
NR93	400	20	3	360	105	9	10	183.75	10	1.8	0.5	0.45	0.595	13.97	14.8	1.35
NR93	400	20	3	360	105	9	10	183.75	10	1.55	0.75	0.69	0.5	13.97	14.8	1.35
NR93	400	20	3	360	105	9	10	183.75	10	1.85	0.44	0.5	0.49	13.97	14.8	1.35
NR93	400	20	3	360	105	9	12	183.75	10	2.345	1	0.845	0.5525	13.97	14.8	1.92
NR93	400	20	3	360	105	9	12	183.75	10	2.465	0.915	0.75	0.65	13.97	14.8	1.92

Appendix C
All Data Related to Velocities from Hydrodynamic Tests

Test Series	Bottom Width b_w, ft	Water Depth h, ft	Left Bank cot α	Tow Position, S, ft	Barge Width B_s, ft	Barge Draft d, ft	Boat Speed V_s, fps	Inst. Dist. from Left Bank, ft	Inst. Depth from Bottom ft	Velocity Data Measured				Blockage Ratio, Left Side, n	Schijf Calculated	
										x-vel		y-vel				
										Return Current u_r, fps	Bow Current u_b, fps	Max away from Bow u_{yb}, fps	Max to Stern u_{ys}, fps		Limit Speed V_L, fps	Left Side u_r, fps
NR93	400	20	3	360	105	9	12	183.75	10	2.6	1.05	0.75	0.64	13.97	14.8	1.92
NR93	400	20	3	360	105	9	14	183.75	10	3.69	1.345	0.905	0.805	13.97	14.8	3.09
NR93	400	20	3	360	105	9	14	183.75	10	4.175	1.55	1	0.89	13.97	14.8	3.09
NR93	400	20	3	360	105	9	14	183.75	10	3.6	1.85	1.05	0.785	13.97	14.8	3.09
NR93	400	20	3	360	105	9	10	183.75	10	1.805	0.595	0.63	0.525	13.97	14.8	1.35
NR93	400	20	3	360	105	9	10	183.75	10	1.835	0.67	0.6	0.55	13.97	14.8	1.35
NR93	400	20	2	190	105	9	6	88.75	10	1.25	0.35	0.116	0.35	7.20	14.9	0.87
NR93	400	20	2	190	105	9	6	88.75	10	1.6	0.23	0.145	0.4	7.20	14.9	0.87
NR93	400	20	2	190	105	9	6	88.75	10	1.15	0.255	0.595	0.38	7.20	14.9	0.87
NR93	400	20	2	190	105	9	8	88.75	10	1.805	0.305	1	0.5	7.20	14.9	1.25
NR93	400	20	2	190	105	9	8	88.75	10	1.845	0.435	0.85	0.45	7.20	14.9	1.25
NR93	400	20	2	190	105	9	8	88.75	10	1.795	0.345	0.855	0.455	7.20	14.9	1.25
NR93	400	20	2	190	105	9	10	88.75	10	2.455	0.75	1.7	0.42	7.20	14.9	1.74

Appendix C
All Data Related to Velocities from Hydrodynamic Tests

Test Series	Bottom Width b_w, ft	Water Depth h, ft	Left Bank cot α	Tow Position, S, ft	Barge Width B_s, ft	Barge Draft d, ft	Boat Speed V_s, fps	Inst. Dist. from Left Bank, ft	Inst. Depth from Bottom ft	Velocity Data Measured				Blockage Ratio, Left Side, n	Schijf Calculated	
										x-vel		y-vel			Limit Speed V_L, fps	Left Side u_r, fps
										Return Current u_r, fps	Bow Current u_b, fps	Max away from Bow u_{yb}, fps	Max to Stern u_{ys}, fps			
NR93	400	20	2	190	105	9	10	88.75	10	2.535	0.79	1.15	0.55	7.20	14.9	1.74
NR93	400	20	2	190	105	9	10	88.75	10	2.285	0.645	1.1	0.535	7.20	14.9	1.74
NR93	400	20	2	190	105	9	12	88.75	10	3.35	1.06	1.61	0.59	7.20	14.9	2.47
NR93	400	20	2	190	105	9	12	88.75	10	3.49	1.19	1.66	0.65	7.20	14.9	2.47
NR93	400	20	2	190	105	9	12	88.75	10	3.54	1.27	1.555	0.61	7.20	14.9	2.47
NR93	400	20	2	190	105	9	14	88.75	10	4.805	1.67	2	0.935	7.20	14.9	3.93
NR93	400	20	2	190	105	9	14	88.75	10	4.705	2.165	1.975	0.685	7.20	14.9	3.93
NR93	400	20	2	190	105	9	14	88.75	10	4.525	1.85	1.835	0.86	7.20	14.9	3.93
NR93	400	20	3	210	105	9	6	108.75	10	1.398	0.197	0.7	0.3	7.62	14.8	0.86
NR93	400	20	3	210	105	9	6	108.75	10	1.3	0.2	0.695	0.295	7.62	14.8	0.86
NR93	400	20	3	210	105	9	6	108.75	10	1.295	0.145	0.59	0.295	7.62	14.8	0.86
NR93	400	20	3	210	105	9	8	108.75	10	1.95	0.295	0.85	0.405	7.62	14.8	1.23
NR93	400	20	3	210	105	9	8	108.75	10	1.795	0.285	0.905	0.505	7.62	14.8	1.23

Appendix C
All Data Related to Velocities from Hydrodynamic Tests

Test Series	Bottom Width b_w, ft	Water Depth h, ft	Left Bank cot α	Tow Position, S, ft	Barge Width B_s, ft	Barge Draft d, ft	Boat Speed V_s, fps	Inst. Dist. from Left Bank, ft	Inst. Depth from Bottom ft	Velocity Data Measured				Blockage Ratio, Left Side, n	Schijf Calculated	
										x-vel		y-vel			Limit Speed V_L, fps	Left Side u_r, fps
										Return Current u_r, fps	Bow Current u_b, fps	Max away from Bow u_{yb}, fps	Max to Stern u_{ys}, fps			
NR93	400	20	3	210	105	9	8	108.75	10	2.15	0.42	0.855	0.51	7.62	14.8	1.23
NR93	400	20	3	210	105	9	10	108.75	10	2.34	0.755	1.27	0.575	7.62	14.8	1.73
NR93	400	20	3	210	105	9	10	108.75	10	2.545	0.645	1.24	0.55	7.62	14.8	1.73
NR93	400	20	3	210	105	9	10	108.75	10	2.155	0.485	1.175	0.6	7.62	14.8	1.73
NR93	400	20	3	210	105	9	12	108.75	10	3.295	1.135	1.62	0.7	7.62	14.8	2.46
NR93	400	20	3	210	105	9	12	108.75	10	3.345	1.085	1.87	0.79	7.62	14.8	2.46
NR93	400	20	3	210	105	9	12	108.75	10	3.33	1.21	1.81	0.78	7.62	14.8	2.46
NR93	400	20	3	210	105	9	14	108.75	10	4.65	1.945	2.27	0.84	7.62	14.8	3.97
NR93	400	20	3	210	105	9	14	108.75	10	4.75	1.85	2.27	0.825	7.62	14.8	3.97
NR93	400	20	3	210	105	9	14	108.75	10	4.775	1.65	2.18	0.895	7.62	14.8	3.97
NR93	400	20	3	210	105	9	10	108.75	10	1.85	0.755	0.905	0.5	7.62	14.8	1.73
NR93	400	20	3	210	105	9	10	108.75	10	2.065	0.74	0.99	0.3	7.62	14.8	1.73
NR93	400	15	2	180	105	9	6	78.75	7.5	1.7	0.395	0.745	0.25	5.24	11.7	1.3

Appendix C
All Data Related to Velocities from Hydrodynamic Tests

Test Series	Bottom Width b_w, ft	Water Depth h, ft	Left Bank cot α	Tow Position, S, ft	Barge Width B_s, ft	Barge Draft d, ft	Boat Speed V_s, fps	Inst. Dist. from Left Bank, ft	Inst. Depth from Bottom ft	Velocity Data Measured				Blockage Ratio, Left Side, n	Schijf Calculated	
										x-vel		y-vel			Limit Speed V_L, fps	Left Side u_r, fps
										Return Current u_r, fps	Bow Current u_b, fps	Max away from Bow u_{yb}, fps	Max to Stern u_{ys}, fps			
NR93	400	15	2	180	105	9	6	78.75	7.5	1.855	0.35	0.73	0.305	5.24	11.7	1.3
NR93	400	15	2	180	105	9	6	78.75	7.5	1.705	0.335	0.855	0.348	5.24	11.7	1.3
NR93	400	15	2	180	105	9	8	78.75	7.5	2.685	0.645	1.16	0.445	5.24	11.7	1.97
NR93	400	15	2	180	105	9	8	78.75	7.5	2.755	0.535	1.2	0.36	5.24	11.7	1.97
NR93	400	15	2	180	105	9	8	78.75	7.5	2.69	0.59	1.05	0.355	5.24	11.7	1.97
NR93	400	15	2	180	105	9	10	78.75	7.5	4.245	1.857	1.395	0.67	5.24	11.7	3.06
NR93	400	15	2	180	105	9	10	78.75	7.5	4.165	1.435	1.29	0.705	5.24	11.7	3.06
NR93	400	15	2	180	105	9	10	78.75	7.5	4	1.1	1.365	0.65	5.24	11.7	3.06
NR93	400	15	2	180	105	9	12	78.75	7.5	6.08	1.64	1.485	0.625	5.24	11.7	6.04
NR93	400	15	2	180	105	9	12	78.75	7.5	5.325	2	1.725	0.55	5.24	11.7	6.04
NR93	400	15	2	180	105	9	12	78.75	7.5	6.08	2	2.095	0.725	5.24	11.7	6.04
NR93	400	15	3	195	105	9	6	93.75	7.5	1.995	0.83	0.81	0.455	5.48	11.6	1.25
NR93	400	15	3	195	105	9	6	93.75	7.5	2.215	0.56	0.775	0.48	5.48	11.6	1.25

Appendix C
All Data Related to Velocities from Hydrodynamic Tests

Test Series	Bottom Width b_w, ft	Water Depth h, ft	Left Bank cot α	Tow Position, S, ft	Barge Width B_s, ft	Barge Draft d, ft	Boat Speed V_s, fps	Inst. Dist. from Left Bank, ft	Inst. Depth from Bottom ft	Velocity Data Measured				Blockage Ratio, Left Side, n	Schijf Calculated	
										x-vel		y-vel				
										Return Current u_r, fps	Bow Current u_b, fps	Max away from Bow u_{yb}, fps	Max to Stern u_{ys}, fps		Limit Speed V_L, fps	Left Side u_r, fps
NR93	400	15	3	195	105	9	6	93.75	7.5	1.965	0.264	0.81	0.375	5.48	11.6	1.25
NR93	400	15	3	195	105	9	8	93.75	7.5	2.86	0.61	1.08	0.599	5.48	11.6	1.89
NR93	400	15	3	195	105	9	8	93.75	7.5	3.195	0.145	1.1	0.14	5.48	11.6	1.89
NR93	400	15	3	195	105	9	8	93.75	7.5	2.56	0.77	0.935	0.265	5.48	11.6	1.89
NR93	400	15	3	195	105	9	10	93.75	7.5	3.755	1.59	1.605	0.545	5.48	11.6	2.95
NR93	400	15	3	195	105	9	10	93.75	7.5	4.45	0.6695	1.74	0.745	5.48	11.6	2.95
NR93	400	15	3	195	105	9	10	93.75	7.5	3.36	1.72	2.105	1.02	5.48	11.6	2.95
NR93	400	15	3	195	105	9	12	93.75	7.5	4.7	1.865	1.65	0.595	5.48	11.6	5.88
NR93	400	15	3	195	105	9	12	93.75	7.5	4.4	1.94	1.64	0.495	5.48	11.6	5.88
NR93	400	15	3	195	105	9	12	93.75	7.5	4.6	2.17	1.68	0.985	5.48	11.6	5.88
NR93	400	15	3	195	105	9	10	93.75	7.5	2.895	1.455	1.385	0.475	5.48	11.6	2.95
NR93	400	15	3	195	105	9	10	93.75	7.5	3.125	1.11	1.36	0.51	5.48	11.6	2.95
NR93	400	15	2	230	105	3.75	6	103.75	7.5	0.532	0.095	0.54	0.105	16.38	15	0.43

Appendix C
All Data Related to Velocities from Hydrodynamic Tests

Test Series	Bottom Width b_w, ft	Water Depth h, ft	Left Bank cot α	Tow Position, S, ft	Barge Width B_s, ft	Barge Draft d, ft	Boat Speed V_s, fps	Inst. Dist. from Left Bank, ft	Inst. Depth from Bottom ft	Velocity Data Measured				Blockage Ratio, Left Side, n	Schijf Calculated	
										x-vel		y-vel			Limit Speed V_L, fps	Left Side u_r, fps
										Return Current u_r, fps	Bow Current u_b, fps	Max away from Bow u_{yb}, fps	Max to Stern u_{ys}, fps			
NR93	400	15	2	230	105	3.75	6	103.75	7.5	0.5105	0.3055	0.14	0.145	16.38	15	0.43
NR93	400	15	2	230	105	3.75	6	103.75	7.5	0.56	0.1575	0.15	0.05	16.38	15	0.43
NR93	400	15	2	230	105	3.75	8	103.75	7.5	0.86	0.3	0.25	0.16	16.38	15	0.63
NR93	400	15	2	230	105	3.75	8	103.75	7.5	0.93	0.223	0.2	0.1	16.38	15	0.63
NR93	400	15	2	230	105	3.75	8	103.75	7.5	0.94	0.19	0.25	0.215	16.38	15	0.63
NR93	400	15	2	230	105	3.75	10	103.75	7.5	1	0.395	0.25	0.205	16.38	15	0.89
NR93	400	15	2	230	105	3.75	10	103.75	7.5	1.06	0.449	0.25	0.25	16.38	15	0.89
NR93	400	15	2	230	105	3.75	10	103.75	7.5	1.182	0.369	0.355	0.165	16.38	15	0.89
NR93	400	15	2	230	105	3.75	12	103.75	7.5	1.505	0.685	0.249	0.2	16.38	15	1.29
NR93	400	15	2	230	105	3.75	12	103.75	7.5	1.39	0.695	0.3	0.199	16.38	15	1.29
NR93	400	15	2	230	105	3.75	12	103.75	7.5	1.44	0.605	0.29	0.3	16.38	15	1.29
NR93	400	15	2	230	105	3.75	14	103.75	7.5	2.025	1.105	0.345	0.25	16.38	15	2.14
NR93	400	15	2	230	105	3.75	14	103.75	7.5	2.001	1.053	0.439	0.23	16.38	15	2.14

Appendix C
All Data Related to Velocities from Hydrodynamic Tests

Test Series	Bottom Width b_w, ft	Water Depth h, ft	Left Bank cot α	Tow Position, S, ft	Barge Width B_e, ft	Barge Draft d, ft	Boat Speed V_s, fps	Inst. Dist. from Left Bank, ft	Inst. Depth from Bottom ft	Velocity Data Measured				Blockage Ratio, Left Side, n	Schijf Calculated	
										x-vel		y-vel				
										Return Current u_r, fps	Bow Current u_b, fps	Max away from Bow u_{yb}, fps	Max to Stern u_{ys}, fps		Limit Speed V_L, fps	Left Side u_r, fps
NR93	400	15	2	230	105	3.75	14	103.75	7.5	2	1	0.225	0.362	16.38	15	2.14
NR93	400	15	2	230	105	3.75	14.9	103.75	7.5	2.355	1.231	0.425	0.265	16.38	15	3.52
NR93	400	15	2	230	105	3.75	14.9	103.75	7.5	2.42	1.165	0.443	0.44	16.38	15	3.52
NR93	400	15	2	230	105	3.75	14.9	103.75	7.5	2.364	1.362	0.385	0.33	16.38	15	3.52
NR93	400	15	3	245	105	3.75	6	118.75	7.5	0.678	0.155	0.195	0.195	16.95	14.9	0.42
NR93	400	15	3	245	105	3.75	6	118.75	7.5	0.556	0.195	0.245	0.14	16.95	14.9	0.42
NR93	400	15	3	245	105	3.75	6	118.75	7.5	0.61	0.35	0.35	0.11	16.95	14.9	0.42
NR93	400	15	3	245	105	3.75	8	118.75	7.5	0.745	0.305	0.186	0.25	16.95	14.9	0.61
NR93	400	15	3	245	105	3.75	8	118.75	7.5	0.8	0.255	0.192	0.237	16.95	14.9	0.61
NR93	400	15	3	245	105	3.75	8	118.75	7.5	0.888	0.247	0.27	0.19	16.95	14.9	0.61
NR93	400	15	3	245	105	3.75	10	118.75	7.5	0.985	0.41	0.243	0.263	16.95	14.9	0.86
NR93	400	15	3	245	105	3.75	10	118.75	7.5	0.935	0.5	0.28	0.315	16.95	14.9	0.86
NR93	400	15	3	245	105	3.75	10	118.75	7.5	1	0.39	0.215	0.33	16.95	14.9	0.86

Appendix C
All Data Related to Velocities from Hydrodynamic Tests

Test Series	Bottom Width b_w, ft	Water Depth h, ft	Left Bank cot α	Tow Position, S, ft	Barge Width B_s, ft	Barge Draft d, ft	Boat Speed V_s, fps	Inst. Dist. from Left Bank, ft	Inst. Depth from Bottom ft	Velocity Data Measured				Blockage Ratio, Left Side, n	Schijf Calculated	
										x-vel		y-vel				
										Return Current u_r, fps	Bow Current u_b, fps	Max away from Bow u_{yb}, fps	Max to Stern u_{ys}, fps		Limit Speed V_L, fps	Left Side u_r, fps
NR93	400	15	3	245	105	3.75	12	118.75	7.5	1.305	0.695	0.325	0.42	16.95	14.9	1.27
NR93	400	15	3	245	105	3.75	12	118.75	7.5	1.34	0.73	0.34	0.29	16.95	14.9	1.27
NR93	400	15	3	245	105	3.75	12	118.75	7.5	1.34	0.745	0.24	0.429	16.95	14.9	1.27
NR93	400	15	3	245	105	3.75	14	118.75	7.5	2.265	1.1	0.25	0.295	16.95	14.9	2.14
NR93	400	15	3	245	105	3.75	14	118.75	7.5	2.3	1.185	0.55	0.225	16.95	14.9	2.14
NR93	400	15	3	245	105	3.75	14	118.75	7.5	2.265	1.2	0.31	0.385	16.95	14.9	2.14
NR93	400	15	3	245	105	3.75	14.9	118.75	7.5	2.775	1.38	0.33	0.475	16.95	14.9	3.48
NR93	400	15	3	245	105	3.75	14.9	118.75	7.5	2.6	1.455	0.395	0.49	16.95	14.9	3.48
NR93	400	15	3	245	105	3.75	14.9	118.75	7.5	2.42	1.37	0.38	0.53	16.95	14.9	3.48

(Concluded)

Appendix D
All Data Related to Wave Heights From Hydrodynamic Tests

Appendix D
All Data Related to Wave Heights from Hydrodynamic Tests

Test Series	Bottom Width b_w, ft	Water Depth h, ft	Left Bank cot α	Tow Position S, ft	Barge Width B_s, ft	Barge Draft d, ft	Boat Speed V_s, fps	Inst. Dist. from Left Bank, ft	Barge Edge to Inst. ft	Wave Data Measured		Sec. Wave H_i, ft	Wave Period T_i, sec	Blockage Ratio Left Side, n	Schijf Calculated	
										Draw-Down z_{max}, ft	Max. Wave H_{max}, ft				Limit Speed V_L, fps	Draw-Down z_{ave}, ft
TT	280	14	2	168	105	9	8.66	28	87.5	1.5	1.2			4.56	9.2	1.45
TT	280	14	2	168	105	9	8.36	28	87.5	1.6	1			4.56	9.2	1.23
TT	280	14	2	168	105	9	8.51	28	87.5	1.7	0.8			4.56	9.2	1.33
TT	280	14	2	168	105	9	8.36	28	87.5	1.5	0.5			4.56	9.2	1.23
TT	280	14	2	168	105	9	8.07	28	87.5	1.4	0.8			4.56	9.2	1.07
TT	280	14	2	168	105	9	7.63	28	87.5	0.8	0.3			4.56	9.2	0.88
TT	280	14	2	168	105	9	7.48	28	87.5	1.2	0.2			4.56	9.2	0.82
TT	280	14	2	168	105	9	7.19	28	87.5	0.8	0.2			4.56	9.2	0.73
TT	280	14	2	168	105	9	6.75	28	87.5	0.8	0.1			4.56	9.2	0.61
TT	280	14	2	168	105	9	6.45	28	87.5	0.5	0.1			4.56	9.2	0.54
TT	280	14	2	168	105	9	6.01	28	87.5	0.6	0			4.56	9.2	0.45
TT	280	14	2	168	105	9	6.01	28	87.5	0.6	0			4.56	9.2	0.45
TT	280	14	2	168	105	9	6.75	28	87.5	0.6	0			4.56	9.2	0.61
TT	280	14	2	168	105	9	6.45	28	87.5	0.6	0.1			4.56	9.2	0.54
TT	280	14	2	168	105	9	7.04	28	87.5	0.8	0.2			4.56	9.2	0.69

Appendix D
All Data Related to Wave Heights from Hydrodynamic Tests

Test Series	Bottom Width b_w, ft	Water Depth h, ft	Left Bank cot α	Tow Position S, ft	Barge Width B_s, ft	Barge Draft d, ft	Boat Speed V_s, fps	Inst. Dist. from Left Bank, ft	Barge Edge to Inst. ft	Wave Data Measured		Sec. Wave H_i, ft	Wave Period T_i, sec	Blockage Ratio Left Side, n	Schijf Calculated	
										Draw-Down z_{max}, ft	Max. Wave H_{max}, ft				Limit Speed V_L, fps	Draw-Down z_{ave}, ft
TT	280	14	2	168	105	9	7.48	28	87.5	0.7	0.2			4.56	9.2	0.82
TT	280	14	2	168	105	9	7.78	28	87.5	1.2	0.3			4.56	9.2	0.94
TT	280	14	2	168	105	9	7.78	28	87.5	1.3	0.4			4.56	9.2	0.94
TT	280	14	2	168	105	9	8.22	28	87.5	1.2	0.7			4.56	9.2	1.15
TT	280	14	2	168	105	9	8.36	28	87.5	1.8	1.2			4.56	9.2	1.23
TT	280	14	2	168	105	9	8.36	28	87.5	1.8	0.4			4.56	9.2	1.23
TT	280	14	2	168	105	9	8.95	28	87.5	2	1.3			4.56	9.2	1.76
TT	280	14	2	168	105	9	8.36	28	87.5	2	0.3			4.56	9.2	1.23
TT	280	14	2	168	105	9	8.36	28	87.5	2.1	1			4.56	9.2	1.23
TT	280	14	2	168	105	9	7.92	28	87.5	2	1			4.56	9.2	1
TT	280	14	2	168	105	9	8.51	28	87.5	2.1	2			4.56	9.2	1.33
TT	280	14	2	168	70	2	12.91	28	105	2.3	1.7			10.5		
TT	280	14	2	168	70	2	12.62	28	105	2.3	0.9			10.5		
TT	280	14	2	168	70	2	13.20	28	105	2.2	1.6			10.5		
TT	280	14	2	168	70	2	13.20	28	105	2.8	1.7			10.5		

Appendix D
All Data Related to Wave Heights from Hydrodynamic Tests

Test Series	Bottom Width b_w, ft	Water Depth h, ft	Left Bank cot α	Tow Position S, ft	Barge Width B_s, ft	Barge Draft d, ft	Boat Speed V_s, fps	Inst. Dist. from Left Bank, ft	Barge Edge to Inst. ft	Wave Data Measured		Sec. Wave H_i, ft	Wave Period T_i, sec	Blockage Ratio Left Side, n	Schijf Calculated	
										Draw-Down z_{max}, ft	Max. Wave H_{max}, ft				Limit Speed V_L, fps	Draw-Down z_{ave}, ft
TT	280	14	2	168	70	2	12.91	28	105	2.1	1.4			10.5		
TT	280	14	2	168	70	2	13.35	28	105	2.5	1.8			10.5		
TT	280	14	2	168	70	2	13.20	28	105	2.4	1.5			10.5		
TT	280	14	2	168	70	2	12.91	28	105	2.4	1.1			10.5		
TT	280	14	2	168	70	2	13.35	28	105	2.7	1.6			10.5		
TT	280	14	2	168	70	2	13.06	28	105	3.2	3.1			10.5		
TT	280	14	2	168	70	2	13.06	28	105	3	2.7			10.5		
TT	280	14	2	168	70	2	13.06	28	105	3.5	3.3			10.5		
TT	280	14	2	168	70	2	13.06	28	105	3.2	2.6			10.5		
TT	280	14	2	168	70	2	13.35	28	105	2.6	2			10.5		
TT	280	14	2	168	70	2	13.06	28	105	2.5	1.2			10.5		
TT	280	14	2	168	70	2	13.35	28	105	2.3	1.2			10.5		
TT	280	14	2	168	70	2	13.06	28	105	2.9	1.9			10.5		
TT	280	14	2	168	70	2	13.06	28	105	3.5	3.3			10.5		
TT	280	14	2	168	70	2	13.35	28	105	3.5	3.4			10.5		

Appendix D
All Data Related to Wave Heights from Hydrodynamic Tests

Test Series	Bottom Width b_w, ft	Water Depth h, ft	Left Bank cot α	Tow Position S, ft	Barge Width B_s, ft	Barge Draft d, ft	Boat Speed V_s, fps	Inst. Dist. from Left Bank, ft	Barge Edge to Inst. ft	Wave Data Measured		Sec. Wave H_i, ft	Wave Period T_i, sec	Blockage Ratio Left Side, n	Schijf Calculated	
										Draw-Down z_{max}, ft	Max. Wave H_{max}, ft				Limit Speed V_L, fps	Draw-Down z_{ave}, ft
TT	280	14	2	168	70	2	13.35	28	105	2.1	1.6			10.5		
TT	280	14	2	168	70	2	13.06	28	105	2	1.7			10.5		
TT	280	14	2	168	70	2	12.47	28	105	1.4	1.1			10.5		
TT	280	14	2	168	70	2	12.47	28	105	1.8	1.3			10.5		
TT	280	14	2	168	70	2	12.03	28	105	1.3	1			10.5		
TT	280	14	2	168	70	2	12.03	28	105	1	0.6			10.5		
TT	280	14	2	168	70	2	10.86	28	105	1.1	0.9			10.5		
TT	280	14	2	168	70	2	10.71	28	105	0.5	0.5			10.5		
TT	280	14	2	168	70	2	9.98	28	105	0.4	0.4			10.5		
TT	280	14	2	168	70	2	9.83	28	105	0.4	0.3			10.5		
TT	280	14	2	168	70	2	10.56	28	105	0.6	0.5			10.5		
TT	280	14	2	168	70	2	10.86	28	105	0.7	0.6			10.5		
TT	280	14	2	168	70	2	11.15	28	105	0.9	0.7			10.5		
TT	280	14	2	168	70	2	11.88	28	105	1.3	0.8			10.5		
TT	280	14	2	168	70	2	12.03	28	105	1.6	0.8			10.5		

Appendix D
All Data Related to Wave Heights from Hydrodynamic Tests

Test Series	Bottom Width b_w, ft	Water Depth h, ft	Left Bank cot α	Tow Position S, ft	Barge Width B_s, ft	Barge Draft d, ft	Boat Speed V_s, fps	Inst. Dist. from Left Bank, ft	Barge Edge to Inst. ft	Wave Data Measured		Sec. Wave H_i, ft	Wave Period T_i, sec	Blockage Ratio Left Side, n	Schijf Calculated	
										Draw-Down z_{max}, ft	Max. Wave H_{max}, ft				Limit Speed V_L, fps	Draw-Down z_{ave}, ft
TT	280	14	2	168	70	2	12.76	28	105	1.2	0.8			10.5		
TT	280	14	2	168	70	2	13.06	28	105	2.2	2			10.5		
TT	280	18	2	176	105	9	11.00	36	87.5	2	1.6			6.02	11.9	1.61
TT	280	18	2	176	105	9	10.86	36	87.5	2.1	1.3			6.02	11.9	1.51
TT	280	18	2	176	105	9	10.56	36	87.5	2	1.4			6.02	11.9	1.34
TT	280	18	2	176	105	9	10.86	36	87.5	2.2	1.9			6.02	11.9	1.51
TT	280	18	2	176	105	9	10.86	36	87.5	2	1.4			6.02	11.9	1.51
TT	280	18	2	176	105	9	11.15	36	87.5	2.2	1.4			6.02	11.9	1.72
TT	280	18	2	176	105	9	10.86	36	87.5	2.1	1.6			6.02	11.9	1.51
TT	280	18	2	176	105	9	10.71	36	87.5	2	1.1			6.02	11.9	1.42
TT	280	18	2	176	105	9	10.42	36	87.5	2	1.5			6.02	11.9	1.27
TT	280	18	2	176	105	9	10.27	36	87.5	1.7	1.1			6.02	11.9	1.2
TT	280	18	2	176	105	9	9.98	36	87.5	1.7	0.9			6.02	11.9	1.09
TT	280	18	2	176	105	9	8.80	36	87.5	1.4	0.9			6.02	11.9	0.73
TT	280	18	2	176	105	9	8.51	36	87.5	1	0.5			6.02	11.9	0.67

Appendix D
All Data Related to Wave Heights from Hydrodynamic Tests

Test Series	Bottom Width b_w, ft	Water Depth h, ft	Left Bank cot α	Tow Position S, ft	Barge Width B_s, ft	Barge Draft d, ft	Boat Speed V_s, fps	Inst. Dist. from Left Bank, ft	Barge Edge to Inst. ft	Wave Data Measured		Sec. Wave H_i, ft	Wave Period T_i, sec	Blockage Ratio Left Side, n	Schijf Calculated	
										Draw-Down z_{max}, ft	Max. Wave H_{max}, ft				Limit Speed V_L, fps	Draw-Down z_{ave}, ft
TT	280	18	2	176	105	9	8.22	36	87.5	1.1	0.4			6.02	11.9	0.61
TT	280	18	2	176	105	9	7.48	36	87.5	0.6	0.3			6.02	11.9	0.47
TT	280	18	2	176	105	9	7.19	36	87.5	0.9	0.3			6.02	11.9	0.43
TT	280	18	2	176	105	9	7.78	36	87.5	0.8	0.3			6.02	11.9	0.52
TT	280	18	2	176	105	9	7.92	36	87.5	0.9	0.4			6.02	11.9	0.55
TT	280	18	2	176	105	9	8.51	36	87.5	0.8	0.6			6.02	11.9	0.67
TT	280	18	2	176	105	9	8.80	36	87.5	1.3	0.6			6.02	11.9	0.73
TT	280	18	2	176	105	9	9.24	36	87.5	1.1	0.7			6.02	11.9	0.85
TT	280	18	2	176	105	9	9.54	36	87.5	1.6	0.8			6.02	11.9	0.93
TT	280	18	2	176	105	9	9.98	36	87.5	1.4	0.9			6.02	11.9	1.09
TT	280	18	2	176	105	9	10.42	36	87.5	1.7	1.4			6.02	11.9	1.27
TT	280	18	2	176	105	9	10.71	36	87.5	1.4	0.6			6.02	11.9	1.42
TT	280	18	2	176	105	9	10.86	36	87.5	2	1.3			6.02	11.9	1.51
TT	280	18	2	176	105	9	11.15	36	87.5	1.8	1.2			6.02	11.9	1.72
TT	280	18	2	176	105	9	11.30	36	87.5	2	1.7			6.02	11.9	1.85

Appendix D
All Data Related to Wave Heights from Hydrodynamic Tests

Test Series	Bottom Width b_w, ft	Water Depth h, ft	Left Bank cot α	Tow Position S, ft	Barge Width B_s, ft	Barge Draft d, ft	Boat Speed V_s, fps	Inst. Dist. from Left Bank, ft	Barge Edge to Inst. ft	Wave Data Measured		Sec. Wave H_i, ft	Wave Period T_i, sec	Blockage Ratio Left Side, n	Schijf Calculated	
										Draw-Down z_{max}, ft	Max. Wave H_{max}, ft				Limit Speed V_L, fps	Draw-Down z_{ave}, ft
TT	280	17.5	2	175	70	2	15.40	35	105	2	1.7			13.40		
TT	280	17.5	2	175	70	2	15.40	35	105	3.2	3.2			13.40		
TT	280	17.5	2	175	70	2	15.40	35	105	2.2	2			13.40		
TT	280	17.5	2	175	70	2	15.11	35	105	2	1.4			13.40		
TT	280	17.5	2	175	70	2	15.11	35	105	3	3			13.40		
TT	280	17.5	2	175	70	2	15.11	35	105	3.1	2			13.40		
TT	280	17.5	2	175	70	2	14.82	35	105	2	1.7			13.40		
TT	280	17.5	2	175	70	2	14.82	35	105	3.1	3.2			13.40		
TT	280	17.5	2	175	70	2	14.52	35	105	1.5	0.8			13.40		
TT	280	17.5	2	175	70	2	14.52	35	105	1.4	1.1			13.40		
TT	280	17.5	2	175	70	2	14.38	35	105	1.9	1.5			13.40		
TT	280	17.5	2	175	70	2	14.08	35	105	1.7	1.4			13.40		
TT	280	17.5	2	175	70	2	13.94	35	105	2.7	1.7			13.40		
TT	280	17.5	2	175	70	2	13.35	35	105	0.9	1			13.40		
TT	280	17.5	2	175	70	2	13.06	35	105	1.3	1.3			13.40		

Appendix D
All Data Related to Wave Heights from Hydrodynamic Tests

Test Series	Bottom Width b_w, ft	Water Depth h, ft	Left Bank cot α	Tow Position S, ft	Barge Width B_s, ft	Barge Draft d, ft	Boat Speed V_s, fps	Inst. Dist. from Left Bank, ft	Barge Edge to Inst. ft	Wave Data Measured		Sec. Wave H_i, ft	Wave Period T_i, sec	Blockage Ratio Left Side, n	Schijf Calculated	
										Draw-Down z_{max}, ft	Max. Wave H_{max}, ft				Limit Speed V_L, fps	Draw-Down z_{ave}, ft
TT	280	22	2	184	105	9	13.20	44	87.5	1.8	2.1			7.54	14.2	1.82
TT	280	22	2	184	105	9	12.47	44	87.5	1.8	2.4			7.54	14.2	1.41
TT	280	22	2	184	105	9	12.03	44	87.5	1.8	2.3			7.54	14.2	1.23
TT	280	22	2	184	105	9	11.74	44	87.5	1.6	1.6			7.54	14.2	1.13
TT	280	22	2	184	105	9	11.44	44	87.5	1.6	1.8			7.54	14.2	1.04
TT	280	22	2	184	105	9	11.15	44	87.5	1.3	1.4			7.54	14.2	0.95
TT	280	22	2	184	105	9	10.56	44	87.5	1.3	1			7.54	14.2	0.81
TT	280	22	2	184	105	9	9.54	44	87.5	0.6	0.5			7.54	14.2	0.61
TT	280	22	2	184	105	9	9.39	44	87.5	1	0.5			7.54	14.2	0.58
TT	280	22	2	184	105	9	8.66	44	87.5	0.5	0.4			7.54	14.2	0.48
TT	280	22	2	184	105	9	8.22	44	87.5	0.7	0.4			7.54	14.2	0.42
TT	280	22	2	184	105	9	8.07	44	87.5	0.4	0.2			7.54	14.2	0.4
TT	280	22	2	184	105	9	8.07	44	87.5	0.6	0.3			7.54	14.2	0.4
TT	280	22	2	184	105	9	8.51	44	87.5	0.5	0.4			7.54	14.2	0.45
TT	280	22	2	184	105	9	8.95	44	87.5	0.8	0.4			7.54	14.2	0.52

Appendix D
All Data Related to Wave Heights from Hydrodynamic Tests

Test Series	Bottom Width b_w, ft	Water Depth h, ft	Left Bank cot α	Tow Position S, ft	Barge Width B_s, ft	Barge Draft d, ft	Boat Speed V_s, fps	Inst. Dist. from Left Bank, ft	Barge Edge to Inst. ft	Wave Data Measured		Sec. Wave H_i, ft	Wave Period T_i, sec	Blockage Ratio Left Side, n	Schijf Calculated	
										Draw-Down z_{max}, ft	Max. Wave H_{max}, ft				Limit Speed V_L, fps	Draw-Down z_{ave}, ft
TT	280	22	2	184	105	9	9.54	44	87.5	1	0.6			7.54	14.2	0.61
TT	280	22	2	184	105	9	10.56	44	87.5	1.2	1			7.54	14.2	0.81
TT	280	22	2	184	105	9	11.15	44	87.5	1.5	1.1			7.54	14.2	0.95
TT	280	22	2	184	105	9	11.44	44	87.5	1.2	1.1			7.54	14.2	1.04
TT	280	22	2	184	105	9	11.74	44	87.5	1.8	1.5			7.54	14.2	1.13
TT	280	22	2	184	105	9	12.18	44	87.5	1.6	1.8			7.54	14.2	1.29
TT	280	21	2	182	70	2	16.72	42	105	2.6	2.9			16.40		
TT	280	21	2	182	70	2	16.72	42	105	3	3.1			16.40		
TT	280	21	2	182	70	2	16.72	42	105	2.8	2.5			16.40		
TT	280	21	2	182	70	2	16.58	42	105	2.8	2.3			16.40		
TT	280	21	2	182	70	2	16.58	42	105	2.8	3			16.40		
TT	280	21	2	182	70	2	15.70	42	105	2	1.6			16.40		
TT	280	21	2	182	70	2	15.70	42	105	1.9	1.3			16.40		
TT	280	21	2	182	70	2	15.99	42	105	2.2	1.3			16.40		
TT	280	21	2	182	70	2	15.99	42	105	2.5	1.4			16.40		

Appendix D
All Data Related to Wave Heights from Hydrodynamic Tests

Test Series	Bottom Width b_w, ft	Water Depth h, ft	Left Bank cot α	Tow Position S, ft	Barge Width B_s, ft	Barge Draft d, ft	Boat Speed V_s, fps	Inst. Dist. from Left Bank, ft	Barge Edge to Inst. ft	Wave Data Measured		Sec. Wave H_i, ft	Wave Period T_i, sec	Blockage Ratio Left Side, n	Schijf Calculated	
										Draw-Down z_{max}, ft	Max. Wave H_{max}, ft				Limit Speed V_L, fps	Draw-Down z_{ave}, ft
TT	280	21	2	182	70	2	15.99	42	105	1.7	1.6			16.40		
TT	280	21	2	182	70	2	15.99	42	105	2.3	2.1			16.40		
TT	280	21	2	182	70	2	15.26	42	105	1.5	1.3			16.40		
TT	280	21	2	182	70	2	15.26	42	105	1.2	1.6			16.40		
TT	280	21	2	182	70	2	14.96	42	105	1.3	1.3			16.40		
TT	280	21	2	182	70	2	15.11	42	105	1.1	1.7			16.40		
TT	280	21	2	182	70	2	13.35	42	105	0.7	1.2			16.40		
TT	280	21	2	182	70	2	12.03	42	105	0.4	0.6			16.40		
TT	280	21	2	182	70	2	15.55	42	105	1.4	1.5			16.40		
TT	280	21	2	182	70	2	14.82	42	105	0.8	1.2			16.40		
TT	280	21	2	182	70	2	12.62	42	105	0.7	1.1			16.40		
GAL	425	15	3	167.5	105	9	7.34	45	70	0.93	0.6			4.60	12	0.45
GAL	425	15	3	167.5	105	9	7.92	45	70	1.02	0.46			4.60	12	0.55
GAL	425	15	3	167.5	105	9	7.34	45	70	0.79	0.51			4.60	12	0.45
GAL	425	15	3	167.5	105	9	7.92	45	70	0.79	0.51			4.60	12	0.55

Appendix D
All Data Related to Wave Heights from Hydrodynamic Tests

Test Series	Bottom Width b_w, ft	Water Depth h, ft	Left Bank cot α	Tow Position S, ft	Barge Width B_s, ft	Barge Draft d, ft	Boat Speed V_s, fps	Inst. Dist. from Left Bank, ft	Barge Edge to Inst. ft	Wave Data Measured		Sec. Wave H_i, ft	Wave Period T_i, sec	Blockage Ratio Left Side, n	Schijf Calculated	
										Draw-Down z_{max}, ft	Max. Wave H_{max}, ft				Limit Speed V_L, fps	Draw-Down z_{ave}, ft
GAL	425	15	3	167.5	105	9	8.07	45	70	0.93	0.6			4.60	12	0.57
GAL	425	15	3	167.5	105	9	8.51	45	70	1.2	0.81			4.60	12	0.66
GAL	425	15	3	167.5	105	9	8.51	45	70	1.02	0.69			4.60	12	0.66
SCT	400	20	0	200	105	9	6	73.75	73.75	0.285	0.365			8.47	15	0.17
SCT	400	20	0	200	105	9	8	73.75	73.75	0.585	0.371			8.47	15	0.33
SCT	400	20	0	200	105	9	10	73.75	73.75	0.648	0.384			8.47	15	0.58
SCT	400	20	0	200	105	9	12	73.75	73.75	1.117	0.831			8.47	15	0.99
SCT	400	20	0	200	105	9	13	73.75	73.75	1.487	1.093			8.47	15	1.32
SCT	400	20	0	200	105	9	6	36.88	110.62	0.308	0.289			8.47	15	0.17
SCT	400	20	0	200	105	9	8	36.88	110.62	0.566	0.385			8.47	15	0.33
SCT	400	20	0	200	105	9	10	36.88	110.62	0.698	0.379			8.47	15	0.58
SCT	400	20	0	200	105	9	12	36.88	110.62	1.167	1.053			8.47	15	0.99
SCT	400	20	0	200	105	9	13	36.88	110.62	1.571	1.183			8.47	15	1.32
SCT	400	20	0	200	105	9	6	110.63	36.87	0.331	0.237			8.47	15	0.17
SCT	400	20	0	200	105	9	8	110.63	36.87	0.509	0.338			8.47	15	0.33

Appendix D
All Data Related to Wave Heights from Hydrodynamic Tests

Test Series	Bottom Width b_w, ft	Water Depth h, ft	Left Bank cot α	Tow Position S, ft	Barge Width B_s, ft	Barge Draft d, ft	Boat Speed V_s, fps	Inst. Dist. from Left Bank, ft	Barge Edge to Inst. ft	Wave Data Measured		Sec. Wave H_i, ft	Wave Period T_i, sec	Blockage Ratio Left Side, n	Schijf Calculated	
										Draw-Down z_{max}, ft	Max. Wave H_{max}, ft				Limit Speed V_L, fps	Draw-Down z_{ave}, ft
SCT	400	20	0	200	105	9	10	110.63	36.87	0.674	0.42			8.47	15	0.58
SCT	400	20	0	200	105	9	12	110.63	36.87	1.142	0.828			8.47	15	0.99
SCT	400	20	0	200	105	9	13	110.63	36.87	1.536	1.162			8.47	15	1.32
SCT	400	20	0	200	105	9	6	73.75	73.75	0.302	0.414			8.47	15	0.17
SCT	400	20	0	200	105	9	8	73.75	73.75	0.576	0.752			8.47	15	0.33
SCT	400	20	0	200	105	9	10	73.75	73.75	0.965	1.411			8.47	15	0.58
SCT	400	20	0	200	105	9	12	73.75	73.75	1.08	1.791			8.47	15	0.99
SCT	400	20	0	200	105	9	13	73.75	73.75	1.205	1.97			8.47	15	1.32
SCT	400	20	0	200	105	9	6	36.88	110.62	0.348	0.476			8.47	15	0.17
SCT	400	20	0	200	105	9	8	36.88	110.62	0.535	0.706			8.47	15	0.33
SCT	400	20	0	200	105	9	10	36.88	110.62	0.926	1.322			8.47	15	0.58
SCT	400	20	0	200	105	9	12	36.88	110.62	1.073	1.781			8.47	15	0.99
SCT	400	20	0	200	105	9	13	36.88	110.62	1.316	2.175			8.47	15	1.32
SCT	400	20	0	200	105	9	6	110.63	36.87	0.394	0.525			8.47	15	0.17
SCT	400	20	0	200	105	9	8	110.63	36.87	0.649	0.852			8.47	15	0.33

Appendix D
All Data Related to Wave Heights from Hydrodynamic Tests

Test Series	Bottom Width b_w, ft	Water Depth h, ft	Left Bank cot α	Tow Position S, ft	Barge Width B_s, ft	Barge Draft d, ft	Boat Speed V_s, fps	Inst. Dist. from Left Bank, ft	Barge Edge to Inst. ft	Wave Data Measured		Sec. Wave H_i, ft	Wave Period T_i, sec	Blockage Ratio Left Side, n	Schijf Calculated	
										Draw-Down z_{max}, ft	Max. Wave H_{max}, ft				Limit Speed V_L, fps	Draw-Down z_{ave}, ft
SCT	400	20	0	200	105	9	10	110.63	36.87	0.95	1.352			8.47	15	0.58
SCT	400	20	0	200	105	9	12	110.63	36.87	1.131	1.847			8.47	15	0.99
SCT	400	20	0	200	105	9	13	110.63	36.87	1.357	2.177			8.47	15	1.32
SCT	400	20	0	200	105	9	6	73.75	73.75	0.255	0.461			8.47	15	0.17
SCT	400	20	0	200	105	9	8	73.75	73.75	0.495	0.7327			8.47	15	0.33
SCT	400	20	0	200	105	9	10	73.75	73.75	0.714	1.133			8.47	15	0.58
SCT	400	20	0	200	105	9	12	73.75	73.75	0.859	1.513			8.47	15	0.99
SCT	400	20	0	200	105	9	13	73.75	73.75	1.185	1.94			8.47	15	1.32
SCT	400	20	0	200	105	9	6	36.88	110.62	0.233	0.389			8.47	15	0.17
SCT	400	20	0	200	105	9	8	36.88	110.62	0.401	0.65			8.47	15	0.33
SCT	400	20	0	200	105	9	10	36.88	110.62	0.688	0.976			8.47	15	0.58
SCT	400	20	0	200	105	9	12	36.88	110.62	0.915	1.378			8.47	15	0.99
SCT	400	20	0	200	105	9	13	36.88	110.62	1.09	1.632			8.47	15	1.32
SCT	400	20	0	200	105	9	6	110.63	36.87	0.383	0.454			8.47	15	0.17
SCT	400	20	0	200	105	9	8	110.63	36.87	0.497	0.684			8.47	15	0.33

Appendix D
All Data Related to Wave Heights from Hydrodynamic Tests

Test Series	Bottom Width b_w, ft	Water Depth h, ft	Left Bank cot α	Tow Position S, ft	Barge Width B_s, ft	Barge Draft d, ft	Boat Speed V_s, fps	Inst. Dist. from Left Bank, ft	Barge Edge to Inst. ft	Wave Data Measured		Sec. Wave H_i, ft	Wave Period T_i, sec	Blockage Ratio Left Side, n	Schijf Calculated	
										Draw-Down z_{max}, ft	Max. Wave H_{max}, ft				Limit Speed V_L, fps	Draw-Down z_{ave}, ft
SCT	400	20	0	200	105	9	10	110.63	36.87	0.724	1.04			8.47	15	0.58
SCT	400	20	0	200	105	9	12	110.63	36.87	0.953	1.439			8.47	15	0.99
SCT	400	20	0	200	105	9	13	110.63	36.87	0.995	1.67			8.47	15	1.32
NR93	400	20	2	240	105	9	6	113.75	72.5	0.1125	0.0625			9.31	14.9	0.16
NR93	400	20	2	240	105	9	6	113.75	72.5	0.1125	0.0525			9.31	14.9	0.16
NR93	400	20	2	240	105	9	8	113.75	72.5	0.41	0.385			9.31	14.9	0.3
NR93	400	20	2	240	105	9	8	113.75	72.5	0.36	0.27			9.31	14.9	0.3
NR93	400	20	2	240	105	9	10	113.75	72.5	0.7025	0.4925	0.275	2.835	9.31	14.9	0.53
NR93	400	20	2	240	105	9	10	113.75	72.5	0.7025	0.5	0.275	2.835	9.31	14.9	0.53
NR93	400	20	2	240	105	9	12	113.75	72.5	1.1475	0.8275	0.75	2.835	9.31	14.9	0.91
NR93	400	20	2	240	105	9	12	113.75	72.5	1	0.775	1.05	2.835	9.31	14.9	0.91
NR93	400	20	2	240	105	9	14	113.75	72.5	1.5	1.2825	1.825	3.095	9.31	14.9	1.74
NR93	400	20	2	240	105	9	14	113.75	72.5	1.68	1.4925	1.8	3.22	9.31	14.9	1.74
NR93	400	20	3	260	105	9	6	133.75	72.5	0.0675				9.74	14.8	0.15
NR93	400	20	3	260	105	9	6	133.75	72.5	0.0775				9.74	14.8	0.15

Appendix D
All Data Related to Wave Heights from Hydrodynamic Tests

Test Series	Bottom Width b_w, ft	Water Depth h, ft	Left Bank cot α	Tow Position S, ft	Barge Width B_s, ft	Barge Draft d, ft	Boat Speed V_s, fps	Inst. Dist. from Left Bank, ft	Barge Edge to Inst. ft	Wave Data Measured		Sec. Wave H_i, ft	Wave Period T_i, sec	Blockage Ratio Left Side, n	Schijf Calculated	
										Draw-Down z_{max}, ft	Max. Wave H_{max}, ft				Limit Speed V_L, fps	Draw-Down z_{ave}, ft
NR93	400	20	3	260	105	9	8	133.75	72.5	0.455	0.4925			9.74	14.8	0.29
NR93	400	20	3	260	105	9	8	133.75	72.5	0.455	0.4525			9.74	14.8	0.29
NR93	400	20	3	260	105	9	10	133.75	72.5	0.91	1.135	0.325	2.5195	9.74	14.8	0.51
NR93	400	20	3	260	105	9	10	133.75	72.5	0.92	1.1575	0.325	2.5195	9.74	14.8	0.51
NR93	400	20	3	260	105	9	12	133.75	72.5	1.3725	1.895	1.45	3.095	9.74	14.8	0.88
NR93	400	20	3	260	105	9	12	133.75	72.5	1.598	2.155	1.275	3.06	9.74	14.8	0.88
NR93	400	20	3	260	105	9	14	133.75	72.5	1.883	2.72	1.6	3.35	9.74	14.8	1.7
NR93	400	20	3	260	105	9	14	133.75	72.5	1.575	2.2425	1.65	3.095	9.74	14.8	1.7
NR93	400	20	2	340	105	9	6	163.75	123.75	0.225	0.228			13.54	14.9	0.14
NR93	400	20	2	340	105	9	6	163.75	123.75	0.225	0.263			13.54	14.9	0.14
NR93	400	20	2	340	105	9	8	163.75	123.75	0.425	0.385			13.54	14.9	0.27
NR93	400	20	2	340	105	9	8	163.75	123.75	0.425	0.375			13.54	14.9	0.27
NR93	400	20	2	340	105	9	10	163.75	123.75	0.775	0.725	0.225	2.735	13.54	14.9	0.47
NR93	400	20	2	340	105	9	10	163.75	123.75	0.8	0.75	0.225	2.715	13.54	14.9	0.47
NR93	400	20	2	340	105	9	12	163.75	123.75	1.35	1.3	0.725	3.275	13.54	14.9	0.8

Appendix D
All Data Related to Wave Heights from Hydrodynamic Tests

Test Series	Bottom Width b_w, ft	Water Depth h, ft	Left Bank cot α	Tow Position S, ft	Barge Width B_s, ft	Barge Draft d, ft	Boat Speed V_s, fps	Inst. Dist. from Left Bank, ft	Barge Edge to Inst. ft	Wave Data Measured		Sec. Wave H_i, ft	Wave Period T_i, sec	Blockage Ratio Left Side, n	Schijf Calculated	
										Draw-Down z_{max}, ft	Max. Wave H_{max}, ft				Limit Speed V_L, fps	Draw-Down z_{ave}, ft
NR93	400	20	2	340	105	9	12	163.75	123.75	1.375	1.283	0.8	3.095	13.54	14.9	0.8
NR93	400	20	2	340	105	9	14	163.75	123.75	1.8	1.7	1.375	3.27	13.54	14.9	1.53
NR93	400	20	2	340	105	9	14	163.75	123.75	1.9	1.8	1.375	3.365	13.54	14.9	1.53
NR93	400	20	2	340	105	9	10	163.75	123.75	0.775	0.62			13.54	14.9	0.47
NR93	400	20	2	340	105	9	10	163.75	123.75	0.9	0.755			13.54	14.9	0.47
NR93	400	20	3	360	105	9	6	183.75	123.75	0.1725	0.13			13.97	14.8	0.13
NR93	400	20	3	360	105	9	6	183.75	123.75	0.15	0.11			13.97	14.8	0.13
NR93	400	20	3	360	105	9	8	183.75	123.75	0.225	0.395			13.97	14.8	0.25
NR93	400	20	3	360	105	9	8	183.75	123.75	0.275	0.51			13.97	14.8	0.25
NR93	400	20	3	360	105	9	10	183.75	123.75	0.6	0.94	0.225	2.735	13.97	14.8	0.45
NR93	400	20	3	360	105	9	10	183.75	123.75	0.75	1.148			13.97	14.8	0.45
NR93	400	20	3	360	105	9	12	183.75	123.75	1.45	2.025			13.97	14.8	0.77
NR93	400	20	3	360	105	9	12	183.75	123.75	1.525	2.16	0.9	3.125	13.97	14.8	0.77
NR93	400	20	3	360	105	9	14	183.75	123.75	2.625	3.45	1.65	3.625	13.97	14.8	1.5
NR93	400	20	3	360	105	9	14	183.75	123.75	2.735	3.56	1.5	3.655	13.97	14.8	1.5

Appendix D
All Data Related to Wave Heights from Hydrodynamic Tests

Test Series	Bottom Width b_w, ft	Water Depth h, ft	Left Bank cot α	Tow Position S, ft	Barge Width B_s, ft	Barge Draft d, ft	Boat Speed V_s, fps	Inst. Dist. from Left Bank, ft	Barge Edge to Inst. ft	Wave Data Measured		Sec. Wave H_i, ft	Wave Period T_i, sec	Blockage Ratio Left Side, n	Schijf Calculated	
										Draw-Down z_{max}, ft	Max. Wave H_{max}, ft				Limit Speed V_L, fps	Draw-Down z_{ave}, ft
NR93	400	20	2	190	105	9	6	88.75	48.75	0.365	0.455			7.20	14.9	0.17
NR93	400	20	2	190	105	9	6	88.75	48.75	0.35	0.445			7.20	14.9	0.17
NR93	400	20	2	190	105	9	8	88.75	48.75	0.43	0.34			7.20	14.9	0.34
NR93	400	20	2	190	105	9	8	88.75	48.75	0.43	0.37			7.20	14.9	0.34
NR93	400	20	2	190	105	9	10	88.75	48.75	0.965	0.99	0.375	2.735	7.20	14.9	0.59
NR93	400	20	2	190	105	9	10	88.75	48.75	0.975	0.94	0.3	2.735	7.20	14.9	0.59
NR93	400	20	2	190	105	9	12	88.75	48.75	1.78	1.84	1.075	3.125	7.20	14.9	1.02
NR93	400	20	2	190	105	9	12	88.75	48.75	1.86	1.794	1.05	3.095	7.20	14.9	1.02
NR93	400	20	2	190	105	9	14	88.75	48.75	1.6	1.405	1.545	3.525	7.20	14.9	1.95
NR93	400	20	2	190	105	9	14	88.75	48.75	1.775	1.56	1.475	3.365	7.20	14.9	1.95
NR93	400	20	3	210	105	9	6	108.75	48.75	0.25	0.26			7.62	14.8	0.17
NR93	400	20	3	210	105	9	6	108.75	48.75	0.225	0.23			7.62	14.8	0.17
NR93	400	20	3	210	105	9	8	108.75	48.75	0.375	0.415			7.62	14.8	0.33
NR93	400	20	3	210	105	9	8	108.75	48.75	0.385	0.4			7.62	14.8	0.33
NR93	400	20	3	210	105	9	10	108.75	48.75	0.85	1.035	0.375	2.63	7.62	14.8	0.58

Appendix D
All Data Related to Wave Heights from Hydrodynamic Tests

Test Series	Bottom Width b_w, ft	Water Depth h, ft	Left Bank cot α	Tow Position S, ft	Barge Width B_s, ft	Barge Draft d, ft	Boat Speed V_s, fps	Inst. Dist. from Left Bank, ft	Barge Edge to Inst. ft	Wave Data Measured		Sec. Wave H_i, ft	Wave Period T_i, sec	Blockage Ratio Left Side, n	Schijf Calculated	
										Draw-Down z_{max}, ft	Max. Wave H_{max}, ft				Limit Speed V_L, fps	Draw-Down z_{ave}, ft
NR93	400	20	3	210	105	9	10	108.75	48.75	0.85	1.065	0.4	2.595	7.62	14.8	0.58
NR93	400	20	3	210	105	9	12	108.75	48.75	2	2.6	1.725	3.41	7.62	14.8	1.01
NR93	400	20	3	210	105	9	12	108.75	48.75	2	2.625	1.7	3.375	7.62	14.8	1.01
NR93	400	20	3	210	105	9	14	108.75	48.75	3.185	3.875	2.875	3.625	7.62	14.8	1.97
NR93	400	20	3	210	105	9	14	108.75	48.75	3.21	3.945	2.625	3.815	7.62	14.8	1.97
NR93	400	20	3	210	105	9	10	108.75	48.75	0.75	0.735			7.62	14.8	0.58
NR93	400	20	3	210	105	9	10	108.75	48.75	0.875	1.035			7.62	14.8	0.58
NR93	400	15	2	180	105	9	6	78.75	48.75	0.475	0.575			5.24	11.7	0.27
NR93	400	15	2	180	105	9	6	78.75	48.75	0.475	0.5			5.24	11.7	0.27
NR93	400	15	2	180	105	9	8	78.75	48.75	0.775	0.65			5.24	11.7	0.55
NR93	400	15	2	180	105	9	8	78.75	48.75	0.7	0.63			5.24	11.7	0.55
NR93	400	15	2	180	105	9	10	78.75	48.75	1.575	1.405	0.45	2.995	5.24	11.7	1.1
NR93	400	15	2	180	105	9	10	78.75	48.75	1.85	1.68	0.7	3.29	5.24	11.7	1.1
NR93	400	15	2	180	105	9	12	78.75	48.75	2.425	2.175			5.24	11.7	2.75
NR93	400	15	2	180	105	9	11.5	78.75	48.75	2.15	1.92	1.35	3.27	5.24	11.7	2.34

Appendix D
All Data Related to Wave Heights from Hydrodynamic Tests

Test Series	Bottom Width b_w, ft	Water Depth h, ft	Left Bank cot α	Tow Position S, ft	Barge Width B_s, ft	Barge Draft d, ft	Boat Speed V_s, fps	Inst. Dist. from Left Bank, ft	Barge Edge to Inst. ft	Wave Data Measured		Sec. Wave H_i, ft	Wave Period T_i, sec	Blockage Ratio Left Side, n	Schijf Calculated	
										Draw-Down z_{max}, ft	Max. Wave H_{max}, ft				Limit Speed V_L, fps	Draw-Down z_{ave}, ft
NR93	400	15	3	195	105	9	6	93.75	48.75	0.275	0.395			5.48	11.6	0.26
NR93	400	15	3	195	105	9	6	93.75	48.75	0.3	0.35			5.48	11.6	0.26
NR93	400	15	3	195	105	9	8	93.75	48.75	0.675	1.025			5.48	11.6	0.53
NR93	400	15	3	195	105	9	8	93.75	48.75	0.695	0.825			5.48	11.6	0.53
NR93	400	15	3	195	105	9	10	93.75	48.75	1.6	1.69	0.6	2.92	5.48	11.6	1.05
NR93	400	15	3	195	105	9	10	93.75	48.75	1.825	2.005			5.48	11.6	1.05
NR93	400	15	3	195	105	9	12	93.75	48.75	3.498	4.3075	0.65	2.865	5.48	11.6	2.65
NR93	400	15	3	195	105	9	11.8	93.75	48.75	3.5	4.3	0.625	3.025	5.48	11.6	2.65
NR93	400	15	3	195	105	9	10	93.75	48.75	2.7	3.48			5.48	11.6	1.05
NR93	400	15	3	195	105	9	10	93.75	48.75	2.68	3.5			5.48	11.6	1.05
NR93	400	15	2	230	105	3.75	6	103.75	73.75	0.13	0.07			16.38	14.9	0.08
NR93	400	15	2	230	105	3.75	6	103.75	73.75	0.125	0.095			16.38	14.9	0.08
NR93	400	15	2	230	105	3.75	8	103.75	73.75	0.205	0.15			16.38	14.9	0.16
NR93	400	15	2	230	105	3.75	8	103.75	73.75	0.2025	0.14			16.38	14.9	0.16
NR93	400	15	2	230	105	3.75	10	103.75	73.75	0.42	0.3			16.38	14.9	0.29

Appendix D
All Data Related to Wave Heights from Hydrodynamic Tests

Test Series	Bottom Width b_w, ft	Water Depth h, ft	Left Bank cot α	Tow Position S, ft	Barge Width B_s, ft	Barge Draft d, ft	Boat Speed V_s, fps	Inst. Dist. from Left Bank, ft	Barge Edge to Inst. ft	Wave Data Measured		Sec. Wave H_i, ft	Wave Period T_i, sec	Blockage Ratio Left Side, n	Schijf Calculated	
										Draw-Down z_{max}, ft	Max. Wave H_{max}, ft				Limit Speed V_L, fps	Draw-Down z_{ave}, ft
NR93	400	15	2	230	105	3.75	10	103.75	73.75	0.395	0.335			16.38	14.9	0.29
NR93	400	15	2	230	105	3.75	12	103.75	73.75	0.58	0.415	0.75	2.895	16.38	14.9	0.51
NR93	400	15	2	230	105	3.75	12	103.75	73.75	0.455	0.4	0.625	2.605	16.38	14.9	0.51
NR93	400	15	2	230	105	3.75	14	103.75	73.75	0.825	0.705	1.375	3.205	16.38	14.9	1
NR93	400	15	2	230	105	3.75	14	103.75	73.75	0.625	0.52	1.35	3.315	16.38	14.9	1
NR93	400	15	2	230	105	3.75	14.9	103.75	73.75	0.94	0.84	1.7	3.32	16.38	14.9	1.82
NR93	400	15	2	230	105	3.75	14.9	103.75	73.75	0.9625	0.88	1.775	3.335	16.38	14.9	1.82
NR93	400	15	3	245	105	3.75	6	118.75	73.75	0.145	0.11			16.95	14.9	0.08
NR93	400	15	3	245	105	3.75	6	118.75	73.75	0.125	0.08			16.95	14.9	0.08
NR93	400	15	3	245	105	3.75	8	118.75	73.75	0.19	0.2			16.95	14.9	0.16
NR93	400	15	3	245	105	3.75	8	118.75	73.75	0.1875	0.297			16.95	14.9	0.16
NR93	400	15	3	245	105	3.75	10	118.75	73.75	0.43	0.57			16.95	14.9	0.28
NR93	400	15	3	245	105	3.75	10	118.75	73.75	0.415	0.59			16.95	14.9	0.28
NR93	400	15	3	245	105	3.75	12	118.75	73.75	0.695	0.915	0.725	2.795	16.95	14.9	0.5
NR93	400	15	3	245	105	3.75	12	118.75	73.75	0.715	0.985	0.8	2.835	16.95	14.9	0.5

Appendix D
All Data Related to Wave Heights from Hydrodynamic Tests

Test Series	Bottom Width b_w, ft	Water Depth h, ft	Left Bank cot α	Tow Position S, ft	Barge Width B_s, ft	Barge Draft d, ft	Boat Speed V_s, fps	Inst. Dist. from Left Bank, ft	Barge Edge to Inst. ft	Wave Data Measured		Sec. Wave H_i, ft	Wave Period T_i, sec	Blockage Ratio Left Side, n	Schijf Calculated	
										Draw-Down z_{max}, ft	Max. Wave H_{max}, ft				Limit Speed V_L, fps	Draw-Down z_{ave}, ft
NR93	400	15	3	245	105	3.75	14	118.75	73.75	0.99	1.3575	1.575	3.27	16.95	14.9	1
NR93	400	15	3	245	105	3.75	14	118.75	73.75	0.97	1.395	1.325	3.205	16.95	14.9	1
NR93	400	15	3	245	105	3.75	14.9	118.75	73.75	1.125	1.565	1.875	3.245	16.95	14.9	1.79
NR93	400	15	3	245	105	3.75	14.9	118.75	73.75	1.16	1.6	1.85	3.35	16.95	14.9	1.79

(Concluded)

REPORT DOCUMENTATION PAGE

Form Approved
OMB No. 0704-0188

1. AGENCY USE ONLY *(Leave blank)*	2. REPORT DATE	3. REPORT TYPE AND DATES COVERED
	April 1997	Final report

4. TITLE AND SUBTITLE
Physical Model Studies for Riprap Design of Tow-Induced Forces

5. FUNDING NUMBERS

6. AUTHOR(S)
Sandra K. Martin

7. PERFORMING ORGANIZATION NAME(S) AND ADDRESS(ES)
U.S. Army Engineer Waterways Experiment Station
3909 Halls Ferry Road
Vicksburg, MS 39180-6199

8. PERFORMING ORGANIZATION REPORT NUMBER
Technical Report CHL-97-7

9. SPONSORING/MONITORING AGENCY NAME(S) AND ADDRESS(ES)
U.S. Army Corps of Engineers
Washington, DC 20314-1000

10. SPONSORING/MONITORING AGENCY REPORT NUMBER

11. SUPPLEMENTARY NOTES
Available from National Technical Information Service, 5285 Port Royal Road, Springfield, VA 22161.

12a. DISTRIBUTION/AVAILABILITY STATEMENT
Approved for public release; distribution is unlimited.

12b. DISTRIBUTION CODE

13. ABSTRACT ***(Maximum 200 words)***

Navigable waterways can be subjected to bank erosion caused by effects from commercial vessel traffic. Since riprap is an accepted and dependable means to protect banks from failure, this means could be, and has been, used to armor banks subject to tow-induced forces. Minimization of rock size can result in substantial savings in a bank protection project. While much research has been conducted to optimize riprap sizes for open channel flow and wave impact in coastal areas, little research has been conducted in the United States to expand this for waves and currents produced by vessels. Most research regarding vessel-induced waves and currents has been conducted at the Delft Hydraulics Laboratory in The Netherlands and has not been specifically verified for effects produced by commercial tow traffic such as those found in the United States on the inland navigable waterways. The intent of this research was to assemble previous physical model data taken from tests that used typical navigation vessels found in the United States, conduct additional physical model tests as necessary, evaluate the applicability of previously developed techniques and guidance, and then modify existing or develop valid, riprap design criteria for tow-induced forces.

14. SUBJECT TERMS

Angle of repose	Navigation effects	Waves
Drawdown	Riprap	
Navigation channels	Towboat	

15. NUMBER OF PAGES
260

16. PRICE CODE

17. SECURITY CLASSIFICATION OF REPORT	18. SECURITY CLASSIFICATION OF THIS PAGE	19. SECURITY CLASSIFICATION OF ABSTRACT	20. LIMITATION OF ABSTRACT
UNCLASSIFIED	UNCLASSIFIED		